
PHD THESIS

*OPTIMIZATION OF RADIONUCLIDIC PURITY AND
YIELD OF CYCLOTRON BASED NUCLEAR
REACTIONS IN THE PRODUCTION OF METALLIC
PET RADIOISOTOPES.*

Submitted in fulfilment of the requirement for the degree of
Doctor of Philosophy in Medical Physics

By

ADAM DABKOWSKI

B.Sc., M.Sc.

School of Medicine

Cardiff University

UK

2020

Summary

Cyclotron productions for the radiometals of ^{89}Zr , ^{48}V , $^{99\text{m}}\text{Tc}$ and ^{68}Ga were investigated to find optimal conditions according to results of FLUKA code Monte Carlo modelling irradiation processes, nuclear reactions and target design. Experimental validation (making cyclotron productions for expected high product yield and low impurities' levels followed by activity measurements, spectra acquisitions and chemical separation procedures) for strategies developed by computer models' analysis were carried out in the IBA CYCLONE[®] 18/9 cyclotron, permitting a comparison of the predicted and actual yields of produced radiometals and isotopic by-products (impurities) mostly for ^{89}Zr and ^{48}V . Once the *in-silica* model was validated experimentally, then optimal method of the radiometal production in the cyclotron was developed.

Results achieved with ^{89}Zr and ^{48}V , enabled expansion of the FLUKA model to other radiometal isotopes like $^{99\text{m}}\text{Tc}$ and ^{68}Ga . Optimisation of cyclotron production for those radiometals may help to keep the high rate of innovation and development in domains of theranostics, nuclear medicine and positron emission tomography (PET). Providing a wide range of isotopes with a variety of parameters like half-lives will help labelling new agents more specific for the tasks of molecular imaging and therapy. Optimized cyclotron production of $^{99\text{m}}\text{Tc}$ may solve problems with resources of the ^{99}Mo for generators of $^{99\text{m}}\text{Tc}$ eluents used in nuclear medicine. Aging nuclear reactor fleet and planned shutdowns of key reactors can cause serious problems especially in Canada and United States.

In this project a tool for optimization of the solid target production of radiometals was developed, that can be easily modified for the most common and commercially available types of the solid target stations (STS). One such solid target system is the COSTIS STS, also known as the Nitra Solid Compact, designed by Elex Commerce for IBA cyclotrons.

Table of Contents

Summary	i
Acknowledgments.....	1
Introduction	3
Hypothesis an Aims	7
Hypothesis.....	7
Aims.....	7
Literature Review	9
Materials and Methods	35
Cyclotron	35
Targets.....	35
Choice of Reaction	37
Energy Degradation	42
Target Design and Preparation	44
Irradiation of targets in the cyclotron.....	44
Target post processing: unloading and separation.....	45
Measurements of the activity and gamma spectroscopy.....	45
FLUKA modelling of the nuclear reactions and cyclotron beam parameters used for production of radiometals	49
Monte Carlo Method and FLUKA	49
Statistical Errors	53
Sources of Systematic Errors.....	54
Results	55
Production of ⁸⁹ Zr.....	55
Introduction.....	55
Modelling in FLUKA software	56
Experimental validation of the simulations' results.....	58
Results	60
Discussion.....	63

Conclusion.....	66
Production of ^{48}V	67
Introduction	67
Materials and Methods.....	70
Results.....	71
Discussion.....	78
Conclusion.....	82
Production of $^{99\text{m}}\text{Tc}$	83
Introduction	83
Materials and Methods.....	95
Results.....	101
Discussion.....	105
Conclusion.....	112
Production of ^{68}Ga	113
Introduction	113
Materials and Methods.....	121
Results.....	122
Discussion.....	146
Conclusion.....	151
Final Conclusions.....	151
References.....	153
Appendix	169

Acknowledgments

I would like to express my special gratitude to my boss, supervisor and guide Prof. Christopher Marshall for his constant support and patience in all these years of my studies and work at Cardiff University. His ease of teaching and discussing scientific problems inspired me. He always gave me the possibility to grow and to improve my competences, also at an international level.

Also, special thanks and respects to my former bosses in PETIC: Ian Davies and Dr Stephen Daniels, which encouraged me to take this challenge.

I would like to thank my co-supervisors: Prof. John Chester for his big support especially at the beginning of my PhD studies and Dr Emiliano Spezi for introducing me to the scientists from University of Bologna and community working with Monte Carlo Method and FLUKA. Their patience and critical feedback were priceless.

I deeply appreciate hospitality and help which I received from the University of Bologna team, especially from Dr Mario Marengo and invaluable Dr Angelo Infantino showing me the tips & tricks of FLUKA code and Monte Carlo Method.

Massive thanks for ICNAS team from University of Coimbra and Prof. Francisco Alves, Dr Antero Abrunhosa and Vítor Alves for their support in ^{68}Ga project and time spent on discussions with excellent food from Portuguese cuisine.

A big “thank you” to my mentor Prof. William David Evans for his constant support, friendship, and reliance in all these years. It was a pleasure to discuss the nuclear medicine problems with him and gain experience listening to his advice.

I am very grateful all the people of science which ongoing work and published literature inspired me and helped to solve the issues that I came across during my studies: Dr C. Hoehr, Dr K. Gagnon, Dr M. Walther, Prof. M. Sadeghi and many others that are listed in references.

Many thanks to all the people from TRIUMF centre in Vancouver for their hard work and contribution to cyclotron science. A special acknowledge goes also to Dr Ken Buckley and Stuart McDiarmid for their support and cooperation with $^{99\text{m}}\text{Tc}$ production.

The special acknowledge goes to the group of people that worked with me in PETIC, to my colleagues for all those years, for their support, kindness, and professionalism. For Dr Stephen Paisey, Dr Katrin Probst, Dr Peter Llewelyn, Dr Andrew Watkins, Donata Hardwick, Dr Matthew Tallboys, Dr Ansam Abd Alrasool

Ali Al-Obaidi, Syed Bukhari, Vito Constanza, Dr Guillaume Marie and all the others that work for Cardiff University in Wales.

I dedicate this work to my wonderful family: Mum, Dad, my lovely wife, my amazing brother and sister and their families.

Adam Dabkowski
June 30th, 2020
Cardiff, UK

Introduction

The development of biological targeting agents such as proteins, peptides, antibodies, exosomes, cells and nanoparticles with biological-effective levels (biological distribution times or biological half-lives) lasting many hours and days requires the production of radionuclides for nuclear imaging and therapy with physical (radioactive) half-lives complementary to the lifetime of these biological agents. Potentially useful radionuclides for labelling and tracking these agents with PET include radiometals such as zirconium-89 (^{89}Zr), yttrium-86 (^{86}Y), copper-64 (^{64}Cu), vanadium-48 (^{48}V), gallium-68 (^{68}Ga), niobium-90 (^{90}Nb) and many others [1-3]. In this project, the optimisation of cyclotron production for the positron emitting radioisotopes of zirconium, vanadium and gallium was investigated. The same optimization method was also tested for technetium-99m ($^{99\text{m}}\text{Tc}$), the most popular single photon emission computed tomography (SPECT) radiometal. The choice of which radioisotopes to investigate was motivated by the highest interest among the local researchers in PETIC in using agents labelled with these radioisotopes. Zirconium-89 is currently a radioisotope widely used for the investigation of processes lasting several days. Vanadium-48, with its longer half-life (15.97 days) could be useful in the research of longer-lasting processes such as stem cells distribution and assimilation or tracking the systemic delivery of antibiotics by liposomes.

In addition, we decided to investigate optimisation of cyclotron production of two other radionuclides:

- Technetium-99m ($^{99\text{m}}\text{Tc}$) – the “work horse” of nuclear medicine [4] and SPECT [5] and
- ^{68}Ga – in PET [6] one of the most popular and promising next to fluorine-18 (^{18}F) [7].

Below a short subjective choice of the most popular and novel radioisotopes is presented. Those radioisotopes are potentially easy to produce in a small (up to 18 MeV beam energy) medical cyclotron equipped with solid or solution liquid target [8-10].

Zirconium-89 is very popular radionuclide in the development of new immuno-PET¹ agents for in vivo imaging of cancerous tumours and radioimmunotherapy² (RIT) planning [11]. Besides the convenient half-life of 78.4 h, ⁸⁹Zr has a beta plus emission rate of 23% and its low maximum energy of 0.9 MeV, delivering good spatial resolution as a result of short positron range in tissue (around 1 mm) [12].

In cancer therapy there is a move to the application of therapies based on antibody targeting of specific pathways that drive the transition from normal to cancerous cell type (immunotherapy) [13]. For example, humanized monoclonal antibody (mAb) trastuzumab (Herceptin ®) which targets the cell surface antigen HER2 (also known as erbB2 or EGFR2), over-expressed in many epithelial tumours [14-16]. Immunotherapies are designed to specifically target molecules known to be associated with malignant processes and to reduce the side-effects associated with cytotoxic drugs. However, the drugs are expensive and occasionally give rise to significant side-effects [17-20]. It is important, therefore, to know whether a therapeutic does target the intended pathway in specific patient. The 78 hour half-life of ⁸⁹Zr, in comparison with physiological time frames typical for antibodies (1 to 10 days, for trastuzumab mean biological half-life is 6 days), makes it very attractive for extended imaging studies, which allows optimal tumour to non-tumour ratios to be achieved [15] given the relatively long (days) biological clearance of large drug molecules such as mAbs [21]. Furthermore, the separate preparation of the mAb-chelating complex and incorporation of the positron emitting ⁸⁹Zr isotope represents an optimized methodology for radiotracer production, of interest to chemists, bio-imaging specialists and clinicians [22, 23].

Yttrium-86 is also an attractive radionuclide for PET studies in patient specific dosimetry for ⁹⁰Y therapy, can provide the necessary information on biodistribution and kinetics required for treatment planning [18]. Yttrium-86 has a half-life of 14.7 h and decays by beta plus in 34% and in 77% by gamma emission. Yttrium-90 with half-life of 64.1 h, 100 % beta minus emission and features of its ⁸⁶Y isotope is one of the best therapeutic isotopes. The limitation of the beta plus emitter is the presence of additional gamma rays emitted during its decay. Emitted positrons have high energy of 3.14 MeV and with mentioned 1.08 MeV gamma rays can

¹ PET imaging used to investigate the specificity of the antibody for its antigen, binding kinetics, exact localization, internalization, stability of the antibody ligand complex, and biodistribution of the antibody.

² RIT uses an antibody labeled with a radionuclide to deliver cytotoxic radiation to a target cell.

interfere with accurate detection of the annihilation photons. To maintain the good image quality, the appropriate corrections are necessary [24].

Charged particle bombardment of natural or enriched titanium targets produces several radionuclides useful in medical and biological fields like intravascular brachytherapy (IVBT) using **vanadium-48** which can be produced by proton or deuteron activation of ready-to-use titanium-rich stents [25]. One interesting study [26] describes the activation of nickel-titanium alloy (nitinol) stents with protons creating ^{48}V , a mixed positron/gamma emitter. Stents are bombarded with 8.5 MeV protons in a cyclotron at a beam flux of 45 mA/mm² producing vanadium-48 in a $^{48}\text{Ti}(p,n)^{48}\text{V}$ reaction. Vanadium-48 has a half-life of 15.97 days and decays by positron (β^+) emission and electron capture (β^+ : 50% with 0.696 MeV of E_{max} ; γ emissions with photon energies of 0.511, 0.944, 0.983, 1.312, and 2.241 MeV). Although other short-lived isotopes are produced, ^{48}V is the only detectable isotope 3 days after activation.

Vanadium-48 is frequently used in nuclear medicine [27] and for checking the sealing capability of used fuel storage tanks in nuclear power plants. Recently it has been proposed for routine transmission scanning in PET as an alternative to germanium-68 [28].

Technetium-99m is the most widely used radionuclide in nuclear medicine, ideal single-photon emitter, because of its favourable half-life (~6 hours), photon energy, and radiopharmaceutical chemistry. The use of $^{99\text{m}}\text{Tc}$ continues to grow worldwide. $^{99}\text{Mo}/^{99\text{m}}\text{Tc}$ generators remain the main source of radioisotopes for nuclear medicine for more than 50 years. In those generators the short-lived $^{99\text{m}}\text{Tc}$ isotope is generated by radioactive decay of molybdenum-99 (with a much longer half-life of 66 h). Research nuclear reactors have been the main source of ^{99}Mo for decades. The fragility of ^{99}Mo supply for $^{99}\text{Mo}/^{99\text{m}}\text{Tc}$ generator production was highlighted by recent shutdowns of the leading production sites for ^{99}Mo creating a risk for loss of a long-term, stable supply of ^{99}Mo for medical purposes [29]. Alternative methods of ^{99}Mo production or direct production of $^{99\text{m}}\text{Tc}$ are investigated. The feasibility of direct production of $^{99\text{m}}\text{Tc}$ was first reported in 1971 employing the $^{100}\text{Mo}(p,2n)^{99\text{m}}\text{Tc}$ reaction [30]. Other method is the photonuclear reaction $^{100}\text{Mo}(\gamma, n)^{99}\text{Mo}$ with gamma radiation generated in electron accelerator. This method is an alternative for production of ^{99}Mo through uranium-235 fission, but its efficiency is much lower, which results in low specific activity (LSA) of ^{99}Mo . These requires efficient methods of separating $^{99\text{m}}\text{Tc}$ from the excess of molybdenum and/or utilizing new adsorbents, which are selective for $^{99\text{m}}\text{Tc}$ or have a large adsorption volume for Mo.

Gallium-68 becomes interesting radiometal in recent years due to its broadening clinical applications [31-33]. In oncology, diagnostic examinations using gallium-based molecules are made. The same compounds are later labelled with a therapeutic radionuclide such as ^{90}Y or ^{177}Lu for treatment. ^{68}Ga can be produced directly in cyclotron by induced nuclear reactions (solid and liquid targets) [8], but it is more commonly provided using $^{68}\text{Ge}/^{68}\text{Ga}$ generators.

Copper-64 is one of the most useful radionuclides for PET as well as systemic and targeted RIT of tumours. ^{64}Cu has an intermediate half-life (12.7 h) and a multiple decay mode that involves β^- , electron capture, and positron decay (β^+) [34]. That feature qualifies copper-64 as one of the best candidates for use in theranostics. Most popular method used in hospital cyclotrons for ^{64}Cu production uses proton bombardment of ^{64}Ni , which like ^{68}Zn used in cyclotron production of ^{68}Ga is very expensive and both methods need high enriched targets. In both cases production in the so-called solution (liquid) targets is very promising because enables usage of very small amounts of the expensive target materials dissolved in bigger volume of the strong acid.

Among less popular metallic radioisotopes niobium-90 is being also proposed as a potential radioactive tag for production of immuno-PET agents [35]. It has a suitable half-life of 14.6 h to be used for labelling of antibody fragments and some intact antibodies as well. The positron branching of 53% is relatively high with optimal energy of emission (0.35 MeV) providing high quality of imaging with low dose used [36].

Most radionuclides with nuclear properties suitable for imaging and therapy are metals and require the coordination of chelates to form complexes with the appropriate biological targeting properties. Long half-lives are also advantageous for radiochemists using more sophisticated methods for labelling molecules with radiometals.

One of the main aims of this project is to assist in development of novel imaging agents for early and effective diagnosis of cancer and treatment targeting for individual patients, thus realising some of the goals of personalized medicine. Successful treatment outcomes for many disease states rely upon early diagnosis for which modern imaging techniques have become essential.

Hypothesis and Aims

Hypothesis

Through the optimization of basic parameters for the nuclear reactions which produce radiometals such as: ^{89}Zr , ^{48}V , ^{68}Ga and $^{99\text{m}}\text{Tc}$ and for further separation and purification steps, it will be possible to increase both the production yields and isotopic purities of radioisotopes which may be used to form anti-cancer drugs and label imaging agents with long biological half-lives (e.g. monoclonal antibodies).

Aims

The overall aim of this project is to:

- Support the development of novel imaging agents for early and effective diagnosis and immunotherapeutic treatment of individual cancer patients, thereby maximising efficacy and reducing side-effects.
- Radiolabel 'biological' therapeutic agents such as proteins, peptides, antibodies and nanoparticles with long biological half-lives using the radiometals.
- Facilitate personalised cancer medicine with anti-cancer radiometal based agents permitting appropriate use of the right drug for the right patient at the right time.
- Solve problems with resources of the ^{99}Mo for generators of $^{99\text{m}}\text{Tc}$ eluents used in nuclear medicine. Aging nuclear reactor fleet and planned shutdowns of key reactors can cause serious problems especially in Canada and United States.

To help with the implementation of the above aims, a set of specific aims has been set as follows:

- Optimisation of cyclotron nuclear reactions yields by computer modelling of the basic parameters (beam energy, target material composition, beam current and time of target irradiation).
- Determination of the optimal methods for cyclotron production of zirconium-89 and vanadium-48 radiometals.

- Adaptation and optimisation of different approach using method for cyclotron production of ^{68}Ga in the standard medical cyclotron by proton irradiation of the solid and liquid targets with ^{68}Zn or its solution.
- Adaptation and optimisation of cyclotron production method for $^{99\text{m}}\text{Tc}$ in the standard medical cyclotron. One possible solution is the direct production of $^{99\text{m}}\text{Tc}$ from a ^{99}Mo target via the $^{99}\text{Mo}(p,n)^{99\text{m}}\text{Tc}$ reaction.
- Helping to develop effective methods for the chemical separation and purification of radioisotopes from target materials by optimization of the radioisotopic purity of the products to increase radiation safety. This might be verified experimentally and confirmed using analytical techniques such as Multi Channel Analysers (gamma spectrometry), Mass Spectrometry and Thin Layer Chromatography with radio-detection. However, it is not always possible and then results of computer simulations can also provide information about radioisotopical purity of the product.

Literature Review

In 2003, J. Czernin [37, 38] summarised that **Positron Emission Tomography** combined with **Computed Tomography** (PET/CT) was a technical evolution that led to a medical revolution. There was a dramatic raise of PET examinations done in US between 2000 and 2012 from 0.2 million up to 1.85 million and 21% increase in number of those procedures in Europe between 2005 and 2010. Over the last two decades PET has been proven to be a superior technology for non-invasive imaging of physiological processes. Sensitivity of nano or even pico-molar range for this modality is a very good example of de Hevesy [39] “tracer principle”³ and combined with “clever design” radiopharmaceuticals can also utilize the “magic bullet”⁴ concept developed by Paul Ehrlich [40]. PET imaging provides also quantitative map of drug/tracer distribution in the living body. It is therefore a useful tool for determining pharmacokinetics and pharmacodynamics. PET does not compete with other tomography methods, but is rather complementary, what also determined its success [3]. It was aptly claimed by Beyer [38] that: *although PET/CT appears to have replaced stand-alone PET for most oncologic indications, it is reasonable to assume that PET/MRI will be the preferred imaging option for neurologic and central nervous system indications. Without doubt, such dual-modality combinations are here to stay because they incorporate the diagnostic power of PET. Thus, PET/CT and PET/MRI, by virtue of their combined anatomometabolic imaging, will lead to a “new-clear” medicine and the demise of “unclear” medicine.*

Successful treatment outcomes for many disease states rely upon early diagnosis for which modern imaging techniques have become essential [41]. Fluorine-18 (¹⁸F) labelled fluorodeoxyglucose (FDG), as a tracer molecule for PET, which reports glucose metabolic activity, has proven an extremely valuable tool in the early diagnosis of a wide variety of cancers, Alzheimer's disease and in the delineation of epileptogenic zones prior to neurosurgery [42]. With a half-life of nearly two hours and its physical properties “almost tailored” for PET, ¹⁸F became

³ G. de Hevesy based his theory on the principle that radioactivity has the advantage of being easily detected at very low quantities that will not perturb the system enabling probing of biological processes at the cellular or molecular level without disturbing normal physiology.

⁴ Biomolecules, particularly antibodies, could be utilized as targeting molecules to transport toxins or radionuclides selectively to cancerous cells.

“technetium” like isotope expanding dramatically the potential of nuclear medicine. However, FDG is not diagnostic for all cancers, since some are not more metabolically active than normal tissue, nor is it mechanistically specific and thus cannot direct selective therapy [2, 43].

It is desirable to develop new specific PET probes with high affinity to bind to a molecular “manifestation” of a disease. PET isotopes, to be useful, should possess number of properties like low positron energy, high positron decay branching ratio and reasonably long half-life. Length of the half-life should match the biological half-life of the molecule being labelled or the physiological event being probed and should allow for radiochemical synthesis within two half-lives of the isotope [1].

Development and optimization of radiopharmaceuticals focuses on designing and modifying the target selectivity of the molecule, not the mechanism of action, as with other drugs.

Diagnostic agents of nuclear medicine consist of radionuclides decaying by:

- Positron (β^+) emission (e.g. ^{18}F) and its quick conversion to two 511 keV gamma photons (γ) after interaction with electron of the tissue (PET), or
- Direct emission of the gamma photons (e.g. $^{99\text{m}}\text{Tc}$) with high enough energy to penetrate the body and be detected externally but low enough to be collimated by the camera (SPECT).

Therapeutic agents consist of radionuclides that decay by electron (β^-) or α particle emission that can cause ionization and break bonds resulting in the intended ablation.

For years radiopharmaceuticals were designed to be used solely for either imaging or therapy. It was assumed that imaging requires a radionuclide that decays only by photon emission with energy suitable for imaging and that any release of additional particles would give an undesired extra dose to the patient. In the case of therapy situation was analogical and nothing more was considered than dose to both the patient and medical technician when administering radionuclides that emitted additional γ photons [44].

As the development of drugs that target specific pathways advanced, the use of the same targeting biomolecule or organic ligand for both imaging and therapy (e.g. DOTATOC labelled with ^{68}Ga first and then with ^{90}Y) began but with attachment to two different radionuclides [44-48]. One radionuclide would be used to image individual patient (^{89}Zr , ^{124}I , ^{86}Y , ^{68}Ga) disease states and evaluate their

receptor expression, metabolic rate, clearance and handling, and a second radionuclide would be used for therapy (^{90}Y , ^{177}Lu). Problems with this approach arose due to differences in the chemistry of the radionuclides themselves, which have been shown to affect the overall distribution and mechanism of localization, resulting in an over- or underestimation of dose to critical tissues and the dose being outside the optimum range of efficacy. Agents currently being designed utilize radionuclides that give off photons that can be imaged as well as particles that can be used for treatment (^{64}Cu). Advantages are:

- more exact patient assessment and dosage [2, 49],
- significant savings of time and other resources when developing one drug that can serve two purposes rather than two separate drugs [34, 50, 51].

Where the imaging and therapy purposes can be combined by means of one molecule, the domain of new method called theranostics begins. Theranostics, next to the multimodal imaging agents could be an example of synergy and dawn of nanotechnology in medicine [52-54]. Many radiometals have the nuclear properties required for use in applications for imaging and therapy together. Some of them are listed in Table 1 [2].

The radioisotopes of zirconium-89, yttrium-86 and copper-64 are the most common examples of the radiometals, mentioned as the most promising and potentially successful in the near future of PET [1, 3, 22]. Each of those three isotopes illustrates in some degree a different approach in the process of optimization of its production and separation (purification), they also differ in main applications and their range. Basic properties of those radiometals are summarized in Table 2 [1] compared with four standard PET isotopes.

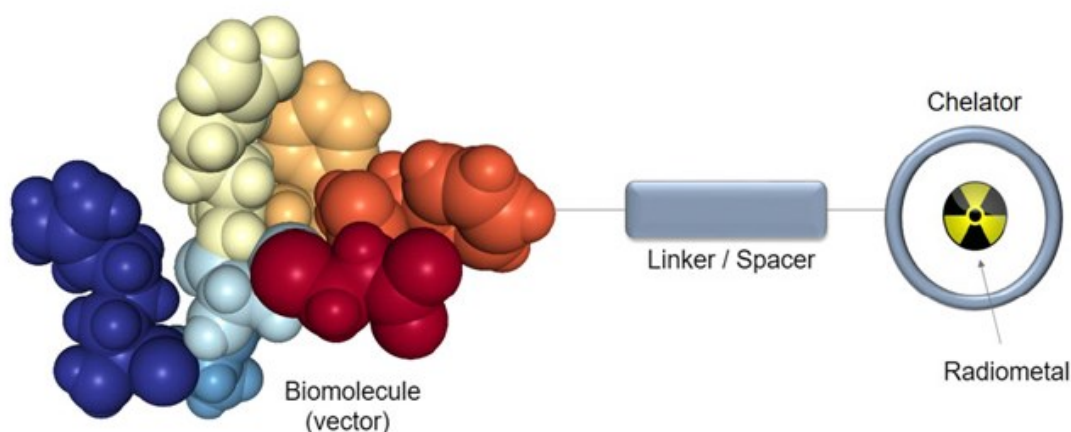


Figure 1 Schematic sketch of targeted metal-based radiopharmaceutical [55].

The potential of radiometals in nuclear imaging goes well beyond the established ^{99m}Tc -radiopharmaceuticals used for SPECT. Concerning diagnostic imaging agents, the use of positron-emitting radiometals for PET is a rapidly growing field. For example, ^{68}Ga has become the clinical standard for the radiolabeling of somatostatin analogs (e.g., DOTATOC/TATE) and prostate-specific membrane antigen (PSMA) ligands (e.g., HBED-cc-PSMA) for the detection of neuroendocrine and prostate tumours, respectively.

Table 1. Nuclear properties of radiometals [2].

radionuclide	decay mode	$T_{1/2}$ (h)	$E_{\max} \beta^-$, MeV (%)	γ energy, keV (%)	theoretical specific activity		achievable specific activity Ci/mg	ref ^a	mean tissue range ^b (mm)
					Ci/ μmol	Ci/mg			
^{198}Au	β^-, γ	64.7	0.96	412 (95.6)	4.8	245	0.095	1	0.38
^{199}Au	β^-, γ	75.4	0.45	208 (9.1) 158 (40)	4.1	210			0.14
^{105}Rh	β^-, γ	35.4	0.57 0.25	319 (19.6) 306 (5)	8.8	843			0.19
^{177}Lu	β^-, γ	161.0	0.50	208 (11) 113 (6.6)	1.9	110	25	1	0.16
^{153}Sm	β^-, γ	46.3	0.81	103 (28.3)	6.7	443	6	1	0.30
^{166}Ho	β^-, γ	26.8	1.86	80.6 (6.2) 1379 (1.13)	11.6	704	22	1	0.84
^{161}Tb	β^-, γ	165.8	0.59	48.9 (17.0) 74.6 (10.2)	1.9	117			0.20
^{149}Pm	β^-, γ	53.1	1.10	286 (3)	5.9	396			0.43
^{186}Re	β^-, γ	89.2	1.10	137 (9)	3.5	189	3	1	0.43
^{188}Re	β^-, γ	16.9	2.10	155 (15)	18.4	984	c	2	0.98
^{44}Sc	β^+, γ	3.9	0.63	511 (94) 1157 (99.9)	79.5	181			
^{47}Sc	β^-, γ	80.4	0.60	159.4 (68)	3.9	830			0.20
^{64}Cu	β^+, β^-, γ (EC)	12.7	0.65 (19) 0.58 (40)	511 (38.6)	24.6	3,855			0.19
^{67}Cu	β^-, γ	61.9	0.58	184.6 (46.7) 93.3 (16.6) 91.3 (7.3)	5.0	755			0.19
^{71}As	β^+, γ	65.3	0.81	175 (82)	4.8	676			
^{72}As	β^+, γ	26.0	3.34	834 (80)	12.0	1674			
^{74}As	β^+, β^-, γ	426.7	1.36 (29) 1.54 (32)	596 (59.3)	0.7	99			0.58
^{77}As	β^-, γ	38.8	0.68	239 (1.6)	8.0	1048			0.24
^{212}Pb	β^-, γ	10.6	0.57	238.6 (43.1)	29.3	1389			0.19
^{212}Bi	α, β^-	1.0	2.25 (55.5)	727 (11.8)	309.4	1465			
^{213}Bi	α, β^-	0.8	1.43 (97.9)	440 (27.3)	410.1	19324			
^{225}Ac	α	240.0	5.94	99 (5.8)	1.3	58			
^{117m}Sn	IT	326.4	0.13–0.16	156 (2.1) 158.6 (86.3)	1.0	82	0.008–0.010	3	
^{67}Ga	EC	78.3		393.5 (4.2) 300 (15.3) 184.6 (20.8) 93 (38.6)	4.0	598	1.0	4	
^{111}In	EC	67.3		173 (89) 247 (95)	4.6	49	c	5	

^aThe achievable specific activity values were obtained from the following, as referenced: (1) Radioisotopes and radiochemicals. http://www.murr.missouri.edu/ps_radio_isotopes.php (accessed October 1, 2012). (2) Knapp, J., Nuclear medicine program progress report, Oak Ridge National Lab, 1996. (3) Knap, J., Production of Medical radioisotopes in the ORNL high flux isotope reactor (HFIR). 13th Radiochemical conference, Marainske Lazne, Czech Republic, 1999, in press. (4) Ga-67 Fact Sheet. http://www.nordion.com/documents/products/Ga-67_Can.pdf (accessed October 1, 2012). (5) PerkinElmer. <http://www.perkinelmer.com/catalog/category/id/radiochemicals> (accessed October 1, 2012). ^bThe values for the estimated mean tissue range were calculated by following the standard formula referenced in Loveland, W. D.; Morrissey, D. J.; Seaborg, G. T. *Modern Nuclear Chemistry*; John Wiley & Sons: Hoboken, NJ, 2005. ^cNo carrier added.

In most targeted **radiometal-based radiopharmaceuticals**, the metal is bound to a pharmacophore by a bifunctional chelating agent (BFCA), which forms a stable covalent linkage between the label and the targeting ligand (vector) and ensures the stable complexation of the metal in vivo (Figure 1). In many instances, the chelator and the vector are connected via a spacer moiety to separate the individual components of the conjugate to avoid potential interference. Chelators contain several functional groups for coordination to the radiometal of choice. This structural feature results not only in high kinetic and thermodynamic stability of the complex but also usually in its fast and quantitative formation (chelate effect). Radiometal complexation with chelator-modified vectors offers convenient access to radiopharmaceuticals, for example, by enabling kit formulations. The choice of a chelator depends on the radiometal, which in turn is determined by the intended application. There are chelators that can be used in combination with different radiometals (e.g., DOTA for radiolabeling with ^{68}Ga , ^{111}In , or ^{177}Lu); however, optimized chelating systems tailor-made for individual radiometals are often available [55].

Table 2. Comparison of some properties for chosen PET isotopes [1].

Isotope	Half-life	$E_{\beta+\text{max}}$ (MeV)	Mode of decay (β^+ %)
Standard isotopes			
^{15}O	2 min	1.74	100
^{13}N	10 min	1.19	100
^{11}C	20.3 min	0.96	99
^{18}F	110 min	0.64	97
Nonstandard isotopes			
^{64}Cu	12.7 h	0.655	18
^{86}Y	14.7 h	1.2	33
^{89}Zr	3.27 days	0.897	23

^{11}C : Carbon-11; ^{64}Cu : Copper-64; ^{18}F : Fluorine-18; ^{15}O : Oxygen-15; ^{13}N : Nitrogen-13; ^{86}Y : Yttrium-86; ^{89}Zr : Zirconium-89.

From Table 2, radiometals (nonstandard isotopes) have optimal half-lives for the novel PET applications presented before, but their branching ratios (modes of decay) for positron emissions are much lower than for standard isotopes. This situation may lead to a statistically lower rate of true coincident gamma detections in PET scanner and result in worse image quality [56]. However, combining a radiometal with a properly selected targeting compound, of high specificity, could compensate that and give better signal to noise ratio of the image.

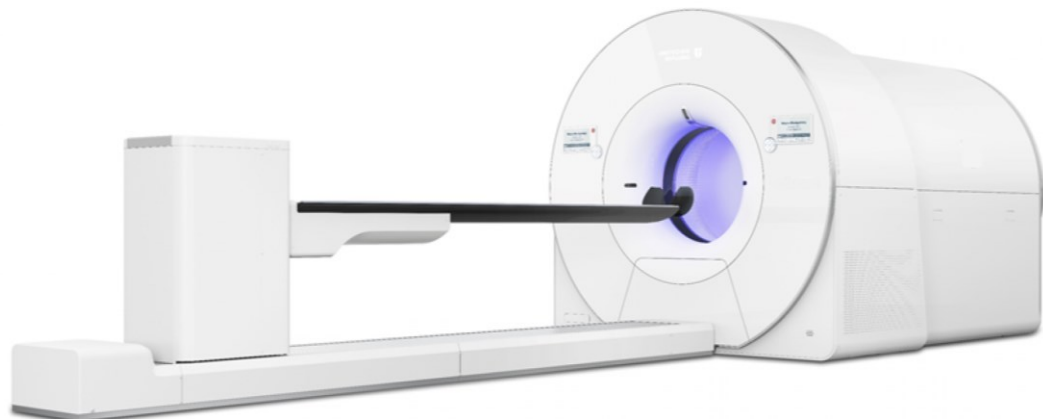
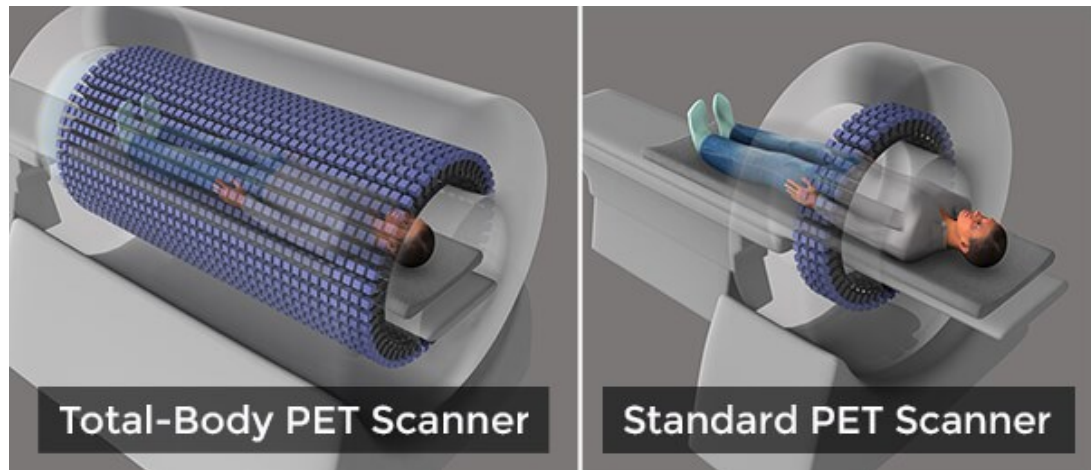


Figure 2 A depiction of the completed uEXPLORER scanner to be installed at University of California, Davis Health in April 2019 [www.explorer.ucdavis.edu].

For imaging applications, the physical half-life of a radionuclide should match its intended application, or more specifically, the biologic half-life of the vector it is conjugated to. Short-lived radiometals are ideal in combination with vectors that exhibit fast pharmacokinetics (e.g., small molecules and peptides), whereas longer-lived radiometals are best suited for the imaging of slow biologic processes, such as the biodistribution of antibodies (immuno-PET). A low β^+ energy is another important aspect, since the positron's energy, and consequently its tissue penetration range till annihilation with an electron, determines the resolution of the PET image. A high positron intensity is also desired, as well as preferably no other radiation emitted from the same nucleus. Concomitant high-energy γ or particle (α , β^-) radiation can

affect the quality of PET images or cause an unnecessary radiation dose to the patient [55]. Problems of radiometals are the high radiation doses to the patients. They could be overcome with both digital and **total body PET** requiring much less signal (i.e. lower doses) to obtain diagnostic images. A medical imaging device that can create 3D renderings of the entire human body in as little as 20 seconds could soon be used for a wide variety of research and clinical applications [57]. The modified PET scanner is faster than conventional PET scans, which can take an average of 20 minutes and requires less radiation exposure for the person being imaged. The EXPLORER scanner (Figure 2) has an effective sensitivity for total-body imaging that is 40-fold higher than current commercial scanners and is expected to open completely new ways in which PET can be used in biomedical research and ultimately in clinical practice. This massive increase in sensitivity can be used in several ways, for example:

- to perform scans at extremely low radiation doses
- to perform scans much more quickly (potentially in less than a minute)
- to track the fate of radiotracers for much more time after injection

Additional factor motivating for usage of nonstandard isotopes in PET is a rapid development in detector technology [58, 59]. The digital detector built into the PET/CT scanner improves sensitivity and, consequently, the detectability of small lesions. And it does so while reducing scan time. The digital photon counting detector, uses solid-state sensors to count the individual scintillation photons created during a PET scan (Figure 3). Analog PET detectors cannot count individual photons. Instead, these detectors, which are built into the vast majority of installed PET/CTs, record flashes of light. The digital detector counts optical photons individually (one-to-one coupling between the scintillation crystals and the digital sensors results in many channels, each with a relatively low count rate, so we end up with good count rate performance), Alternatively, the **digital PET/CT** might maintain image quality achieved over a substantially reduced scan time, as low as one-third or less of the typical 10 to 15 minutes. Physicians might choose a third option: to maintain image quality and scan time but reduce the dose of radiopharmaceutical injected into the patient [G. Freiherr, *ITN*, Oct. 17, 2018].

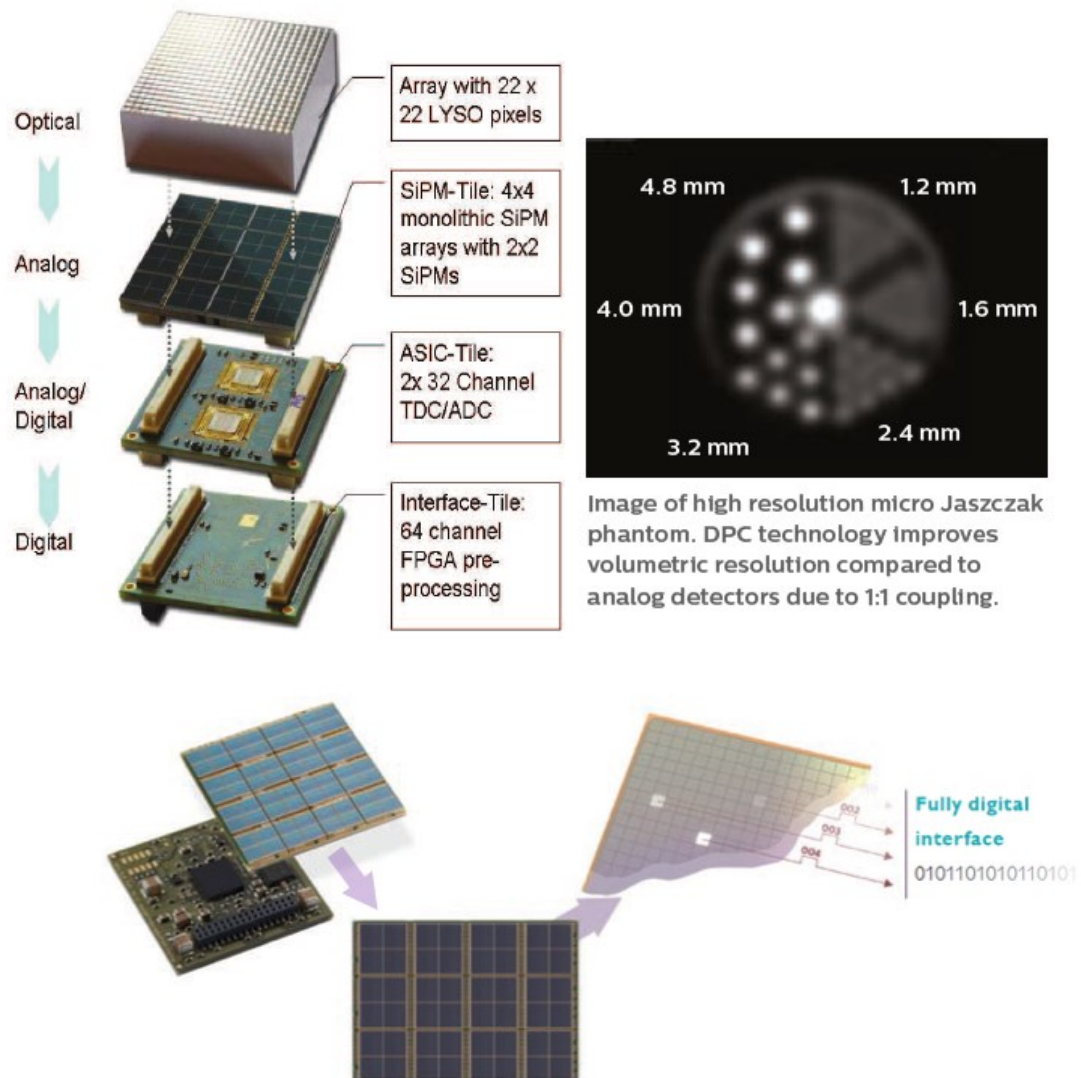


Figure 3 Digital PET detectors replacing traditional photomultiplier PET detector assemblies is a major technological change [www.usa.philips.com].

Properties like maximum energy of emitted positrons and their range in the human tissue (affecting imaging resolution) are comparable for both groups of isotopes from Table 2.

Wide range of nonconventional radionuclides potentially useful in production of new radiopharmaceuticals and their physical properties is presented in [60].

In this project, optimisation plays a crucial role in determining simplest and optimal methods to produce high yields of radioisotopically pure radionmetals using a common, low energy medical cyclotron.

Nuclear medicine procedures, whether performed for diagnostic or for therapeutic purposes, rely on the decay of a radioisotope of adequate radiation characteristics. These unstable isotopes are not available in nature and therefore must be artificially produced, through nuclear reactions. Three main direct or indirect nuclear processes leading to the production of the intended radioisotopes can be identified:

- Nuclear reactions performed in particle accelerators, namely cyclotrons
- Nuclear reactions performed in nuclear reactors
- Nuclear reactions performed in Generators

In other words: radionuclides can be subdivided into three main categories based on their method of production:

- Generator
- Cyclotron
- Reactor.

Generator produced radionuclides are particularly attractive for use in biomedical applications as they are both cost-effective and can also be used in locations remote from cyclotron or reactor facilities. However, reactor production facilities and ready availability of the parent radionuclides are essential for development and wide usage of generator-based systems. The extremely high cost, fragile supply chain and numbers of highly skilled workers required to operate a nuclear reactor makes these facilities operational only at the national level [61-63]. Problems with the closing down old fleet of nuclear reactors automatically generate the shortage of the generator produced radionuclides supply [64].

As of July 2017, almost all molybdenum-99 (moly-99) for medical use was being produced by irradiating solid uranium targets in the six research reactors listed below (available production capacity of the reactors is shown in parentheses) and illustrated in Figure 4.

BR-2, Belgium (7,800 six-day Ci/week)

HFR, Netherlands (6,200 six-day Ci/week)

LVR-15, Czech Republic (3,000 six-day Ci/week)

Maria, Poland (2,700 six-day Ci/week)

OPAL, Australia (2,150 six-day Ci/week)

SAFARI-I, South Africa (3,000 six-day Ci/week)

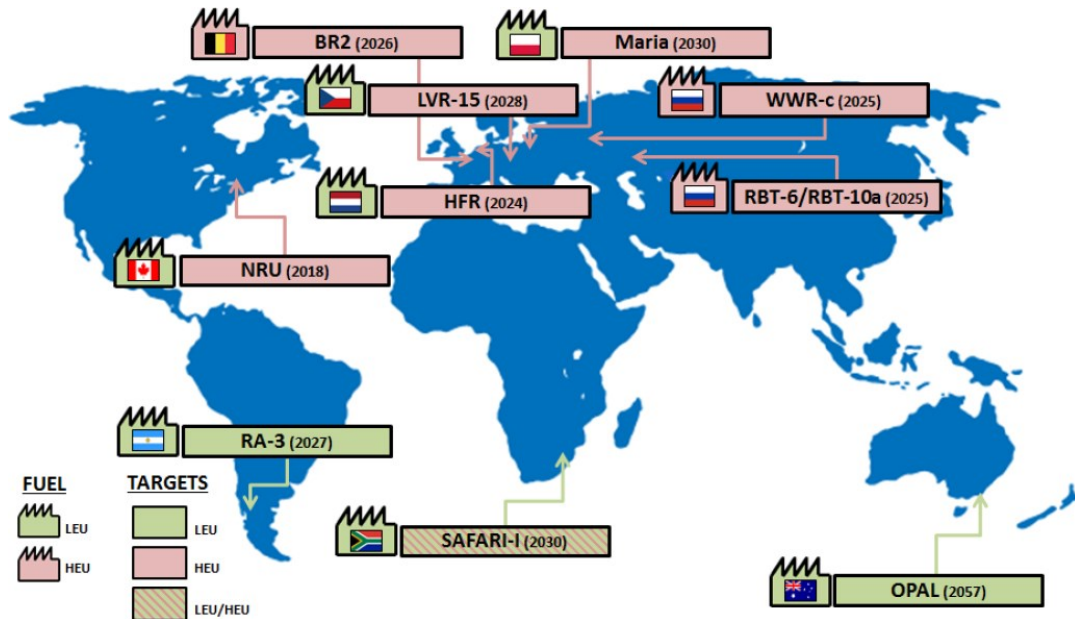


Figure 4 Molybdenum-99 supply map as of July 2017. Most moly-99 was produced in reactors in Belgium (BR-2), Netherlands (HFR), the Czech Republic (LVR-15), Poland (Maria), Australia (OPAL), and South Africa (SAFARI-I). Smaller amounts of moly-99 were produced in Russia (RBT-6/RBT-10a and WWR-c) and Argentina (RA-3). The NRU reactor in Canada was on “hot standby” and could resume production until March 2018 to support global moly-99 supply. The estimated end of operation for the reactors is shown in parentheses. The schematic indicates whether a reactor irradiates HEU or LEU targets and whether it operates using HEU or LEU fuel [65].

All reactors except OPAL and SAFARI-I (since August 2017) irradiate highly enriched uranium (HEU) targets. Moly-99 produced in these reactors is supplied to the global market by four companies in Australia (Australian Nuclear Science and Technology Organisation [ANSTO]), Belgium (Institut National des Radioelements [IRE]), Netherlands (Curium), and South Africa (NTP Radioisotopes). In addition to these reactors, smaller amounts of Moly-99 are produced in other reactors, for example, the RBT-6 and RBT-10a (available production capacity is 1,000 six-day Ci/week) and WWR-c (350 six-day Ci/week) in Russia, and the RA-3 reactor (400 six-day Ci/week) in Argentina. The Russian reactors irradiate HEU targets, and the Argentinian reactor irradiates low-enriched uranium (LEU) targets.

All moly-99 suppliers except those in Russia are either in the final stages of converting production from using HEU to LEU targets or already produce Moly-99 using LEU targets.

Two irradiation facilities, the OSIRIS reactor in France and the NRU reactor in Canada, contributed to the moly-99 supply until December 2015 and October 2016, respectively. The OSIRIS reactor permanently stopped operating; the NRU reactor is kept in hot standby and could resume production until March 2018 to support global moly-99 supply and avoid moly-99 shortages.

The following section summarize information that was provided at the symposium OPPORTUNITIES AND APPROACHES FOR SUPPLYING MOLYBDENUM-99 AND ASSOCIATED MEDICAL ISOTOPES TO GLOBAL MARKETS on the countries and companies that supply moly-99 produced in currently operating reactors.

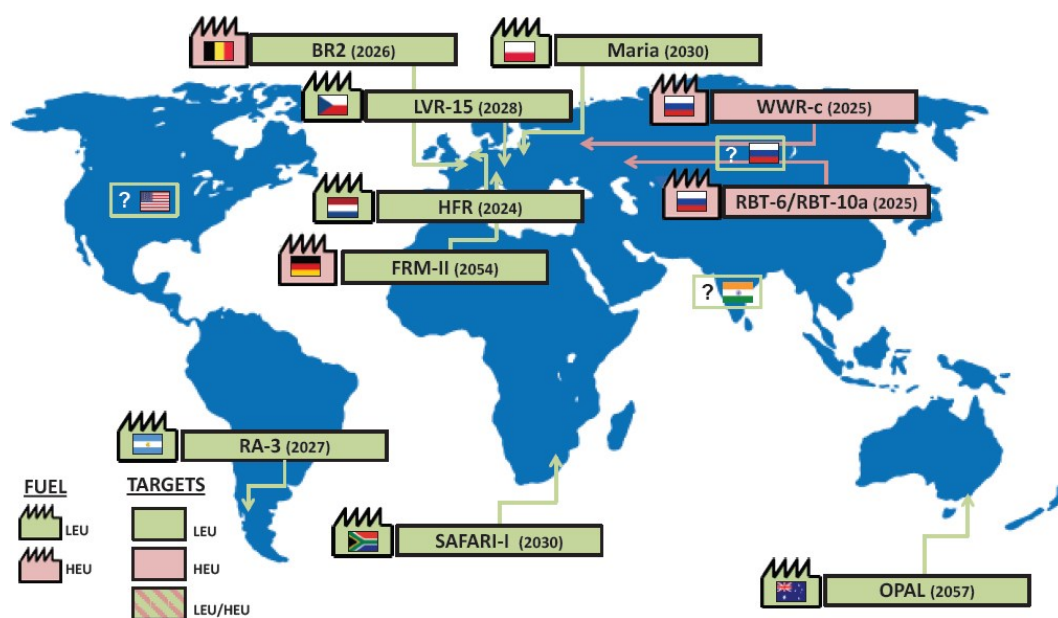


Figure 5 Speculative map of moly-99 supply in 2020. Reactors that irradiated highly enriched uranium (HEU) targets for ^{99}Mo production in July 2017 (BR-2, HFR, LVR-15, Maria, and SAFARI-I) will likely be irradiating low-enriched uranium (LEU) targets by 2020. Russia's reactors will likely continue to irradiate HEU targets if they still produce moly-99. Canada's NRU reactor will have permanently shut down. The United States, Russia, and India may have started producing moly-99 using non-HEU-sourced production methods. The question marks on the left of the three country flags indicate the uncertainties associated with the production plans and schedules [65].

Dr. Ourania Kosti (National Academies) noted several changes in the moly-99 supply that could occur by 2020.

For example,

- Irradiation facilities that currently irradiate HEU targets for moly-99 production for medical use (i.e., BR-2, HFR, LVR-15, Maria) may only irradiate LEU targets.
- Existing reactor FRM-II, Germany, could start producing moly-99 for medical use.
- One or more companies in the United States could start producing moly-99.
- One or more companies in Canada could start producing moly-99 or technetium-99m.
- Russia could increase moly-99 production by introducing additional capacity from existing production facilities and/or from new projects [65].

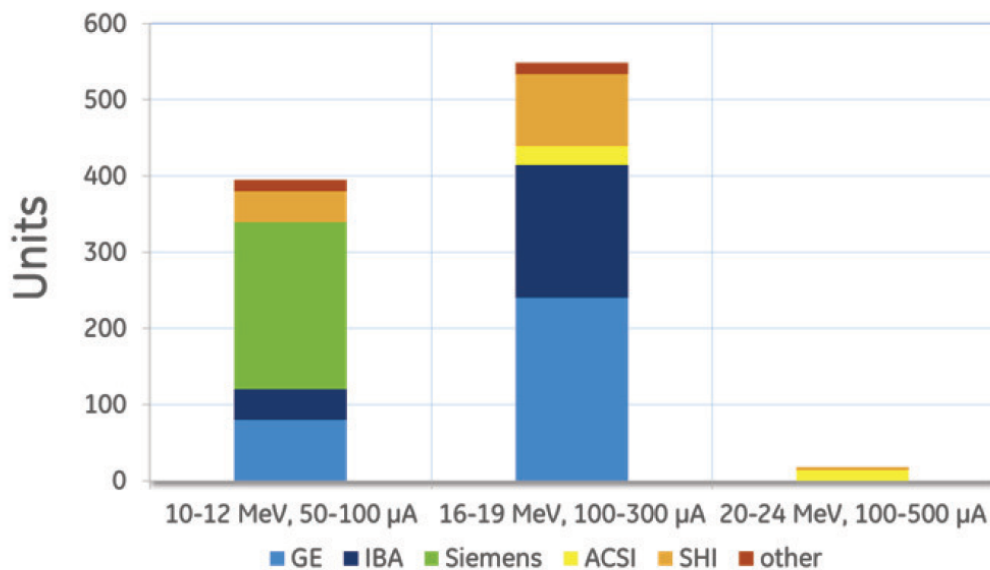


Figure 6 Estimated PET cyclotron numbers by manufacturers [66].

The future of the nuclear medicine seems to belong to the cyclotron produced isotopes [67, 68]. Cyclotrons and cyclo-synchrotrons are also getting more popular nowadays (Figure 6) as they are being used in proton or heavy ion therapy, much more effective than radiotherapy based on beams generated by linear accelerators [69, 70].

As it was summarized by Alves et al. [71, 72] in cyclotrons radioisotopes can be created through nuclide transmutation by bombarding stable target nuclei with charged particles (protons, deuterons or alpha particles). These charged particles

need to be accelerated to energies of at least several MeV in order to overcome the target nucleus Coulomb barrier and lead to the nuclear reaction. Because of their practical characteristics and high current performance for the entire energy range of interest (10–100 MeV), cyclotrons have been almost exclusively chosen as the most convenient option for radioisotope production since the 1950s. The choice and characterisation – and therefore determination of the feasibility and yield – of a nuclear reaction to be performed in a cyclotron require study and knowledge of physical quantities such as beam **range**, target material **stopping power**, **cross section** and **thick target yield**.

Radioisotope production in cyclotrons is based on charged projectile particles impinging on a medium containing the target material. This medium, which can be a gas, a liquid or a solid, slows down the particles as they penetrate. The average energy degradation of the beam per unit length of its path in the absorbing medium, dE/dx , termed as the **stopping power** and usually expressed in $\text{keV}\cdot\mu\text{m}^{-1}$, is given by Bethe's formula:

$$-\frac{dE}{dx} = \frac{4\pi z^2 q_e^4}{m_e v^2} N Z \ln\left(\frac{2m_e v^2}{I}\right)$$

Equation 1

where m_e and q_e are the mass and charge of the electron, z and v the atomic number and velocity of the particles of the beam, Z and N are the atomic number and number of atoms per volume of the target material crossed by the beam and I is the average excitation potential of an atom of this material. Stopping power values are available in the literature for most elements and beam energy ranges, based on experimental measurements. Although precise theoretical calculations are complex, simpler semi-empirical expressions produce a good approximation. As can be seen in Figure 7, the stopping power decreases with the projectile energy and increases for heavier projectiles and with the medium density.

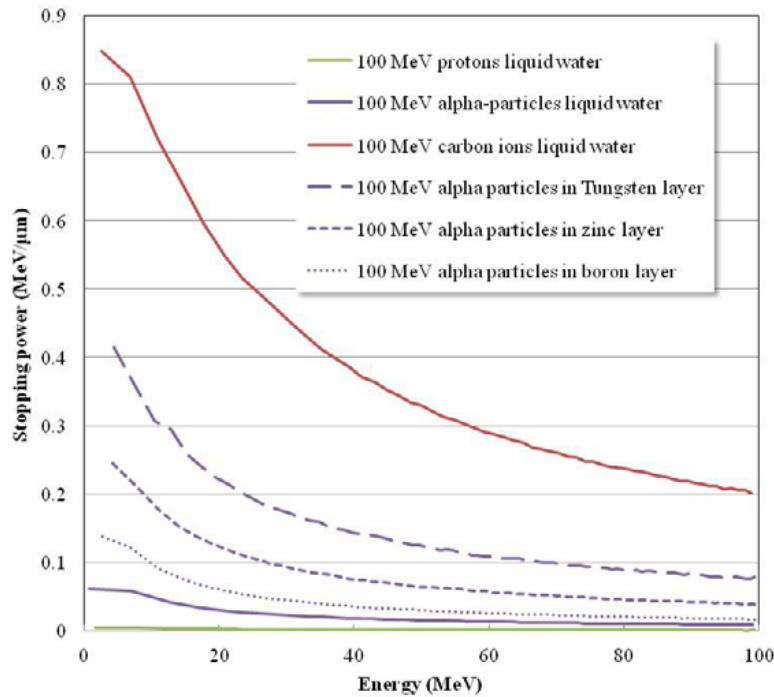


Figure 7 Examples of stopping powers in liquid water.

The knowledge of stopping power variation with energy enables determination of the distance travelled by the beam through a medium until complete rest, as illustrated in Figure 8 and Figure 9. This distance, denominated as **range, R** , corresponds to the integral of the inverse of the stopping power for the beam in this material, where the integration limits are the initial energy when entering the material, E_i , and 0 :

$$R = \int_0^{E_i} -\frac{dx}{dE} dE$$

Equation 2

Typically, for common energy ranges, targets for radioisotope production are:

- less than 1 cm thick when considering solid targets,
- a few centimetres long when impinging on boiling liquids,
- 10–20 cm long for gaseous targets.

Figure 8 and Figure 9 show that the stopping power increases sharply within a very short distance when the beam energy slows down almost to rest, originating a small and well-defined volume where a significant amount of energy is deposited. Known

as the **Bragg peak**, this is the fundamental characteristic exploited in **particle therapy**.

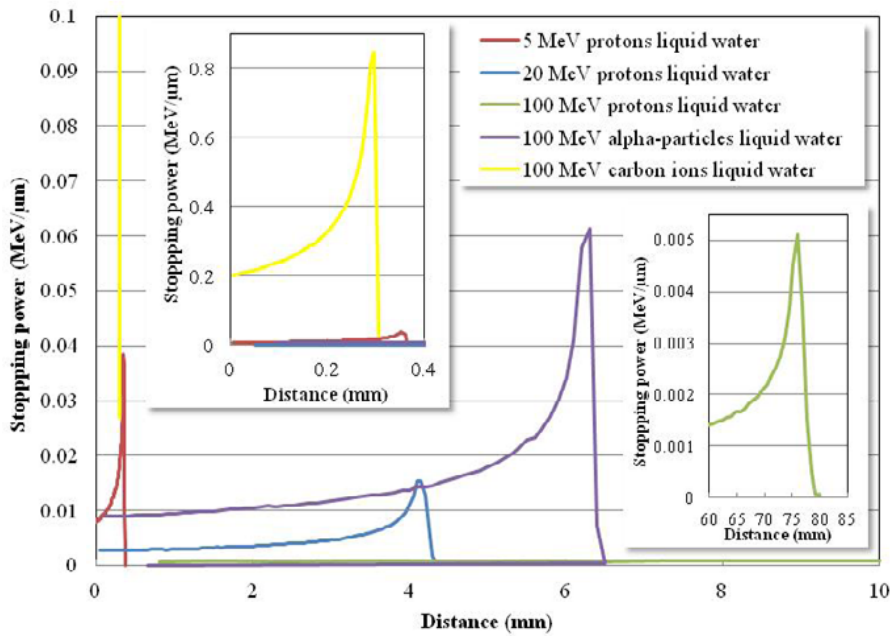


Figure 8 Stopping powers in liquid water at atmospheric pressure for distinct energies and for different particles of equal energy.

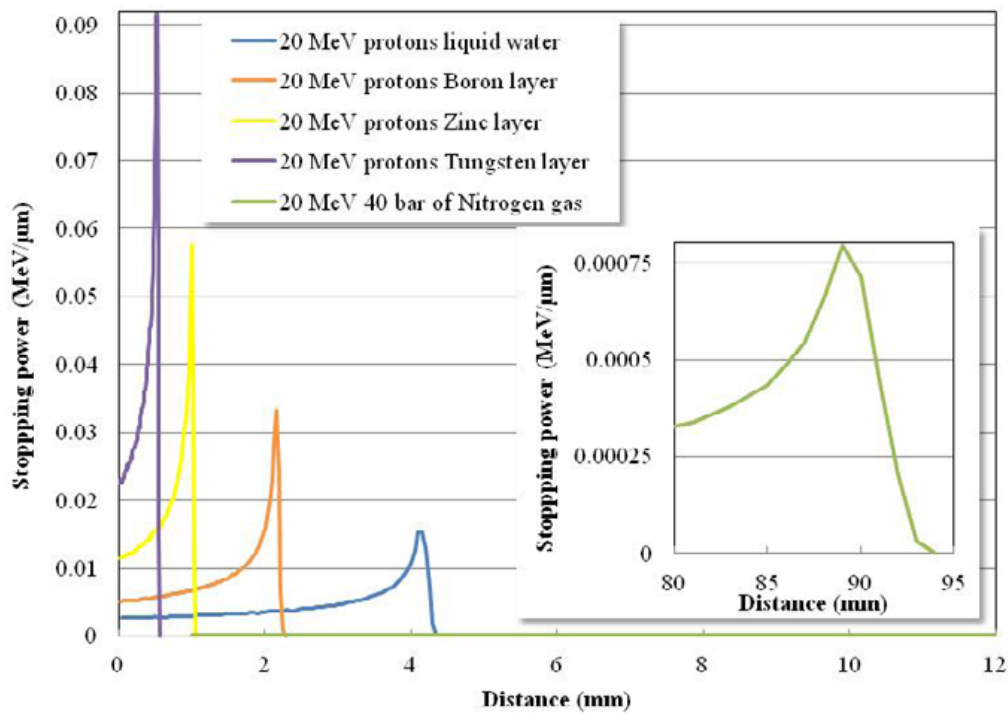


Figure 9 Stopping powers for 20 MeV protons in different absorbing media.

The **cross section** is the metric that quantifies the probability that a given nuclear reaction will occur, per projectile and per target density unit. The cross section of a nuclear reaction is usually denominated and is defined by:

$$N_{NR} = N_p N_{target} \sigma$$

Equation 3

where N_{NR} is the number of nuclear reactions induced when a beam of N_p particles hits a surface with N_{target} nuclei per unit area. Cross section is related to event probability and has area dimensions. It is usually expressed using the unit **barn**, b, defined as: $1 \text{ b} = 10^{-28} \text{ m}^2$.

Cross sections are energy dependent, meaning that nuclear reaction probability depends on the energy of the incident projectile. The set of cross section values for a relevant particle energy range is denominated as the **excitation function** of the given nuclear reaction. The excitation function is usually depicted as an example shown in Figure 10 for the $^{68}\text{Zn}(p,n)^{68}\text{Ga}$ nuclear reaction.

Since a projectile impinging on a target slows down as it penetrates the media, the amount of radioisotope produced by a particular nuclear reaction in a target can be estimated by integrating its excitation function over the range of beam energies over the target material. The production route efficiency, termed as **thick target yield Y**, thus correlated to the beam stopping power and the reaction cross sections, is defined as:

$$Y = C \frac{N_A H}{M} \int_{E_f}^{E_i} \left(\frac{dE}{d(\rho x)} \right)^{-1} \sigma(E) dE$$

Equation 4

where N_A is the Avogadro number, ρ is the medium density M and H are respectively the atomic mass and the target material isotopic enrichment, and C is the concentration of the target nuclei in the target medium. The inverse of the stopping power multiplied by the excitation function $\sigma(E)$ is integrated along the beam energy values, from entering E_i to emerging from the target E_f . Although Y evaluates the absolute number of radioisotope nuclei produced per incident projectile, it is more conveniently (and therefore more commonly) defined as the

activity production yield per unit of beam current and is thus expressed in terms of MBq/ μ A.

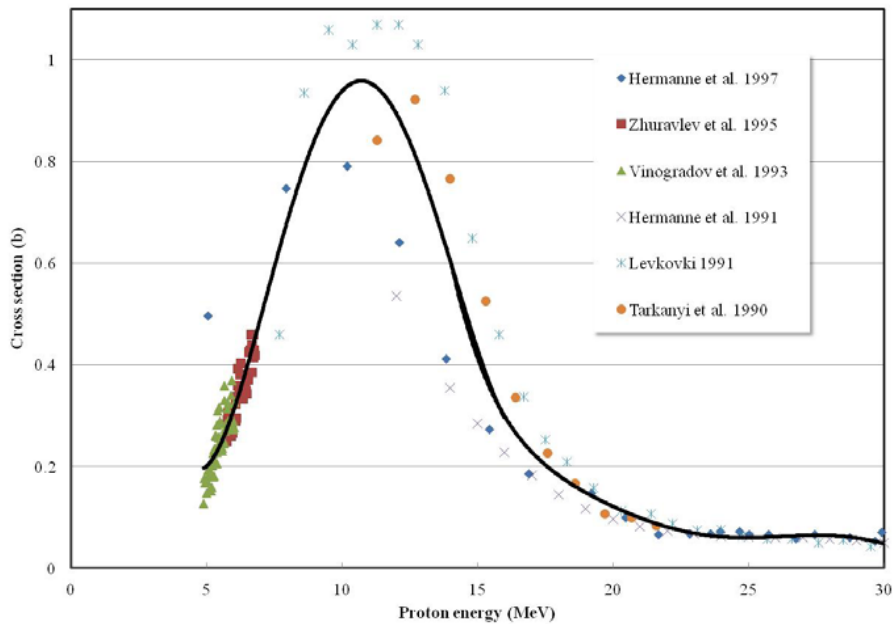


Figure 10 Excitation function of the $^{68}\text{Zn}(p,n)^{68}\text{Ga}$ reaction, obtained from experimental measurements. The line shown is a guide for the eye.

Since there is limited interest in considering the production yield without taking into account its decay during the irradiation duration, it is necessary to consider simultaneously the production rate and the decay during the irradiation to evaluate the activity produced. The temporal evolution of the number N of radioactive nuclei in the target during bombardment is given by:

$$\frac{dN(t)}{dt} = -\lambda N(t) + YI$$

Equation 5

where I is the beam current and λ the produced radioisotope decay constant. The product YI corresponds to the production rate. As a result, the activity $A(t)$ of the radioisotope produced (null at the beginning of the irradiation) after an irradiation duration t is:

$$A(t) = \lambda N(t) = YI(1 - e^{-\lambda t}) = \frac{c N_A H}{M} (1 - e^{-\lambda t}) I \int_{E_f}^{E_i} \left(\frac{dE}{d(\rho x)} \right)^{-1} \sigma(E) dE$$

Equation 6

Equation 6 shows that a saturation condition is reached for long irradiation times and that the activity then tends to equalise, asymptotically, the rate of production (Figure 11), since a balance is reached between the number of nuclides being produced and the decay. In such conditions, a maximum producible activity is obtained, which equals the product YI . For that reason, the thick target yield is also referred to as the expected activity, per unit of beam current, in saturation and is thus also expressed as MBq / μ Asat. It is then seen that the thick target yield must refer to a range of energies or only to an incident energy if the beam is completely stopped within the target.

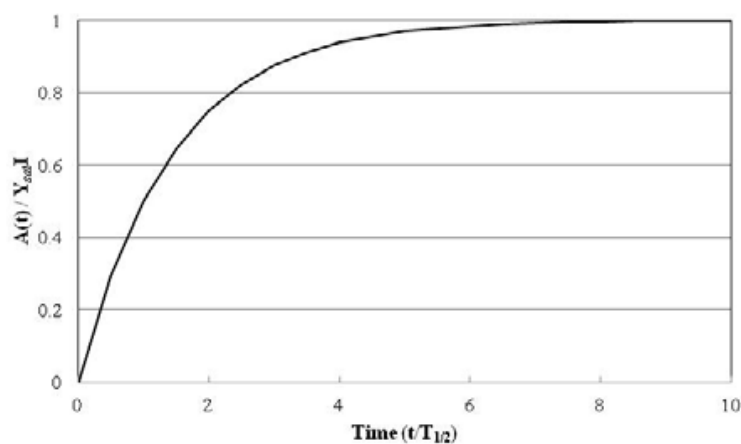


Figure 11 Ratio between the activity A and the rate of production $Y_{sat}I$, as a function of time in units of half-life.

When studying distinct possible routes to produce a given radioisotope, there are several parameters that need to be considered simultaneously. As several different nuclear reactions can lead to production of the same nuclide, knowledge of their excitation functions is fundamental, keeping in mind the practical possibilities in terms of projectiles available and respective energy ranges. Then, to compare all the production possibilities and their optimisation, in terms of not only yield but also radionuclidic purity of the product, it is mandatory to evaluate fundamental parameters:

- The thick target yield at saturation for the intended production channel, as this represents the maximum yield that can be obtained for a target.
- Thick target yields for nuclear reactions leading to radionuclidic impurities: while radioisotopes from other elements can be removed chemically, radionuclidic impurities will remain in the final product and therefore must be kept below acceptable levels.

- The evaluations provided from the thick target yields are used to determine carefully the most suitable energy range to minimise radioisotope impurities, especially if these have longer half-lives than the intended radioisotope as they will worsen the radionuclidic purity with time.
- Depending on the former results, it is also possible to establish the target material purity to be required, concerning both the enrichment in the target nuclide and minimisation of specific unwanted stable isotopes.
- Such calculations must consider the length of practical irradiations according to the half-life of the intended radioisotope.
- It is also fundamental to consider the radionuclidic purity of the product after the irradiation, so that it remains in agreement with the quality control (QC) requirements sufficiently long to enable its clinical use.

Knowledge and simultaneous optimisation of all these parameters are fundamental and equally important. Failure to maintain the quality levels definitively discards a production route regardless of its production yield [71].

Medical cyclotrons are often distinguished basing on their maximum proton (E_p) or deuteron (E_d) beam particle energies (Table 3).

Table 3 Cyclotron types regarding beam particle energy [Goethals and Zimmermann, 2015].

Cyclotron type	Energy Range (MeV)	Approximate number	Typical location
Small medical cyclotron (SMC)	< 20 MeV	1050	- hospitals - universities - local commercial plants
Intermediate energy cyclotron	20–35 MeV	100	- regional commercial plants - research institutes
High energy cyclotron	> 35 MeV	50 ^a	- research institutes - cancer proton therapy centers

^aExcluding proton therapy cyclotrons

Low-energy (small medical) cyclotrons are the least expensive and most popular in biomedical applications. They use common low-energy transmutation reactions: (p,n) , (p,α) , (d,n) and (d,α) and the majority of the radionuclides currently used in the nuclear medicine can be produced via these simple nuclear reactions. Typically, they are produced routinely on an almost daily basis and therefore present the bulk of targetry solutions offered by the cyclotron manufacturers. Among these classical radionuclides are: ^{18}F , ^{13}N , ^{11}C and ^{15}O . These four PET radionuclides are also commonly referred to as “standard” radionuclides in literature and are mostly

produced using low energy medical cyclotrons. ^{123}I and ^{111}In are two of the cyclotron-produced radionuclides used in SPECT studies that can be regarded as classical. However, these are produced by intermediate energy cyclotrons. The novel cyclotron produced radionuclides are defined as all others [73].

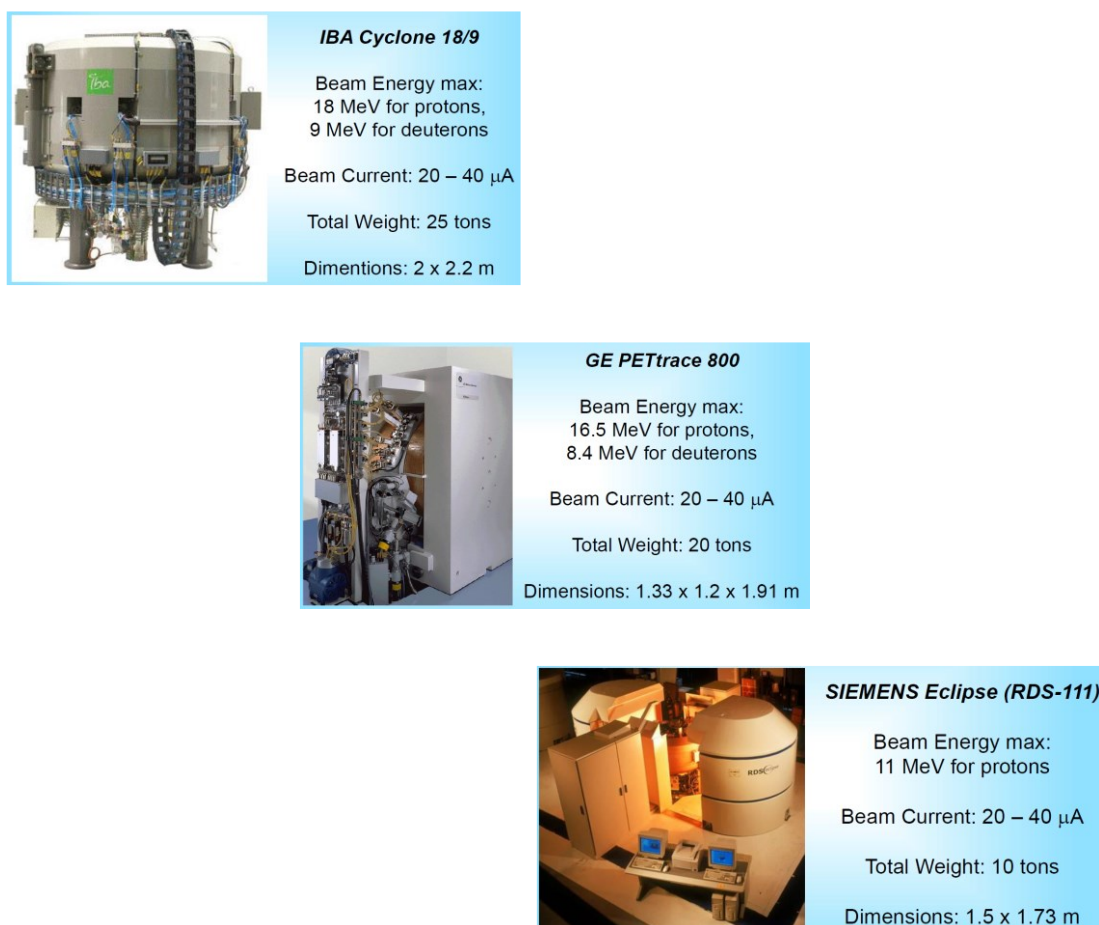


Figure 12 Some most common small medical cyclotron examples.

Small (low energy) cyclotrons (Figure 12) represent the most available method for producing a wide range of conventional (standard) and unconventional PET radionuclides (Table 2). Careful optimization of the cyclotron targets (including the chemical composition and standard state of the target material, target thickness and geometry) and particle beam parameters such as particle energy and beam current, as well as irradiation times can help to produce high yields (measured in units of $\text{MBq}/\mu\text{Ah}$) of many of the radionuclides given in Table 4 [60]. Careful selection of the irradiation parameters can also minimize the production of unwanted radionuclidic impurities [74, 75].

Table 4 Physical decay characteristics for chosen nonstandard cyclotron-produced PET radionuclides [60].

Radionuclide	Half-Life (error)	Decay Mode (% branching ratio)*	Production Route	E(β^-)/keV	β^- End-Point Energy/keV	Abundance, I_p /%	E_p /keV (intensity, I_p /%)	
^{34m} Cl	14.60 (5) h	$\epsilon + \beta^+$ (55.4 [6]) β^+ (54.3 [8]) IT (44.6 [6])	³⁴ S(<i>p,n</i>) ^{34m} Cl	554.81 (24)	1,311.43 (8)	25.6 (5)	511.0 (108.5)	
			³² S(α,pn) ^{34m} Cl	1,099.01 (21)	2,488.08 (8)	28.4 (7)	146.4 (40.5)	
								1,176.6 (14.1)
								2,127.5 (42.8)
³⁸ K	7.636 (18) m	$\epsilon + \beta^+$ (100) β^+ (99.53 [5])	³⁸ Ar(<i>p,n</i>) ³⁸ K	1,212.08 (20)	2,724.4 (4)	99.333 (13)	511.0 (199.1)	
								2,167.5 (99.9)
⁴⁵ Ti	184.8 (5) m	$\epsilon + \beta^+$ (100) β^+ (84.82 [13])	⁴⁵ Sc(<i>p,n</i>) ⁴⁵ Ti	1,040.1 (5)	438.93 (22)	84.80 (13)	511.0 (169.6)	
⁵¹ Mn	46.4 (1) m	$\epsilon + \beta^+$ (100%) β^+ (97.08 [7])	⁵⁰ Cr(<i>d,n</i>) ⁵¹ Mn	963.67 (19)	2,185.5 (4)	96.86 (7)	511.0 (194.17)	
			⁵⁰ Cr(<i>p,x</i>) ⁵¹ Mn					
⁵² Mn	5.591 (3) d	$\epsilon + \beta^+$ (100) β^+ (29.6 [4])	⁵⁰ Cr(<i>p,xn</i>) ⁵² Mn	241.8 (9)	575.6 (19)	29.6 (4)	511.0 (59.2)	
							744.2 (90.0)	
⁵² Fe	8.275 (8) h	$\epsilon + \beta^+$ (100) β^+ (99.58)	⁵⁰ Ni(<i>p,x</i>) ⁵² Fe	1,990 (64)	4,473 (6)	99.58	935.5 (94.5)	
							1,434.1 (100.0)	
⁵⁵ Co	17.53 (3) h	$\epsilon + \beta^+$ (100) β^+ (76 [3])	⁵⁶ Fe(<i>p,2n</i>) ⁵⁵ Co	435.68 (20)	1,021.3 (4)	25.6 (15)	511.0 (152)	
			⁵⁴ Fe(<i>d,n</i>) ⁵⁵ Co	648.98 (20)	1,498.5 (4)	46 (3)	931.1 (75)	
			⁵⁸ Ni(<i>p,α)</i> ⁵⁵ Co				1,408.5 (16.9)	
⁶⁰ Cu	23.7 (4) m	$\epsilon + \beta^+$ (100) β^+ (93 [4])	⁶⁰ Ni(<i>p,n</i>) ⁶⁰ Cu	872.0 (10)	1,980.8 (21)	49.0 (23)	511.0 (185)	
				1,324.9 (10)	2,946.0 (21)	15.0 (12)	826.4 (21.7)	
⁶¹ Cu	3.333 (5) h	$\epsilon + \beta^+$ (100) β^+ (61 [5])	⁶¹ Ni(<i>p,n</i>) ⁶¹ Cu	523.69 (54)	1,215.2 (12)	51 (5)	511.0 (123)	
			⁶⁰ Ni(<i>d,n</i>) ⁶¹ Cu				656.0 (10.8)	
⁶⁴ Cu	12.701 (2) h	$\epsilon + \beta^+$ (61.5 [3]) β^+ (17.60 [22]) β^- (38.5 [3])	⁶⁴ Ni(<i>p,n</i>) ⁶⁴ Cu	278.21 (9)	653.03 (20)	17.60 (22)	511.0 (35.2)	
			⁶⁷ Zn(<i>p,α)</i> ⁶⁴ Cu				1,332.5 (88.0)	
⁶⁶ Ga	9.49 (7) h	$\epsilon + \beta^+$ (100) β^+ (56.0 [15])	⁶⁶ Zn(<i>p,n</i>) ⁶⁶ Ga	1,904.1 (15)	4,153 (3)	50.0 (15)	511.0 (112)	
			⁶⁴ Cu(α,n) ⁶⁶ Ga				1,039.2 (36.9)	
⁷¹ As	65.28 (15) h	$\epsilon + \beta^+$ (100) β^+ (28.3 [8])	⁷⁰ Ge(<i>p,γ)</i> ⁷¹ As	352.0 (18)	816 (4)	27.9 (8)	2,751.75 (23.3)	
							511.0 (56.5)	
⁷² As	26.0 (1) h	$\epsilon + \beta^+$ (100) β^+ (87.8 [23])	⁷⁰ Ge($\alpha,2n$) ⁷² Se/ ⁷² As	1,117.0 (19)	2,500 (4)	64.2 (15)	511.0 (176)	
			⁷² Ge(<i>p,n</i>) ⁷² As	1,528.5 (19)	3,334 (4)	16.3 (17)	834.0 (79.5)	
⁷⁴ As	17.77 (2) d	$\epsilon + \beta^+$ (66 [2]) β^+ (29 [3]) β^- (34(2)%)	⁷⁴ Ge(<i>p,n</i>) ⁷⁴ As	408.0 (8)	944.6 (17)	26.1 (22)	511.0 (58)	
			⁷³ Ge(<i>d,n</i>) ⁷⁴ As				595.8 (59)	
⁷⁵ Br	96.7 (13) m	$\epsilon + \beta^+$ (100) β^+ (73 [5])	⁷⁶ Se(<i>p,2n</i>) ⁷⁵ Br	758 (7)	1,721 (14)	52 (3)	634.8 (15.4)	
							511.0 (146)	
⁷⁶ Br	16.2 (2) h	$\epsilon + \beta^+$ (100%) β^+ (55 [3])	⁷⁶ Se(<i>p,n</i>) ⁷⁶ Br	1,532 (8)	3,383 (9)	25.8 (19)	511.0 (109)	
			⁷³ As($\alpha,3n$) ⁷⁶ Br				559.1 (74)	
^{82m} Rb	6.472 (6) h	$\epsilon + \beta^+$ (100%) β^+ (21.2 [16])		352 (11)	798 (7)	19.7 (16)	657.0 (15.9)	
							1,853.7 (14.7)	
⁸⁶ Y	14.74 (2) h	$\epsilon + \beta^+$ (100) β^+ (31.9 [21])	⁸⁶ Sr(<i>p,n</i>) ⁸⁶ Y	535 (7)	1,221 (14)	11.9 (5)	511.0 (42)	
							554.4 (62.4)	
⁸⁹ Zr	78.41 (12) h	$\epsilon + \beta^+$ (100) β^+ (22.74 [24])	⁸⁹ Y(<i>p,n</i>) ⁸⁹ Zr	395.5 (11)	902 (3)	22.74 (24)	619.1 (38.0)	
							698.4 (26.3)	
⁹⁰ Nb	14.60 (5) h	$\epsilon + \beta^+$ (100) β^+ (51.2 [18])	⁹⁰ Zr(<i>p,n</i>) ⁹⁰ Nb	662.2 (18)	1,500 (4)	51.1 (18)	776.5 (84.4)	
							827.8 (21.0)	
^{94m} Tc	52.0 (10) m	$\epsilon + \beta^+$ (100) β^+ (70.2 [4])	⁹⁴ Mo(<i>p,n</i>) ^{94m} Tc	1,094	2,439 (5)	67.6 (4)	1,044.1 (32.1)	
							1,317.4 (23.7)	
¹²⁰ I	81.6 (2) m	$\epsilon + \beta^+$ (100) β^+ (68.2 [12])	¹²² Te(<i>p,3n</i>) ¹²⁰ I	1,845.0 (72)	4,033 (15)	29.3 (7)	1,474.9 (15.5)	
				2,099.3 (70)	4,593 (15)	19.0 (7)	511.0 (136.5)	
¹²⁴ I	4.1760 (3) d	$\epsilon + \beta^+$ (100) β^+ (22.7 [13])	¹²⁴ Te(<i>p,n</i>) ¹²⁴ I	687.04 (85)	1,534.9 (19)	11.7 (10)	560.4 (69.6)	
				974.74 (85)	2,137.6 (19)	10.7 (9)	1,523.0 (10.9)	
						511.0 (45)		
						602.7 (62.9)		
						722.8 (10.4)		
						1,691.0 (11.2)		

ϵ = electron capture; IT = isomeric transition; m = minutes.

*Where positrons or γ -rays with different energies are emitted, only those with abundance > 10% are listed.

Unless otherwise stated and where available, standard deviations are given in parentheses.



Figure 13 Further cyclotron examples for small, intermediate high energy machines and cyclotron systems (IBA, ACSI).

Cyclotrons next to the linear accelerators (linacs) are the most used devices for acceleration of particles (Figure 14) to energies sufficient to enable the required nuclear reactions. It was the remarkable idea of E. Lawrence to bend the path of the particles in a linac into a circle and therefore to use the same electrode system repeatedly to accelerate the particles. This idea is the basis of all modern cyclotrons and has made the cyclotron the most widely used type of particle accelerator. The first model was built in 1930, with proof of particle acceleration being provided by Livingston in 1931.

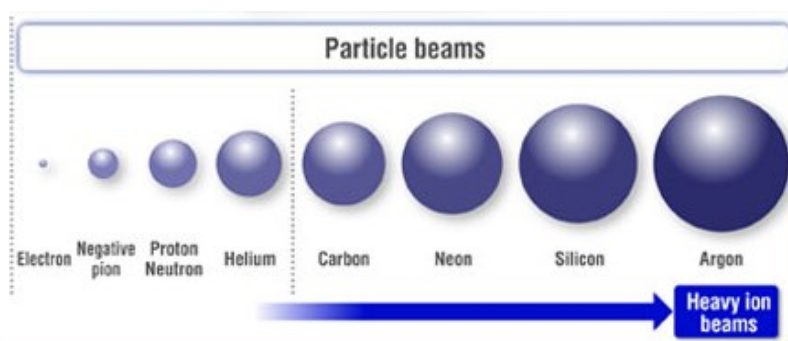


Figure 14 Types of particle beams that can be generated by accelerators.

The literature on cyclotrons for medical purposes base on book by Livingood published in 1961 [76] and a more recent review by Scharf [77]. Those are general texts on cyclotrons and other particle accelerators.

The production of radionuclides with a cyclotron demands that particle beams are delivered with two specific characteristics. The beam must have enough energy to initiate required nuclear reactions, and there must be enough beam current to give practical yields. Noting that beam of protons, considered in this thesis, is the beam of particles with the same charge, it is clear that a number of nontrivial solutions for focusing of the beam must be used to optimise the production of the PET isotopes. However, it is not within the scope of this project to discuss all the engineering solutions and parameters (hill-valley magnet geometry, stripping foils, isochronism, all types of beam focusing etc.) used in the modern cyclotrons that are different that first machines of this type (Figure 15). Very good, detailed discussion of these aspects is available in IAEA publication [67] and book by *Alves et al.* [72].

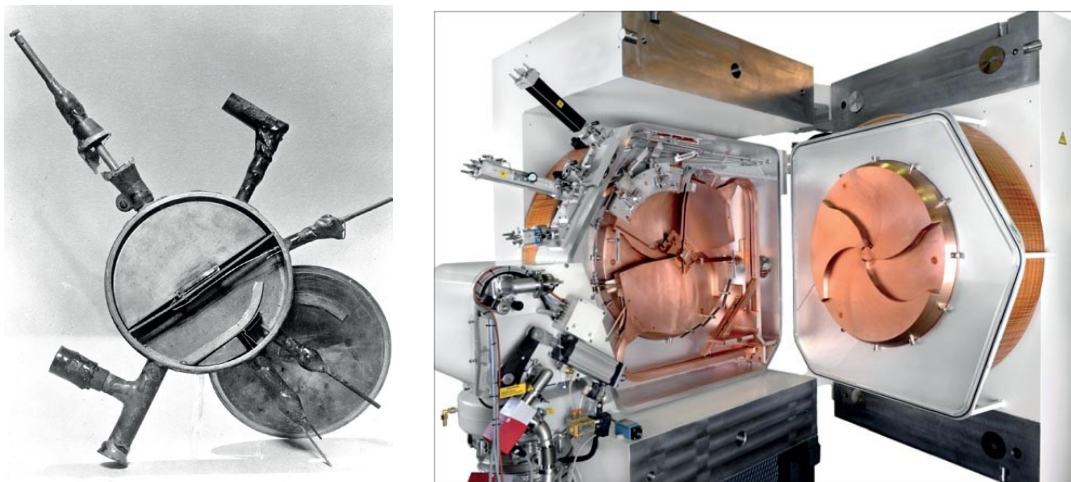
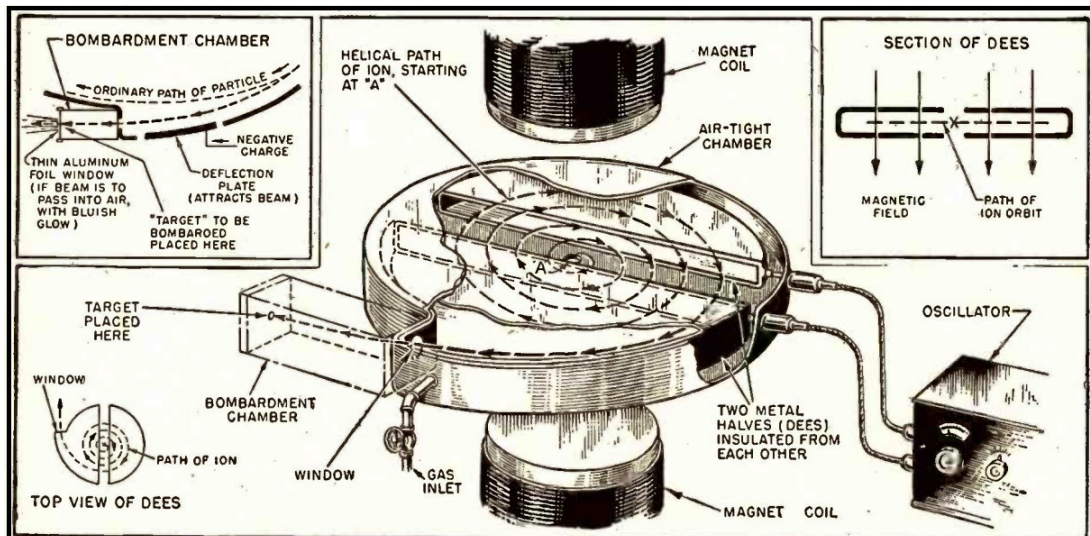


Figure 15 Comparison one of the first prototypes of the cyclotron with standard modern “PET isotope generator” with vertical plane of acceleration.

According to the theory of electrodynamics, the rotational frequency of a charged particle travelling in a magnetic field is independent of the radius of its orbit. The energy of the particle increases as the velocity of the particle increases. The cyclotron utilizes this fact to produce particles of reasonably high energy in a relatively confined space. The acceleration chamber of the cyclotron is placed

between the poles (magnet coils) of a homogeneous magnetic field, as shown in Figure 16.



How the cyclotron works. Size of the magnets has been kept down to show dees path of the electron. See photo above for their true size.
 RADIO-CRAFT for JUNE 1947 23

- Since magnetic force is perpendicular to velocity, we get centripetal acceleration.

$$m \frac{v^2}{R} = qvB$$

- Electric charges will spiral around magnetic field lines with radius: (with higher speed, bigger)

$$R = \frac{mv}{qB}$$

- But, the frequency (period) of orbit turns out to be independent of speed. Cyclotron frequency depends only on charge to mass ratio.

$$f = \frac{v}{2\pi R} = \frac{B}{2\pi} \left(\frac{q}{m} \right)$$

Figure 16 Diagram of a cyclotron, a particle accelerator invented by Ernest O. Lawrence in 1932 [78] and basic cyclotron equations [*Magnetostatics*, B. Pezzaglia, 2012].

The cyclotron's magnetic field causes particles to travel in circular orbits but also focuses the beam. Ions are produced in an ion source at the centre of the machine and are accelerated out from the centre. The ions are accelerated by a high frequency electric field through two or more hollow electrodes called 'dees'. The ions are accelerated as they pass from one dee to the next through a gap between the dees. Since the rotational frequency of the particles remains constant as the energy of the particles increases, the diameter of the orbit increases until the

particle can be extracted from the outer edge of the machine. The limit on the energy of a particle is determined on a practical basis by the diameter of the magnet pole face. In modern cyclotrons the so called EPR probes with carbon foils are used to adjust the radius and by this energy of the extracted beam instead of using magnet deflectors.

For routine production of radioisotopes in cyclotron targets, the practical yield can be quite different from the saturation yield of a radionuclide usually stated in the literature. Saturation occurs when the production rate of the radionuclide equals the decay rate. In a practical sense, this limit is reached at about five half-lives. For example, the irradiation time for ^{18}F production to reach saturation is about 9 hours, which is much longer than one would normally irradiate this type of target. ^{15}O production, on the other hand, reaches saturation at about 10–12 min, which is a more practical irradiation time. Currently, each manufacturer will offer customers a 'guaranteed' yield of radionuclides under defined conditions. This is a primary consideration, especially if clinical applications are considered.

The chemical form of the radionuclide is also of major interest in considering the attributes of any machine. The target material must withstand the intensely ionizing particle beam and must be able to withstand the intense radiation field accompanying particle bombardment. The questions of the chemical form of the radioisotope coming from the target, which target material to use and the specific bombardment conditions have been the subjects of research since the early 1950s. Target conditions can be manipulated to some extent to provide the desired precursors for syntheses of labelled compounds directly from the target.

Another aspect relating to chemistry is the choice between proton-only machines and two particle, proton and deuteron, machines. If a proton-only machine is chosen, enriched isotopes are needed to produce some of the four PET standard radionuclides (Table 2). If a dual particle machine is chosen, ^{15}O and ^{13}N can be produced from natural abundance target materials. Other radioisotopes may require enriched isotope targets with either protons or deuterons.

The main aim of this project was to investigate how the yield of the radiometal isotope produced in a typical medical cyclotron varies with beam energy and target thickness, and how these values can be modified to optimize production. In other words how to use Monte Carlo method for simulation of the thick target yields instead measuring them experimentally. Previously published work [79] has discussed how the product yield is dependent on the excitation function and have presented thick target yields and reported thresholds for main impurities. However,

results of the simulations presented in this thesis suggest the optimization of cyclotron production is slightly more complicated. Optimization of radiometals cyclotron productions is not just about maximising the amount of isotope produced. It is also important to minimise the production of long lived radionuclidic impurities in the final product [12, 15, 28, 80-84].

Materials and Methods

Cyclotron

The IBA CYCLONE® 18/9 Cyclotron used in this project is one of the most used type among small medical accelerators used for production of the PET isotopes in hospitals and small production centres. The cyclotron version used at Cardiff University is equipped with two types of ion source for negative ions acceleration:

- Negative Hydrogen Ions Source (called proton source) H⁻
- Negative Deuterium Ions Source (called deuterium source) D⁻.

Negative hydrogen ions can be accelerated up to a beam energy of 18 MeV and then converted to protons using carbon stripper foil inserted into the beam at the outermost orbit and then focused on to one of the eight targets located in the ports around the cyclotron. Negative deuterium targets operate in a similar manner but can only be accelerated up to a beam energy of 9 MeV before being converted to deuterons using the same carbon stripper foil before hitting the target.

Targets

Eight ports (outputs) located around the IBA CYCLONE® 18/9 cyclotron vacuum chamber can be equipped with a variety of gas, liquid and solid-state targets of different types and volumes. The most used method for production of the radiometals is still using solid targets of the amazing variety of types [73]. Recently the liquid (solution) target production of the radiometals (⁸⁹Zr, ⁶⁴Cu, ⁶⁸Ga, ⁸⁶Y, ^{94m}Tc) is getting very popular however the production yields are still much higher in the solid targets [8, 85-88].

In this project we have developed a tool for optimization of the solid target production of radiometals that can be easily modified for the most common and commercially available types of the solid target stations (STS). One such solid target system is the COSTIS STS, also known as the Nitra Solid Compact (Figure 17), designed by Elex Commerce for IBA cyclotrons. The basic method of irradiation

used in this type of targets is also most popular - a coin shaped solid target irradiated by the perpendicular proton beam whose energy can be reduced by the use of a degrader foil installed inside the STS.



Figure 17 Three examples of the STS from Elex Commerce family. From left: Nirta Solid Compact Model, COSTIS Model TS04 and HighPIT Model PI01 for irradiation of inclined targets (elexcomm.com).

The verification of the beam shape and its positioning in the plane perpendicular to the incoming beam (face of the target disc), to ensure the most intensive part of the beam reach the centre of the target, was optimized using the paper burn method [89] (Figure 18 c). Mechanical adjustments of the beam line were further verified using Thin Layer Chromatography (TLC) scanning of the Al blank disc after 2 minutes of irradiation (Figure 18 a, b). Results, in form of gamma chromatograms along the horizontal (a) and vertical axis (b) of the target disc, demonstrated a good axial alignment of the beam and a Gaussian beam profile that enabled irradiation also of the target regions that are located away of the target discs centre instead of focusing of all of the beam energy in a small very dense hot central point.

Water cooling of the COSTIS STS was also improved (Figure 56) by increasing the water flow from 4 l/min up to 6 l/min which allowed solid targets irradiations with currents of up to 50 μA (max. 20 μA current was used before).

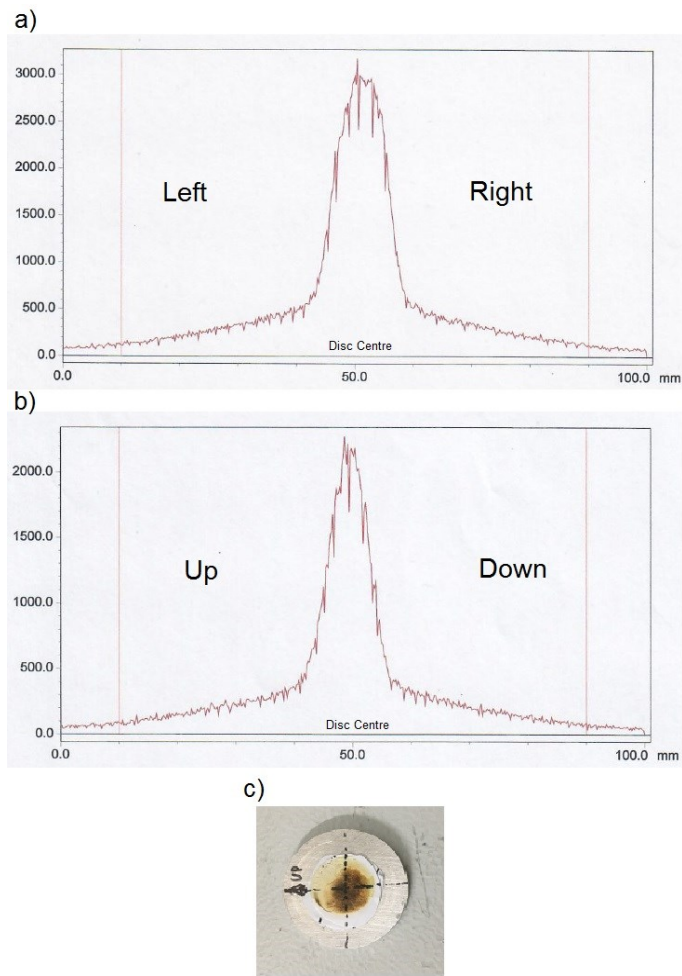


Figure 18 Beam positioning results.

Choice of Reaction

Following [72], particle irradiation, leading to nuclide transmutation, is performed in a cyclotron. A target material is irradiated with accelerated particles (protons, deuterons, and in some cases, α particles), leading to a nuclear reaction. This type of nuclear reaction, induced by cyclotron beam particle irradiation, can be described using Bothe's notation:

$$A(a,b)B$$

Equation 7

The target nucleus appears before the first bracket and the resulting nucleus after the final bracket. Inside the brackets, the irradiating and emitted particles are separated by commas.

A process involving interaction with a particular nucleus leading to the alteration of its original state is known, in general terms, as a nuclear reaction. A set consisting of a projectile and a target nucleus and their energy characteristics is called the entrance channel of a given nuclear reaction. The exit channel is the name given to the set of products of a nuclear reaction that are characterized by their respective energy or internal excitation status. If a certain channel is not physically possible (e.g., if not enough energy is available), it is said to be closed. Otherwise, it is open. The total relativistic energy, momentum, angular momentum, total charge, and number of nucleons are conserved in a nuclear reaction. Parity is also conserved, as interactions in a nuclear reaction are defined by the strong nuclear interaction, which conserves this nuclear state wave-function property.

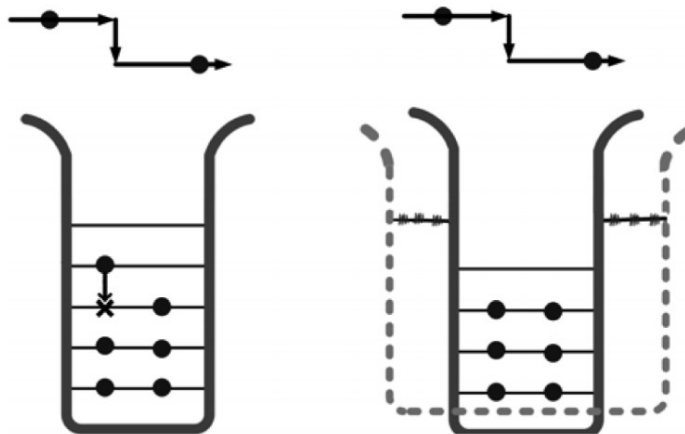


Figure 19 Diagram of examples of direct reactions, involving only energy transfer (elastic dispersion): excitation of a single nucleon (left) and collective excitation of a rotational or vibrational state (right).

Two main mechanisms can be observed in typical nuclear reactions induced by protons or deuterons in a cyclotron: direct reactions and compound nucleus mechanisms. A nuclear reaction is called direct (or sometimes, peripheral) when it involves interaction leading to energy and/or particle transfer between the projectile and the outer (peripheral) nucleons of the target nuclei, without interference to other nucleons. Figure 19 and Figure 20 illustrate some reaction types that can be considered direct. A direct reaction involves only a small number of system degrees

of freedom and is characterized by a significant overlap of the initial and final wave functions. Therefore, the transition from the initial to the final state takes place in a very short time (about 10^{-22} s, the order of magnitude of transit time of a nucleon through a nucleus) and with minimum rearrange processes. Consequently, a strong interdependence between the pre- and postreaction energy states of the projectile, emitted particles and target nucleus can be observed. This interdependence causes (and is seen in) the anisotropic angular distribution of the emitted particles, resulting from a strong correlation with the projectile incident direction.

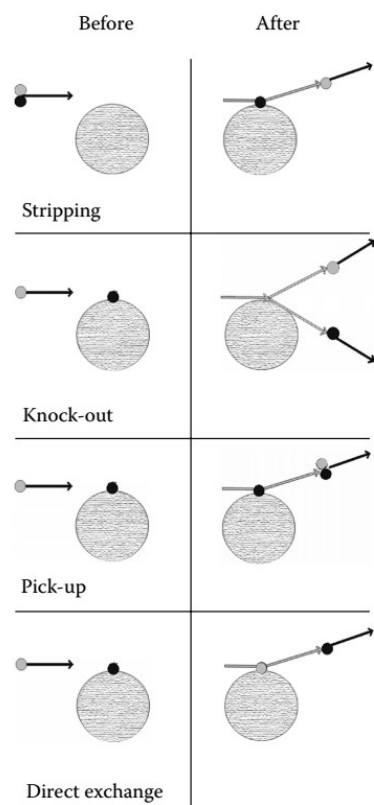


Figure 20 Diagram of some types of direct reactions involving the exchange of the nucleons.

In a compound nucleus reaction mechanism, the projectile is captured in the target-nucleus potential; and a highly excited system, the compound nucleus, is formed. Projectile energy is distributed throughout all the compound nucleus nucleons, reaching a state comparable to thermal equilibrium. Even though the average energy per nucleon is insufficient to overcome the binding potential, since the system particle number is relatively small, important fluctuations in energy distribution will occur, until one or more nucleons gathers enough energy to exit the

nucleus. The typical time interval between projectile target penetration and particle emission is in the order of 10^{-16} s.

It may be possible that, in a compound nucleus reaction, no particle is emitted, and all the excess energy is released through γ radiation emission. This is the case in *capture reactions*, a mechanism predominant in thermal neutron irradiation (and used in nuclear reactor radionuclide production), but it is relatively infrequent in charged particle irradiation.

The process of forming the compound nucleus and the energy states that are assumed characterize and define the specific properties of this type of nuclear reaction. Since the compound nucleus is essentially a nuclear excited state in which energy is distributed through many particles, it can assume many different states, called *many-particle states*. These excited states result from possible energy distributions among the different nucleons (which should not be confused with individual nucleon energy states) and are quantified states defined by quantum numbers and properties, such as spin or parity. However, their energy state value is associated with an intrinsic uncertainty resulting from Heisenberg's principle, corresponding to approximately an electron-volt (calculated basing on an energy state lifetime in the order of 10^{-16} s). If the energy available from the nuclear reaction equals one of the many particles' energy states in the compound nucleus to be formed, a resonance phenomenon will occur and there will be maximum probability of compound nucleus formation. Compound nucleus resonances are characteristic of this type of nuclear reaction. However, these resonances are easy to observe only when the projectile is a relatively low-energy nucleon, because in many particles, the separation of energy states rapidly decreases as energy increases, and energy width increases at the same rate. An important specific property of compound nucleus reactions is the verification of the independence hypothesis, according to which the formation and decay of the compound nucleus are independent processes. Therefore, the relative probabilities of possible decay mechanisms will be independent of each other and independent of the process leading to compound nucleus formation. Therefore, the emission angular distribution is expected to be isotropic. Although the clear and total separation of direct and compound nucleus reactions may be pedagogically convenient, these mechanisms are not mutually exclusive over the whole projectile energy range for a given reaction. Usually, even for the same projectile energy value, mechanisms of both types and intermediate processes can be observed, even when, as in most cases, one of the mechanisms is predominant. The relative importance of the different mechanisms to a given nuclear reaction depends on projectile energy and

on the Q value⁵, as can be observed in Figure 21. In this example, the upward trend (corresponding to a compound nucleus mechanism) is inverted when the (p,n) channel is opened, as this channel statistically competes with the (p,p') channel for compound nucleus decay. The corresponding effect is particularly important, as, for emitted neutrons, the Coulomb barrier is transparent. Experimental evidence of combined mechanisms can be seen in the degree of spatial anisotropy (even if sometimes very slight) that can always be found in the nuclear reaction emission. This anisotropy is present even in reactions characterized by compound nucleus formation, because of the interdependence between the entrance and exit channels due to the laws of conservation, as the initial constants are determined by the entrance channel [72].

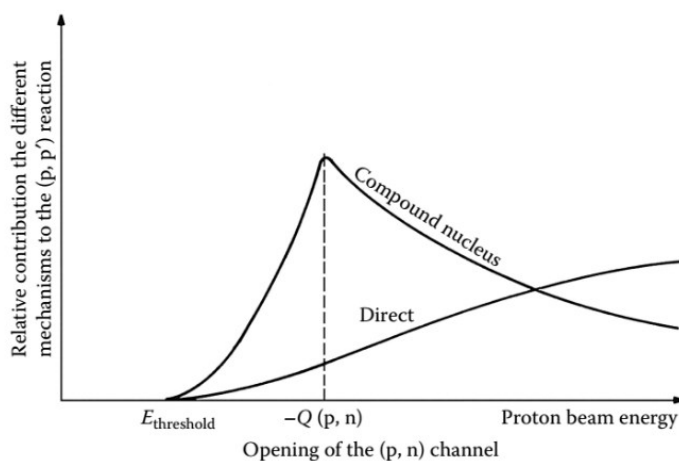


Figure 21 Relative contribution of direct and compound nucleus mechanisms to a (p,p') reaction, as a function of projectile energy.

Low-energy medical cyclotrons use common low-energy direct transmutation reactions: (p,n), (p,α), (d,n) and (d,α). The CYCLONE® 18/9 cyclotron installed in PETIC can only accelerate deuterons up to 9 MeV and this energy is not high enough for the (d,n) and (d,α) reactions' to take place as for the all known radiometals useful for PET, their production methods need deuterons with energy higher than 9 MeV [73]. The only choice remains to optimize the proton induced nuclear reactions. Further it will be described what determines reaction and its energy range for each of the radiometals separately.

⁵ One important characteristic of a nuclear reaction is the difference between the kinetic energy of the initial participants and final products of the reaction in the laboratory referential system (in which the target nucleus is considered at rest). This difference is the Q value of the nuclear reaction.

Energy Degradation

The proton beam energy E_p in CYCLONE® 18/9 cyclotron can be degraded from initial 18 MeV down to value from the range of 16.6 to 9.8 MeV using disc of thickness L_{Nb} [μm] made of Niobium as an energy degrader installed in the COSTIS STS as a vacuum window. Figure 22 shows one of the Nb foil (500 μm) that has been used in ^{89}Zr cyclotron production and there is a clearly seen trace of the beam. The spot on the Nb foil shows the Gaussian shape of the beam and a shift that should be corrected to get a centrally positioned beam.

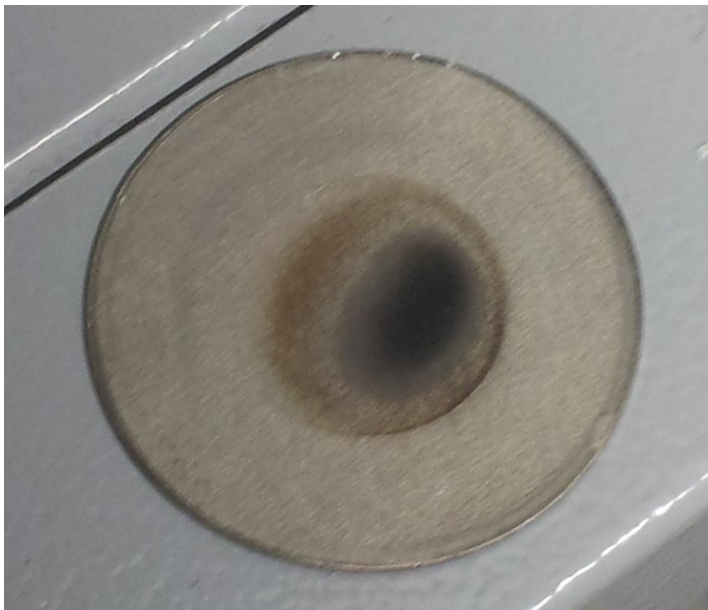


Figure 22 Niobium vacuum window – beam energy degrader.

Each Nb foil from the set of thicknesses L_{Nb} , modifies the beam energy $E_i = 18$ MeV to specified value E_p from the range mentioned above according to relation shown in Figure 23.

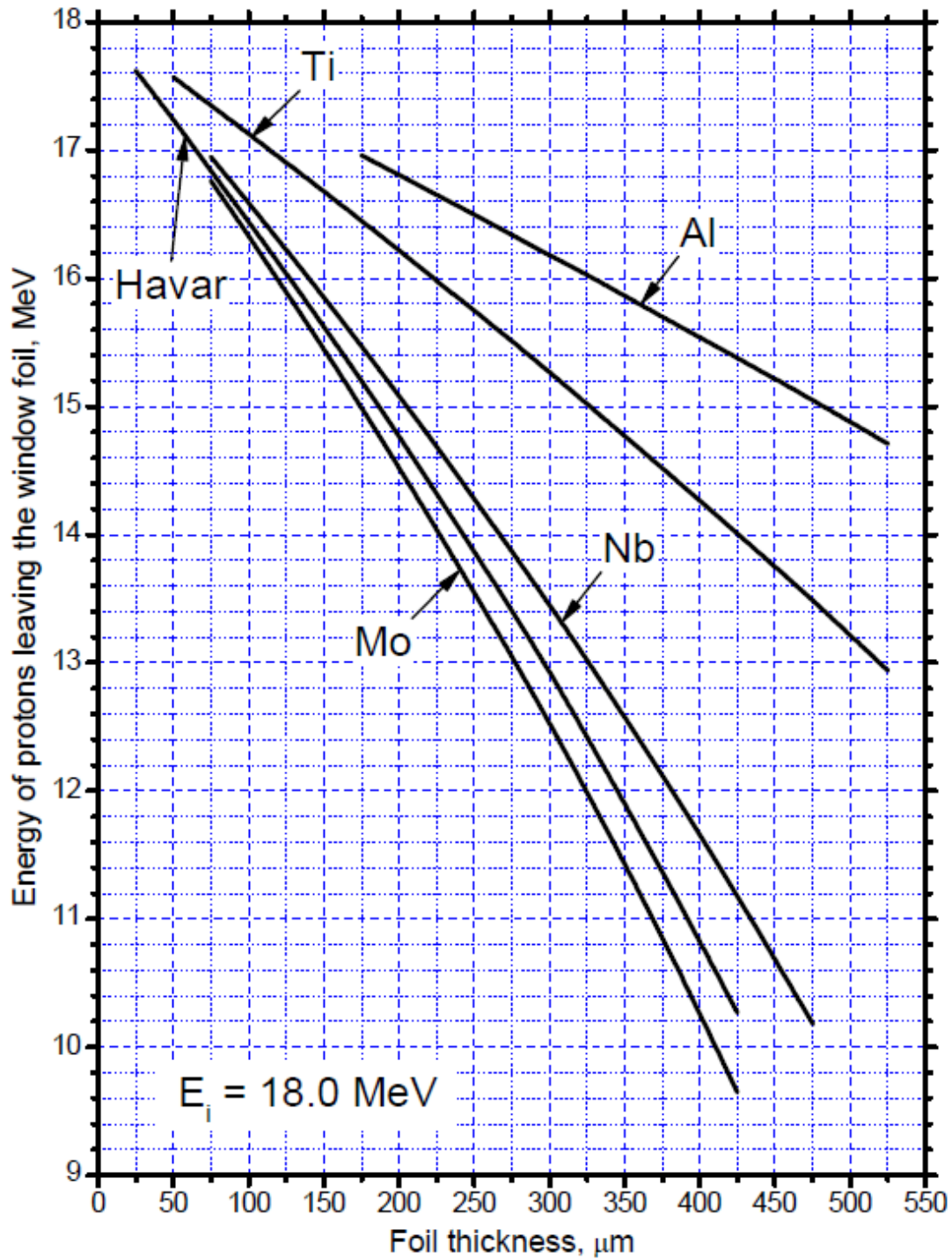


Figure 23 Degradation of $E_i = 18.0$ MeV proton beam energy by window foils made of common materials [90].

Target Design and Preparation

Target design for zirconium-89 and vanadium-48 production was based on the concept of Walther et al. [81] as the Al holder (coin) with target material (foil) enclosed inside. This solution seems to be a fastest and easiest solution, especially in small hospital PET departments and is also recommended for gallium-68. For this method irradiated foil must be in very good contact with Al holder walls to enable good thermal conductivity. However, when target material is very expensive and not available as the thin foil like moly-100 and zinc-66, then sintered or electroplated coin targets (also available commercially) can be used [91-93].

More details will be discussed further in the text, especially in the chapter about zirconium-89 and technetium-99m results.

Irradiation of targets in the cyclotron

For several combinations of the target thickness L_Y and beam energy E_p (determined by L_{Nb}) the set of data is received that shows the relation of the basic production parameters (L_Y , L_{Nb}) and yields of ^{89}Zr expressed in Bq/ μ Ah and they are the thick target yields. Yields for radioactive impurities can be also investigated for each combination using gamma spectrometry. Ideal situation would be to receive the experimental value from irradiation in cyclotron for each simulated combination of production parameters from realistically chosen range. Only certain experimental values were available as the cyclotron productions are expensive. The biggest set of real production values were available for zirconium-89 and vanadium-48 and those productions were crucial for validation of the simulation method for direct nuclear reactions used for production optimization. Validation was also based on values available in literature for similar experiments done by other research groups. In case of technetium-99m and gallium-68 the validated earlier Monte Carlo model was used to verify further its accordance to other results (received during other projects) in process of planning other radiometals productions with maximized yields and minimized amounts of by-products.

Target post processing: unloading and separation

The COSTIS STS is equipped with a conveyor belt (FlexLink) that allows the safe transportation of solid targets from the vault (Figure 15) to a target loading lead pig. After irradiation, the coin is released and dropped into an open transport shuttle and waits for a signal from the COSTIS STS to start delivery. Both COSTIS STS and conveyor belt are operated by panels located outside the vault. The automatic closing mechanism was removed from the vault and located on the other end of conveyor belt. Coins are delivered in lead pigs using the lift from cyclotron suite located one level under the lab. The hot cell has its own loading system (independent from the main hot cell door) with a drawer and hoist for automatic lead pig opening and delivery of radioactive coin. The coin is opened, and the target foil released for further processing using in house equipment.

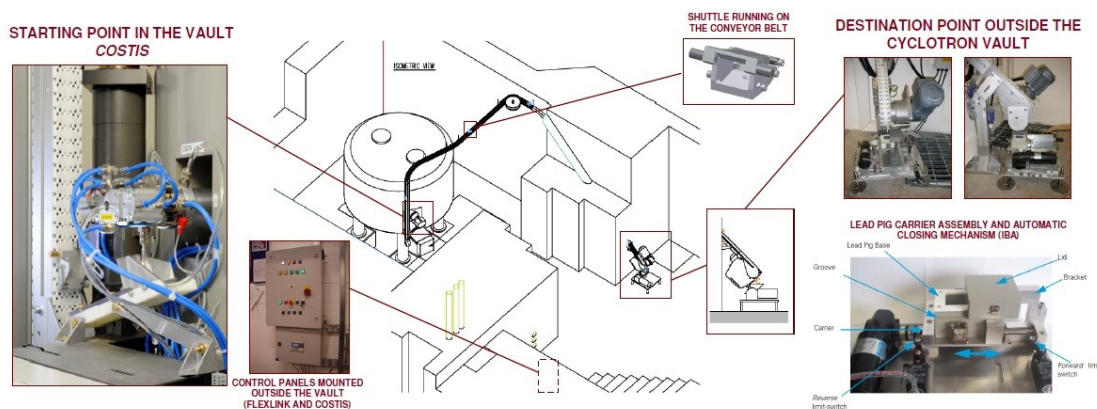


Figure 24 Schematic view of the solid target disc transportation system.

Target foil activity is measured in the dose calibrator, then dissolved in acid and purified using methods specific for each isotope. More detailed example of the purification method is described in the chapter about zirconium-89 production results.

Measurements of the activity and gamma spectroscopy

The activities of the produced radiometals were measured using a CRC 25R CAPINTEC Dose (Activity) Calibrator set to a dial factors recommended by CAPINTEC or estimated by comparison (cross-calibration) with measurements done in other types of dose calibrators (CRC-15R) for which those factors are available.

Activity measurements were usually delayed at least few hours after the end of beam, to allow for the decay of short-lived by-products which are also produced alongside, and results were decay corrected to End of Beam (EOB).

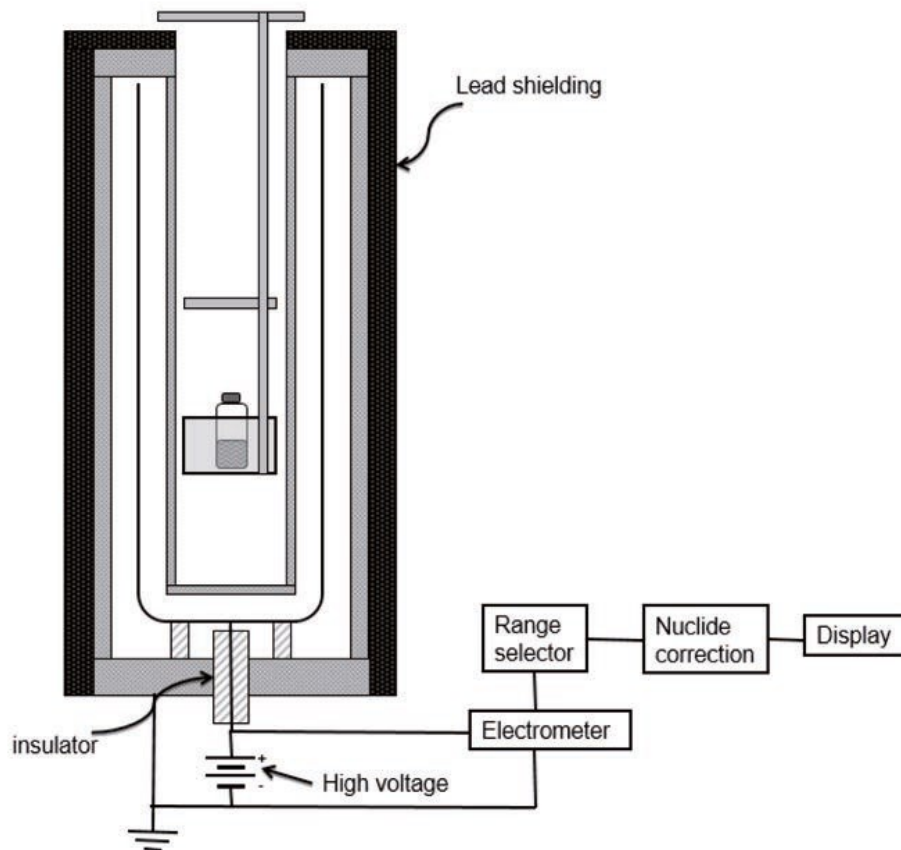


Figure 25 Ionization chamber [94].

A radionuclide activity (dose) calibrator is a specific type of ionization chamber [94] in which the radiation detector has a cylindrical, well-shaped geometry. Once a radioactive sample (dose) is placed into the well, the measurement geometry is approximately 4π granting a limited effect of variations in the sample shape and position; radiation emitted by the sample produces ionization in the gas filling the chamber and the resulting current is measured by an electrometer, producing a signal that is proportional to the sample's activity (see Figure 25). The chamber is sealed and typically contains argon under pressure. The voltage applied to the electrodes and the gas pressure determines the response of the system and is chosen to obtain optimal response, according to the use. The detector is essentially sensitive to X ray and gamma radiation, but also penetrating beta radiation can reach the sensitive volume. For activity calibrators aimed at

measuring single photon emitting radionuclides the voltage is frequently (depending on the design of the manufacturer) of about 150 V, with argon gas at a pressure of about 1 MPa. In the case of positron emitters, the voltage is typically higher, frequently about 500 V, while the pressure of the argon gas is reduced to about 0.5 MPa. The ionization current is measured in the electrometer associated with the chamber; a microprocessor then applies radionuclide specific correction factors to convert the reading to an activity value in Bq, that is eventually further corrected to take into account factors for the shape and material of the sample container (plastic syringes of different shapes and volumes, glass vials). By selecting the radionuclide and the type of container, the operator determines the choice of the correction factor, so that 'a priori' knowledge of the radionuclide in measurement is necessary: the radionuclide activity calibrator is not a discriminating detector, performing an analysis of the spectra of the radiation emitted by the sample, but rather an integral detector measuring all the charge produced by all radiation emitted by the sample in the sensitive volume. It is then wrong to think that the operator, by selecting the type of radionuclide, sets a 'window' peaked only on the gamma radiation emitted by a specific radionuclide, as in analogy to what happens during an acquisition with a gamma camera. By selecting the radionuclide instead, a specific calibration factor is used to proportionally convert the current produced by all radiation emitted by a radionuclide to the corresponding activity. Radionuclide activity calibrator can be installed as a 'stand-alone' instrument; that is, placed on a workbench, or included into a shielded hot cell for samples manipulation or for automatic operation of radiopharmaceutical synthesis modules or dispensing equipment (e.g., unit doses dispensers or vial filling stations). The chamber of the detector can then be shielded differently, the shielding being mainly aimed at avoiding interference from radiation coming from the surrounding environment in the measurement process, as well as at protecting the operator, limiting the radiation from the detector. The amount of shielding surrounding the detector determines a variable amount of sample's radiation backscatter into the chamber, thus influencing the final measurement. Despite the apparently simple operation of the equipment, calibration of the radionuclide activity meters is then a delicate process, in which many factors need to be taken into proper account. In order to obtain proper traceability to the international standards of the measured quantity (activity), calibration needs to be made with certified standards of each specific radionuclide in current clinical use. The fact that an instrument's results are properly calibrated when tested with a certified source of a specific long lived radionuclide (e.g. ^{137}Cs) do not automatically means that it will correctly measure other radionuclides, such as $^{99\text{m}}\text{Tc}$, ^{18}F or ^{131}I . Factory stored calibration factors cannot be assumed to be accurate if traceability to

international standards is not certified (e.g., by a secondary standard radioactivity laboratory), or certified standard sources of the specific radionuclide are used. This aspect is particularly challenging when short lived radionuclides are involved. In these cases, however, the following approaches are possible:

- (a) Cross calibration with a chamber calibrated by a secondary standards laboratory within specified limits of accuracy.
- (b) Use of 'mock' standards, for example a standard based on a long-lived radionuclide that emits the same radiation as the clinically used short lived radionuclide, and is certified in terms of equivalence to the short lived radionuclide and traceable to international standards. As an example, standards of this type have been produced for the short-lived positron emitter ^{18}F , based on $^{68}\text{Ge}/^{68}\text{Ga}$.
- (c) Use of an accurate Monte Carlo simulation of both the ionization chamber and the sample, to derive calibration factors; this methodology is currently under investigation. Some promising results have been published and its effective role will be clarified by further research.

When pure beta emitters are considered (e.g., ^{90}Y), the signal produced in the detector is mostly due to bremsstrahlung radiation produced in the interaction of beta particles within the sample itself and its container. In this case, geometric factors become extremely important and specific calibration procedures are necessary.

A radionuclide activity calibrator is typically supplied with several accessories, such as a syringe/vial dipper, allowing for reproducible sample positioning, and a plastic lined cover for easy decontamination of the ionization chamber well. When acquiring a new meter, it is good practice to buy spare parts of these simple but essential components. Modern calibrators are frequently computer controlled. The software allows for introducing patient's name, weight and information on the batch of the radiopharmaceutical in use. This makes possible to print patient specific labels, reporting these data and the measured activity and reference time that can be stick to individual syringes (or their container), helping traceability and limiting the risk of mis-administration [94].

Basing on PETIC experience and other authors' papers [95], the total accuracy of measurements done by CRC 25R CAPINTEC Dose Calibrator are assumed as $\pm 5\%$ by the rule of thumb (considering linearity accuracy and secondary standard comparison).

Effectiveness of irradiation and separation methods, when possible, were verified using analytical techniques: gamma spectrometry (Multi Channel Analyser), mass spectrometry and half-life measurements.

Long lived impurities were assessed using an EG & G Ortec (NaI and HPGe) detectors with Canberra Multi Channel Analysers.

FLUKA modelling of the nuclear reactions and cyclotron beam parameters used for production of radiometals

This project investigated the optimization of specific nuclear reactions using computer modelling of irradiation processes, nuclear reactions and target design using simulation package developed in CERN as a general-purpose Monte Carlo code FLUKA [96-98]. The first part of the model was created in FLUKA's combinatorial geometry editor and contains the Aluminium beam line pipe, Niobium energy degrader, Aluminium target holder, target material and target cooling (Figure 27). The aim was to use this model to investigate the effect of altering both the target thickness and beam energy in order to determine the optimum conditions for the nuclear reaction in order to increase the yields of radiometals, whilst limiting radio-impurities by ensuring the competing nuclear reactions are minimized. The validity of the model was also verified through experimental measurements of target irradiations on the IBA Cyclotron when it was possible. Most important and detailed validation was done for zirconium-89 and vanadium-48 as those isotopes are routinely produced in PETIC (Wales Positron Emission Tomography Imaging Centre) and lot of production data were available. For other two isotopes (^{99m}Tc and ^{68}Ga) evaluation of the model was continued basing on less numerous results of experimental productions or other reports available in literature.

Monte Carlo Method and FLUKA

The Monte Carlo method was invented by John von Neumann, Stanislaw Ulam and Nicholas Metropolis (who named the method), and independently by Enrico Fermi. Originally it was not a simulation method, but a device to solve a multidimensional integro-differential equation by building a stochastic process such that some parameters of the resulting distributions would satisfy that equation. The

equation itself did not necessarily refer to a physical process, and if it did, that process was not necessarily stochastic. It was soon realised, however, that when the method was applied to an equation describing a physical stochastic process, such as neutron diffusion, the model (in this case a random walk) could be identified with the process itself. In these cases, the method (analogue Monte Carlo) has become known as a simulation technique since every step of the model corresponds to an identical step in the simulated process. Particle transport is a typical physical process described by probabilities (cross sections are interaction probabilities per unit distance). Therefore, it lends itself naturally to be simulated by Monte Carlo [99].

The analysis technique called Monte Carlo is, in essence, a methodology to use sample means to estimate population means. More broadly, Monte Carlo is a widely used numerical procedure that allows people to estimate answers to a wide variety of problems. Monte Carlo is a highly flexible and powerful form of quadrature⁶, or numerical integration, that can be applied to a very wide range of problems, both direct and inverse [100].

In this work, the FLUKA code [96, 101] was used to perform all the simulations (see Appendix for FLUKA code and file example). FLUKA is a fully integrated particle physics Monte Carlo simulation package. FLUKA is a general-purpose tool for calculations of particle transport and interactions with matter, covering an extended range of applications spanning from proton and electron accelerator shielding to target design, calorimetry, activation, dosimetry, detector design, Accelerator Driven Systems, cosmic rays, neutrino physics, radiotherapy, radiobiology. It was developed and it is maintained under an INFN-CERN agreement. The highest priority in the design and development of FLUKA has always been the implementation and improvement of sound and modern physical models. Microscopic models are adopted whenever possible, consistency among all the reaction steps and/or reaction types is ensured, conservation laws are enforced at each step, and results are checked against experimental data at single interaction level. As a result, final predictions are obtained with a minimal set of free parameters fixed for all energy/target/projectile combinations. Therefore, results in complex cases, as well as properties and scaling laws, arise naturally from the underlying physical models, predictivity is provided where no experimental data are directly

⁶ Quadrature is a historical mathematical term which means determining area. Quadrature problems have served as one of the main sources of problems for mathematical analysis. Mathematicians of ancient Greece, according to the Pythagorean doctrine, understood determination of area of a figure as the process of geometrically constructing a square having the same area (squaring). Thus, the name quadrature for this process. The term numerical quadrature (often abbreviated to quadrature) is a synonym for numerical integration, especially as applied to one-dimensional integrals.

available, and correlations within interactions and among shower components are preserved. The FLUKA physical models are described in several journal and conference papers [102-106] on the technical side the stress has been put on four apparently conflicting requirements, namely efficiency, accuracy, consistency and flexibility. FLUKA can simulate with high accuracy the interaction and propagation in matter of about 60 different particles, including photons and electrons from 1 keV to thousands of TeV, neutrinos, muons of any energy, hadrons of energies up to 20 TeV and all the corresponding antiparticles, neutrons down to thermal energies and heavy ions. The program can also transport polarised photons (e.g., synchrotron radiation) and optical photons. Time evolution and tracking of emitted radiation from unstable residual nuclei can be performed online. FLUKA can handle even very complex geometries, using an improved version of the well-known Combinatorial Geometry (CG) package. The FLUKA CG has been designed to track correctly also charged particles (even in the presence of magnetic or electric fields). Various visualization and debugging tools are also available. For most applications, no programming is required from the user. However, several user interface routines (in Fortran 77) are available for users with special requirements [107].

For many years FLUKA has been known as one of the main tools for designing shielding of proton accelerators in the multi-GeV energy range (its hadron event generator has been adopted by the majority of the existing high-energy transport codes, including those used for particle physics simulations). In the last years, however, FLUKA has gone through an important process of transformation which has converted it from a specialized to a multi-purpose program, not restricted to a limited family of particles or to a particular energy domain. If in its original high energy field FLUKA has few competitors, this is not the case in the intermediate and in the low energy range, where several well-established transport codes exist. However, FLUKA can compare favourably with most of them, thanks to some important assets. One of them is the adoption of modern physical models, especially in the description of nuclear interactions. Some of these models have even been updated and extended with original contributions. Other advantages are the special care devoted to low-energy electromagnetic effects and the accurate combined treatment of multiple scattering and magnetic fields near material boundaries, essential for a correct simulation of many synchrotron radiation problems [104]. In the last years, FLUKA has been widely used in the medical field to study different kinds of applications [108-113]. Even if FLUKA has been validated in the high energy range [114-116] no specific validations in the energy range of medical application have been published. As it will be shown in this work a possibly accurate

validation of FLUKA, in terms of physical and transport parameters, was conducted in the energy range of interest in the medical field of small cyclotrons (16 – 18 MeV).

FLUKA reads user input from an ASCII text file with extension “.inp”. The input consists of a variable number of “*commands*” (called also “options”), each consisting of one or more “lines” (called also “*cards*” for historical reasons). Each card contains one keyword (the name of the command), six floating point values called *WHATs* and one-character string called *SDUM*. The typical structure of a FLUKA input file is the following [105]:

- Titles and comments for documentation purposes (optional but recommended).
- Description of the problem geometry (solid bodies and surfaces, combined to partition space into regions), (mandatory).
- Definition of the materials (mandatory unless pre-defined materials are used).
- Material assignments (correspondence material–region, mandatory).
- Definition of the particle source (mandatory).
- Definition of the requested “detectors”. Each of these is a phase space domain (region of space, particle direction and energy) where the user wants to calculate the expectation value of a physical quantity such as dose, fluence, etc. Various kinds of detectors are available, corresponding to different quantities and different algorithms used in the estimation (“estimators”). Detectors are optional, but one at least is expected, at least in the production phase.
- Definition of biasing schemes (optional).
- Definition of problem settings such as energy cut-offs, step size, physical effects not simulated by default, particles not to be transported, etc. (optional).
- Initialisation of the random number sequence (mandatory if an estimation of the statistical error is desired).
- Starting signal and number of requested histories (mandatory).

In addition, special commands are available in FLUKA for more advanced problems involving magnetic fields, time-dependent calculations, writing of history files (so-called “collision tapes”), transport of optical photons, event-by-event scoring, calling user-written routines, etc. Details on the cards, the setup and the parameters used in this work will be given in the following chapters.

Statistical Errors

- Statistical Errors can be calculated for single histories (not in FLUKA), or for batches of several histories
- Distribution of scoring contributions by single histories can be very asymmetric (many histories contribute little or zero)
- Scoring distribution from batches tends to Gaussian for $N \rightarrow \infty$, provided $\sigma^2 \neq \infty$ (thanks to Central Limit Theorem)
- The standard deviation of an estimator calculated from batches or from single histories is an estimate of the standard deviation of the actual distribution (“error of the mean”)
- How good is such an estimate depends on the type of estimator and on the particular problem (but it converges to the true value for $N \rightarrow \infty$)
- The variance of the mean of an estimated quantity x (e.g., fluence), calculated in N batches, is:

$$\sigma_{\langle x \rangle}^2 = \frac{1}{N-1} \left[\frac{\sum_1^N n_i X_i^2}{n} - \left(\frac{\sum_1^N n_i X_i}{n} \right)^2 \right]$$

mean of squares - square of means

Equation 8

where:

n_i number of histories in the i^{th} batch

$n = \sum n_i$ total number of histories in the N batches

x_i average of x_i in the i^{th} batch:

$$x_i = \sum_{j=1}^{n_i} \frac{X_{ij}}{n_i}$$

x_{ij} is the contribution to x of the j^{th} history in the i^{th} batch

In the limit $N = n$, $n_i = 1$, the formula applies to single history statistics

Practical tips:

- Using always at least 5-10 batches of comparable size
- Variance itself is a stochastic variable subject to fluctuations
- Being careful about the way convergence is achieved: often (particularly with biasing) apparent good statistics with few isolated spikes could point to a lack of sampling of the most

- relevant phase-space part
- Relative error Quality of Tally
 - 50 to 100% Garbage
 - 20 to 50% Factor of a few
 - 10 to 20 Questionable
 - < 10% Generally reliable
 - Why does a 30% σ mean an uncertainty of a “factor of a few”?
 - Because: σ is a stochastic variable
 - Its evaluation is valid only in the Gaussian approximation
 - If large then probably not Gaussian
 - The MCNP guideline is empirically based on experience, not on a mathematical proof. But it has been generally confirmed as working also with other codes
 - Small penetrations and cracks are very difficult to handle by MC, because the “detector” is too small and too few non-zero contributions can be sampled, even by biasing

[lectures from www.fluka.org]

Sources of Systematic Errors

- physics: codes are based on physics models, which cannot be perfect (especially in nuclear physics). Model quality is best shown by benchmarks at the microscopic level (e.g. thin targets)
- artifacts: due to imperfect algorithms, e.g., energy deposited in the middle of a step*, inaccurate path length correction for multiple scattering*, missing correction for cross section and dE/dx change over a step*, etc. Algorithm quality is best shown by benchmarks at the macroscopic level (thick targets, complex geometries)
- data uncertainty: results can never be better than available experimental data!
- material composition: not always well known. In particular concrete/soil composition (how much water content?). Air contains humidity and pollutants, has a density variable with pressure
- presence of additional material, not well defined (cables, supports)
- geometries cannot be reproduced exactly (or would require too much effort)

[lectures from www.fluka.org]

Results

Production of ^{89}Zr

Introduction

The $^{89}\text{Y}(p,n)^{89}\text{Zr}$ reaction was investigated in order to determine the optimal methodology for cyclotron production of the promising immuno-PET radiometal ^{89}Zr . FLUKA, a fully integrated particle physics Monte Carlo simulation was used to model irradiation processes, nuclear reactions, and the solid target of the IBA CYCLONE[®] 18/9 cyclotron, to estimate the yields of ^{89}Zr and isotopic by-products for a range of different production conditions. The results of the FLUKA simulations were also validated experimentally by performing irradiations on Cardiff University IBA CYCLONE[®] 18/9 cyclotron. Isotopically pure yields up to 41.7 MBq/ μAh were achieved and it is possible to produce more than 1 GBq of ^{89}Zr using a beam time of 1.5 hours and beam current of 20 μA .

Since naturally occurring Yttrium is isotopically pure, ^{89}Zr can be easily generated by bombarding Y foils with a proton beam via the $^{89}\text{Y}(p,n)^{89}\text{Zr}$ reaction [82]. The excitation function for this reaction (Figure 26) reaches maximum values of the cross section for energy range (7 – 18 MeV) that that is achievable for the beams generated in small biomedical cyclotrons, like IBA CYCLONE[®] 18/9.

The aim of this part of the project was to simulate the $^{89}\text{Y}(p,n)^{89}\text{Zr}$ reaction using a FLUKA model *in silico*, validate the model experimentally and then use the model in order to determine the optimal method of production in order to maximise the yield of isotopically pure ^{89}Zr and other radiometals with high potential in nuclear medicine.

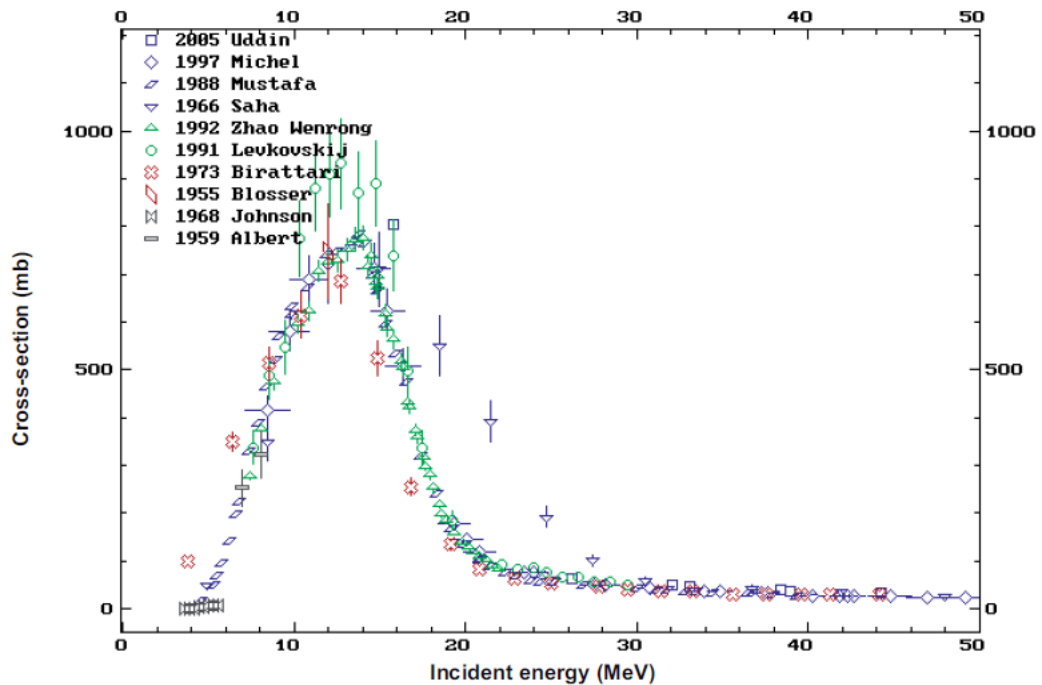


Figure 26 Excitation function for the $^{89}\text{Y}(p,n)^{89}\text{Zr}$ reaction [68].

Modelling in FLUKA software

Figure 27 a) shows a 3D model of the hardware used in the production and optimization of ^{89}Zr . Figure 27 b) shows the details of the different components of the modelled cyclotron parts. Figure 27 c) depicts the several regions created in the FLUKA CG editor for simulation of the materials used in the cyclotron.

Basic beam parameters such as the proton energy, the Gaussian beam shape and the dimensions of the Yttrium target disc and Niobium degrader were defined in the model (see Appendix). Between 10^6 and 10^8 of primary beam particles (protons) were used in Monte Carlo simulations. Calculation time for one simulation including 5 runs (batches) took less than 10 h. This is in line with data reported in other studies [109]. The statistical uncertainty of the simulation was defined as the standard deviation of the results of 5 repeated runs and is dependent upon the target and degrader thickness. For thinner degraders and targets, the number of primary protons was increased to reduce the statistical uncertainty in generated ^{89}Zr yields to below 2% and produce an accuracy comparable to results for thicker targets and degraders where reactions for production of ^{89}Zr and impurities are more frequent and simulation is statistically better. However for reactions that are not so frequent, the statistical noise oscillations are so high that

for their proper modelling much longer simulations would need to be used. It will be rather seen further for other radiometals with higher number of trace amount of impurities than for ^{89}Zr .

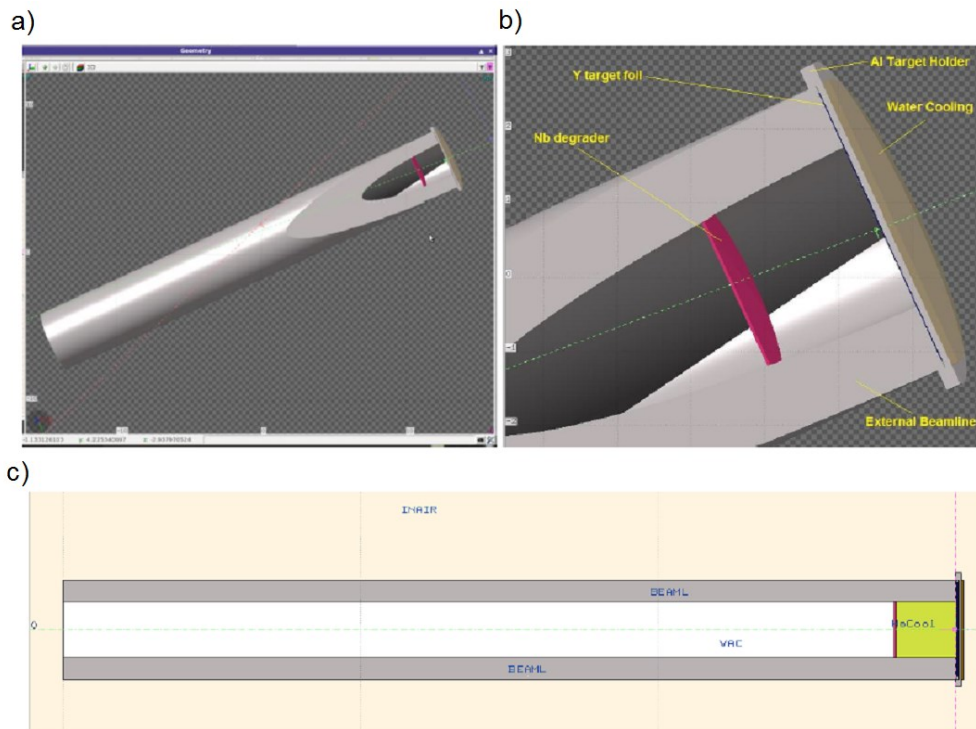


Figure 27 Model created with FLUKA's combinatorial geometry editor.

The target material ^{89}Y (100% natural abundance) was modelled in form of discs of varying thicknesses enclosed in the Aluminium holder shown in the Figure 29. L_Y was defined as the thickness of the Yttrium target disc and was modelled using a range of commercially available thicknesses (5, 25, 50, 100, 150, 200, 250, 300, 350, 400, 500, 700, 1000 μm) that could either be placed in the Aluminium holder (Figure 29) or loaded directly in the COSTIS STS.

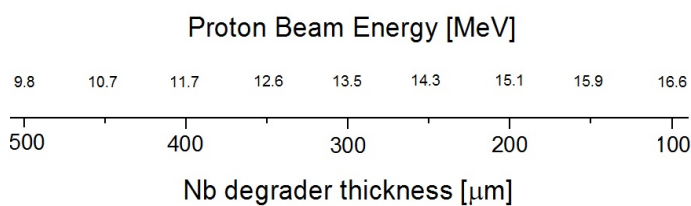


Figure 28 Relation between proton beam energy and Nb degrader thickness.

The proton beam energy E_p in the IBA CYCLONE® 18/9 cyclotron was modelled between the range of 16.6 to 9.8 MeV using a Niobium foil beam degrader of varying thickness L_{Nb} : 100, 150, 200, 250, 300, 350, 400, 450, 500 μm , installed in the COSTIS STS as a vacuum window (Figure 22).

For each FLUKA simulation, one combination of the target thickness and beam energy was considered. Results of the simulations were presented by FLUKA in terms of the radioactivity in the Y target generated after 1 h of irradiation with 1 μA of the beam current. The set of data received from the simulations shows the relation of the basic production parameters (L_Y , L_{Nb}) and yields of ^{89}Zr produced expressed in $\text{Bq}/\mu\text{Ah}$. Yields for radioactive impurities were also generated as FLUKA includes models of the other competing reactions that can result in by-products produced by the proton beam used in the model.

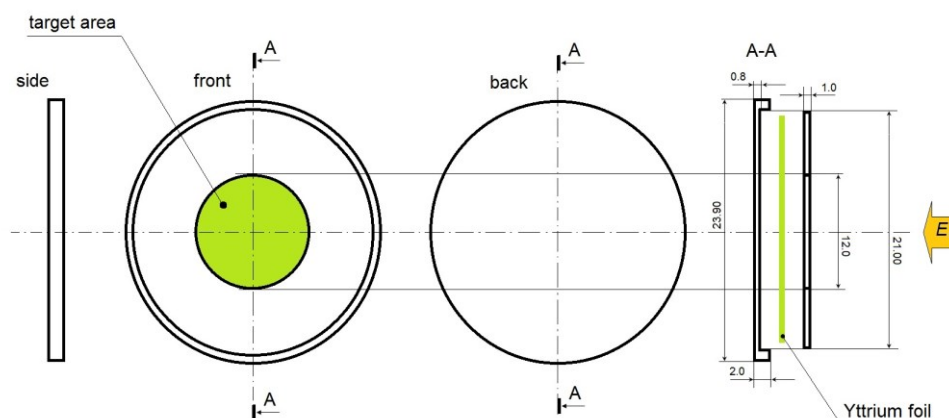


Figure 29 Solid target “coin” design.

Experimental validation of the simulations' results

Results from the simulated range of values were verified experimentally in the IBA CYCLONE® 18/9 cyclotron and COSTIS STS setup. The simulated productions selected to be validated experimentally were based on reasonable optimisation of the product yield with possibly lowest rates of impurities generated (Figure 30).

Another issue shown in the Figure 30 is that the Yttrium target thickness should not be increased more than necessary as the target material also degrades beam energy internally. As a result, the production yield of ^{89}Zr is not the same in all regions of Yttrium along the direction of the incoming beam. In addition, it is only possible to place an Yttrium disc with a max thickness of 400 μm in the target holder (Figure 29).

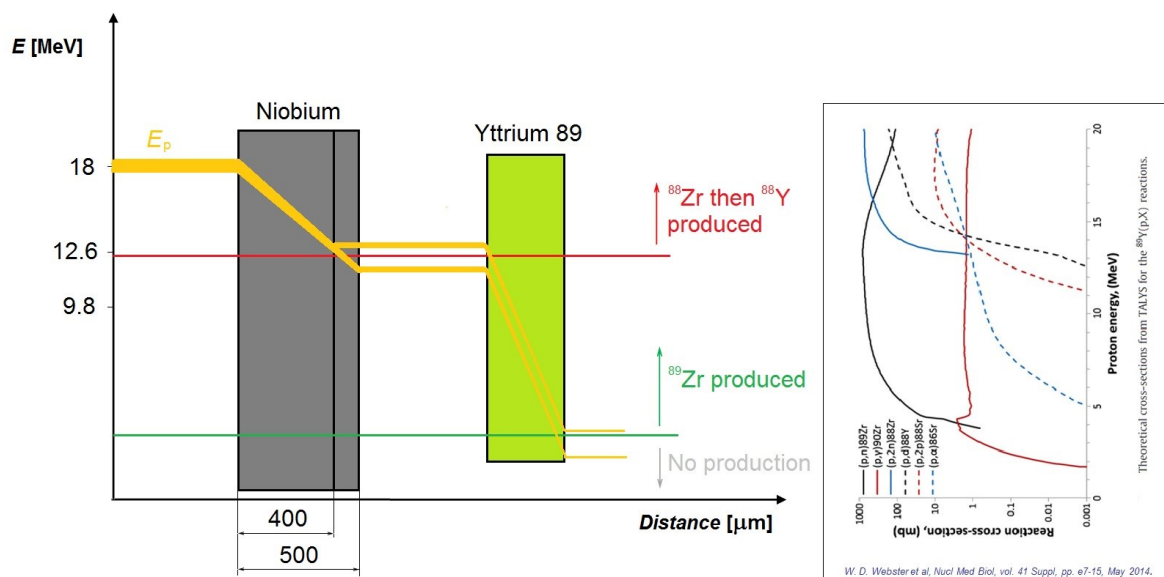


Figure 30 Schematic picture of the relationship between the Niobium foil thickness and the ^{89}Zr production yield/purity (energy drop in the stopping material is shown in simplified way for schematic purpose).

The activity of the ^{89}Zr produced was measured using a CRC 25R CAPINTEC Dose Calibrator (set to a dial factor of 490) at least 1 h after the end of beam, to allow for the decay of short lived $^{89\text{m}}\text{Zr}$ which is also produced alongside ^{89}Zr [109], and decay corrected to end of beam (EOB). The CAPINTEC CRC-25PET dose calibrator does not have a published calibration factor for ^{89}Zr , so a suitable calibration factor was determined through cross-calibration with a CRC-15R dose calibrator which has a published factor of 465 for ^{89}Zr [117, 118].

The chemical separation and purification were based on previously described methods [12, 81, 119]. An Yttrium disc (supplied by *Testbourne* and

Goodfellow) was released from its Al holder after irradiation and dissolved in 2 to 6 M HCl and 30% H₂O₂ heated to 110 °C, washed with HCl and water through a separation column. A hydroxamate functionalized ion exchange resin was used for separation of ⁸⁹Zr.

Following experimental validation of our model, we then identified the optimal methodology for production of ⁸⁹Zr by finding the maximum yield for product free of impurities in the available set of the simulated values.

Results

FLUKA simulations

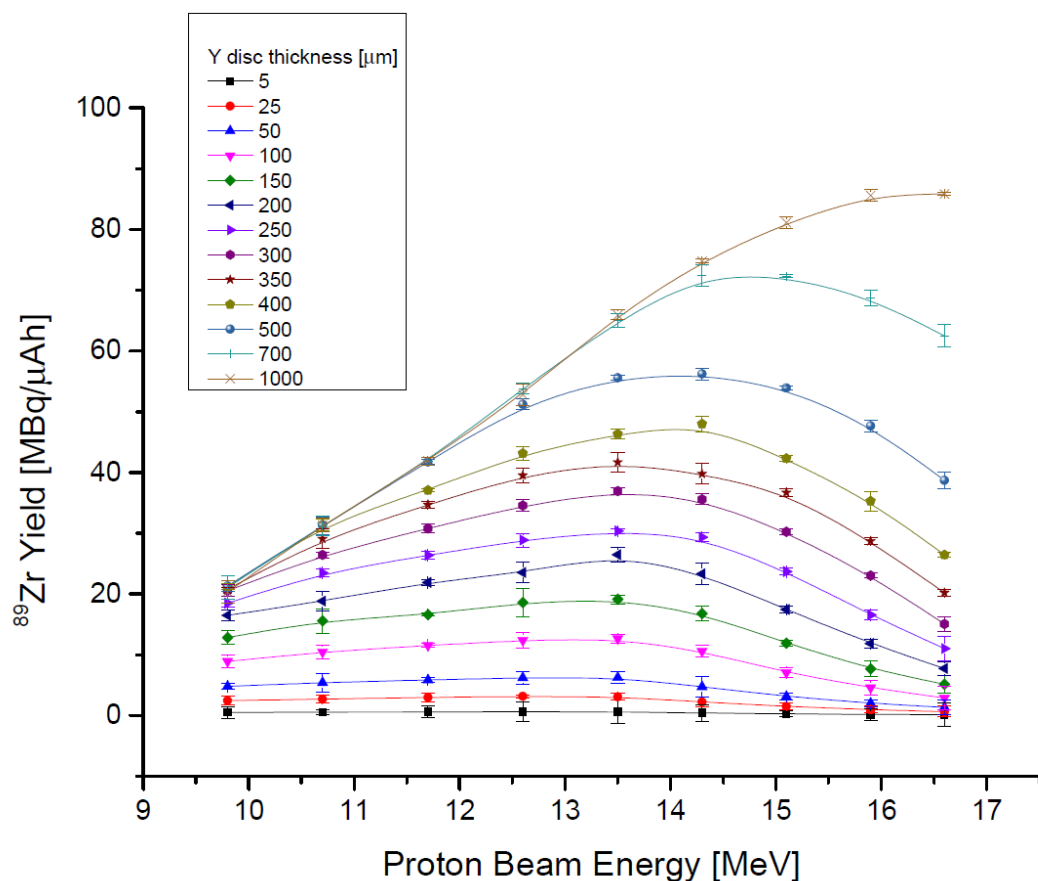


Figure 31 Yields of ⁸⁹Zr isotope generated by FLUKA simulations modelling IBA CYCLONE® 18/9 cyclotron production in a range of Yttrium targets thicknesses irradiated in proton beam of energies from 9.8 up to 16.6 MeV achieved by the use of Nb beam degraders of different thicknesses.

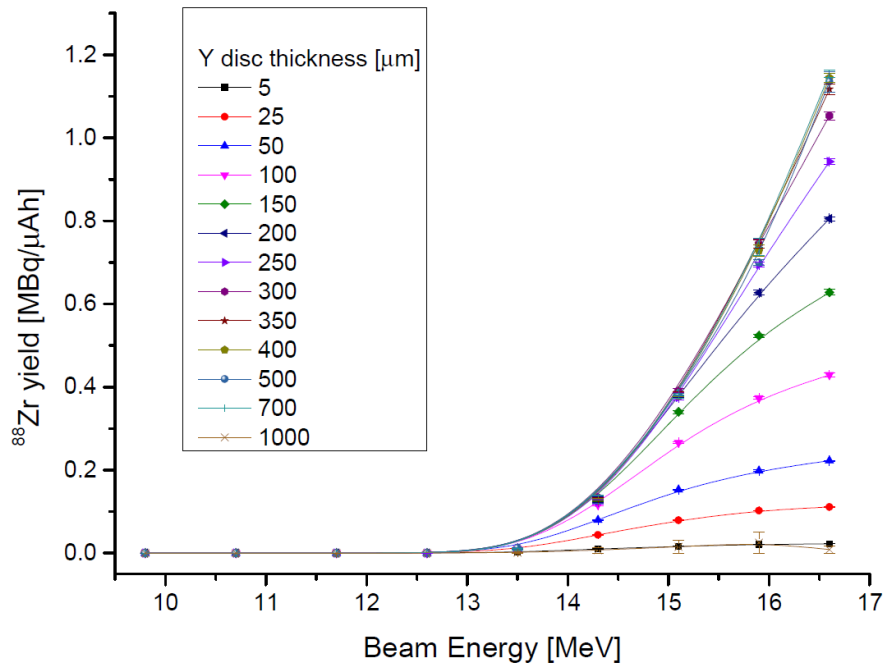


Figure 32 Yields of ^{88}Zr isotope depending on the beam energy modelled in FLUKA for range of Y solid target discs.

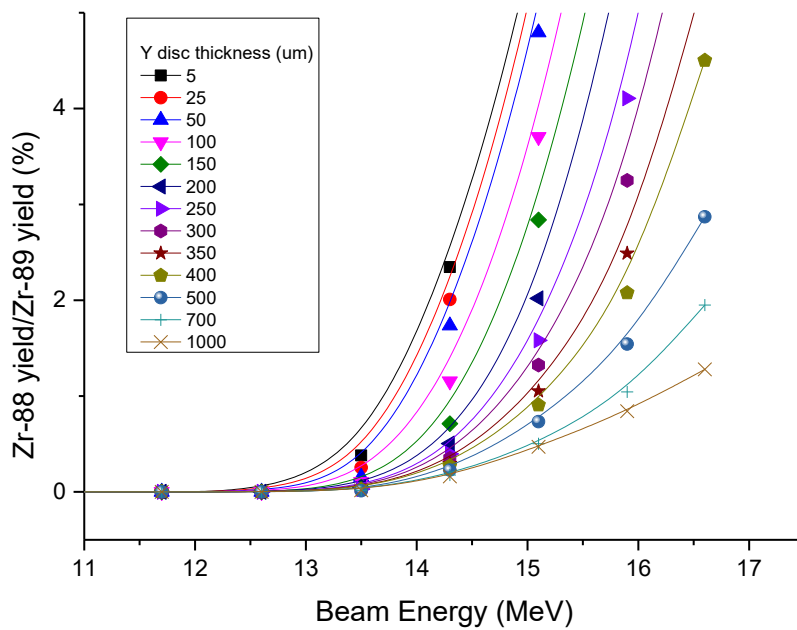


Figure 33 Yields of ^{88}Zr isotope as a fraction of ^{89}Zr yield depending on the beam energy.

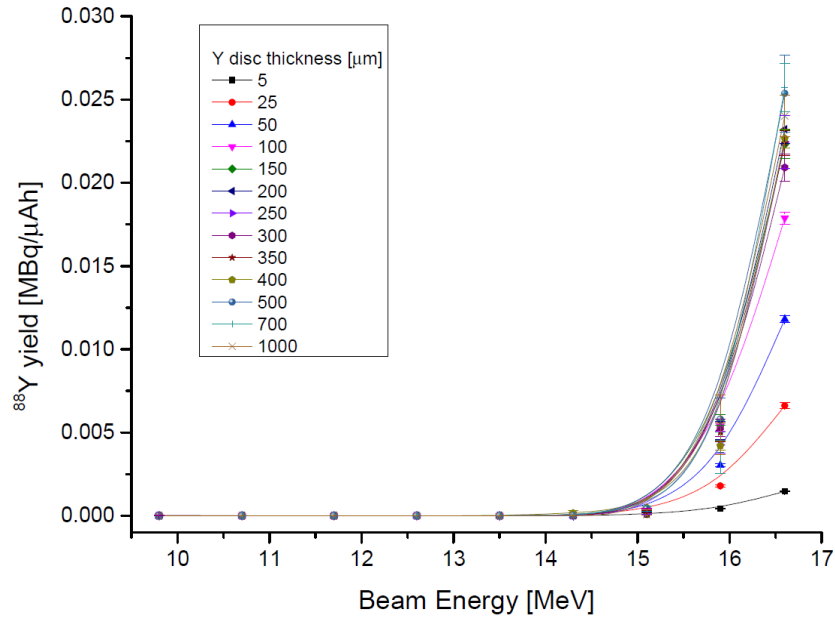


Figure 34 Yields of ^{88}Y (impurity generated for values of $E_p > 13.5$ MeV) according to the FLUKA simulations in the energy range of 9.8 - 16.6 MeV and range of Y solid target discs are at least 10 times lower than yields for ^{88}Zr .

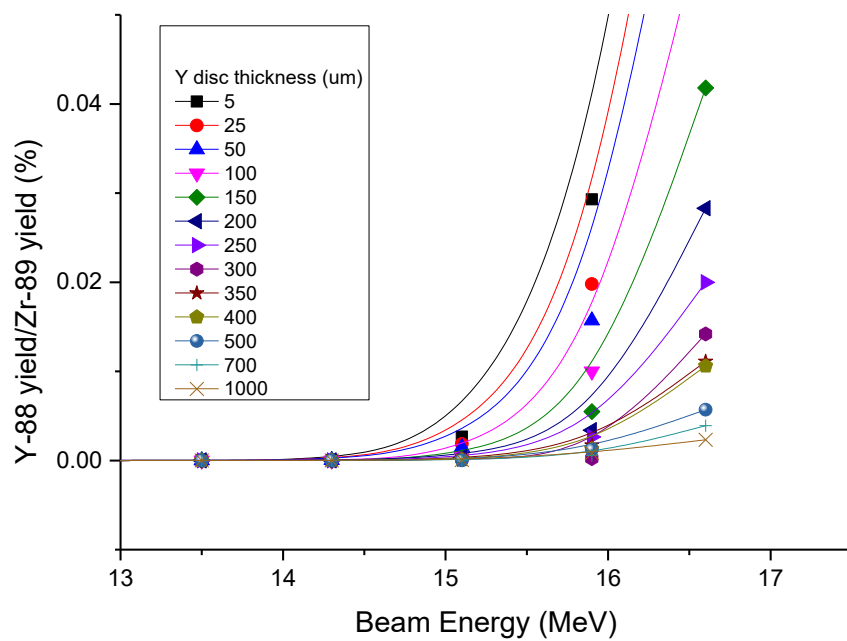


Figure 35 Yields of ^{88}Y isotope as a fraction of ^{89}Zr yield depending on the beam energy zoomed to show the threshold of the energy where ^{88}Y impurity appears.

Comparison of the FLUKA results with experimental production yields

Table 5 ^{89}Zr yields for experimental cyclotron productions compared to FLUKA simulation results.

L_{Nb} [μm] (E_p [MeV])	L_Y [μm]	Experimental ^{89}Zr Yield [MBq/uAh] (Accuracy $\pm 5\%$)	Simulated ^{89}Zr Yield [MBq/uAh] (Accuracy $\pm 3\sigma$)	Statistical Uncertainty of Simulated Yield (Standard Deviation σ) [%]
500 (9.8)	100	8.83	8.90	1.1
450 (10.7)	200	18.12	18.82	1.64
	400	31.68	31.42	0.98
400 (11.7)	100	9.76	11.55	0.36
	150	15.56	16.62	0.22
	200	23.30	21.88	0.48
	300	30.74	30.79	0.68
	400	36.83	37.07	0.25
350 (12.6)	100	9.76	12.37	1.32
	150	18.68	18.58	2.342
	200	24.41	23.55	1.75
	300	33.68	34.58	0.99
	350	36.57	39.52	1.258
	400	41.68	43.13	1.05
250 (14.3)	150	18.67	16.79	1.148
	200	24.18	23.31	1.802
	300	36.82	35.59	0.886

Discussion

The main aim of this project was to investigate how the yield of the ^{89}Zr isotope produced in a typical medical cyclotron varies with L_{Nb} and L_Y and how these values can be modified to optimize production. Previously published work [79] has discussed how the product yield is dependent on the excitation function and have presented thick target yields and reported thresholds for main impurities. However, results of the simulations presented in Figure 31 – Figure 35 suggest the optimization of production is slightly more complicated. Figure 31 demonstrates how the yield of ^{89}Zr in FLUKA simulations varies with L_{Nb} and L_Y and clearly demonstrates that thicker targets produce higher yields. The maximum ^{89}Zr yield for thin targets (5-350 μm) are achieved with a proton beam energy of approximately 13.5 MeV, comparable to the excitation function presented in Figure 26. However,

as the target thickness increases above 350 μm , the peak in the yield of ^{89}Zr production shifts towards higher beam energies. The reason for this is due to beam energy degradation within the Y target material and the location of the nuclear cross section maximum value within the target. With higher beam energies and thinner targets, the ^{89}Zr yield drops due to the maximum of the nuclear cross section no longer occurring within the target material.

However, optimization of ^{89}Zr production is not just about maximising the amount of ^{89}Zr produced. It is also important to minimise the production of long-lived radionuclidic impurities in the final product. Previous studies have reported that the main impurities, ^{88}Zr and ^{88}Y [12, 15, 80-82], may be generated in significant amounts within the range of energies used in small medical cyclotrons. As ^{88}Zr is a long-lived radioisotope ($t_{1/2} = 83.4$ d) that cannot be chemically separated from ^{89}Zr , it is crucial to minimise the yield of this isotope during target bombardment. Figure 30 shows how the yield of ^{88}Zr from FLUKA simulations varies in relation to L_{Nb} and L_{Y} . Simulations demonstrate that the threshold for production of ^{88}Zr is approximately 12.5 MeV, in agreement with previously reported values [118], and that the yield of ^{88}Zr increases with increasing beam energy. Therefore, to degrade the beam energy from 18 MeV to below 12.5 MeV (Figure 29) and to avoid any production of ^{88}Zr (Figure 32), it is necessary to use a Niobium beam degrader with a thickness of 350 μm .

It could be justifiable to accept a small of ^{88}Zr in the final product if the yield of ^{89}Zr can be substantially improved. Figure 33 shows the ratio of ^{88}Zr to ^{89}Zr produced for varying target thickness and beam energy. The ratio of $^{88}\text{Zr}/^{89}\text{Zr}$ increases with increasing beam energy and decreases with increasing target thickness. For the maximum achievable target thickness of 400 μm on our cyclotron, the maximum yield would occur at around 14.5 MeV and would result in a $^{88}\text{Zr}/^{89}\text{Zr}$ ratio of around 1%. However, the increase in the yield of ^{89}Zr is between 5 to 10 % which is not enough to justify increasing the $^{88}\text{Zr}/^{89}\text{Zr}$ ratio from 0 to 1%.

Figure 34 and Figure 35 describe how the yield of ^{88}Y varies in relation to L_{Nb} and L_{Y} . The yields are at least a factor of 10 lower than ^{88}Zr and do not begin to increase significantly until the beam energy incident on the target is greater than approximately 14.5 MeV. As with ^{88}Zr , the yield of ^{88}Y also increases with increasing beam energy. The $^{88}\text{Y}/^{89}\text{Zr}$ ratio also increases with increasing beam energy and decreases with increasing target thickness. It is also worth noting that ^{88}Y is less of a concern than ^{88}Zr as ^{88}Y can also be chemically separated from Zirconium, thus reducing the percentage of ^{88}Y in the final product even further.

Whilst the main impurities generated in FLUKA model were ^{88}Zr and ^{88}Y , it is worth noting that model also predicted the production of ^{90}Y and ^{85}Sr , with yields significantly lower than ^{88}Y at energies higher than 16 MeV. ^{85}Sr has previously been mentioned in the literature [120, 121] as a by-product, with significant yields for much higher beam energies ($E_p > 18$ MeV). For ^{90}Y , negligible amounts (less than 0.1 %) appear in the simulation results for the unlikely (n,γ) reactions. It is not possible to verify those values experimentally. Again, given that ^{90}Y ($t_{1/2} = 64$ h) and ^{85}Sr ($t_{1/2} = 64.8$ d) can be separated by chemical methods [12, 81, 119] from the product and are only produced at energies above 16 MeV, they are unlikely to impact upon the production of ^{89}Zr .

In case of the STS and target holder available in our institution, the thickest target that can be used is 400 μm . We concluded that it was not practical to repeat each modelled reaction and decided to validate modelled reactions in the range of reactions where production of ^{89}Zr would appear to be optimal. We validated our simulated values experimentally for a range of readings with beam energy between 9.8 MeV and 14.3 MeV and target thickness between 100 and 400 μm . All simulated and experimental results showed good agreement regarding the yield of ^{89}Zr (Table 5). The values shown in Table 5 are well confirmed by the experimental results and both sets are comparable with the yields reported by other authors, especially by *Walther et al.* (2011) [81], *Poniger et al.* (2015) [122], and *Link et al.* (2017) [12, 123]. The setup described by *Walther et al.* (2011) [81] is a home-made solid target system with 2 m long external beam on an IBA cyclotron, similar to the COSTIS STS with helium and water cooling of the solid target. The aluminium disc holder and target foil are also almost identical to our experimental set up. After irradiation with 12 μA proton beam for 120 minutes of the 150 μm thick, *Walther et al.* reported that a square shaped foil gave 12.5 ± 0.5 MBq/mAh average yield (for 15, 12 and 10 MeV beam energy) of the $^{89}\text{Y}(p,n)^{89}\text{Zr}$ nuclear reaction. In comparison, our results for a 150 μm thick Y foil with beam energy between 11.7 and 14.3 MeV were slightly higher and in the range of 15.6 to 18.7 MBq/mAh. This may be explained by a difference in the area of the Yttrium target volume irradiated by the proton beam and the different shape of the target foil.

Poniger (2015) [122] also reported on ^{89}Zr production using a COSTIS STS installed on the CYCLONE[®] 18/9 IBA cyclotron with 2 m long beamline and reported yields of 22.6 MBq/ μAh and 15.9 MBq/ μAh for 0.25 mm thick Y discs irradiated by 14.9 MeV and 13 MeV beam respectively. In comparison, our results for 250 μm thick Y targets gave a yield of approximately 18 MBq/ μAh for a beam energy at 12.6 and 14.3 MeV.

Link et al. irradiated Yttrium targets on a Siemens Eclipse cyclotron with an on-target beam energy of 10.7 MeV and reported yields of 20.5 MBq/ μAh for a 250 μm thick Yttrium target. This is in good agreement with our reported yield of approximately 18 MBq/ μAh for a 200 μm thick target at 10.7 MeV.

Conclusion

The combination of a comprehensive set of modelled results and results of their experimental validation enables determination of the strategy for optimizing the production ^{89}Zr in a manner that maximises yield and minimises the radionuclidic impurity ^{88}Zr , by varying both L_{Nb} and L_{Y} . It was shown by FLUKA simulations and experimental validation that using a Niobium degrader thickness of 350 μm to lower the beam energy to 12.6 MeV, enables production of the ^{89}Zr which is still free of the ^{88}Zr and contains insignificant amounts (less than 10^{-2} MBq/ μAh) of the other (non Zr) impurities which can be easily removed by either chemical separation or physical decay for isotopes with short half-lives. When used in combination with a target with a thickness of 400 μm , a yield more than 40 MBq/ μAh was achievable in good agreement with the simulated value.

Production of ^{48}V

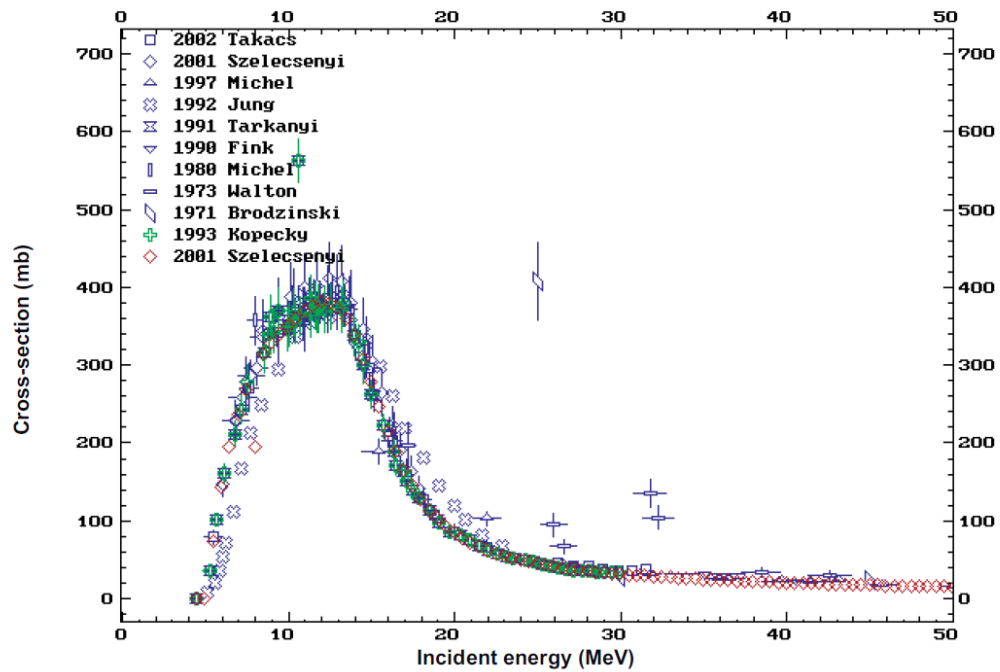
Introduction

Vanadium-48 has a half-life of 16 days and 50% of its decay is by positron emission with two high abundance gamma rays (984 keV and 1312 keV). Its main applications are mainly non-medical and it has been suggested as an alternative for the $^{68}\text{Ge}/^{68}\text{Ga}$ generator system for calibrating PET scanners [28]. To date, only one medical application involving the use of ^{48}V in radioactive stents in renal artery brachytherapy has been reported [27]. Local researchers in PETIC have expressed an interest in using this radiotracer to label several biological probes such as stem cells, exosomes and monoclonal antibodies and then track their distribution in vivo for many weeks and months. As a result, it was decided to explore the production of this rarely used radioisotope to determine the optimal methodology for its production in terms of yield and radionuclidic purity.

Vanadium-48 can be easily produced in cyclotrons by irradiation of a natural titanium target by protons with an energy of between 8 to 21 MeV via the $^{48}\text{Ti}(p,n)^{48}\text{V}$ reaction. This can be achieved with a reasonable degree of isotopic purity due to the high natural abundance 73.8% of ^{48}Ti [68]. ^{48}V in no-carrier-added (NCA) form was produced by *Bonardi et al.* via proton irradiation on Ti targets of natural isotopic composition. Metallic Ti targets irradiated with 21 MeV proton beam were submitted to a selective radiochemical separation resulting in very high specific activity ^{48}V , at levels of hundreds MBq/ μg [124].

Additionally, ^{48}V is also produced in following reactions involving less abundant Titanium isotopes present in natural Titanium such as ^{47}T (7.3%) via the $^{47}\text{Ti}(p,\gamma)^{48}\text{V}$ reaction and ^{49}T (5.5%) via the $^{49}\text{Ti}(p,2n)^{48}\text{V}$ reaction [125]. The estimated experimental value for the production yield of ^{48}V for irradiation at ~20 MeV was calculated by *Sadeghi et al.* was ~22 MBq/mAh at the end of the bombardment. The $^{50}\text{Ti}(p,3n)^{48}\text{V}$ reaction is not considered in this work as the threshold for proton beam energy is of 24.36 MeV (Figure 36) and is well above the maximum proton beam energy used in most small medical PET cyclotrons.

a)



b)

Contributing reactions	Q-value [MeV]	Threshold [MeV]	Abundance of target nucleus [%]
$^{47}\text{Ti}(p, \gamma)^{48}\text{V}$	6.83	0	7.3
$^{48}\text{Ti}(p, n)^{48}\text{V}$	-4.79	4.89	73.8
$^{49}\text{Ti}(p, 2n)^{48}\text{V}$	-12.93	13.20	5.5
$^{50}\text{Ti}(p, 3n)^{48}\text{V}$	-23.88	24.36	5.4

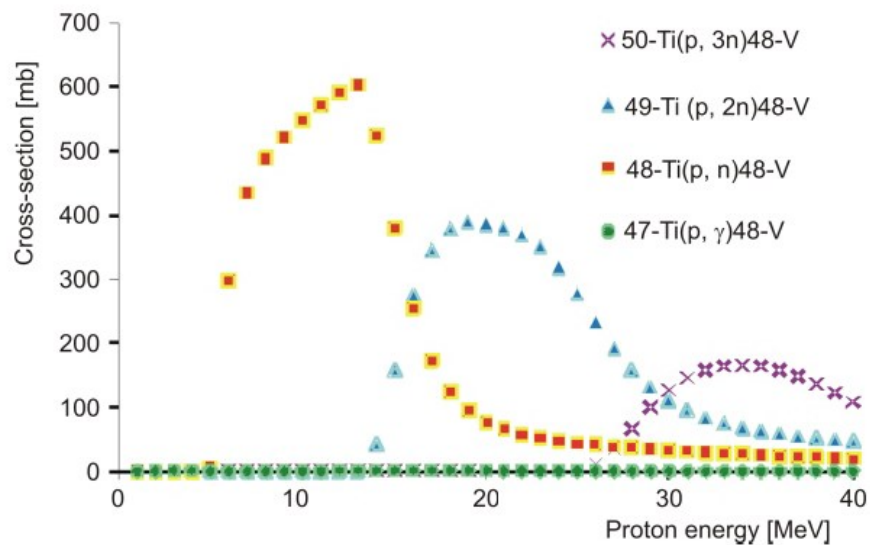


Figure 36 Excitation function for the $^{48}\text{Ti}(p,n)^{48}\text{V}$ reaction only [68] a) and generated in TALYS [125] excitation function for all ^{48}V production channels by irradiation of natural Titanium b).

Excitation functions for both ${}^{\text{nat}}\text{Ti}(p,xn)$ and ${}^{\text{nat}}\text{Ti}(d,xn)$ nuclear reactions are known with good accuracy and precision [126]. No advantages using deuteron induced nuclear reaction, compared to protons, have been identified due to the lower cross sections and higher stopping power, lower deuteron beam current, higher deuteron beam time cost and the higher energy required (Figure 37).

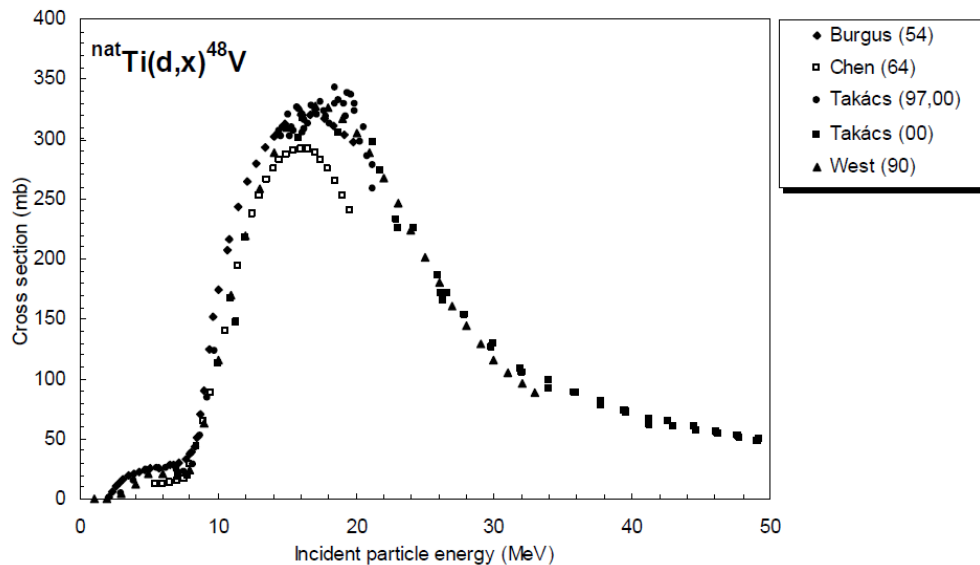


Figure 27 Excitation function for the ${}^{48}\text{Ti}(d,x){}^{48}\text{V}$ reaction [126].

It is also possible to produce ${}^{48}\text{V}$ via the ${}^{45}\text{Sc}(\alpha,n){}^{48}\text{V}$ reaction as Scandium-45 has 100% natural abundance [124]. Since the chemistries of Sc^{III} , $\text{Ti}^{\text{III,IV}}$ and $\text{V}^{\text{III,IV,V}}$ differ significantly, a very selective and fast radiochemical separation was developed. Unfortunately, the nuclear yield of this alternative nuclear reaction is about 40 times lower compared to the (p,xn) one and poses severe limitations when large activities are required [127].

Unfortunately, acceleration of α particles at all and deuterons of energy above 9 MeV is not possible on the IBA CYCLONE[®] 18/9 or on most of the small medical accelerators used for production of PET isotopes and is not considered in this thesis.

Materials and Methods

The experimental setup and *in silico* model for vanadium-48 production are almost identical to the methods used for zirconium-89 production. The same FLUKA model as utilised with the Yttrium target is replaced with a natural Titanium target. Unlike the case of natural Yttrium (where there is only one isotope ^{89}Y) natural Titanium consists of a mixture of Titanium isotopes: ^{48}Ti (73.72%), ^{46}Ti (8.25%), ^{47}Ti (7.44%), ^{49}Ti (5.41%), ^{50}Ti (5.18%) [125]. With FLUKA, we have investigated the analogical set of $^{\text{nat}}\text{Ti}$ disc thicknesses to investigated in the ^{89}Zr chapter (5, 25, 50, 10, 150, 200, 250, 300, 350, 400, 500, 700, 1000 μm). The production model and energies used for the proton beam irradiating of the Titanium targets are the same and we have also used Niobium degraders of the same range of thicknesses as used in ^{89}Zr production model.

In the experimental cyclotron productions, we used the same Al target holder and natural Titanium discs with 99.6% purity (*Goodfellow*) instead of Yttrium-89 ones. The remaining 0.4% of impurities contains [ppm]: Al 300, Ca 20, Cr 50, Cu 5, Fe 1500, Mn 100, Ni 50, Si 300, Sn 200, C 300, H 60, N 150, O 2000. We were unable to obtain extensive experimental productions of vanadium-48 in PETIC as this isotope is not manufactured on a regular basis unlike zirconium-89. However, given the similarities between the method of both zirconium-89 and vanadium-48 production, it is reasonable to assume that the validation of the *in silico* model with zirconium 89 together with even small number of ^{48}V productions provides some evidence of validation that applies also to the production of vanadium-48.

Irradiated discs were unloaded, transferred to a research hot cell at least after 24 hours from the End of Beam (EOB) and measured in a Capintec CRC 25R dose calibrator set at calibration factor 569. Measurements were repeated 4-5 times every 2-3 days. Values of activities measured at CRC 25R were divided by 2 (according to Capintec's algorithm) and decay corrected to the EOB time assuming a 6 h half-life. For EOB activity calculation, measurements 2-7 days after end of production were used.

Results

Table 6 ^{48}V yields for some experimental cyclotron productions compared to FLUKA simulation results.

L_{Nb} [μm] (E_p [MeV])	L_{Ti} [μm]	Experimental ^{48}V Yield [MBq/uAh] (Accuracy $\pm 5\%$)	Simulated ^{48}V Yield [MBq/uAh] (Accuracy $\pm 3\sigma$)	Statistical Uncertainty of Simulated Yield (Standard Deviation σ) [%]
400 (11.7)	150	3.80	3.79	1.53
	200	5.62 6.42*	5.22	0.98
350 (12.6)	150	3.97 4.06	3.99	1.96
	300	7.95	7.85	2.21
300 (13.5)	150	5.6*	4.22	2.80

*Results for measurements done less than 48 and more than 24 hours from EOB.

Other (not marked) results were received for the yields based on activity measurements done a week after the EOB and time corrected to get values at the EOB.

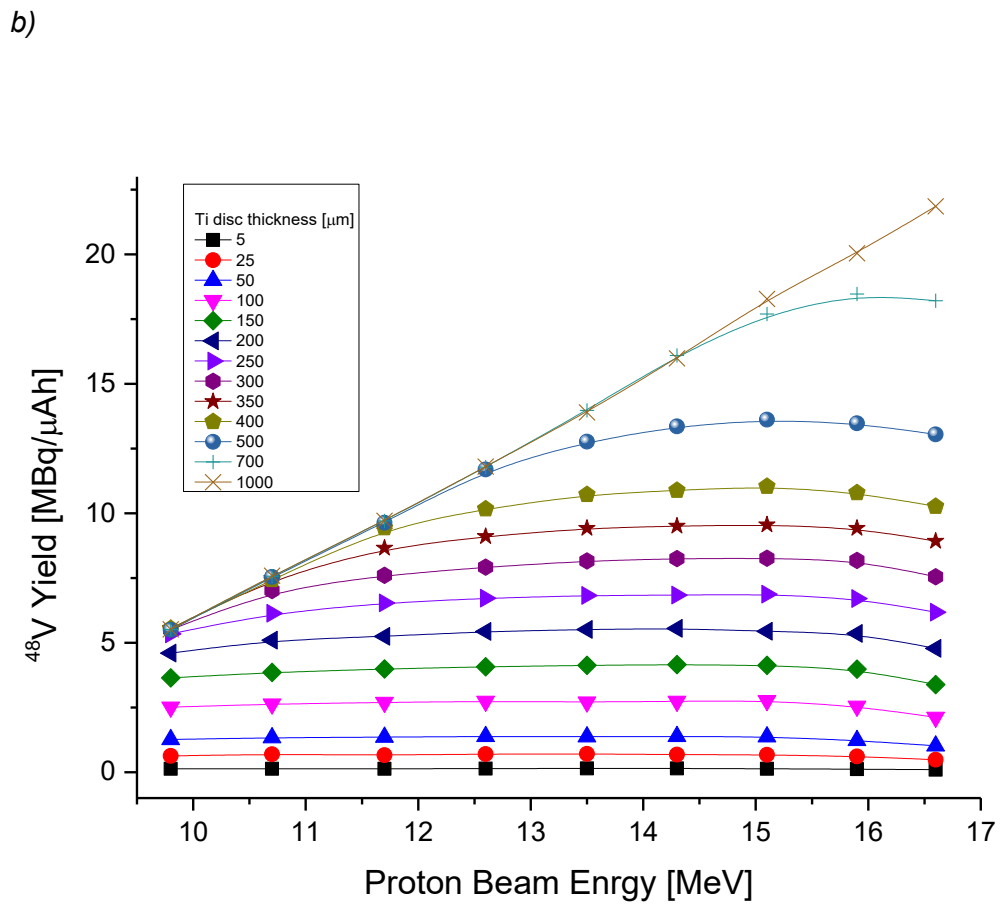
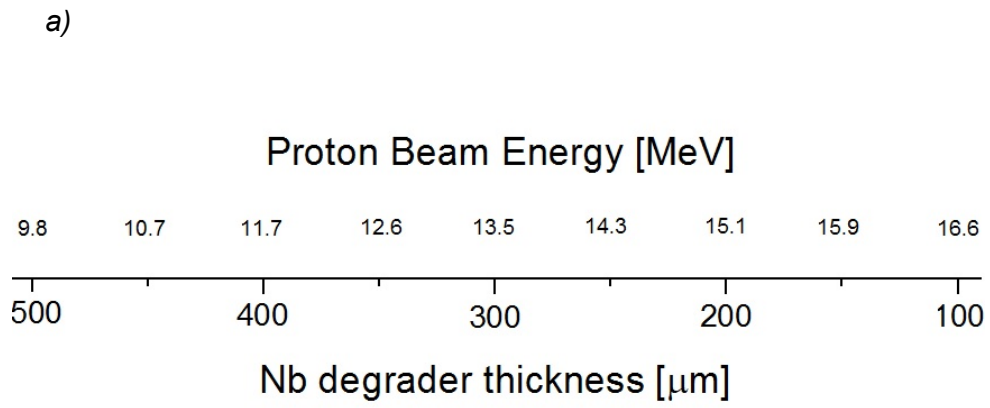


Figure 38 a) Relation between proton beam energy and Nb degrader thickness and b) Vanadium-48 yields calculated in FLUKA for range of proton beam energies and Ti target thicknesses.

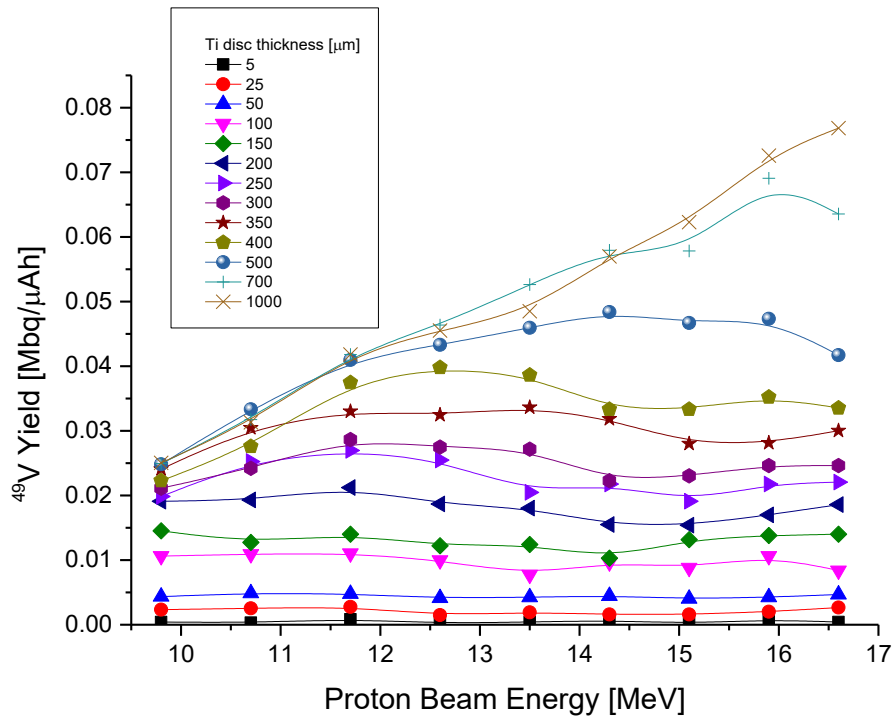


Figure 39 Vanadium-49 yields calculated in FLUKA. For impurities that are very low abounding and reactions where they are produced are less probable, their statistical errors' and yield values' oscillations appear.

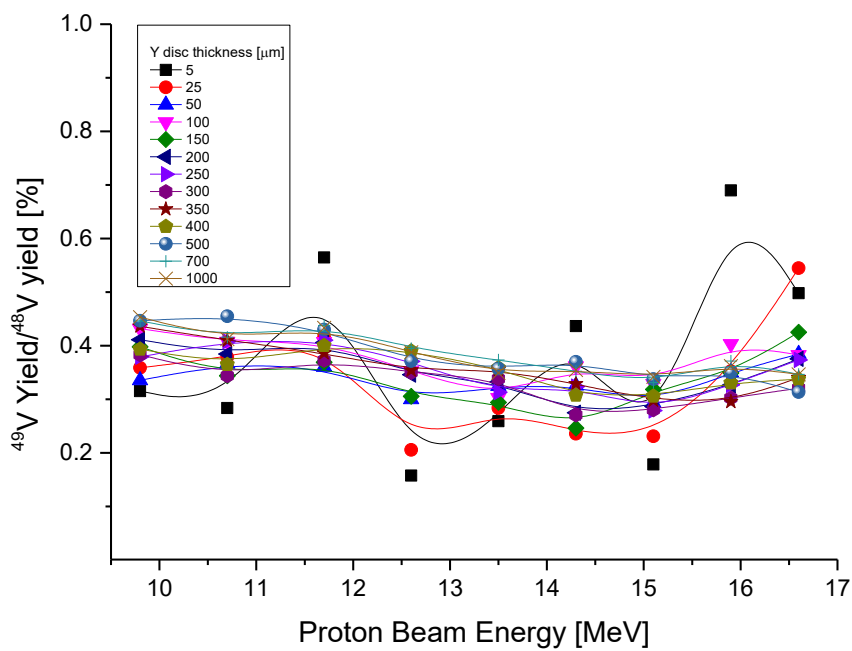


Figure 40 Ratios of the Vanadium-49 yield to the Vanadium 48 yield vs proton beam energy.

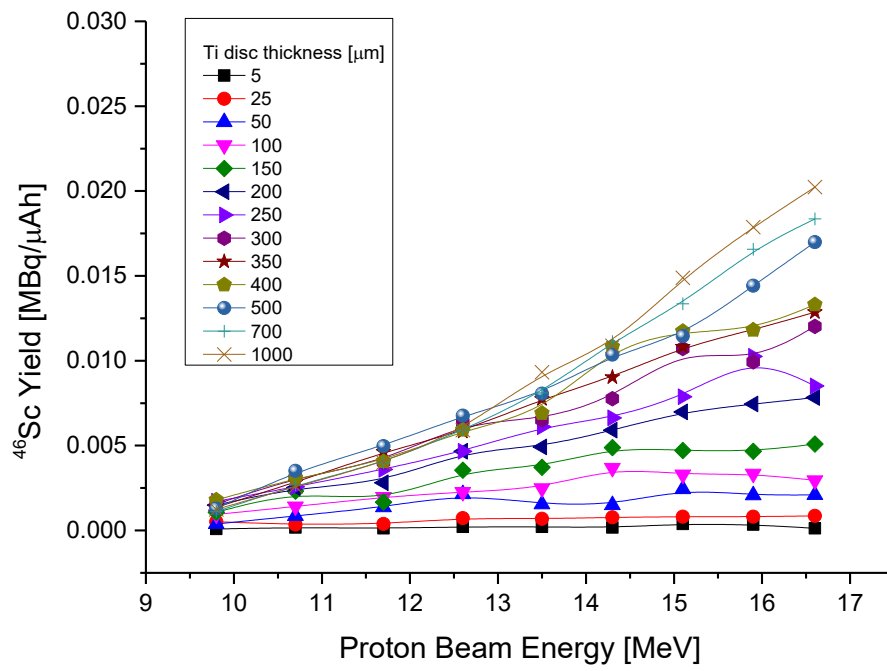


Figure 41 Scandium-46 yields calculated in FLUKA.

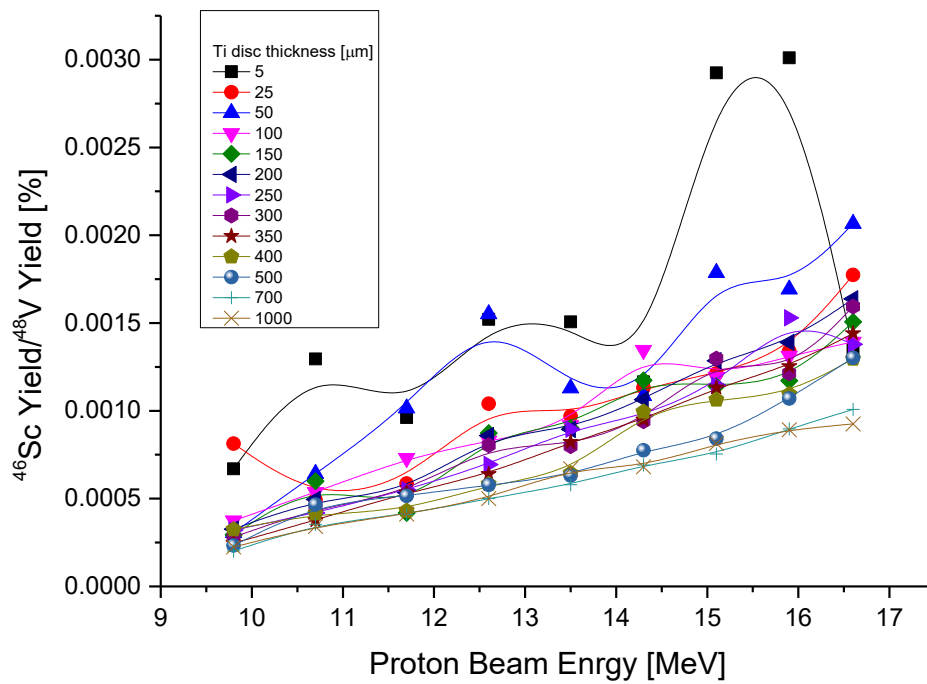


Figure 42 Ratios of the Scandium-46 yield to the Vanadium 48 yield vs proton beam energy.

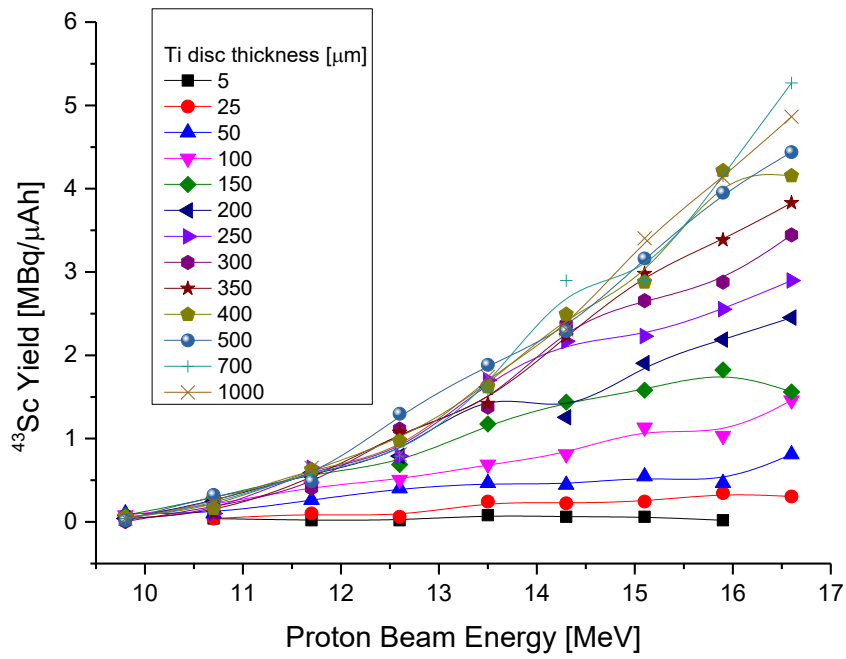


Figure 43 Scandium-43 yields calculated in FLUKA.

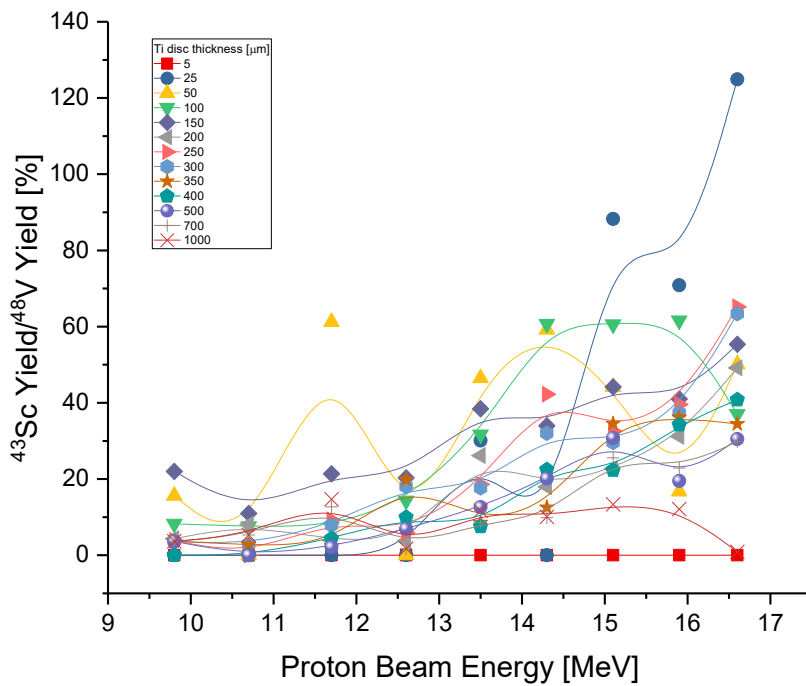
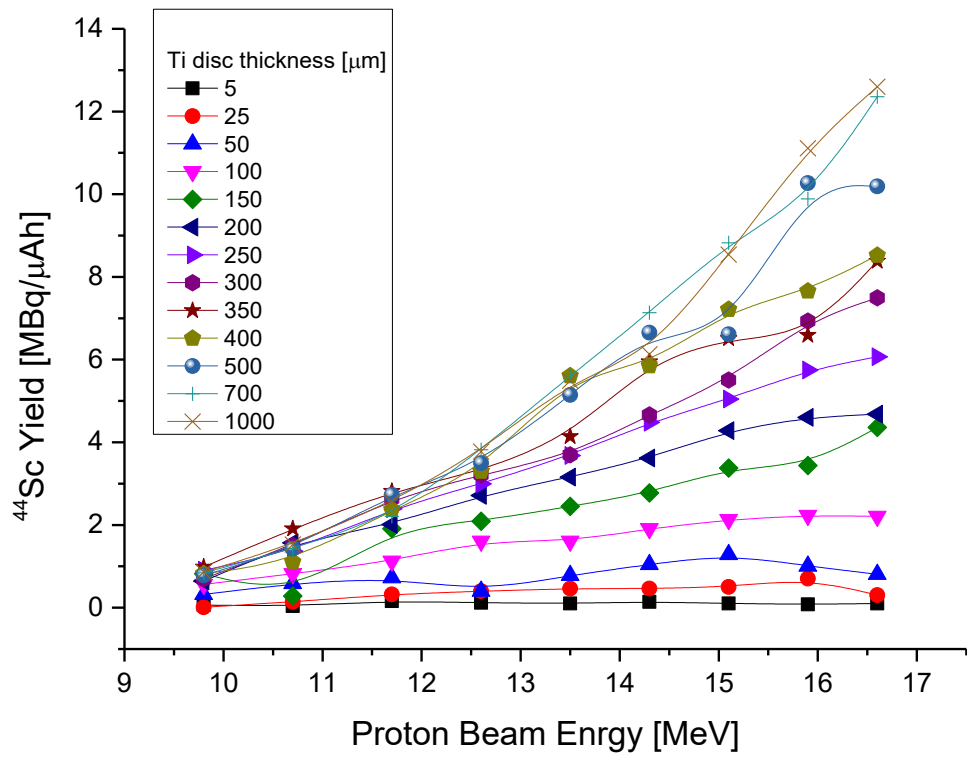
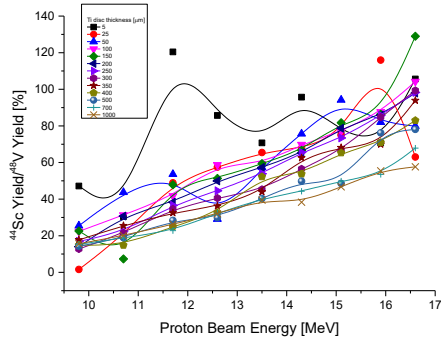


Figure 44 Ratios of the Scandium-43 yield to the Vanadium 48 yield vs proton beam energy.

a)



b)



c)

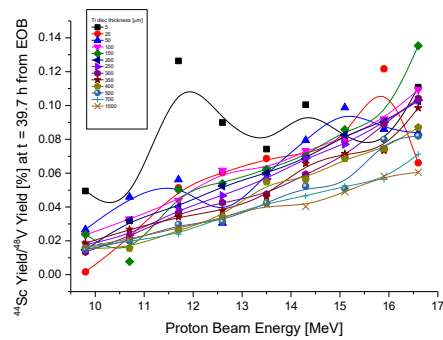
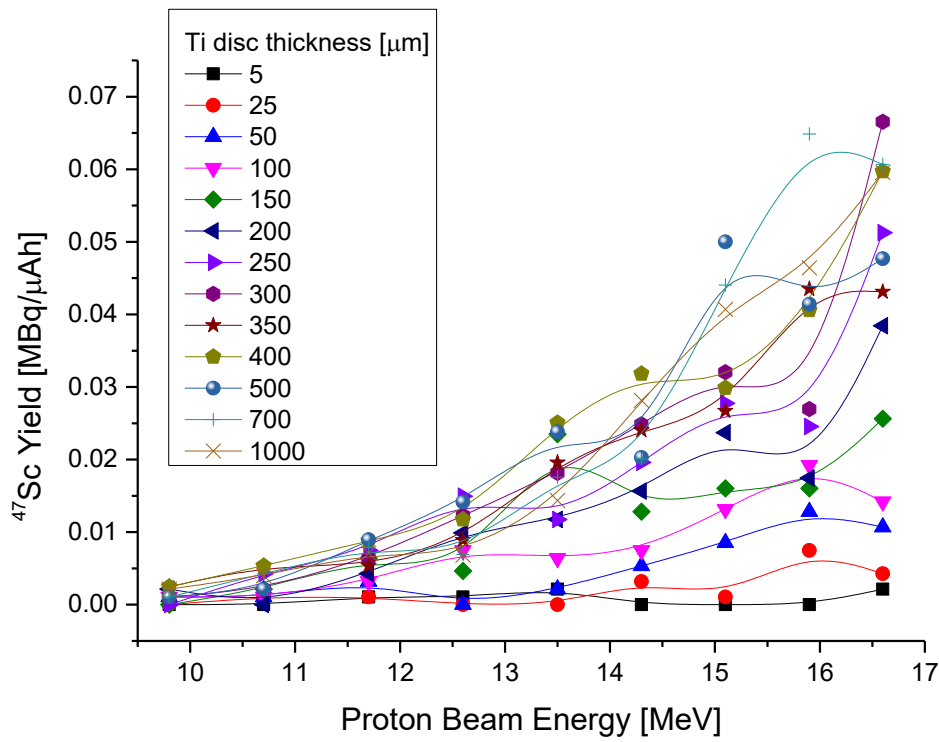
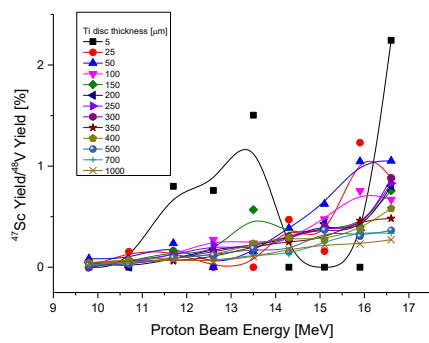


Figure 45 Scandium-44 yields calculated in FLUKA a) and their ratios to the ^{48}V yield at the EOB b) and after 10 half-lives c).

a)



b)



c)

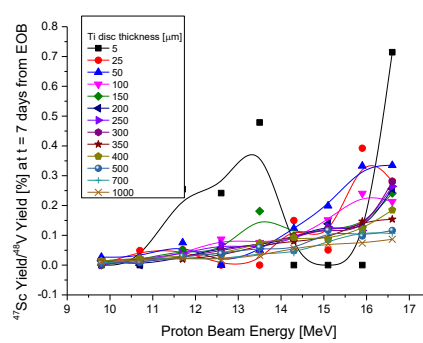


Figure 46 Scandium-47 yields calculated in FLUKA a) and their ratios to the ^{48}V yield at the EOB b) and after 7days c).

Discussion

Figure 38, presenting yields of ^{48}V productions for range of energies and target thicknesses, shows a fully reasonable picture where the maximums lay close or exactly in the same range (14 MeV) like for excitation function shown in Figure 36. For thinner targets effect of energy degradation in the volume of these target is weaker and energy range for maximum yield corresponds to the energy of excitation function's maximum cross-section. The situation is analogical to ^{89}Zr production yields, where thick targets (more than 300 μm) have maximum yield shifted towards energies higher than 14 MeV. This effect gets bigger with growing thickness of the target as the target itself provides additional energy degradation for the proton beam reaching the target with initial energy higher than 14 MeV. This effect might be useful for thin target discs (up to 150 μm) stacked together in one thick target. Titanium is hard to dissolve in acid and single thick targets might be harder to process into further products than two thinner stacked in one.

Table 6 shows first attempt comparing experimental values, based on activity measurements done 2 to 7 days after production, for ^{48}V yields with simulation results for FLUKA model of its cyclotron production. It is clearly seen that experimental yields are higher than their simulated values for measurements done less than 48 hours from EOB (Table 6). This is effect of isotopic impurities with half-lives of few hours or days generated during irradiation of natural Titanium with protons in a cyclotron (Table 7 and Figure 47) especially $^{43,44,47}\text{Sc}$ that have yields higher or comparable to ^{48}V at the EOB (Figure 43, Figure 44, Figure 45 and Figure 46). All the isotopes generated in that process according to FLUKA simulation are listed in Table 7. Due to the target composition, there is a wide range of radioisotopes that are produced alongside ^{48}V when irradiating a natural Titanium target with a proton beam.

From the Figures 39-45 it is clearly seen, that for impurities which are very low abounding and reactions where they are produced are less probable, their statistical errors' and yield values' start to oscillate. It is hard to fit the proper curve (existing one is just to guide an eye across data points) to the data with lower accuracy, as better accuracy will need longer simulation.

Looking at isotopes from Table 7 it is easy to find four groups of impurities that will be characterized below.

Table 7 Isotopes generated by irradiation of ^{nat}Ti target with proton beam 9.8–16.6 MeV of energy according to FLUKA.

Z	23				22	21				
Half-life	15.97 d	32.66 min	422.5 ms	329.86 d	3.08 h	3.35 d	3.89 h	3.97 h	83.78 d	1.82 d
Isotope	^{48}V	^{47}V	^{46}V	^{49}V	^{45}Ti	^{47}Sc	^{43}Sc	^{44}Sc	^{46}Sc	^{48}Sc

- Short lived impurities with half-lives “ultra” much shorter than ^{48}V
- Short lived impurities with half-lives much shorter than ^{48}V
- Short lived impurities with half-lives shorter than ^{48}V
- Long lived impurities with half-lives much longer than ^{48}V
- Trace impurities produced in FLUKA model and not previously mentioned in the literature

Short lived impurities with half-lives “ultra” much shorter than ^{48}V , these are ^{46}V and ^{47}V . With their relatively short half-lives after about 5 hours they decay away by positron emission like ^{48}V only much quicker and decay to ^{46}Ti and ^{47}Ti respectively that are stable. Their yield might be 10 times higher than yield of ^{48}V at the EOB, but after few hours, their amount is negligible. They also appear in simulations done by *Sadeghi et al.* [125] (Figure 47).

Short lived impurities with half-lives much shorter than ^{48}V like ^{43}Sc (3.89 h) and ^{44}Sc (3.97 h) and their yields are comparable to the yields of the product within the wide range of energies. In this case around 1/3 of the product yield for optimal production range of ^{48}V within the simulated energies (compare Figure 38 and Figure 43, Figure 44 and Figure 45). ^{43}Sc decays by positron emission to stable innocuous ^{43}Ca and ^{44}Sc respectively to ^{44}Ca .

The percentage amounts of ^{43}Sc (and long-lived ^{46}Sc) in relation to ^{48}V are very close to values given by *Sadeghi et al.* in [125]. However, absolute values are not comparable as they used 21 MeV proton beam where yields would be higher for the product.

Also, ^{45}Ti (3.08 h) that has half-life no longer than 4 hours has no influence for measurement of the experimental yield of ^{48}V after 4 to 5 days from EOB (10 or more half-lives of this type impurities). ^{45}Ti decays by positron emission to stable harmless ^{45}Sc . Even if amounts of impurities from this group initially are higher (120 %) than ^{48}V like in case of ^{44}Sc after 4 to 5 days their decay out to the negligible

levels (Figure 45). ^{45}Ti that could be generated in (p,pn) reactions from ^{46}Ti , however appears in simulations' results very rarely with high statistical error, and its presence among by-products of ^{48}V generation cannot be confirmed by other authors and it might be also more reasonable to classify this isotope to the last group.

Scandium-47 with its 3.35 days half-life might be more problematic however its amount drops below 0.5 % after a week from EOB (Figure 46) and might be classified as **short lived impurity with half-life shorter than ^{48}V** . Scandium-47 decays by electron emission to stable ^{47}Ti . Scandium-47 can be created via the $^{47}\text{Ti}(p,n)^{47}\text{Sc}$ reaction with low yields due to the low abundance of ^{47}T (7.44 %) in natural Titanium. However, this channel is not mentioned in literature and *Bonardi et al.* [124] propose ^{47}Sc rather as a by-product of (p,axn) reaction on $^{\text{nat}}\text{Ti}$.

Long lived impurities with half-lives much longer than ^{48}V , like ^{49}V and ^{46}Sc with yields not higher than 0.5% and 0.003 % of ^{48}V yield respectively for whole range of simulated energies and should not affect much the measurements of experimental yields from Table 1 and also appear in simulations results of *Sadeghi et al.* [125] (Figure 47). Vanadium-49 in this simulation can be generated via the $^{49}\text{Ti}(p,n)^{49}\text{V}$ reaction, with its low yield due to the low abundance of ^{49}T (5.5%) in natural Titanium. There is no clear energy threshold for the production of ^{49}V (Figure 39) and the ratio of $^{49}\text{V}/^{48}\text{V}$ is consistent across the range of energies (Figure 40). As it would not be possible to easily separate ^{49}V for ^{48}V and there is no optimal energy for minimising the ratio, a degree of impurity of around 0.5% at end of beam will always be present when irradiating natural Titanium. Only way to reduce this impurity will be to produce ^{48}V with an enriched Titanium target with minimal amounts of ^{49}Ti . In addition, the longer half-life of ^{49}V would mean the isotopic purity of ^{48}V would decrease with time following production as amount of ^{49}V present as a percentage would increase as time progressed. ^{49}V decays by electron capture to stable ^{49}Ti , and like other isotopes of Vanadium is innocuous and nutritionally essential for higher animals, including humans as a trace metal [128].

Scandium-46 can be created via the $^{46}\text{Ti}(p,n)^{46}\text{Sc}$ reaction with low yields due to the low abundance of ^{46}T (8.25%) in natural Titanium. There is no clear threshold for its occurrence within simulated range of energies up to around 14 MeV (compare Figure 41 and Figure 42 with Figure 47) and its amount can be further reduced by use of enriched target material with isotopic purity close to 100% ^{48}Ti or by chemical purification methods post irradiation. As with ^{49}V , the longer half-life of ^{46}Sc would mean the isotopic purity of ^{48}V would decrease with time following production as the amount of ^{46}Sc present as a percentage would increase with time passed. ^{46}Sc decays by electron emission to stable ^{46}Ti . Scandium has no biological

role. Only trace amounts reach the food chain, so the average person's daily intake is less than 0.1 microgram. Scandium is harmless, although there have been suggestions that some of its compounds might be carcinogenic [129]. Scandium is a rare element from which different radionuclides with medicinal potential can be produced in reactors or cyclotrons. These radionuclides that are useful for diagnosis and treatment in nuclear medicine are ^{43}Sc , ^{44}Sc , ^{46}Sc , ^{47}Sc and ^{48}Sc [130].

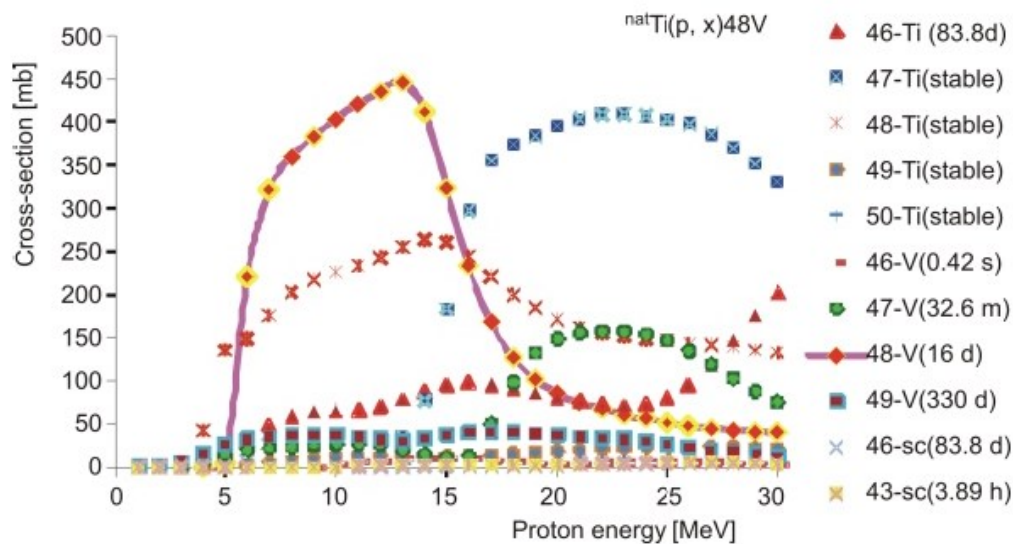


Figure 47 Excitation function for the $^{nat}\text{Ti}(p,x)$ reaction only generated in TALYS [125].

Trace impurities produced in FLUKA model and not previously mentioned in the literature, impurities which traces are questionable, like ^{48}Sc with 1.82 d half-life, its level is very low and appears very irregular might be negligible as not mentioned in literature. Scandium-48 was ignored as its yields are very low, within the statistical error value and appeared 3 times only for all simulated values. Its production with very low probability might be caused by high speed neutrons bombarding Ti [130]. Like for ^{47}Sc its amount will be negligible after a week from EOB anyway.

Impurities like $^{43,44,46,47}\text{Sc}$ and the potential traces of ^{48}Sc can be removed by chemical separation methods [124].

Conclusion

Using FLUKA simulations and slightly modified ^{89}Zr target, it was possible to produce the PET isotope ^{48}V with yields ($\sim 8 \text{ MBq}/\mu\text{Ah}$) that are enough to enable pre-clinical studies of radiopharmaceuticals labelled with ^{48}V .

It is possible to produce around 500 MBq of ^{48}V with 13.5 MeV proton beam 4 h irradiation of the $^{\text{nat}}\text{Ti}$ target on an IBA Cyclone® 18 cyclotron equipped with a COSTIS solid target system.

FLUKA model proves its usefulness not only helping to find maximum yield of the ^{48}V production, but also finding composition (levels of isotopical impurities) of the irradiated target for example when gamma spectroscopy measurements are not possible. As the impurities generated in this production have no sharp energy thresholds, the optimal beam energy would be between 12 and 16 MeV as shown in Figure 38. However, differences in yields due to varying the beam energy do not justify changing the Nb degrader between ^{89}Zr and ^{48}V production and exposing cyclotron operators to radiation doses. Therefore, in PETIC, the standard 300 μm Nb foil is used to produce both isotopes.

Production of ^{99m}Tc

Introduction

^{99m}Tc is the most commonly used radionuclide in nuclear medicine used in approximately 85% of imaging procedures on nearly 40 million patients per year worldwide [131]. Typically, nuclear medicine users produce ^{99m}Tc by eluting ^{99}Mo in licenced generators, manufactured by GE Healthcare, Covidien, BACisBio and Lantheus [132], which make use of the radioactive decay of ^{99}Mo into ^{99m}Tc . Demographic and medical trends suggest that global demand for ^{99m}Tc is growing at an average annual rate of 3–8% as these diagnostic imaging procedures expand to new markets [131].



Figure 48 Nuclear Centre in Świerk (POLATOM), 30 km from Warsaw (Poland) with reactor MARIA that has been converted in 2009 – 2014 from HEU to LEU fuel in its core [133].

^{99}Mo is produced by processing uranium targets irradiated in nuclear reactors situated in Belgium (IRE), Canada (AECL/Nordion), the Netherlands (Covidien), Poland (POLATOM) and South Africa (NTP). After irradiation, the uranium targets are processed to extract ^{99}Mo , which in turn is purified for use in $^{99}\text{Mo}/^{99m}\text{Tc}$ generators that are shipped to radiopharmacies, hospitals and clinics. This provides a convenient supply chain for the inhouse production of ^{99m}Tc labelled radiopharmaceuticals. The success of ^{99m}Tc in the clinic is primarily due to its advantageous physical properties such as a half-life of 6 hours and a low energy 99% γ emission of single peak of 140.5 keV. Other advantages include a low price and availability [134]. The parent radionuclide ^{99}Mo for the generation of ^{99m}Tc is typically produced in a nuclear fission process of $^{235}\text{U}(n,f)^{99}\text{Mo}$ (Figure 49) applied in

a handful of aging high neutron flux nuclear reactors running on Highly Enriched Uranium (HEU).

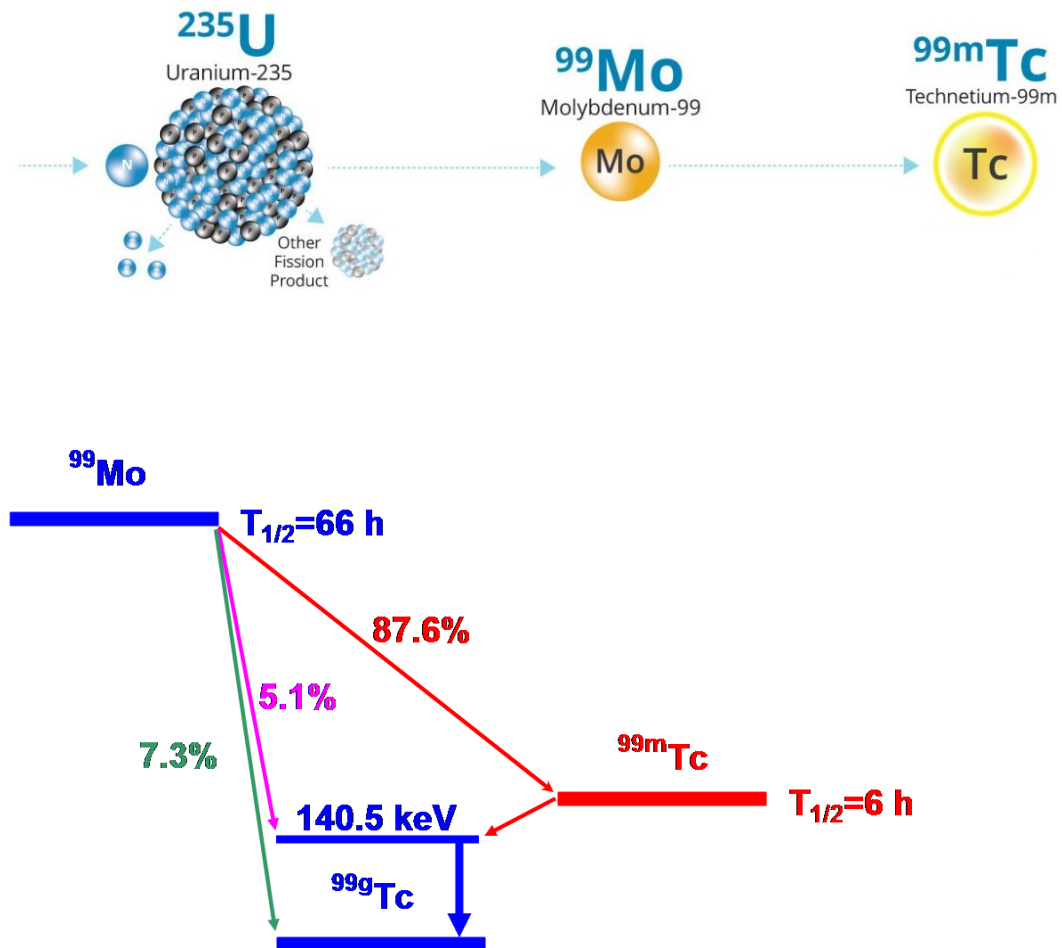


Figure 49 High neutron flux irradiation of ^{235}U (HEU) in nuclear reactor leads to production of ^{99}Mo and other fission products (f). ^{99}Mo is a parent radionuclide for generation of $^{99\text{m}}\text{Tc}$ that decays to $^{99\text{g}}\text{Tc}$ emitting gamma rays 140.5 keV of energy that can be detected by planar or SPECT gamma cameras (graphics – courtesy of SHINE Medical Technologies and [135]).

Due to global shortages of ^{99}Mo caused by the unexpected shutdown of the Chalk River (Canada) and Petten (Netherlands) reactors, and the further suspension of ^{99}Mo production at Chalk River in 2016, the exploration of alternative methods of producing technetium radioisotopes has attracted significant interest. Such alternative methods would enable the continued use of all existing radiopharmaceuticals designed for $^{99\text{m}}\text{Tc}$ in nuclear medicine.

Supply chain issues led to global shortages in 2008 and 2009 [29] made the operators of the existing fleet of reactors used to produce ^{99}Mo are under growing

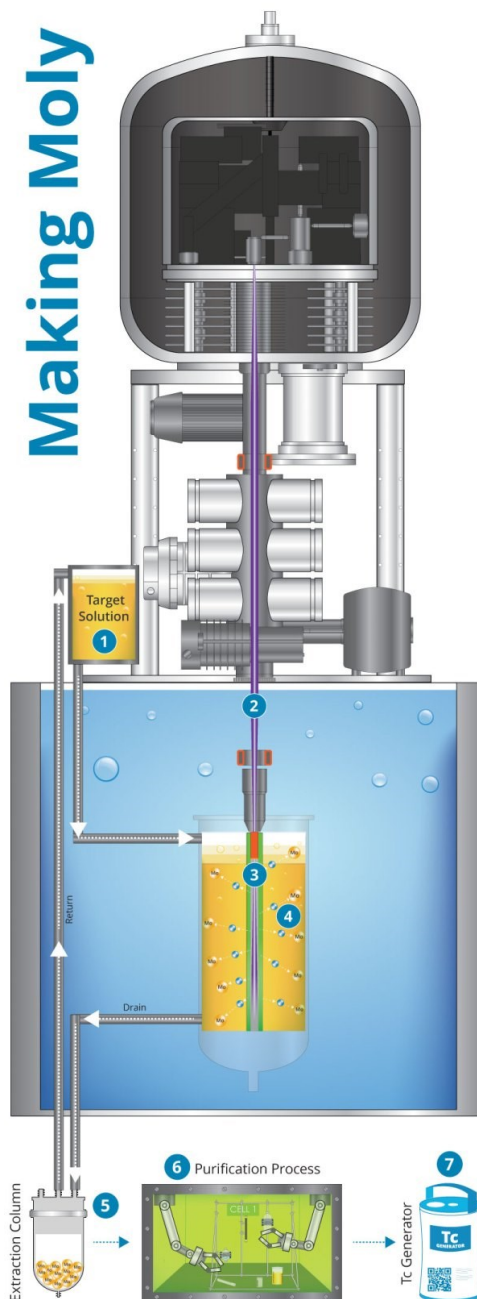
pressure to convert their targets from HEU to low-enriched uranium (LEU). The conversion requires modifying the target itself and the subsequent chemistry. To have the same amount of ^{235}U in the target mix, approximately 5 times the amount of uranium is required (HEU: 93% ^{235}U ; LEU: 20% ^{235}U). The Canadian governments strategy to overcome this issue was to develop alternative sources of supply for the vital medical radioisotope in which it has invested some CAD 60 million. The closure of Chalk River reactor [136] also led to researchers around the globe investigating other methods of production. The threat of possible shortages due to imminent closure of those facilities encouraged many research groups to investigate alternative production methods of $^{99\text{m}}\text{Tc}$ without the use of a nuclear reactor [62]. Such studies are supported by the International Atomic Energy Agency (IAEA) in coordinated research activities like: “Non-HEU Production Technologies for Molybdenum-99 and Technetium-99m”, “Accelerator-based Alternatives to Non-HEU Production of Mo-99/Tc-99m” and “Cyclotron Based Production of Technetium-99m [135, 136].

Potential American solutions to the global supply chain include SHINE Medical Technologies, Northstar and the cyclotron production of $^{99\text{m}}\text{Tc}$ led by ARTMS and ACSI.

SHINE founded in 2010 by Greg Piefer is building its isotope production facility in Janesville, Wisconsin. It will use a patented, proprietary manufacturing process to produce medical isotopes such as molybdenum-99. The SHINE technology does not require a nuclear reactor, uses less electricity, and generates less waste than reactor sites. The first major improvement over existing production methods is the replacement of a highly-specialized nuclear reactor with a low-energy, accelerator-based neutron source. This source functions by colliding deuterium ions with tritium gas to cause fusion. The fusion reaction results in high energy neutrons and ^4He . In other words, the accelerator takes a radioactive by-product created by nuclear power plants (tritium) and turns it into harmless gas. The neutrons produced by this reaction then strike the uranium target to produce moly-99. Removing the nuclear reactor as the neutron source eliminates almost all the nuclear waste associated with production today, resulting in a safer, greener process and giving a significant cost-advantage. Their technology produces moly-99 that is proven to be compatible with the existing global supply chain [136, 137]. The second technological leap forward is the target material itself. Instead of employing solid highly enriched uranium (HEU) plates that are used once and then disposed of, the uranium in SHINE's target is low-enriched uranium (LEU) that is dissolved in a water-based solution. Neutrons from the accelerator enter the water and strike the

uranium, causing fission. ^{99}Mo is created just as in the solid target case but is already dissolved in solution. After several days, the solution is drained and passed through a filter which retains molybdenum but allows the uranium to pass through. The solution is then pumped back into the production system and reused. This recyclable target further reduces waste production, increases the ease of separation, and decreases the amount of uranium required to make a given quantity of $^{99\text{m}}\text{Tc}$ by many times. The LEU target eliminates any chance of highly-enriched uranium (HEU) diversion for nuclear weapons production [138, 139]. SHINE's isotope production facility will be capable of producing up to one-third of the global patient need and will primarily serve the U.S. market. SHINE is planning to build its second facility in Europe and work to identify a site for the European facility is underway. Until recently, all major moly-99 producers used targets made from (HEU) with a composition of 20% uranium-235 or more. Although moly-99 can be produced very efficiently from this material, HEU also can be made into nuclear weapons and is a risk to global security. In the traditional production process, after the moly is separated from the target, almost all of the HEU remains and is not reused. Instead, it is stored indefinitely at a relatively low-security site. Historically, the United States has exported enough HEU for the purpose of making moly-99 to produce a few nuclear bombs each year. This situation has created a conflict between the health and the security of U.S. citizens, because a reliable supply of medical isotopes comes at the expense of the increased threat posed by the potential diversion of HEU [140].

The alternative to HEU is LEU with a composition of less than 20% uranium-235. Because the uranium-235 in LEU is diluted, it cannot be used in a nuclear weapon without very sophisticated modifications and is much less of a proliferation risk. Several scientific investigations [136] have shown that there is no technological barrier preventing the use of LEU in the traditional production process with some modification. However, many producers have proved reluctant to change. SHINE's technology is 100% LEU-based (Courtesy of SHINE Medical Technologies shinemed.com).



1. Target Solution: Low-enriched uranium (LEU) is created by diluting former nuclear weapons to the point of no longer being a threat. Once intended to cause harm to billions, the LEU will be transformed by the SHINE process to help provide healthcare for a billion patients. SHINE receives LEU from the US Government, and dissolves it, creating a uranyl sulphate mixture. This mixture is then pumped into a target solution tank.

2. Accelerator: Electrons are stripped from deuterium using microwave energy. The resulting positively charged deuterium ions are shaped into a beam and accelerated to about 10 million mph.

3. Fusion Chamber: The deuterium ions are accelerated into a gas target made of another isotope of hydrogen (tritium) resulting in clean fusion reactions that generate neutrons. These neutrons then pass into the target solution tank.

4. Fission Target: The neutrons cause the uranium nuclei in the target solution tank to split in a process known as fission. This process creates multiple elements, including moly-99 and other useful isotopes.

5. Moly Extraction: The target solution is irradiated for approximately 1 week, then pumped through an extraction column. Moly sticks to the column and the rest of the target solution is

returned for re-use. A separate solution is then pumped through the extraction column to take the moly to purification.

6. Purification: A proven chemical process purifies the moly-99 to meet pharmaceutical standards and customer specifications.

7. Distribution: Moly-99 decays at a rate of about 1% per hour, so it must be quickly transported for use by doctors. Moly-99 is flown from the SHINE facility to its customers, where it will be packaged and sent to hospitals for use in procedures such as stress tests and bone scans. Moly-99 is used in around 56,000 procedures every day in the U.S. alone.

Figure 50 Production of moly-99 from LEU (graphics – courtesy of SHINE Medical Technologies).

On the 4th of May 2020 World Nuclear News (world-nuclear-news.org) reported that Belgium's Institute of Radioelements (IRE) has produced its first batch of the medical radioisotope molybdenum-99 using LEU target. Also, in Europe the use of HEU is seen as a potential nuclear proliferation risk. The LEU target was irradiated in the Belgian Research Reactor 2 (BR2), one of three operating research reactors at the Belgian Nuclear Research Centre (SCK-CEN) in Mol, northeast Belgium. SCK-CEN is a key partner of IRE in the production of radioisotopes. IRE, based in Fleurus, said the first batch of ^{99}Mo will be sent to the USA. Moly-99 is used in hospitals to produce technetium-99m, which is used in around 56,000 procedures in the USA per day.

NorthStar Medical Radionuclides (USA) is currently finalizing the ^{99}Mo production method from the neutron capture $^{98}\text{Mo}(n,\gamma)^{99}\text{Mo}$ using an old nuclear reactor at the University of Missouri Research Reactor Center (MURR).

Other methods can utilize linear accelerators or lasers. The production of ^{99}Mo by utilizing electron induced brehmsstrahlung photons produced in linear accelerators or rhodotrons is getting popular. These targets require the ^{100}Mo enriched material, but the nuclear reaction pathway is $^{100}\text{Mo}(\gamma,n)^{99}\text{Mo}$. Recent experiments in this field confirmed that this production pathway is feasible [141] and a steady supply of ^{99}Mo is expected to be provided soon by the already commissioned 35 MeV, 40 kW Linear Accelerator (LINAC) at the Canadian Light Source. Similar projects based on the same principle are under development or consideration in other countries. NorthStar Medical Radionuclides plans to expand its capacity by building a single site LINAC farm, comprised of up to 16 LINACs capable of producing ^{99}Mo by a photonuclear reaction on enriched ^{100}Mo targets. The project is estimated to cover half of the USA demand for $^{99\text{m}}\text{Tc}$ (NorthStar Medical Radioisotopes received \$11.75 Million from National Nuclear Security Administration in 2015 – see presentation from Harvey, Isensee, Moffatt, and Messina from 2014). In 2019 NorthStar Medical Radioisotopes signed an agreement with Ion Beam Applications (IBA) to acquire eight Rhodotron TT300 HE electron beam accelerators (Figure 51). NorthStar has issued purchase orders for two initial units and plans to order the remaining units in the coming years. NorthStar president and CEO Stephen Merrick said: “Investing in accelerator technology is a key component of NorthStar’s multi-pronged approach to deliver domestic and non-uranium-based production of the medical radioisotope ^{99}Mo across multiple processing platforms. We plan to use these accelerators to expand production capacity, enhance production efficiencies and create manufacturing redundancies to

further secure reliable, non-uranium based ^{99}Mo radioisotope supply for U.S. customers and patients.” [136]



Figure 51 Rhodotron TT300 HE.

An interesting alternative pathway of cyclotron production of ^{99}Mo has been theoretically examined by a group from the Italian National Institute for Nuclear Physics [142]. They use an α -beam on an enriched ^{96}Zr target, thus inducing a $^{96}\text{Zr}(\alpha, n)^{99}\text{Mo}$ nuclear reaction. The above pathway does not produce enough ^{99}Mo for commercial use. However, it has the advantage of an extremely high specific activity in the range of 106 TBq/g (current large generators have a specific activity of up to 370 TBq/g). A limiting factor for the development of this pathway is the unavailability of high current α beams.

The Lighthouse Consortium, Netherlands, is gathering companies and research institutes under the leadership of ASML, to achieve their goal of building an electron accelerator facility for ^{99}Mo production from enriched ^{100}Mo targets. It is assumed that by 2021 the facility will be able to cover the capacity of the HFR nuclear reactor in Petten (Lighthouse: productie medische isotopen vanaf 2021, 2017).

In Japan, considerations on which technology to rely on for securing the future ^{99m}Tc supply are ongoing. The country already has a greatly developed particle accelerator infrastructure, allowing to diversify between production from linear accelerators, a vast ACSI cyclotron network of appropriate energies or even by using the Japan Proton Accelerator Research Complex (J-PARC) spallation facility [143, 144].

Another alternative is the use of direct laser light that generates proton or electron fluxes further impinging on final targets. The disadvantage of this method is that the particle fluxes are not mono-energetic, which complicates yield calculations for side products. For this reason, a laser facility would require careful optimization of the laser target-nuclear target setup, to obtain a minimum number of co-produced impurities. Theoretical work in this field has been done with promising results [145], yielding 300 GBq of ^{99m}Tc with 0.12% radionuclidic impurities in a 6 h irradiation assuming the utilization of the future International Coherent Amplification Network (ICAN) laser concept. However, in comparison to earlier mentioned advancements of particle accelerators, current laser-based ^{99m}Tc production research and infrastructure is not developed enough for short-term considerations.

Many other countries like Hungary, Saudi Arabia, India, Poland and many more are currently developing their non-HEU or cyclotron based $^{99}\text{Mo}/^{99m}\text{Tc}$ production programs and would be hard to present them all. Very good summary of the technical details of those projects is presented in “Final report of the coordinated research project On Accelerator-based Alternatives to Non-HEU Production of Mo-99/Tc-99m”. Current situation of the moly-99 supply chain and future perspective is well analysed in [137].

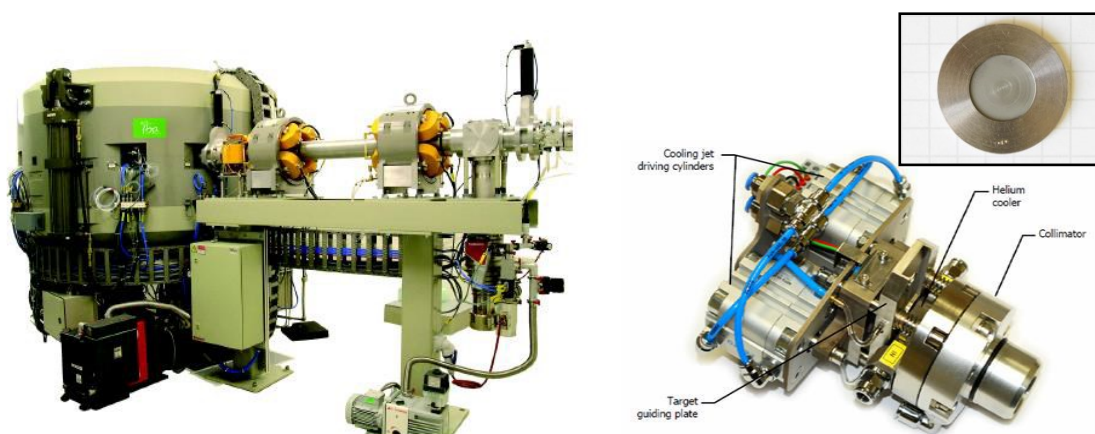


Figure 52 General views of the C-18 cyclotron with extracted beam pipe (left), COSTIS STS (right) and disc type target with compressed natural molybdenum powder (top-right) [146].

The concept of producing sufficient amounts of ^{99m}Tc from enriched ^{100}Mo targets using a cyclotron was first performed in the early 1970's [147]. At the time, the current capacity of fission produced ^{99}Mo for usage in handy $^{99}\text{Mo}/^{99m}\text{Tc}$ generators was deemed enough for years to come with further expansion of the nuclear reactor network to come. As a result, little work was undertaken on the development of this methodology. In the 1990's, several researchers again started the investigation of the nuclear data for proton induced reactions for molybdenum radionuclides, most notably $^{100}\text{Mo}(p,2n)^{99m}\text{Tc}$. The results renewed interest in the production of ^{99m}Tc using cyclotrons and set the optimum production energy using protons in the range of 13.5 – 17 MeV, with a recommendation to avoid higher energies resulting in the production of inseparable impurities such as ^{98}Tc , ^{97}Tc and ^{96}Tc [148].

Target design became the next milestone for successful cyclotron production of ^{99m}Tc , resulting in thick molybdenum coatings for solid targets able to withstand prolonged irradiation of high beam currents accompanied by an easy recovery of ^{99m}Tc and recycling of ^{100}Mo after end of beam [91, 92].

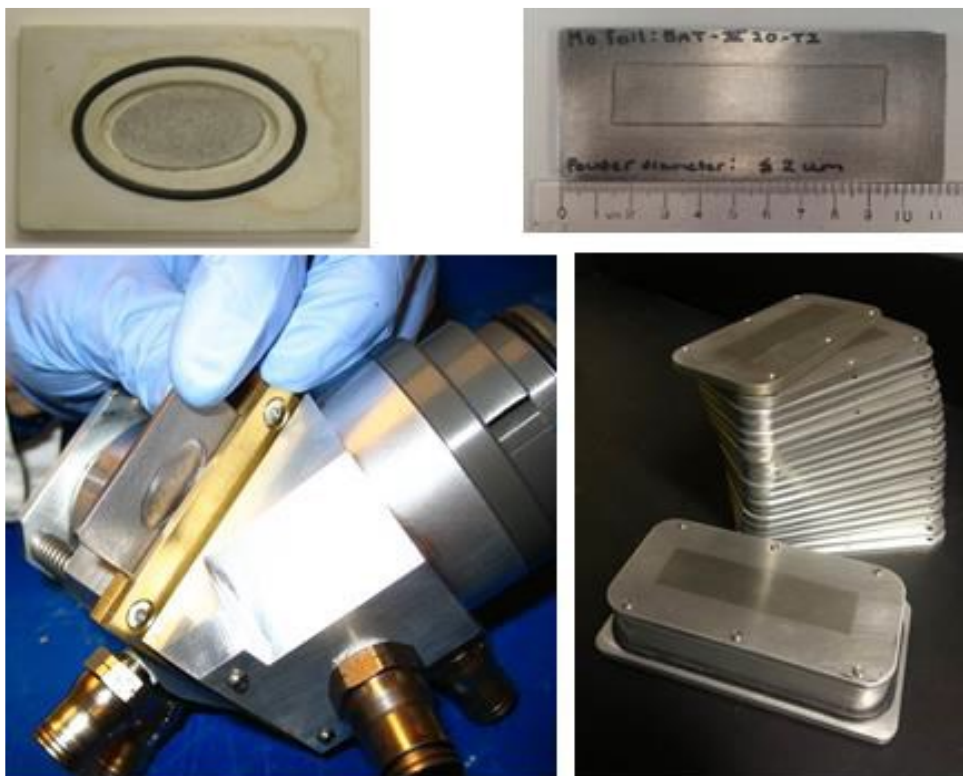


Figure 53 Pictures showing target concept transition from the small low-current TR-19 targets (left –top and bottom), to initial/preliminary foil studies (right - top), and present ARTMS and ACSI commercial high-current TR-24 targets (right - bottom) [146].

The worldwide leading group for the targetry, beam optimization and ion source studies are undoubtedly Canadian researchers gathered under the auspices of the TRIUMF national lab [64]. They used for ^{99m}Tc production the solid targets of enriched ^{100}Mo coatings which resulted in a production yield of up to approximately 513 MBq/ μAh . This further led to 350 GBq of ^{99m}Tc on an ACSI TR-19 cyclotron (6.9 h beam time, 300 μA beam, cyclotron beam energy lowered to 18 MeV protons) and about 170 GBq on GE PETtrace 880 (6 h beam, modified to 130 μA , 16.5 MeV protons). In the case of 18 MeV proton energy irradiations, which are slightly above the recommended energy range for ^{99m}Tc production, the target contained approximately 95% of ^{99m}Tc with 99.5% radionuclidic purity at EOB. The separation efficiency of ^{99m}Tc from a molybdenum target, which can be easily automated, was proved to be in the range of 80% - 90%. With the radiochemical purity of 99.7% of the final pertechnetate [^{99m}Tc]TcO₄ solution, the same U.S. Pharmacopeia (USP) quality requirements (> 95%) as for $^{99}\text{Mo}/^{99m}\text{Tc}$ generator produced pertechnetate are met. The final efficiency of ^{100}Mo recycling is above 90%. Other research groups have produced data on similar experiments that agree with these results [149-151].

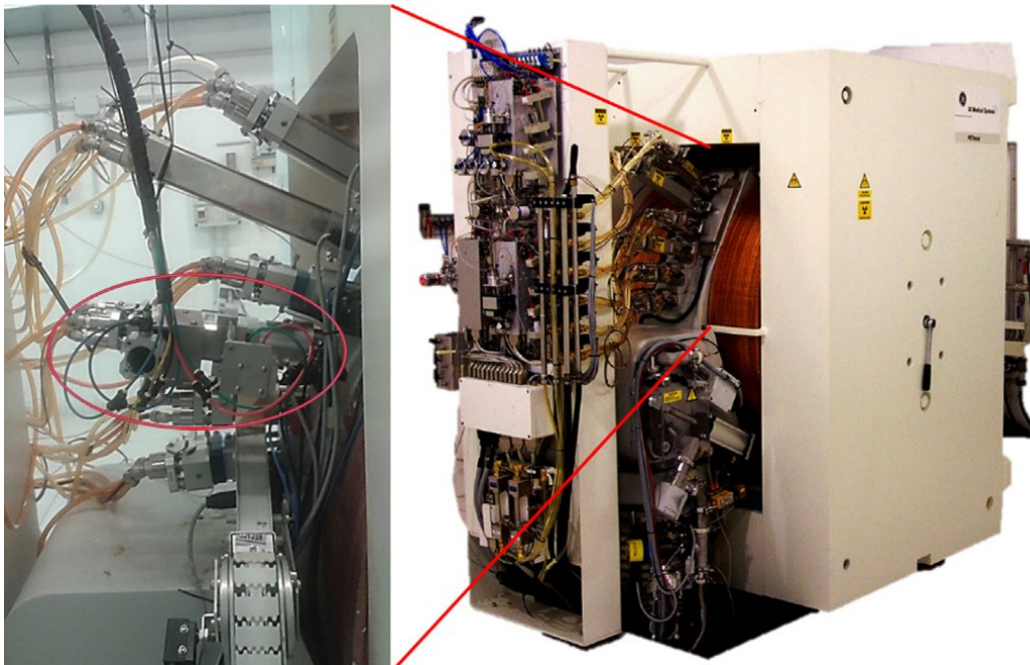


Figure 54 The Solid Target Station assembled with GE-PETtrace cyclotron used for ^{99m}Tc production [150].

Such capacity can satisfy a daily demand for a large area, thus encouraging the Canadian government to co-finance and support The Canadian National

Cyclotron Network project, run by ACSI, which will cover 100% of Canadian needs for ^{99m}Tc (ACSI, n.d.). The project was scheduled to be finalized before closure of the Chalk River nuclear reactor, once one of the leading suppliers of ^{99}Mo , operated as a back-up plant until its closure in March 2018. The project is ongoing, facing several delays caused by regulatory approval issues and logistics considerations [152], but some Canadian nuclear medicine patients are already scanned with cyclotron produced ^{99m}Tc .

The Canadian consortium led by University of Alberta cooperating with Advanced Cyclotron Systems Inc. (ACSI) and the Centre Hospitalier Universitaire de Sherbrooke (CHUS) initiated two new cyclotron facilities, the Medical Isotope and Cyclotron Facility (MICF, Edmonton, AB) and the Centre d'imagerie moléculaire de Sherbrooke (CIMS, Centre Hospitalier Universitaire de Sherbrooke, QC), to help address the expected problems in the supply of $^{99}\text{Mo}/^{99m}\text{Tc}$ generators from aging nuclear reactors. This project demonstrated that cyclotron-produced ^{99m}Tc is feasible and successful implemented of a cyclotron laboratory with associated GMP facility producing cyclotron-based ^{99m}Tc . The processes leading to the final production scheme, as well as $^{99m}\text{Tc}/^{100}\text{Mo}$ separation were developed. Although initially developed for a 19 MeV cyclotron (TR-19) and 100 μA beam current, results were successfully translated to use a higher power cyclotron (TR-24, $E_p=24$ MeV @ 500 μA) in order to meet the needs of a larger patient population (EOB $^{99m}\text{Tc} \approx 1.5$ TBq, experimentally measured saturated yield 6.1 ± 0.2 GBq/ μA .) [146].



Figure 55 The TR-24 cyclotron at MICF (left). One of the two high current target stations in its dedicated “cave” at MICF (right). Having two target stations not only provides redundancy and reliability for ^{99m}Tc production, but also helps to reduce dose received by operators and engineers during maintenance.

In May 2017, Alliance Medical announced that it will use the ACSI and ARTMS technology to supply UK hospitals with ^{99m}Tc and expects to deliver the first doses in 2020. Alliance Medical is finalizing installation of the new ACSI TR-24 cyclotron to make ^{99m}Tc at its facility in Dinnington and will begin production in 2020. If the UK's Medicines and Healthcare products Regulatory Agency gives it the green light for clinical use, a second cyclotron will follow. Both cyclotrons should make enough ^{99m}Tc to cover the vast majority of the UK's needs i.e. more than 600,000 imaging procedures per year.

Canadian ARTMS provides whole range of the solid targets (coins, plates etc.), not only ^{100}Mo , that can be used all around the world for production of radiometals and ^{99m}Tc in highly efficient cyclotron systems like ACSI TR-24 or smaller medical accelerators equipped with COSTIS STS or custom made coin targets stations.

In 2016 PETIC started new project in cooperation with TRIUMF and IBA to determine whether it is possible to produce sufficient quantities of ^{99m}Tc using the $^{100}\text{Mo}(p,2n)^{99m}\text{Tc}$ reaction on IBA CYCLONE® 18/9 cyclotron equipped with a COSTIS solid target system using the targets developed by TRIUMF. Initial meeting took place in September 2016 at World Target and Target Chemistry conference at Los Alamos. Some Environmental Permitting Regulations needed to modify permit granted by Natural Resources Wales (NRW) to enable work to proceed. Ionising Radiation Regulations needed to update Risk Assessments in areas where work was to be undertaken.



Figure 56 Modified water and He cooling of the COSTIS STS.

Technically, the project required small modifications to the cyclotron to eliminate the target degrader and bypassing the He cooling to obtain the maximum beam energy of 18 MeV on target. IBA also provided additional water cooling (Figure 56) that increased the water flow from 4 l/min up to 6 l/min to overcome the missing He cooling which allowed solid targets irradiations with currents of up to 50 μA (max. 20 μA current was used before). It is important to be aware that improved water cooling enables usage of higher currents (up to 50 μA) only in case of the lack of He cooling and beam degrader. When degraders like Nb disc thicker than 300 μm are used then target current is recommended to be set not higher than 30 μA because He cooling is not effective enough to provide heat transfer from thicker discs. Currents higher than 30 μA on degraders thicker than 300 μm can cause fractures caused by overheating and vacuum loss after less than 3 hours of the beam time.

The scope of this project was to confirm that the ARTMS/TRUMF targets could be irradiated on the IBA CYCLONE[®] 18/9 cyclotron and COSTIS solid target, and also to confirm that the yields were comparable to those predicted by TRIUMF and achieved by other research groups [146]. The project scope did not include target processing or Technetium separation after cyclotron production and gamma spectroscopy measurements were impossible due to the high radiation flux from the target.

The aim of this section was to utilise the FLUKA models developed and validated with ⁸⁹Zr and ⁴⁸V to explore the cyclotron production of ^{99m}Tc and compare its results with other models like the one developed by Celler et al. [153] to estimate radioisotope by-products, ^{99m}Tc yields and possible routes of improvement for this production.

Materials and Methods

Environmental Permitting Regulations require the need to determine product radionuclides, daughter radionuclides and likely yields from nuclear reaction. Technetium-99m can be made using a hospital's medical cyclotron to bombard molybdenum with a proton beam, causing the transmutation of some of the molybdenum-100 nuclei into ^{99m}Tc. However, molybdenum-100 enriched targets are expensive, and the technique produces other unwanted isotopes that reduce the diagnostic benefit for the patient. The viability of the technique must therefore be carefully inspected – however, doing experiments is extremely expensive. Before

PETIC received its permit for technetium-99m production studies, it used the theoretical model developed by *Celler et al.* [153] that predicts the viability of the method and estimates logistical parameters, such as the number of cyclotron runs needed to meet the daily demands of a typical nuclear medicine department. The reaction conditions needed for optimal yields, such as beam energy and target geometry, were also identified. The nuclear-reaction model code EMPIRE-3 calculates the cross-section, or probability, of each of the possible molybdenum–proton reactions, across an energy range of 6–30 MeV. The simulation confirmed that the numerous molybdenum–proton reactions produced multiple contaminants, including several technetium, molybdenum, niobium and zirconium isotopes. Together with the yield calculations, the EMPIRE-3 simulation also demonstrated that only molybdenum targets enriched with molybdenum-100 were viable for efficient technetium-99m production. Natural molybdenum, with its composition of several isotopes, produced significant amounts of contaminant isotopes. *Celler et al.* also identified 16–19 MeV as the optimal proton energy range for ^{99m}Tc production. In this range, relative ^{99m}Tc yields were greatest when compared with contaminant isotopes. Shorter, multiple molybdenum-100 irradiation cycles per day, each 3–6 hours long, also proved to be the most efficient production schedule.

Nuclear reactions modelled by *Celler et al.*:

Main Channel $^{100}\text{Mo}(p,2n)^{99m}\text{Tc}$

Additional Reaction $^{100}\text{Mo}(p,pn)^{99}\text{Mo} \rightarrow ^{99m}\text{Tc}$

also need to account for other reactions on ^{100}Mo (Figure 57) and other Mo isotopes (Figure 58). These will be some (p,n) reactions produced during irradiation (Figure 58) and also will see (p,2n) reactions as well (Figure 59).

Although a wide range of radionuclidic impurities would be generated, ^{99m}Tc dominates. Significant quantities of ^{99}Mo are produced alongside trace amounts of other impurities produced including ^{97m}Tc having 91-day half-life and decaying by isomeric transition emitting a gamma ray at 97 keV.

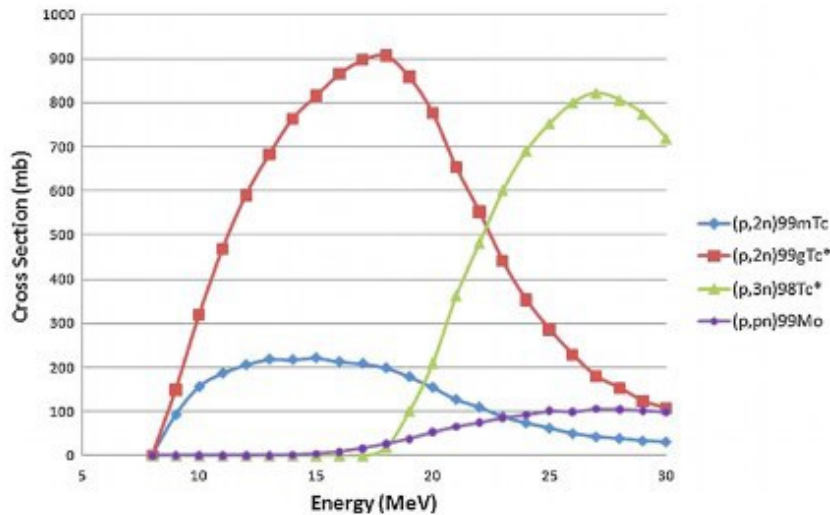


Figure 57 Excitation functions corresponding reaction products with the highest cross sections in the investigated energy range (stable isotopes are marked by the asterisk) for ^{100}Mo irradiation with beam of protons [153].

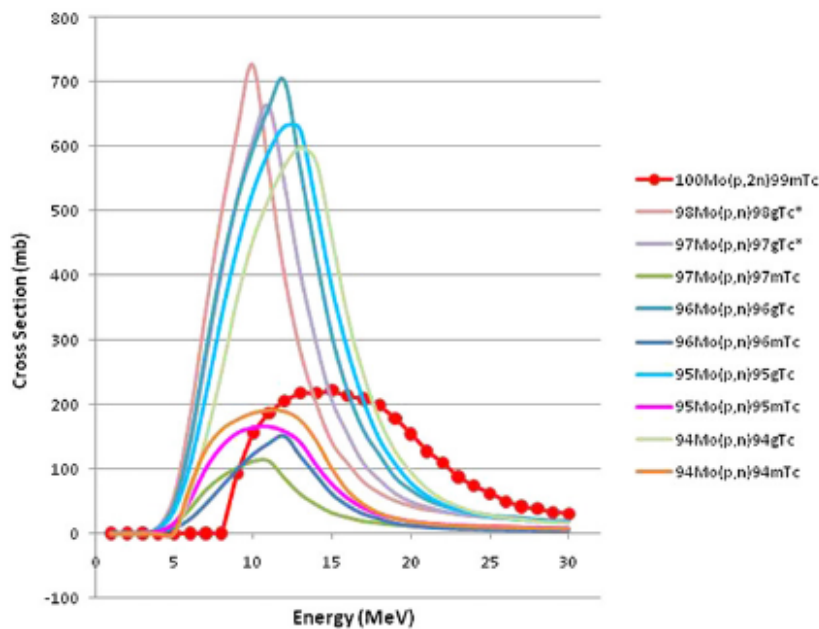


Figure 58 Comparison of the $^{100}\text{Mo}(p,2n)^{99\text{m}}\text{Tc}$ excitation function to the six other technetium isotopes (isomeric and ground states) which are produced through the (p,n) reaction. The excitation function for $^{99\text{m}}\text{Tc}$ is marked with red circles and stable isotopes are marked by an asterisk [153].

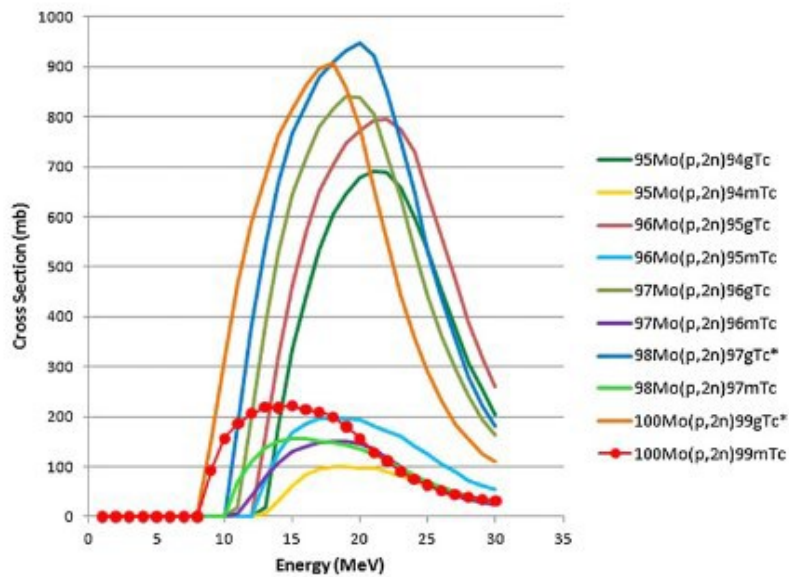


Figure 59 Comparison of the $^{100}\text{Mo}(p,2n)^{99\text{m}}\text{Tc}$ excitation function to the other radioactive and stable technetium isotopes (isomeric and ground states) which are produced through the (p,2n) reaction. The excitation function for $^{99\text{m}}\text{Tc}$ is marked with red circles and stable isotopes are marked by an asterisk [153].

PETIC applied to Natural Resources Wales (NRW) to alter its open source permit to increase $^{99\text{m}}\text{Tc}$ holding limit from 2.1 GBq to 500 GBq. Other radionuclides, excluding alpha emitters was increased from 0.3 GBq to 100 GBq. NRW did not approve the irradiation of a natural molybdenum target.



Figure 60 Mo targets sintered on Cu backing provided by TRIUMF.

Risk assessments did not show any significant additional risk related with technetium-99m production comparing to standard ¹⁸F productions as the shielding for 511 keV would be more than sufficient for the 140 keV gamma rays. Each irradiation expected to produce between 50-100 GBq of ^{99m}Tc. Shielding in all areas designed for 200 GBq of ¹⁸F.

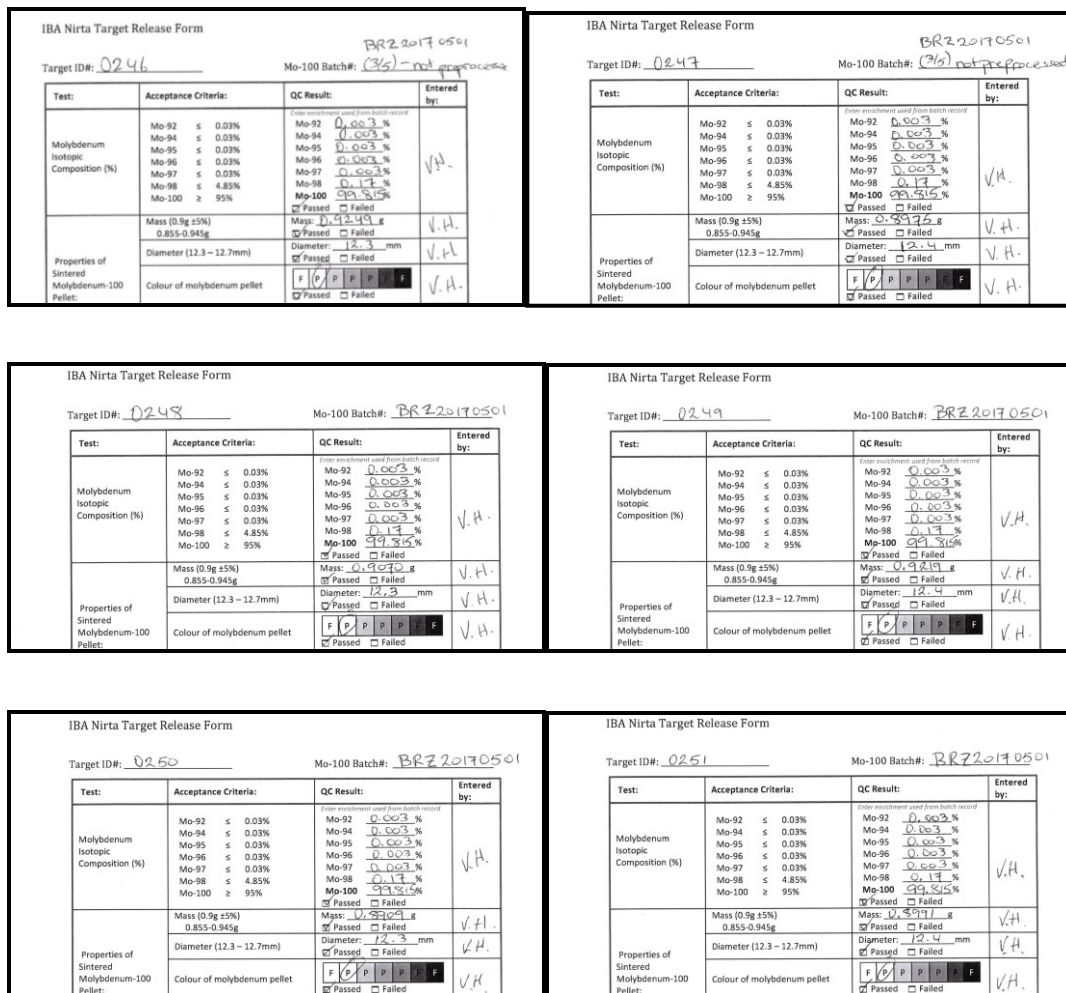


Figure 61 Composition of Mo targets sintered with Cu backing, provided by TRIUMF.

In November 2016, TRIUMF supplied natural Mo targets sintered with copper backing to ensure the system could load and unload the target disks (Figure 60). Due to restrictions imposed by Natural Resources Wales, PETIC was not permitted to irradiate these targets. The original Molybdenum target insert sputtered on Copper back plate was found to be slightly too large and prevent the vacuum being maintained on the target. As a result, the diameter of Mo insert was reduced from 12.5 mm to 12 mm and modified targets were supplied to PETIC. After the

modifications, target loading, and unloading was repeated with new target successfully.

In February 2017, irradiations of 6 enriched targets were undertaken in PETIC in presence of representatives from TRIUMF and IBA: 3 x 1 hour at 50 μ A and 3 x 6 hour at 50 μ A (6 discs with of ^{100}Mo targets 99.815% enriched were irradiated).

Irradiated discs were unloaded, transferred to a research hot cell and measured in a Capintec CRC 25R dose calibrator set at calibration factor 90. Repeated every 5 minutes measurements were taken using NPL data logging software. Activities were decay corrected to End of Beam (EOB) time assuming a 6 h half-life. For EOB activity calculation, measurements 24 h after end of production were used. Due to the high radiation flux, it was not possible to measure the gamma spectrum. No attempts were made to measure gamma spectrum earlier than 2 years after EOB. Targets were visually assessed for damage post irradiation.

The range of examples with proton beam energies across the range of 18→11.6 MeV were simulated with FLUKA model to validate the M-C model for $^{99\text{m}}\text{Tc}$ production and check potential reduction of impurities generated in productions with lower energy beam.

Simulated Irradiations of the TRIUMF type targets with range of proton beams with energies reduced below 18 MeV were done by use of set of Niobium degrader discs of different thicknesses L_{Nb} (50, 100, 150, 200, 250, 300 μm). The use of He cooling (only were Nb degraders were used) was also simulated using FLUKA CG model.

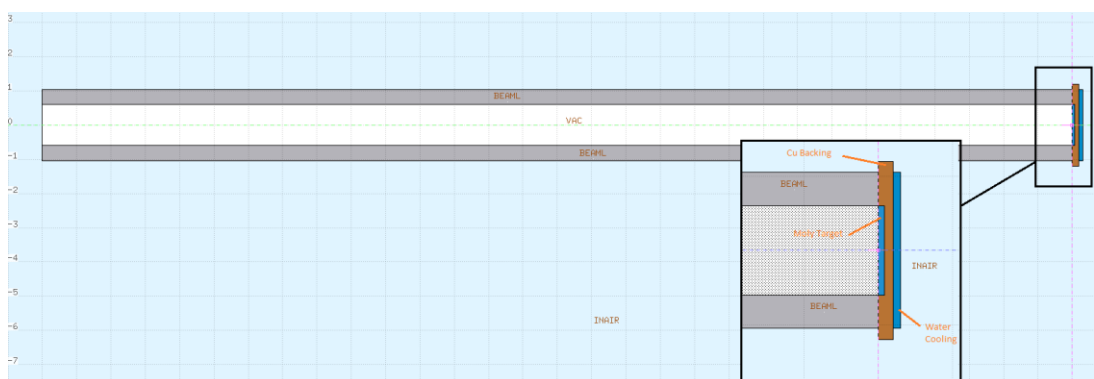


Figure 62 View of the geometry simulated in FLUKA for $^{99\text{m}}\text{Tc}$ production at beam energy 18 MeV without He cooling and Nb degrader.

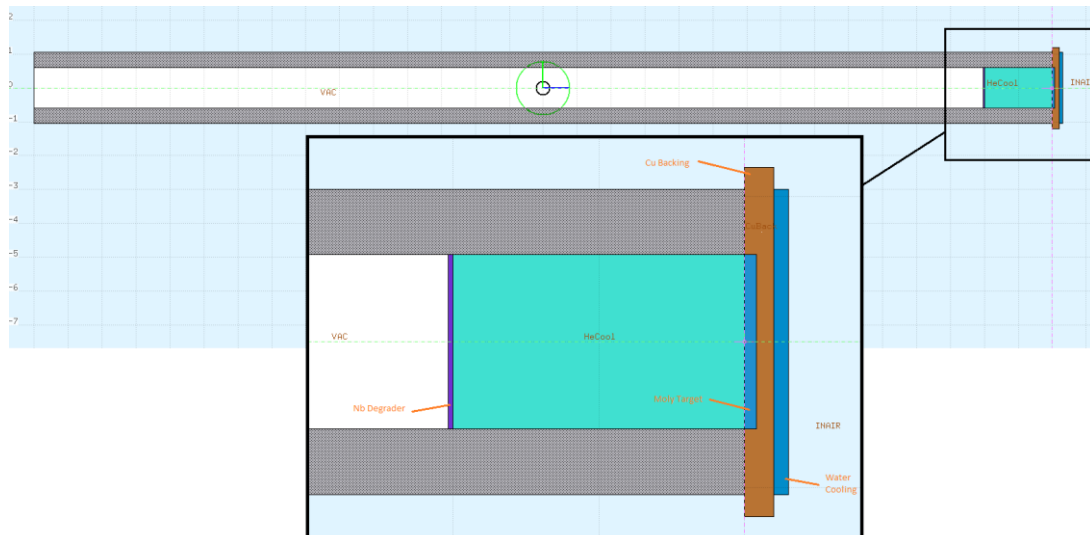


Figure 63 View of the geometry simulated in FLUKA for ^{99m}Tc production at beam energy lower than 18 MeV with He cooling and Nb degrader.

Results

Experimental irradiations of the TRIUMF ¹⁰⁰Mo targets with 18 MeV proton beam of IBA cyclotron were correct with no symptoms of damage or overheating. Basic parameters logs show stable performance for all six irradiations (Figure 64).

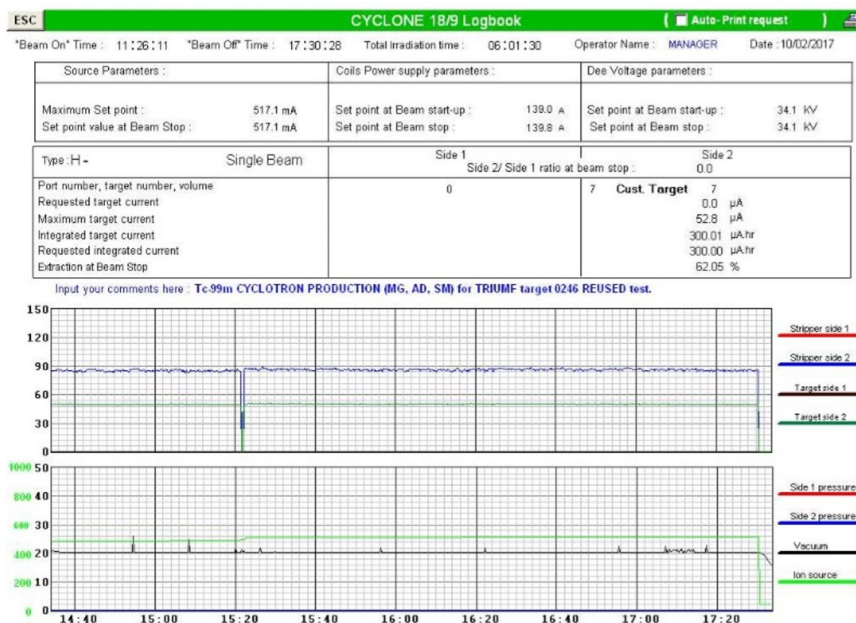


Figure 64 Example of a 6-hour irradiation demonstrating stable cyclotron performance during ^{99m}Tc production

After 1-hour irradiations mean activity produced for each irradiated target disc was 16.1 ± 0.9 GBq of ^{99m}Tc . The 6-hour irradiations produced average 80.2 ± 6 GBq of ^{99m}Tc per disc. Values for each disc are shown in Table 8.

Activity measurements 4 days after production on 6-hour irradiation targets showed less than 500 MBq present.

Table 8 Productions of technetium-99m from moly-100 done in February 2017 in PETIC.

Disc Number	Irradiation Time [h]	EOB [hh:mm]	Activity @ EOB [GBq] (18MeV, 50 μA)
			(Accuracy $\pm 5\%$)
0246	6	17:30	76.4
0247	1	15:08	15
0248	6	13:24	75.0
0249	1	11:48	17.4
0250	1	17:32	15.9
0251	6	12:54	89.2

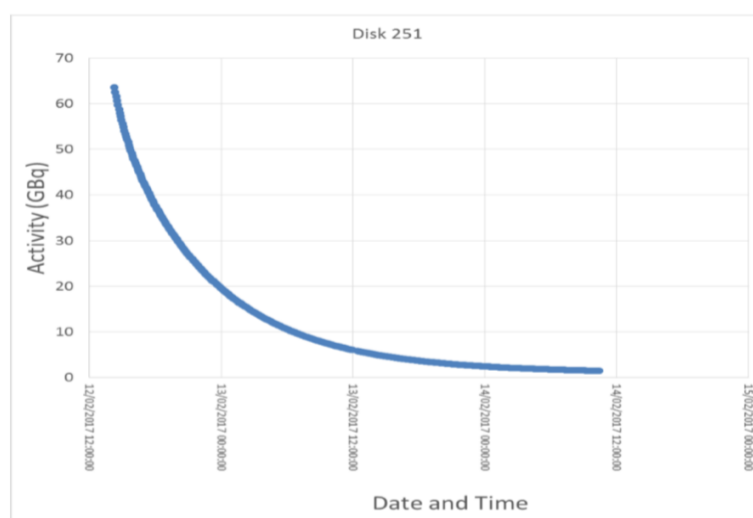


Figure 65 Example of the activity and half-life measurement log used for EOB activity estimation of ^{99m}Tc produced in 6-hour irradiation.

There was no visual evidence of significant damage or degradation post irradiation in the STS or target discs (Figure 66).



Figure 66 COSTIS STS and target discs after irradiations showing no visual evidence of damage

Figures 67 - 69 show results of FLUKA simulations.

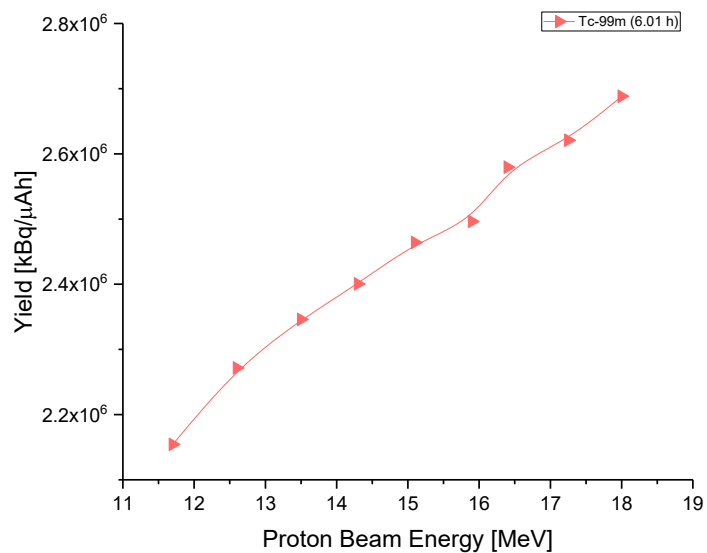


Figure 67 Results of the FLUKA simulation for the TRIUMF ^{100}Mo target irradiation with the proton beams 18 → 11.6 MeV (linear scale for yield axis) for $^{99\text{m}}\text{Tc}$ with highest yield and 6.01 h half-life (shown in brackets).

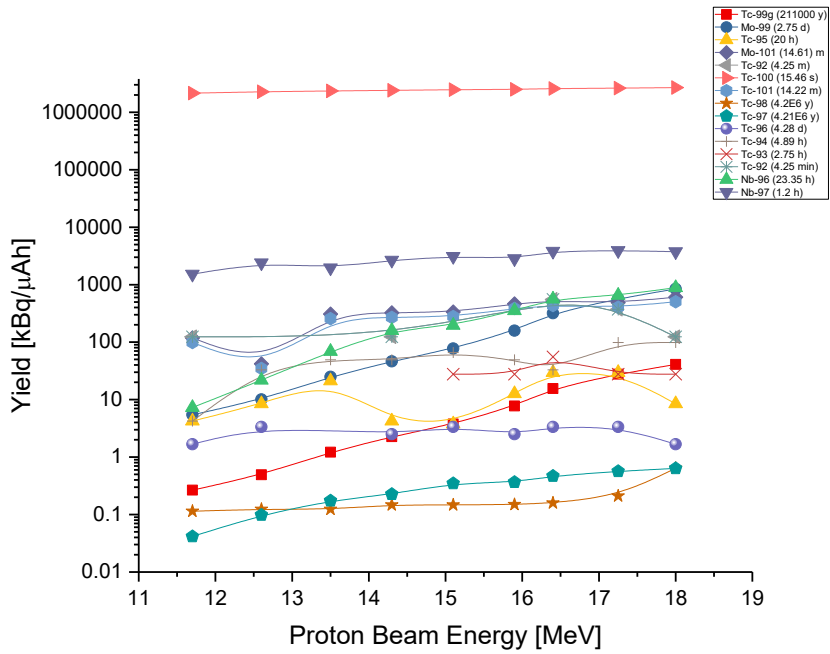


Figure 68 Results of the FLUKA simulation for the TRIUMF ¹⁰⁰Mo target irradiation with the proton beams 18 → 11.6 MeV (log scale for yield axis down to 0.01, half-lives given in brackets).

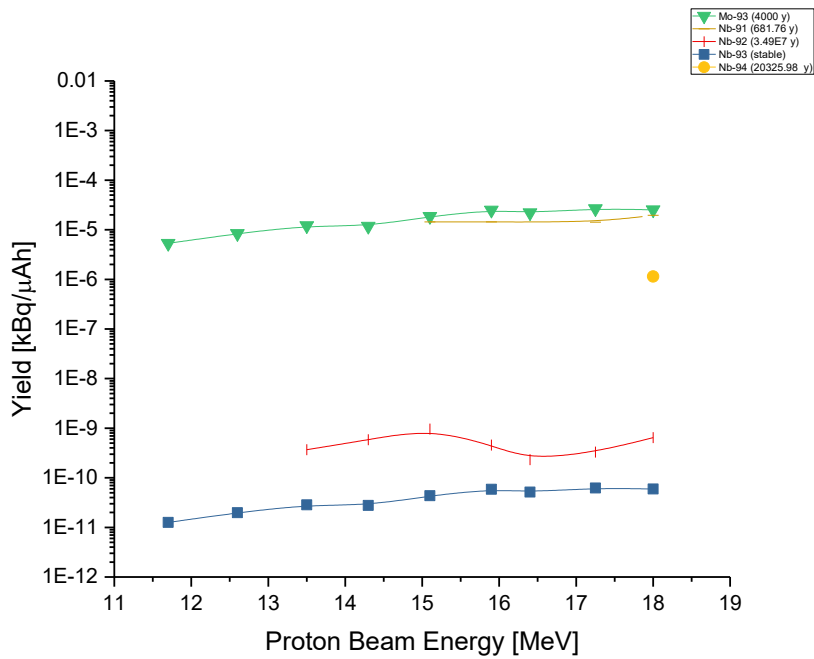


Figure 69 Results of the FLUKA simulation for the TRIUMF ¹⁰⁰Mo target irradiation with the proton beams 18 → 11.6 MeV (log scale starts with 0 and ends with 0.01 for yield axis, half-lives given in brackets).

Discussion

The mean value of the yield calculated (295 MBq/ μ Ah) from activities presented in Table 1 that are results of the test productions done in PETIC in 2017 fully agree with data presented by ARTMS on their website (artms.ca/targets):

~39 Ci (1443 GBq) @ EOB (24 MeV, 500 μ A, 6 h) \rightarrow 481 MBq/ μ Ah

~13.9 Ci (514.3 GBq) @ EOB (18 MeV, 300 μ A, 6 h) \rightarrow 286 MBq/ μ Ah

~4.7 Ci (173.9 GBq) @ EOB (16.5 MeV, 130 μ A, 6 h) \rightarrow 223 MBq/ μ Ah.

However, some ARTMS activity values for production of ^{99m}Tc are higher as the first two lines present results achieved for beams with high currents available at the machines like ACSI TR-24, IBA CYCLONE[®]KIUBE or C-30 equipped with high current inclined targets not like max 50 μ A target current COSTIS STS. Also, energies like 24 MeV are available only for bigger accelerators used rather in commercial sites or national labs. Value of the yield for 18 MeV proton beam calculated for value presented in line two is almost identical with yield achieved in PETIC. For coin targets ARTMS uses the same amount of moly-100 enriched material ~0.9 g like the targets used in PETIC then comparison is straight forward.

IBA advertising its new CYCLONE[®]KIUBE together with COSTIS STS gives a theoretical value for yield 95 mCi/ μ Ah (3.515 GBq/ μ Ah) @ 18 MeV (iba-radiopharmasolutions.com). Their standard runs also last 6 h, but the yield value seems to be much overestimated even considering that they are not mentioning amount of moly used in their targets. Increasing the moly thickness to improve the yield (COSTIS coin targets) makes sense only in some narrow range as the ^{99m}Tc extraction might be problematic. For high yield productions better is to use large surface inclined targets like ones used in STS HighPIT Model PI01 from Elex Commerce or other inclined high current stations used by ARTMS and ACSI at TR-24, also heat transfer is better for those targets.

The experimental yields received in PETIC in 2017 seems to be almost half of the values presented in IAEA publication (Figure 70) about cyclotron production of ^{99m}Tc [135]. It might be caused by bigger amount of used moly-100. However, Figure 67 shows very well how yield depends on beam energy and irradiation time and looks very alike Figure 70 for 1 h irradiation. It is also seen that so-called thick target yields energy trends are different than excitation functions where maximum

yield energy is not always the same as the maximum cross section energy (Figure 57, Figure 67 and Figure 71).

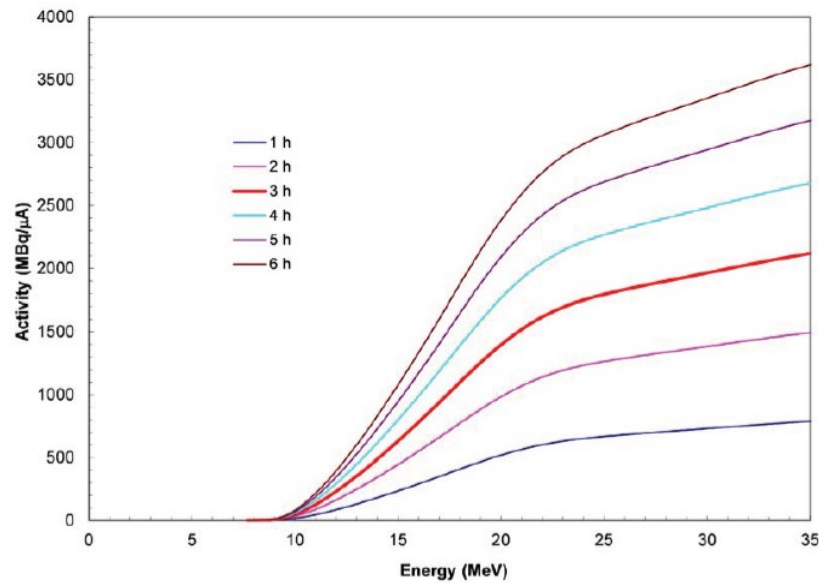


Figure 70 EOB yields as a function of beam energy and irradiation time [135].

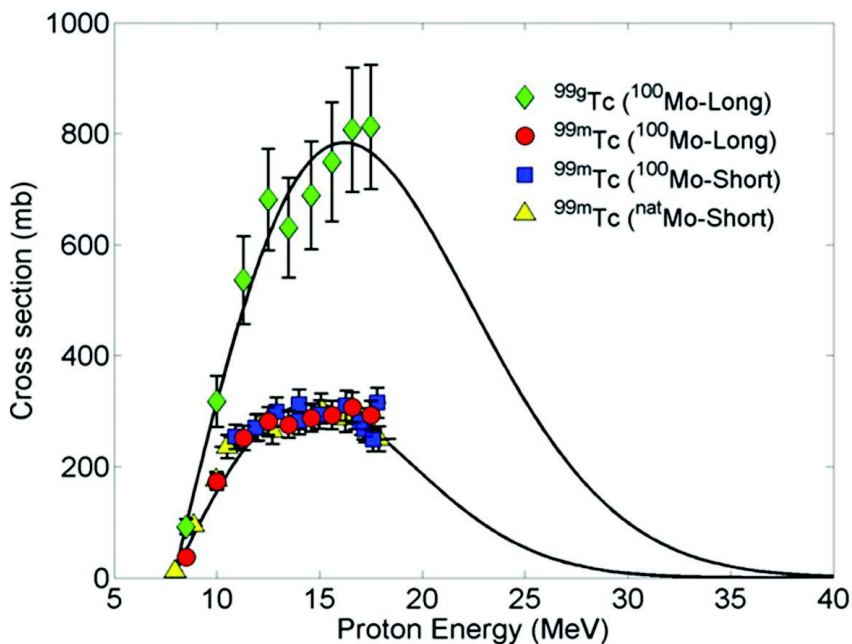


Figure 71 Experimental excitation function for the $^{100}\text{Mo}(p,2n)^{99g}\text{Tc}$ and $^{100}\text{Mo}(p,2n)^{99m}\text{Tc}$ reactions. The 'Short' designation refers to irradiations of $1\ \mu\text{A}$ for 600 seconds while the 'Long' indicates irradiations lasting 10 hours at $20\ \mu\text{A}$. The ^{100}Mo had an enrichment of 97.5% while natural Mo was of natural composition — enrichment of $^{100}\text{Mo}=9.63\%$ [154].

The volume of the simulated moly target in the FLUKA model is slightly bigger than the volume used in experimental runs. It was caused by difference between first batch of natural moly/copper test discs and batch of targets used for irradiations that consist ~0.9 g of moly-100 (Figure 60). Simulated targets consist 8.397 g of moly-100. Taking it into account and dividing maximal simulated yield value by factor of 9.33 (8.397/0.9) we receive 288 MBq/ μ Ah which is in good agreement with experimental 295 MBq/ μ Ah yields. Figure 67 shows how the yield of ^{99m}Tc depends on energy for the simulated range of energies and 288 MBq/ μ Ah represents the yield for 18 MeV of proton beam energy. Energy of 18 MeV is maximal for C-18 cyclotron and optimal for ^{99m}Tc production what is seen comparing ^{99m}Tc yields with yields of other isotopes presented in the Figures 68 and 69 that are at least 10000 times lower within the whole range of simulated energies. Comparing this with results of studies done by Gagnon et al. [146], where energy was also reduced down to 18 MeV, we got quite good agreement with those values that were 169 MBq/ μ Ah (less moly-100 used for target material). Values received by TRIUMF team shows even better agreement for ~242 MBq/ μ Ah at TR-19 with 18 MeV beam and 223 MBq/ μ Ah at GE PETtrace with 16.5 MeV beam that corresponds to 277 MBq/ μ Ah simulated by FLUKA for analogical target irradiated at 16.6 MeV [64, 146]. Small differences might be result of slightly different moly-100 enrichment levels, the stability of the beam current for long irradiations and different amounts of used target material (\pm few grams). It is hard to find exact masses of the used Molybdenum for mentioned reports, but looking at the Figure 67 and 70, expected differences seem to be not high.

In Figure 68 and 69 the logarithmic scales were used to visualize better the yields of other isotopes. The lowest yields' values are seen in the Figure 48 for $^{91-94}\text{Nb}$ isotopes and ^{93}Mo that are stable or have relatively long half-life comparing to ^{99m}Tc . Niobium isotopes can be removed by chemical separation methods. Additionally, Niobium impurities and Moly-93 yields seen in the Figure 69 are less than 10^{-8} % of ^{99m}Tc yields for the simulated energy range of proton beams.

The major radioactive contaminants seen in the Figure 68 are $^{99,101}\text{Mo}$, $^{96,97}\text{Nb}$, $^{92,93,94,95,96}\text{Tc}$ and $^{97,98,99g}\text{Tc}$ where last three can be considered as stable and represent very low part of the total technetium radioactivity (less than 10^{-7} %).

Most of the potential impurities listed in the USP (United States Pharmacopeia) and the EU Pharm (European Pharmacopoeia) are specific to the $^{99\text{Mo}}/^{99\text{mTc}}$ generator production route (such as iodine-131, strontium-98, strontium-90, and ruthenium-103). However, the limit for molybdenum-99 can be used

regardless of the production method for pertechnetate [146]. The USP limit is 0.015% of moly-99, whereas the EU Pharm limit is 0.1% of Moly-99. For results of FLUKA simulation we received moly-99 amounts of 0.032 % at 18 MeV and 0.031% at 16.6 MeV, what makes them acceptable in Europe.

Table 9 Technetium isotopes produced in proton bombardment of ^{100}Mo enriched target material. Dosimetry associated with each of these isotopes also listed. Data presented by Ruth et al. in [146].

Tc isotope	Half-life	Emission energies (intensity) (keV (%))	Patient Dose (Sv/MBq)	Remarks
$^{93\text{m}}\text{Tc}$	43.5min	511 (4.5); 2644.58 (14.3)	8.73	Not considered in imaging study because of short half-life.
$^{93\text{g}}\text{Tc}$	2.75h	1362.9(66.2); 1520.3 (24.4)	7.82	Considered in imaging study
$^{94\text{m}}\text{Tc}$	52min	511(140); 871(94.2)	51	Not considered in imaging study because of short half-life.
$^{94\text{g}}\text{Tc}$	4.88h	702.7 (99.6); 849.7 (95.7); 871.1 (99.9)	96.6	Considered in imaging study
$^{95\text{m}}\text{Tc}$	61d	204.1(63.2); 582.1(30); 835.2 (26.6)	187	Considered in imaging study
$^{95\text{g}}\text{Tc}$	20d	765.8 (93.8)	77.7	Considered in imaging study
$^{96\text{m}}\text{Tc}$	51.5min	1200.2 (1.1)	1.79	Not considered in imaging study because of short half-life and weak gamma emission.
$^{96\text{g}}\text{Tc}$	4.28d	778.1 (99.8); 812.5 (82); 849.9 (98); 1126.9 (15.2)	446.0	Considered in imaging study; The worst impurity which highly increases patient dose.
$^{97\text{m}}\text{Tc}$	91d	96.5 (3)	145	Not considered in imaging study Gamma has low energy cannot be detected in 140 keV window.

Impurities mentioned by Gagnon et al. in [146] for the $^{100}\text{Mo}(p,2n)$ derived pertechnetate are $^{94\text{m}}\text{Tc}$, $^{94\text{g}}\text{Tc}$, ^{95}Tc , ^{96}Tc , $^{93\text{m}}\text{Tc}$, $^{93\text{g}}\text{Tc}$, $^{95\text{m}}\text{Tc}$, $^{97\text{m}}\text{Tc}$, ^{96}Nb , and ^{97}Nb . These radioisotopic impurities are almost the same as presented in Figure 68 and listed in Table 9, and are most easily controlled through reasonable selection of the isotopic impurities in the enriched ^{100}Mo used for the target [155]. However, FLUKA generated additional ^{101}Mo not mentioned by the other authors and does not distinguish between isomeric states and treats for example $^{94\text{m}}\text{Tc}$ and $^{94\text{g}}\text{Tc}$ as the same ^{94}Tc isotope.

For processed targets when small enough sample can be taken, radionuclidic purity can be assessed by gamma ray spectroscopy where the spectrum should be identical to that of a pre-qualified $^{99\text{m}}\text{Tc}$ standard that exhibits a major photopeak with an energy of 140 keV and/or 6.02 h half-life.

Radionuclidic purity may include an assessment for non-technetium as well as technetium radioisotopes. For non-technetium radioisotopes, the European Union Pharmacopoeia mentions possible contamination of generator derived $^{99\text{m}}\text{Tc}$ with ^{99}Mo and other radioisotopes. In addition, and depending on the quality of the ^{100}Mo target, cyclotron produced $^{99\text{m}}\text{Tc}$ might be contaminated by the following radioisotopes:

^{91}Zr ;
 $^{91\text{g}}\text{Nb}$, $^{93\text{g}}\text{Nb}$, $^{94\text{g}}\text{Nb}$, $^{95\text{m}}\text{Nb}$, $^{95\text{g}}\text{Nb}$, ^{96}Nb , ^{97}Nb ;
 $^{91\text{g}}\text{Mo}$, $^{93\text{g}}\text{Mo}$, ^{94}Mo , ^{95}Mo , ^{96}Mo , ^{97}Mo , ^{98}Mo , ^{99}Mo ;
 ^{99}Ru , ^{100}Ru , ^{101}Ru .

A precise analysis using gamma spectroscopy is needed for their identification and quantification [135]. Using this method, the percentage amounts of ^{96}Tc and ^{95}Tc have been specified by *Lapi* [156]. FLUKA simulated values are $6.2 \times 10^{-7} \%$ for ^{96}Tc and $3.1 \times 10^{-6} \%$ for ^{95}Tc . Looking at the values from Table 10, we can find a good agreement for ^{95}Tc amounts and huge underestimation for ^{96}Tc . However, comparing FLUKA results with values of cross sections presented by *Celler et. al.* [153] (Figure 68) we can see that values for 18 MeV for ^{96}Tc and ^{95}Tc are very close each other but percentage values are slightly different ($6.4 \times 10^{-5} \%$ for ^{96}Tc and $1.7 \times 10^{-4} \%$ for ^{95}Tc at 19 MeV).

Table 10 Average isotopic impurities at EOB. Values expressed in percentage relative to $^{99\text{m}}\text{Tc}$ [156].

$^{99\text{m}}\text{Tc}$	^{96}Tc	^{95}Tc
100%	0.08 %	$8.6 \times 10^{-6} \%$

However amounts of isotopic impurities seems to be at the same level as presented by other authors and passing criteria proposed in IAEA CRP reports for Accelerator-based Alternatives to Non-HEU Production of Mo-99/Tc-99m [135, 146] (Table 11 and 12).

Table 11 Acceptance limits and procedures to control the radionuclidic and chemical purity of cyclotron produced ^{99m}Tc [135].

	Acceptance limits	Determined by	Procedure
Radionuclide identity	Half-life between 5.72 and 6.32 h	Half-life determination	United States Pharmacopoeia <821>
	Main emission peaks: 0.141 MeV	Gamma spectrometry	European Pharmacopoeia
Radionuclidic purity	Proposed: Radioisotopic purity >99.5%	Gamma ray spectrometry	
	No gamma ray peaks at 569 keV (^{96}Nb), 658 keV (^{97}Nb), 739 keV (^{98}Mo) are detected		
	Isotopes other than ^{99m}Tc contribute an emission rate of less than 6 000 emissions per second per MBq of ^{99m}Tc	Modified Mo shield assay	
	Not more than: 0.005 % ^{99}Mo 0.005% ^{96}Nb 0.005% ^{97}Nb 0.01% ^{93m}Tc 0.04% ^{93}Tc ; ^{94}Tc 0.02% ^{94m}Tc 0.07% ^{95}Tc 0.07% ^{96}Tc 0.05% ^{95m}Tc 0.01% ^{97m}Tc 0.02% of other gamma impurities	Gamma spectrometry	European Pharmacopoeia (draft version)
	Rf = 0.8–1.0	TLC-radiometric	
	Rf > 0.7	TLC	
	Rf = 0.8	Ascending paper chromatography	
	≥95%	TLC-radiometric	
	>95%	Ascending paper chromatography	
	Aluminium content < 10 µg/mL of solution (10 ppm)	Colorimetric assay	
Mo content < 30 µg/mL of solution (30 ppm)	Photometric assay		
Hydrogen peroxide content < 50 µL/mL of solution (50 ppm)	Colorimetric assay		
Aluminium ≤ 5,000 ppm Ethanol ≤ 5,000 ppm	USP monograph on residual solvents		
Not more than: 5 µg/ml Pb, Al, Ba, Ni 10 µg/ml B, Zn 20 µg/ml Si, Mg, Ca	Spectrometry ICP-OES in-house method		

Table 12 Proposed specifications for cyclotron produced pertechnetate [146].

Parameter	Acceptance Criteria	Test Method
Visual Appearance	Clear, colourless, no particles	Visual Inspection
Radionuclidic purity	Isotopes other than ^{99m}Tc contribute an emission rate of less than 6,000 emissions per second per MBq of ^{99m}Tc	Modified Molybdenum shield assay
Radionuclidic identity	Half-life between 5.72 and 6.32 hours or main gamma photopeak at 140 keV	USP <821> Half-life determination or gamma spectroscopy
Radiochemical purity	$\geq 95\%$	TLC-Radiometric
Radiochemical identity	Rf = 0.8 - 1.0	TLC-Radiometric
pH	4.5 to 7.5	USP <791> (pH paper)
Aluminum content	< 10 $\mu\text{g/mL}$ of solution (10 ppm)	Colorimetric assay
Molybdenum content	< 30 $\mu\text{g/mL}$ of solution (30 ppm)*	Photometric assay
Hydrogen peroxide content	< 50 $\mu\text{L/mL}$ of solution (50 ppm)	Colorimetric assay
Bacterial endotoxins	No more than $175/V$ USP endotoxin units per mL (V = final vial volume in mL)	USP <85> (Gel-clot or kinetic-chromogenic)
Sterility (retrospective)	No growth	USP <71> (Direct inoculation)

Conclusion

With a modified cooling system, it is possible to use up to 50 μA beam current for production of $^{99\text{m}}\text{Tc}$ in small medical cyclotron without target degradation or melting.

It is possible to produce around 75 GBq of $^{99\text{m}}\text{Tc}$ with 6 h irradiation of the ^{100}Mo target (99.815% enriched) on an IBA Cyclone® 18 cyclotron equipped with a COSTIS solid target system using targets designed and produced by TRIUMF without large amounts of long-lived impurities that might be accepted by EU Pharm.

FLUKA model proves its usefulness in finding maximum yield of the $^{99\text{m}}\text{Tc}$, and only in some degree finding composition (levels of isotopical impurities) of the irradiated target for example when gamma spectroscopy measurements are not possible.

Production of ^{68}Ga

Introduction

Interest in the use of PET imaging agents labelled with ^{68}Ga has greatly increased in nuclear medicine diagnostics over last two decades, mainly due to the convenient production of this synthetic isotope eluted from $^{68}\text{Ge}/^{68}\text{Ga}$ generators [8, 157]. Gallium chelation chemistry has also matured due to more than 30 years of research so that the design of ^{68}Ga radiopharmaceuticals, particularly peptide-based radiotracers, has become relatively straightforward for peptides with established high affinity/selectivity for their biological targets. Finally, in parallel to the advances in ^{68}Ga chemistry and radiopharmaceuticals, there has also been tremendous growth in recent years in the development of peptides and other molecules conjugated with radiotherapy isotopes such as ^{177}Lu for the treatment of various tumours. ^{68}Ga represents an ideal diagnostic isotope for pairing with radiometal therapy isotopes, particularly in many examples of molecules that can utilize the same chelator for ^{68}Ga and the therapy isotope (^{90}Y , ^{177}Lu , ^{225}Ac , etc.) [8, 157].

Two other gallium isotopes that are not found in nature are:

- ^{66}Ga ($T_{1/2} = 9.5$ h; 44% $\text{EC}+\beta^+$, 51% β^+_{av} 1904 keV, 37% γ 1039 keV, 23% γ 2751 keV) not used in PET because of its high positron range resulting from high energy and lowering resolution of potential images combined with a high patient dose as it emits multiple γ rays of energies above 1 MeV [158],
- and ^{67}Ga ($T_{1/2} = 78.3$ h; 100% EC; 39% γ 93 keV, 21% γ 185 keV, 17% γ 300 keV) which is less widely used in diagnostics than ^{68}Ga but as a SPECT imaging agent, having big potential for future medical applications. Its most popular tracer is ^{67}Ga citrate used in various inflammatory studies leading to detection of tumours and infections [159]. ^{67}Ga could also become a therapeutic agent in the future due to the emission of Auger electrons [73].

^{68}Ga ($T_{1/2} = 67.7$ min; 100% $\text{EC}+\beta^+$, 88% β^+_{av} 836 keV, 3% γ 1077 keV) is considered as a complementary to ^{18}F in terms of its ease of production (from generator like $^{99\text{m}}\text{Tc}$) and application in nuclear medicine. Its half-life is relatively short, but it is not problematic as the majority of ^{68}Ga is available at nuclear medicine departments from $^{68}\text{Ge}/^{68}\text{Ga}$ generators and the short half-life lowers the patient dose. The ^{68}Ga eluate produced with generators has well-known radiochemistry and kit-based preparation methods that have accelerated applications in peptide-based tracers, antibodies and small research molecules [7, 23, 160]. Many ^{68}Ga -labelled tracers have been used in clinical trials and some are

already approved by local authorities: ^{68}Ga -DOTATATE (approved by the US Food and Drug Agency in the USA) and SomaKit TOC™ (approved by the European Medicines Agency) [73]. For neuroendocrine tumour imaging in the UK, ^{68}Ga based PET scans were recently advised as a replacement for ^{111}In based SPECT scans [161]. ^{68}Ga has become established as a valuable diagnostic isotope, primarily for detection of neuroendocrine tumours (NETs) and Prostate Cancer.

NETs do not metabolize glucose as well as other tumour, this makes their visualization via standard FDG-PET scans sub optimal. However, overexpressed somatostatin receptors (SMSR) that bind, for example, to the PET agent ^{68}Ga -DOTATATE [162] (SMSR PET and PET/CT) have demonstrated high sensitivity and specificity. These accurate techniques should be considered as first-line diagnostic imaging methods in patients with suspicious thoracic and/or gastroenteropancreatic (GEP) NETs [163]. Somatostatin receptor PET tracers such as [^{68}Ga -DOTA,1-Nal(3)]-octreotide (^{68}Ga -DOTANOC) and [^{68}Ga -DOTA,Tyr(3)]-octreotate (^{68}Ga -DOTATATE) have shown promising results in patients with neuroendocrine tumours, with a higher lesion detection rate than is achieved with ^{18}F -fluorodihydroxyphenyl-L-alanine PET, somatostatin receptor SPECT, CT, or MR imaging. ^{68}Ga -DOTANOC has high affinity for somatostatin receptor subtypes 2, 3, and 5 (sst2,3,5). It has a wider receptor binding profile than ^{68}Ga -DOTATATE, which is sst2-selective. The wider receptor binding profile might be advantageous for imaging because neuroendocrine tumours express different subtypes of somatostatin receptors [164].

Recently, PET imaging using PSMA-ligands has gained high attention as a promising new radiotracer in patients with prostate cancer. Several studies promise accurate staging of primary prostate cancer and restaging after biochemical recurrence with ^{68}Ga -PSMA ligand PET/CT. However, prospective trials and clinical guidelines for this new technique are still missing [165].

For staging and restaging performance in patients with prostate cancer, there was no significant difference between Ga-PSMA PET/CT and F-choline PET/CT. Both methods have demonstrated high diagnostic performance for accurate staging and restaging in patients with prostate cancer, and thus both should be considered for staging in this disease [166].

There are also studies showing that ^{18}F -labeled prostate-specific membrane antigen (PSMA)-ligand PET has several principal advantages compared to ^{68}Ga -PSMA. In ^{18}F -PSMA PET, a considerably higher number of lesions with increased PSMA-ligand uptake attributed to benign lesions is present compared to ^{68}Ga -PSMA PET [167].

^{68}Ga is most often used in PET radiopharmaceuticals in oncologic applications, however it has shown good potential for imaging of cardiovascular diseases, pulmonary perfusion and ventilation, inflammation, infection and cell trafficking [33].

^{68}Ga can be produced via several alternative routes:

- Elution from $^{68}\text{Ge}/^{68}\text{Ga}$ generators. The parent isotope ^{68}Ge is the longest-lived (271 days) of the radioisotopes of germanium. It can be produced by several methods for example via $^{\text{nat.}}^{69}\text{Ga}(\text{p},\text{xn})^{68}\text{Ge}$ nuclear reaction in higher than 20 MeV proton energy cyclotrons, capable of delivering beam intensities of up to a few hundred microamperes on target for up to a few weeks of irradiation time [168]. This requires a robust and complex solid target design that can handle a high heat transfer for long irradiation times, as well as reliable purification of the material once the irradiation is complete.

In the United States, it is primarily produced in linear proton accelerators: At Los Alamos National Laboratory, it may be separated out as a product of proton capture, after proton irradiation of Nb-encapsulated gallium metal [169]. At Brookhaven National Laboratories [170], 40 MeV proton irradiation of a gallium metal target produces ^{68}Ge by (p,2n) reaction in nuclei of ^{69}Ga (the most common of two stable isotopes of gallium). This reaction is: $^{69}\text{Ga}(\text{p},2\text{n})^{68}\text{Ge}$ [171].

One Russian manufacturer produces ^{68}Ge from cyclotron-produced helium ion (alpha particle) irradiation of ^{66}Zn , in the nuclear reaction $^{66}\text{Zn}(\alpha,2\text{n})^{68}\text{Ge}$ [172].

Authors often mention need to prevent ^{68}Ge breakthrough that occurs in generators, but this argument seems less relevant since today's modern generators have included mechanisms that drastically reduced that effect [173]. This newer generation of generators, producing ^{68}Ga as $^{68}\text{Ga}[\text{GaCl}_3]$, has solved critical impurity problems and has allowed commercial availability of generators. The greater availability of commercial generators has led to increased efforts on ^{68}Ga radiopharmaceutical production. The small size and mobility of the $^{68}\text{Ge}/^{68}\text{Ga}$ generator has provided improved access of receptor targeting PET radiopharmaceuticals at PET imaging centres. Also, the simple and robust chelation chemistry of ^{68}Ga allows the preparation of ^{68}Ga radiopharmaceuticals via relatively simple methods using commercially manufactured cold kits containing ligand-chelator conjugates. The use of cold kits is analogous to the commonly employed labelling of compounds with $^{99\text{m}}\text{Tc}$ for preparation of SPECT. Thus, many institutions can perform PET studies with ^{68}Ga due to the modest investment to purchase a

generator. Currently, most of the ^{68}Ga used clinically is made using a germanium/gallium generator. Unfortunately, this approach only produces enough ^{68}Ga for two or three patient scans per day. The use of direct cyclotron production has the potential to overcome the limitations caused by the limited amounts of ^{68}Ga available from a generator.

- Direct production in small cyclotron of ^{68}Ga is possible via proton beam bombardment of enriched ^{68}Zn or $^{\text{nat}}\text{Zn}$ target [174] since the nuclear reaction of $^{68}\text{Zn}(p,n)^{68}\text{Ga}$ has a high cross section in the energy range of 11–14 MeV. However, this method cannot compete with the $^{68}\text{Ge}/^{68}\text{Ga}$ generators when it comes to issues such as complex solid target handling and development, the need for enriched material (very expensive), acceptance of inseparable impurities of ^{66}Ga and ^{67}Ga present even for irradiation of pure ^{68}Zn target.

However, recently the solid target production gets very popular again as the Canadian company ARTMS Products presented successful example of developing a low-energy cyclotron direct production of ^{68}Ga from solid ^{68}Zn enriched targets. The company has recently demonstrated record breaking, multi-curie levels of ^{68}Ga production. ARTMS developed the QUANTM Irradiation System (QIS), a ^{68}Ga production scheme that includes enriched ^{68}Zn targets, a transportation device that attaches onto the port of an existing medical cyclotron and a send-and-receive station that terminates inside a shielded workspace. Solution is based on the STS and transportation system used in TR-24 cyclotron for production of $^{99\text{m}}\text{Tc}$ using very efficient inclined targets. This system can be installed on any major cyclotron brand. The hardware enables a technician to load a non-radioactive ^{68}Zn target into the transportation system (Figure 72). Automated pneumatics and robotics then move the target to the cyclotron's target port, where it is irradiated for two hours by a proton beam. This proton irradiation generates ^{68}Ga within the target via the $^{68}\text{Zn}(p,n)^{68}\text{Ga}$ nuclear reaction. The irradiated target is then brought back to the shielded space where the ^{68}Zn can be extracted and purified for use in radiopharmaceuticals. ARTMS demonstrated that QIS can produce ^{68}Ga at levels of 10 Ci (370 GBq) what is 100 to 200 times more activity in a two-hour irradiation than a germanium/gallium generator can put out. This puts the problem not on the amount of gallium that you have but, with its 68 min half-life, the rush to use it all. In this case a hospital might be able to produce about a day's worth of ^{68}Ga and scan several patients following a single cyclotron run. The record-breaking ^{68}Ga production was achieved at Odense University Hospital. The team there demonstrated multi-curie production of two radiopharmaceuticals: ^{68}Ga -Dotatate (known as

NETSPOT) and a prostate-specific membrane antigen (PSMA) radiopharmaceutical for imaging prostate cancer (artms.ca).

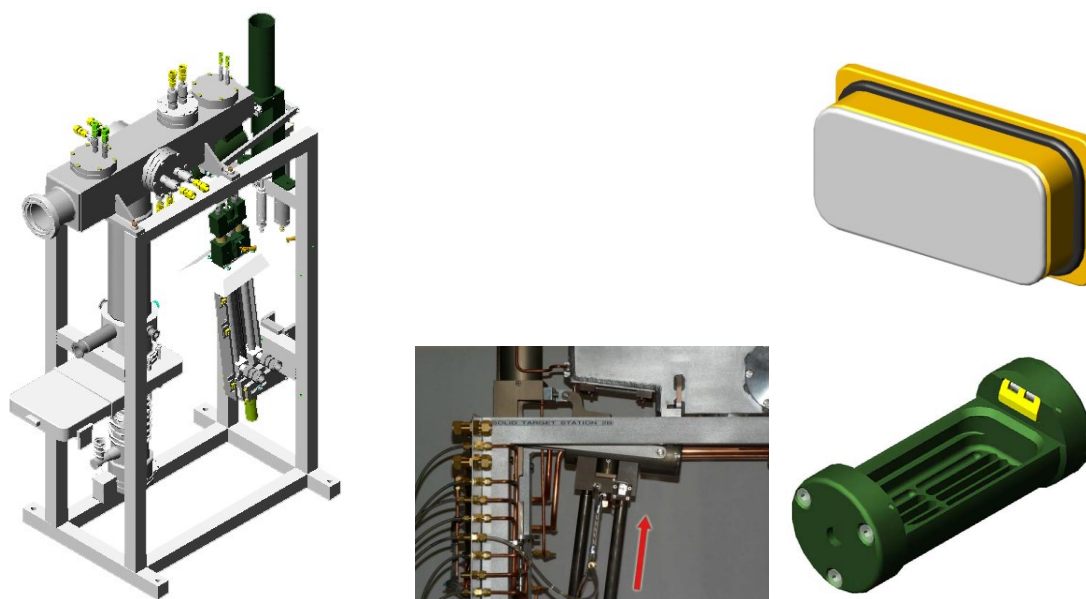


Figure 72 Modern ACSI solid target station (general view - left) loaded and unloaded automatically by the remote controlled manipulator (center) with the inclined target plug (up right) delivered by the rabbit (down right) providing transportation between STS and hot cell via pneumatic post line.

It is generally necessary to bombard isotopically enriched ^{68}Zn since several radioisotopes of gallium with longer half-lives than ^{68}Ga are also co-produced when irradiating natural Zn. However, despite use of isotopically enriched ^{68}Zn , small amounts of ^{66}Ga and ^{67}Ga will occur as it is not possible to acquire 100% pure ^{68}Zn , and even in the event of pure ^{68}Zn being available, the proton irradiation of ^{68}Zn leads to the production of ^{67}Ga radioisotopic impurity through the $^{68}\text{Zn}(p,2n)^{67}\text{Ga}$ reaction for proton energies larger than 12.2 MeV (it will be shown in FLUKA simulations later in the text). Therefore, the composition of the isotopically enriched ^{68}Zn and the proton energy must be selected wisely to balance yield and achieve a purity suitable for human use [8, 9]. It is also important to assess other metal contamination in the ^{68}Zn starting material. Iron may be of concern as (if not purified) it may interfere with labelling of some precursors, for example those with a DOTA chelator. Iron and other metals must be excluded in such case during whole process of production (iron free lab tools, trace grade reagents, transfer lines etc.).

ARTMS also offers coin targets that can be used in smaller STS like COSTIS (Figure 73). Target material zinc-68 (250-300 mg what is the equivalent of 300-350 μm thick ^{68}Zn disc 20 mm diameter used in FLUKA simulations described later) is electroplated or sintered on silver or aluminium backing. Typical yields for those targets are:

> 5 Ci (>180 GBq) @ EOB (12.8 MeV, 1 h, 50 μA)

> 2 Ci (>75 GBq) @ EOB (11.0 MeV, 1 h, 50 μA).

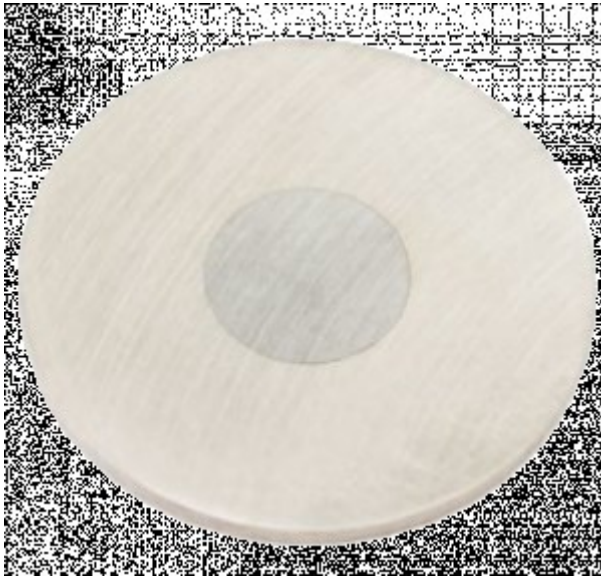


Figure 73 Solid target for production of ^{68}Ga offered by ARTMS (<http://artms.ca/targets>).

- Direct medical cyclotron productions using liquid (solution) targets, allow fast, small scale on-site productions of relatively pure ^{68}Ga in form of $^{68}\text{GaCl}_3$ (provided by extension box preceding synthesis module). Such a method, based on $^{68}\text{Zn}(p,n)^{68}\text{Ga}$ reaction in near future might be very convenient for hospital cyclotron facilities that can afford additional liquid target for ^{68}Ga production and radiochemistry module for synthesis of the ^{68}Ga -based radiotracer in their routine operations. High purity of ^{68}Ga production via direct proton beam irradiation of enriched ^{68}Zn is improved by liquid target technology initiated by Pandey et al. [175, 176], the same group that developed ^{89}Zr liquid target [85]. Dissolution of enriched ^{68}Zn target material in nitric acid enabled a cheap method for producing small quantities of relatively pure ^{68}Ga for 2–4 patients in a beam time of ~ 1 h. Recent study using a novel IBA target (Figure 64) was carried out by Alves et al. in ICNAS (Portugal) [8]. Results look very promising as 45 min irradiation of 30 mg/ml

of ^{68}Zn with a 45 μA proton beam yielded 6 GBq of ^{68}Ga , which can be translated to achieving batches of 40 GBq of ^{68}Ga (pre-purification) by optimization of concentration and beam parameters. This can create a viable alternative for solid target and generator produced ^{68}Ga . Besides general advantages of using a solution target instead of solid target, no long lived ^{68}Ge impurities were found in the final product. Solution target can be remotely loaded into the target body similarly to an ^{18}F target system. After irradiation, the solid target must be removed either manually with the risk of high personnel exposure to the radioactive field of the target itself and activated parts of the cyclotron, or with an automated target transfer system. Again, for a liquid target, the target liquid is remotely pushed into a hot cell through capillary lines with over pressure of air or an inert gas. Once in the hot cell, the solid target must be dissolved. This step adds extra time for the post-process versus the liquid target process. The next step is the same for both solid and liquid target. Namely, the ^{68}Ga must be separated from the bulk parent ^{68}Zn isotope and purified to remove any unwanted metal contaminants. Recycling of the enriched ^{68}Zn starting material can be considered. The end product of the separation can be $[^{68}\text{Ga}]\text{GaCl}_3$, the same as the eluate from the generator. However, the concentration and pH may differ from one method to the other. At this point, labelling the desired radiopharmaceutical with ^{68}Ga is the same for all three production methods, generator, solid and liquid targets. Production of ^{68}Ga amounts exceeding the amount available from current generators is possible with both methods using solid and solution target.



Figure 74 ^{68}Ga solution target used in ICNAS and PETIC.

However, in case of very promising solution target productions of ^{68}Ga there is still a need to optimize these methods as certain problems arise in the phase of their tests. One of them is the target pressure build-up during

irradiation. This effect depends on the beam intensity and concentration of the target material. The irradiation of aqueous solutions leads to water radiolysis and the creation of ions and free radicals of hydrogen, oxygen and hydroxyl groups, which in turn leads to rapid gas evolution in the target chamber (H_2 and O_2). This effect is further promoted by the introduction of certain types of salt cations and anions. Those effects were studied and minimized in a recently published patent invented by *DeGrado et al.* in 2017. In particular cases, the introduction of strong nitric acid proves to minimize the gas evolution in the target because the nitric acid helps to get rid of free radicals. Another solution is the introduction of a backpressure regulator which keeps the in-target pressure at a stable level during irradiation. Authors also point out the importance of carefully selecting salt constituents as certain pairs of metallic cations and acidic anions affect the gas evolution in different ways. Additionally, strong acids used in target may result in corrosion. Other experiments using silver or aluminium targets demonstrated the presence of fine particles, leading to clogging of the transfer lines [86] and thus requiring frequent target maintenance. It is recommended to use heat-resistant and chemically inert materials (such as niobium and tantalum) as target body and window materials. Optimization of target material, metallic salt composition and concentration of acid are all needed to prevent the formation of precipitates. Favourably, the addition of nitric acid also eliminates the precipitation of salts within target (*DeGrado et al.*, 2017). Pandey et al. show high ratios (approximately 85–90%) of enriched material recycling for liquid targets [175], which is a highly desirable and financially advantageous factor for considering the use of solution targets. In general, the liquid target radiometal production technology is not yet mature and requires more studies to optimize production yields. For small facilities and/or facilities at remote locations, the recent liquid target developments allow for in-house production of radionuclides with small cyclotrons.

As the FLUKA model presented in this thesis was validated for ^{89}Zr and ^{48}V , also tested for ^{99m}Tc , it is worth to try it for prediction of the results for solid target production of ^{68}Ga . Gamma spectroscopy studies of other authors usually point out ^{67}Ga and ^{66}Ga as the main impurities having great impact on the shelf life of the ^{68}Ga product. Using FLUKA we hope to receive a more detailed picture for possible optimization of the production. As PETIC was one of the first PET centres where

solution target method was tested, we are also able to compare results from FLUKA simulations with experimental outcomes of ^{68}Ga production in solution target.

Materials and Methods

The *in-silica* model for gallium-68 production is almost identical to the one used for cyclotron production of zirconium-89 and vanadium-48. Our investigation of the FLUKA model for the simulation of gallium-68 production contains two variants: one with isotopically pure ^{68}Zn target and one with ^{68}Zn enriched target instead of the yttrium or titanium ones used for zirconium-89 and vanadium-48. In the case of ^{68}Zn enriched target, FLUKA uses mixture of Zinc isotopes: ^{68}Zn (99.50%), ^{67}Zn (0.30%), ^{70}Zn (0.18%), ^{66}Zn (0.01%), ^{64}Zn (0.01%). Concentration of the isotopes in this variant is analogical to the one reported by FLUIDOMICA (supplier of the ^{68}Zn solution targets) used in Coimbra [8] and Cardiff [83]. Suppliers like Isoflex and American Elements offer this isotope only in the form of a powder which is not possible to be use in the type of Al holder used in this model. Only ARTMS provides coin targets in the form which is comparable with the coin used in this model. Simulated metal foils have concentration of isotopes that can be compared with one used in experimental productions using solution targets (the same impurities expected). The range of ^{68}Zn discs thicknesses for both variants is the same as range of ^{89}Y discs. The production model and used energies for proton beam irradiating ^{89}Zn targets is the same and uses Niobium degraders of the same range of thicknesses as used in ^{89}Zr production model. For simplicity, the same model of the foil target closed in Al holder was used, however results from this part of FLUKA simulations can be easily translated for electroplated, sintered or even solution targets, comparing thicknesses and masses of the used target materials and knowing zin density (7140 mg/cm^3) or just comparing isotopical impurities' content (the same level of enrichment for materials used in two different target types).

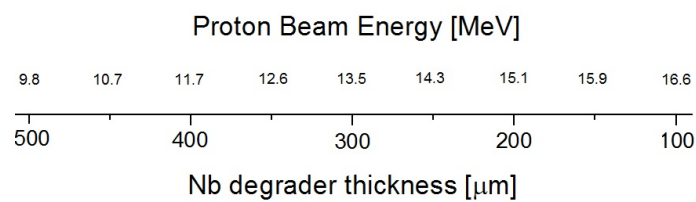
An IBA CYCLONE® 18/9 cyclotron was used for ^{68}Ga radionuclide production in NIRTA solution target (Figure 64) and 4 ml liquid samples were prepared before and after chemical purification of the target material. Activities were measured in a Capintec CRC 25R dose calibrator and corrected to the end-of-beam (EOB) time. After decay of the primary radionuclide, multiple gamma spectra were acquired with a shielded and energy calibrated Ortec LoAx hyper-pure germanium (HPGe) detector. Detector efficiency was measured in the range 35-1115 keV using a variety of radionuclides of known activity. Spectra were analyzed using Canberra

Genie 2000 multi-channel analyzer software to give energy and net count-rate for visible photopeaks. For identified impurities, count-rate was converted to activity, corrected to EOB, and expressed as a percentage of the primary radionuclide activity.

Results

Pure Zinc-68 solid target proton bombardment – FLUKA simulation results

a)



b)

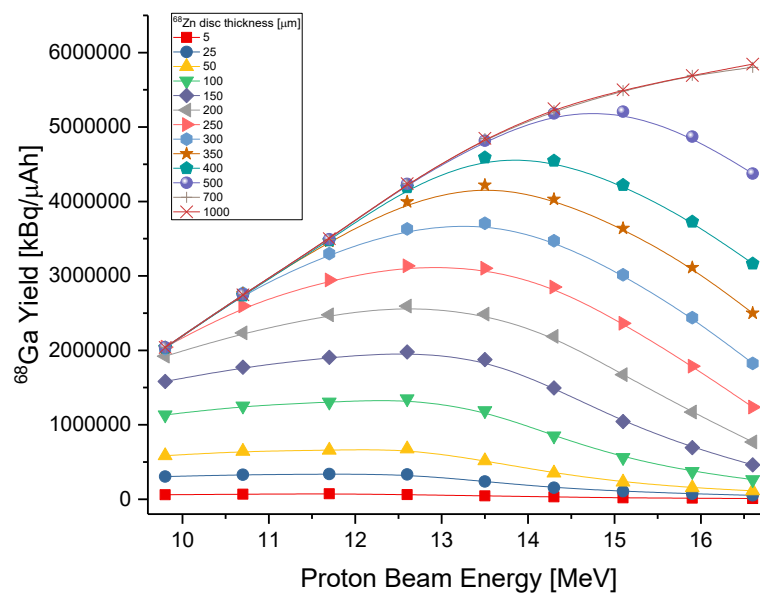


Figure 75 a) Relation between proton beam energy and Nb degrader thickness and b) ^{68}Ga (67.71(9) min) yields calculated in FLUKA for range of proton beam energies and pure ^{68}Zn target thicknesses.

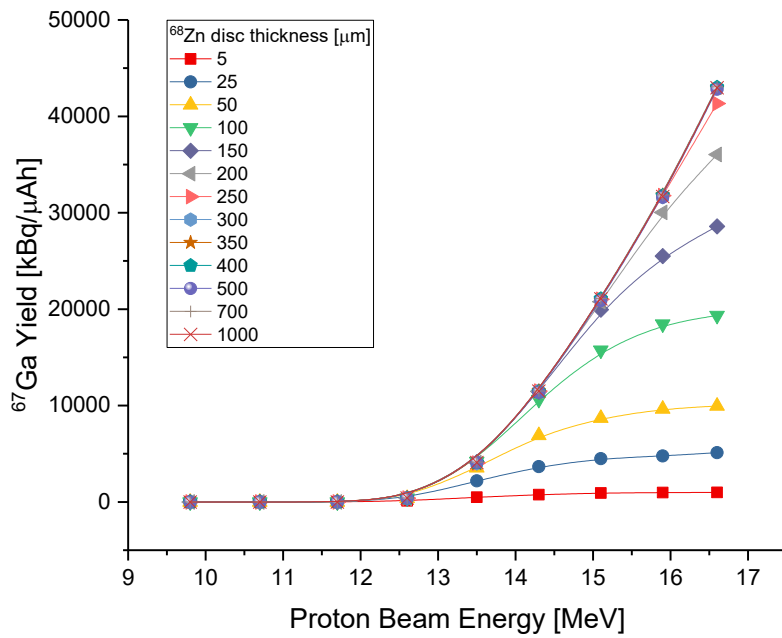


Figure 76 ^{67}Ga (3.2612(6) d) yields calculated in FLUKA for ^{68}Zn pure targets.

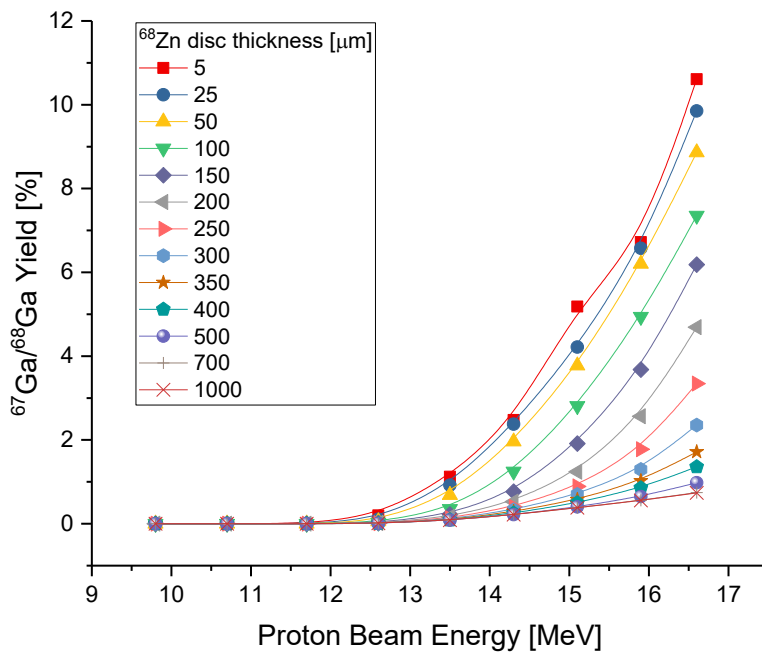


Figure 77 Ratios of the ^{67}Ga to the ^{68}Ga yield vs proton beam energy for ^{68}Zn pure targets.

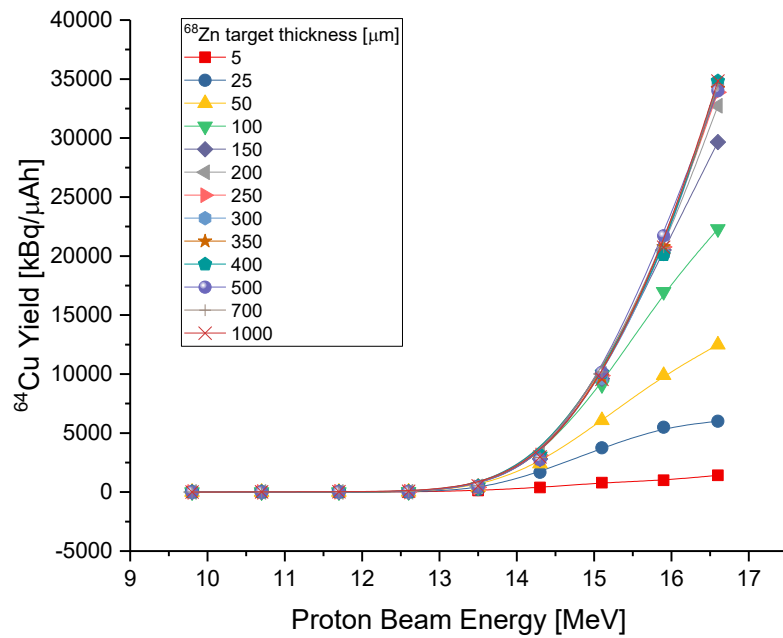


Figure 78 ^{64}Cu (12.700(2) h) yields calculated in FLUKA vs proton beam energy for ^{68}Zn pure targets (copper-64 might be produced with low yields in reaction $^{68}\text{Zn}(p,\alpha+n)^{64}\text{Cu}$ – compare Figure 115).

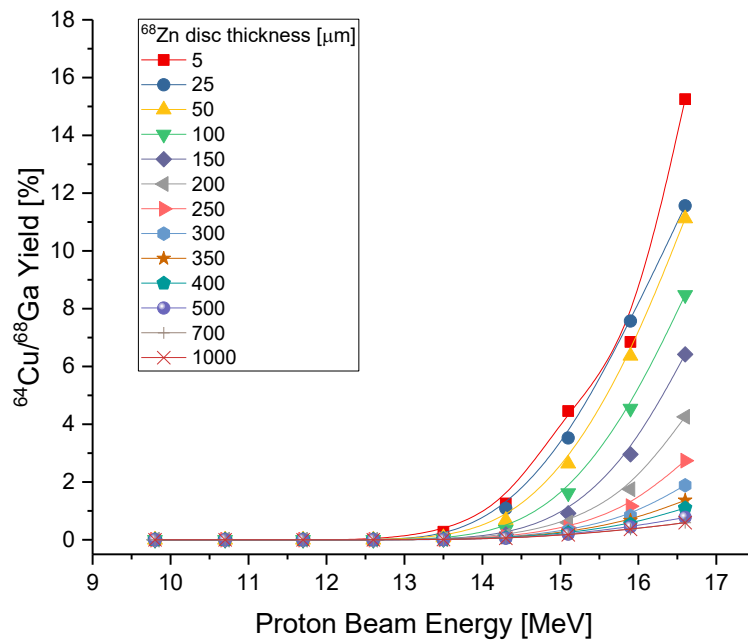


Figure 79 Ratios of the ^{64}Cu yield to the ^{68}Ga yield vs proton beam energy for ^{68}Zn pure targets.

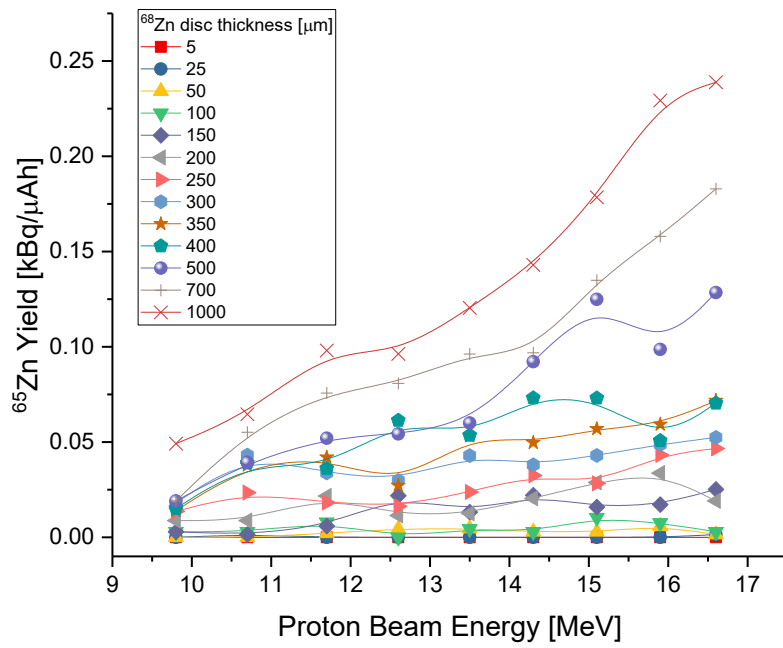


Figure 80 ^{65}Zn (243.66(9) d) yields vs proton beam energy for ^{68}Zn pure targets, calculated in FLUKA.

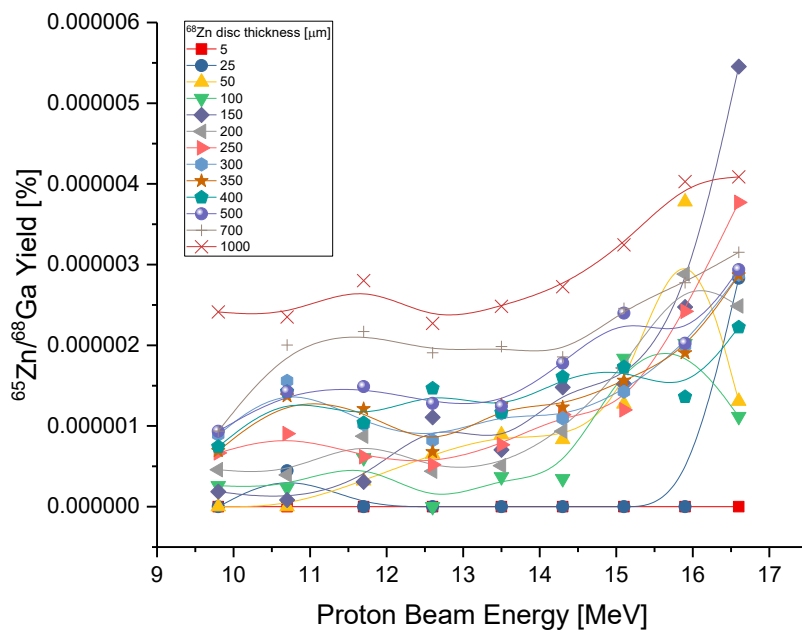


Figure 81 Ratios of the ^{65}Zn yield to the ^{68}Ga yield vs proton beam energy for ^{68}Zn pure targets, calculated in FLUKA.

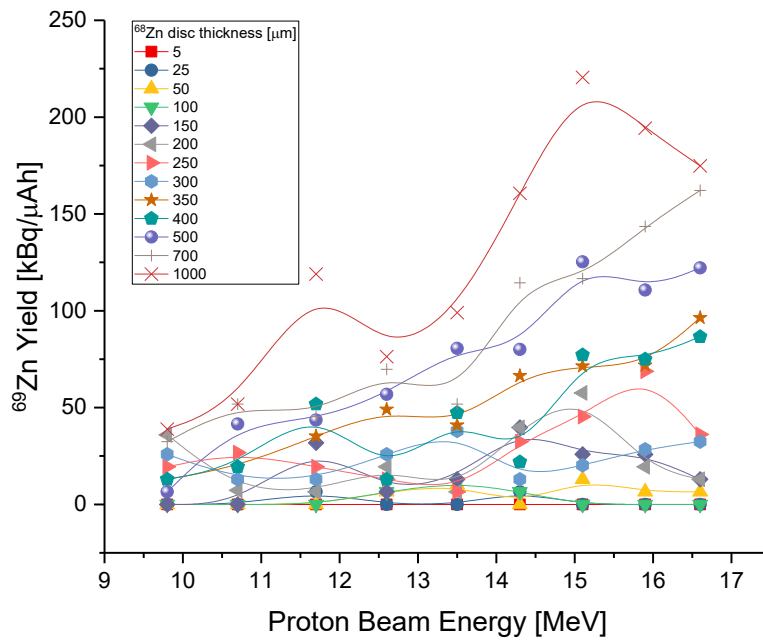


Figure 82 ^{69}Zn (56.4(9) min) yields calculated in FLUKA vs proton beam energy for ^{68}Zn pure targets.

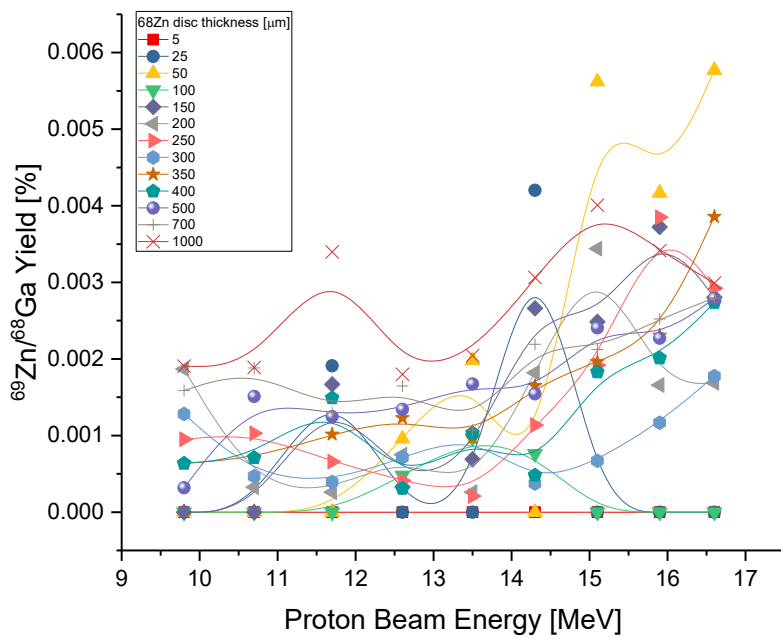
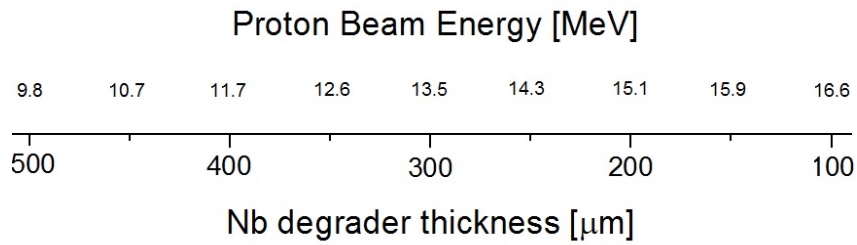


Figure 83 Ratios of the ^{69}Zn yield to the ^{68}Ga yield vs proton beam energy for ^{68}Zn pure targets. Radiation Protection Aspects for Solid Target Production of Radiometals.

Zinc-68 enriched (^{68}Zn : 99.50%, ^{67}Zn : 0.30%, ^{70}Zn : 0.18%, ^{66}Zn : 0.01%, ^{64}Zn : 0.01%)
 solid target proton bombardment – FLUKA simulation results

a)



b)

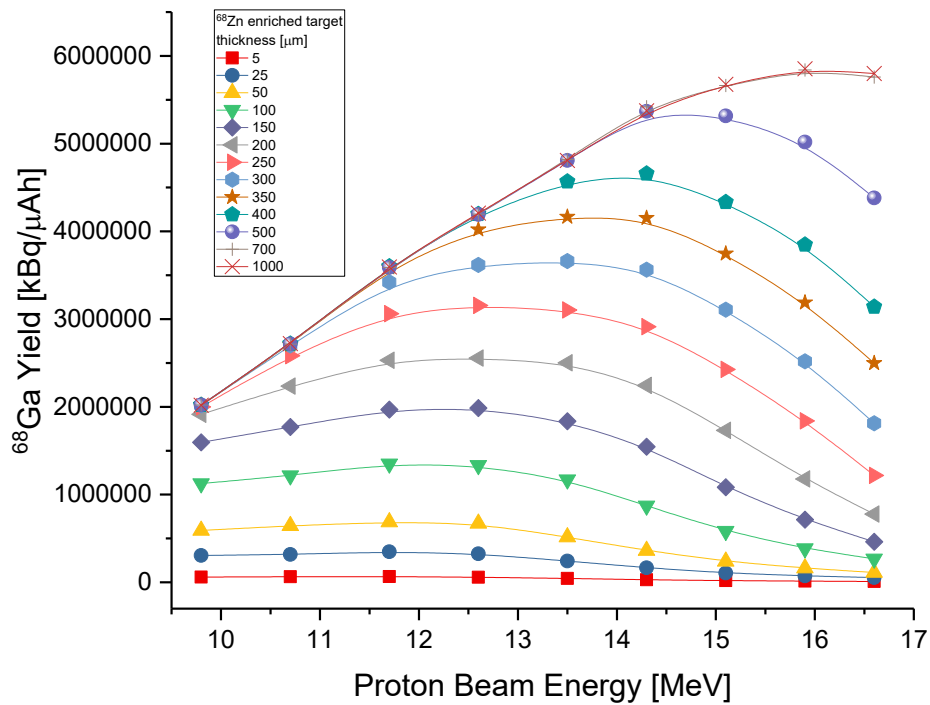


Figure 84 a) Relation between proton beam energy and Nb degrader thickness and b) ^{68}Ga (67.71(9) min) yields calculated in FLUKA for range of proton beam energies and ^{68}Zn enriched target thicknesses.

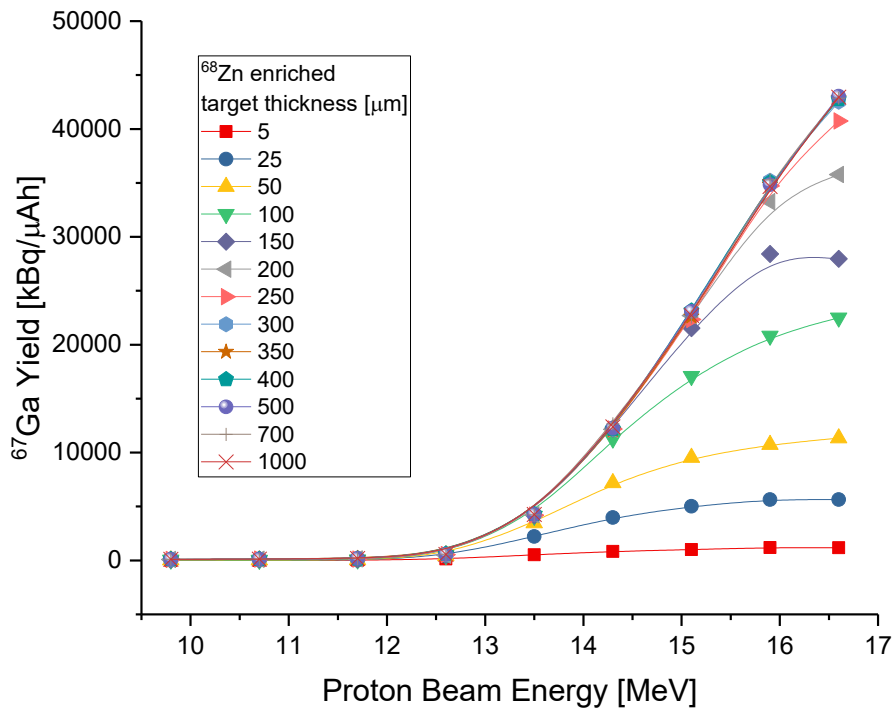


Figure 85 ^{67}Ga (3.2612(6) d) yields calculated in FLUKA for ^{68}Zn enriched target.

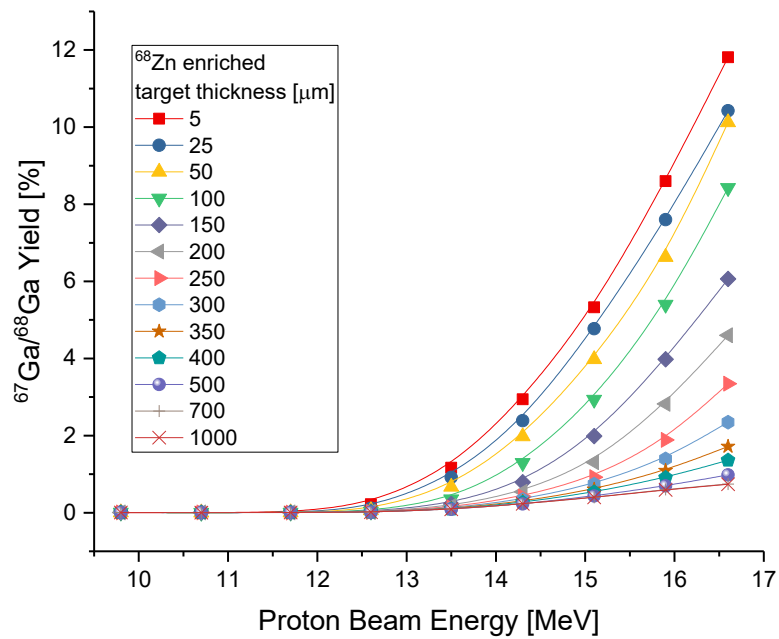


Figure 86 Ratios of the ^{67}Ga to the ^{68}Ga yield vs proton beam energy for ^{68}Zn enriched targets.

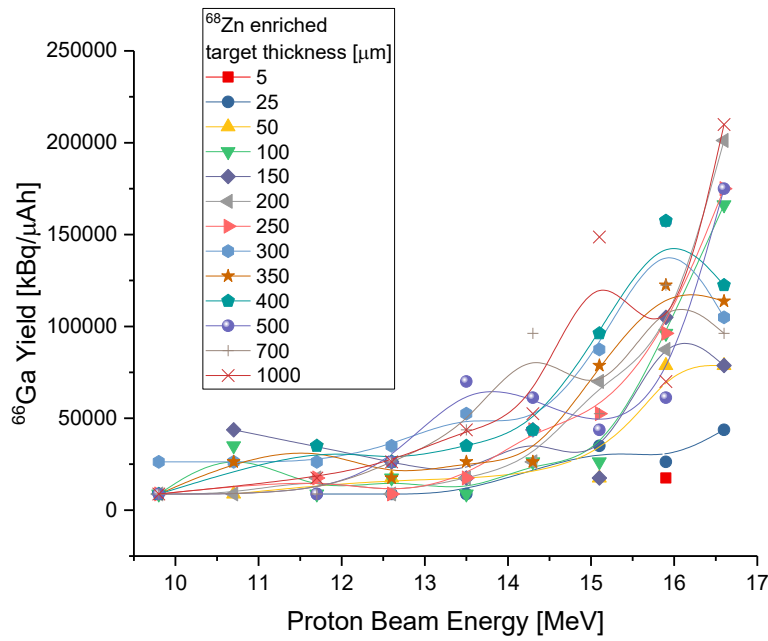


Figure 87 ^{66}Ga (9.49(7) h) yields calculated in FLUKA for ^{68}Zn enriched target.

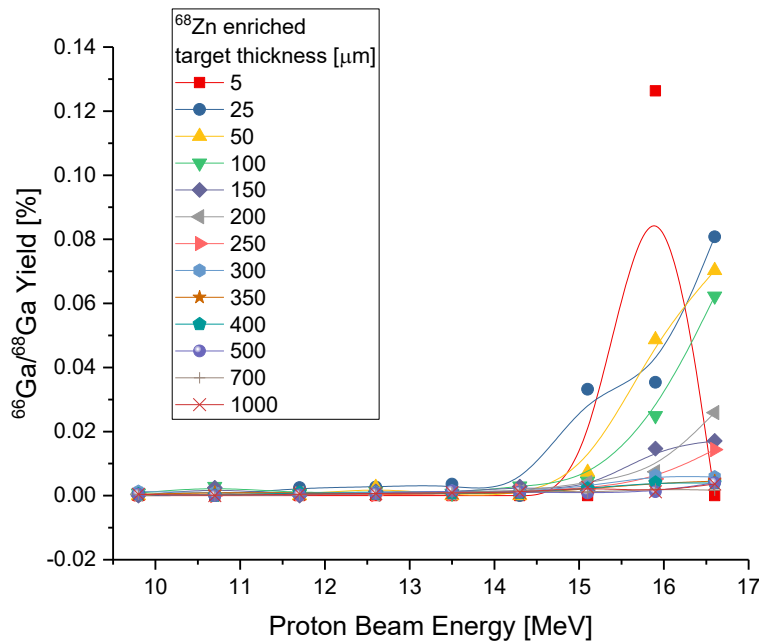


Figure 88 Ratios of the ^{66}Ga to the ^{68}Ga yield vs proton beam energy for ^{68}Zn enriched targets.

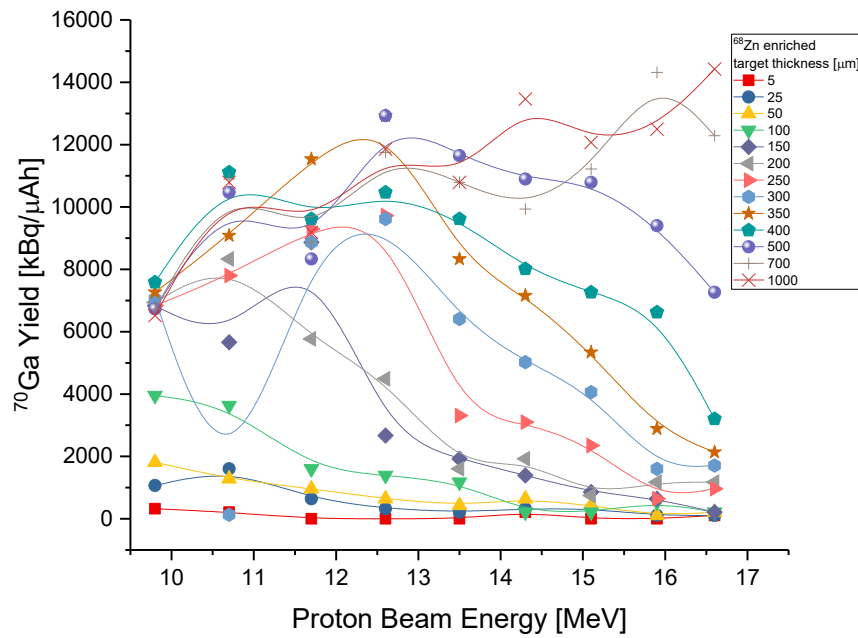


Figure 89 ^{70}Ga (21.14(3) min) yields calculated in FLUKA for ^{68}Zn enriched target.

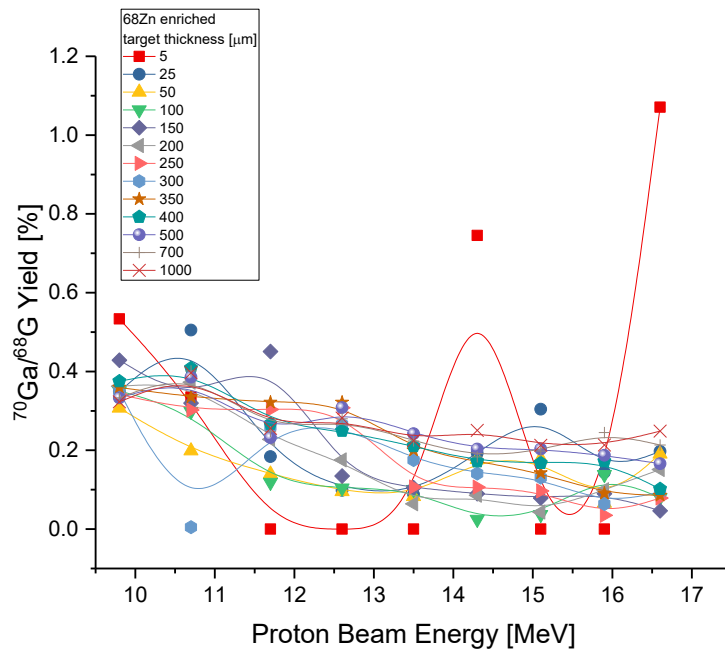


Figure 90 Ratios of the ^{70}Ga to the ^{68}Ga yield vs proton beam energy for ^{68}Zn enriched targets.

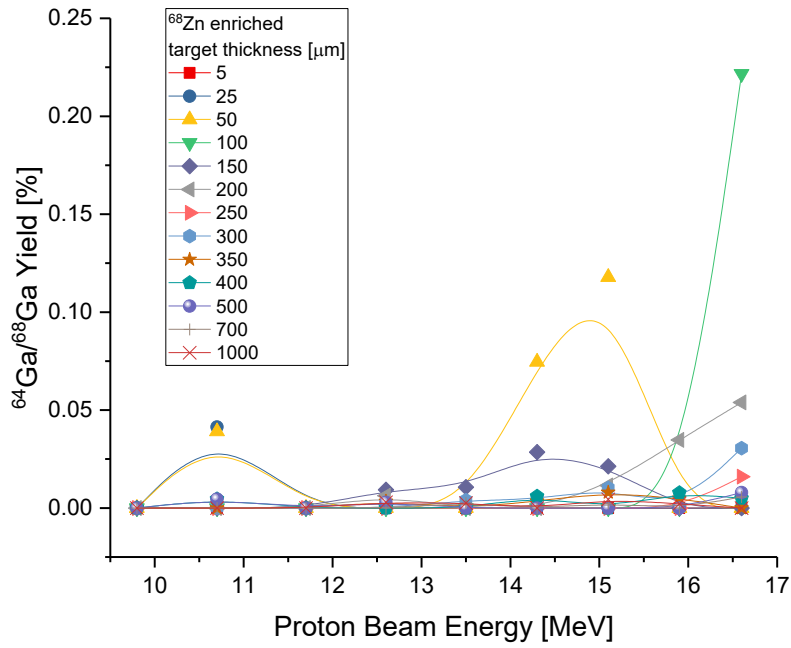


Figure 91 Ratios of the ^{64}Ga (2.627(12) min) to the ^{68}Ga yield vs proton beam energy for ^{68}Zn enriched targets.

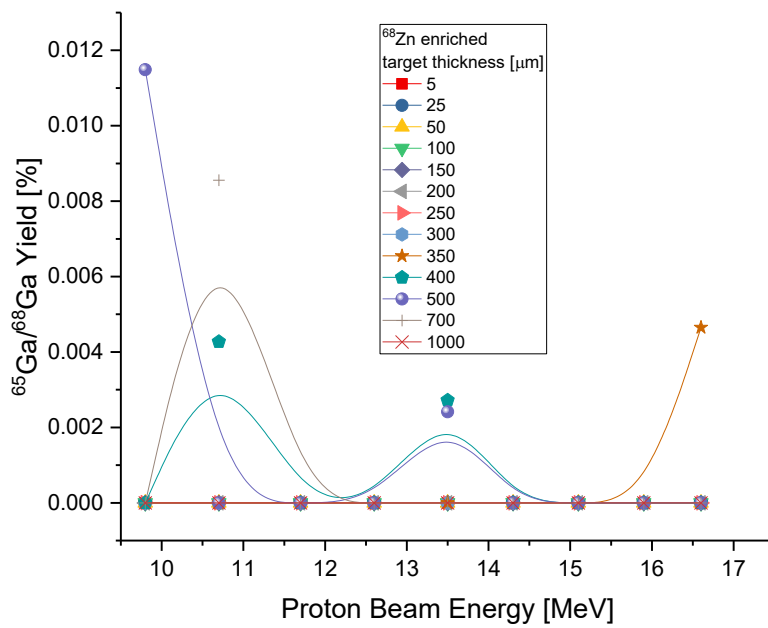


Figure 92 Ratios of the ^{65}Ga (15.2(2) min) to the ^{68}Ga yield vs proton beam energy for ^{68}Zn enriched targets.

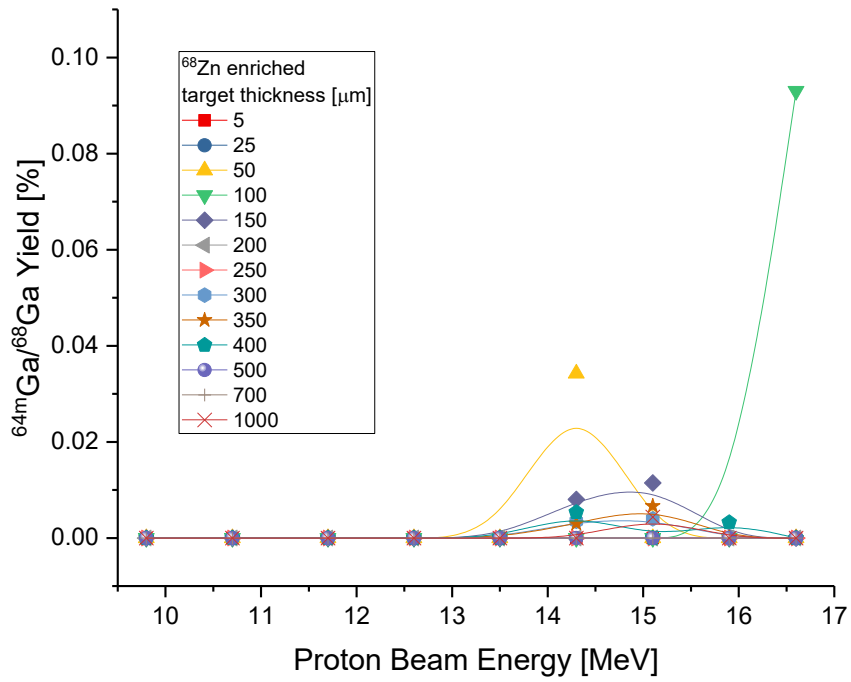


Figure 93 Ratios of the ^{64m}Ga (21.9(7) μs) to the ^{68}Ga yield vs proton beam energy for ^{68}Zn enriched targets.

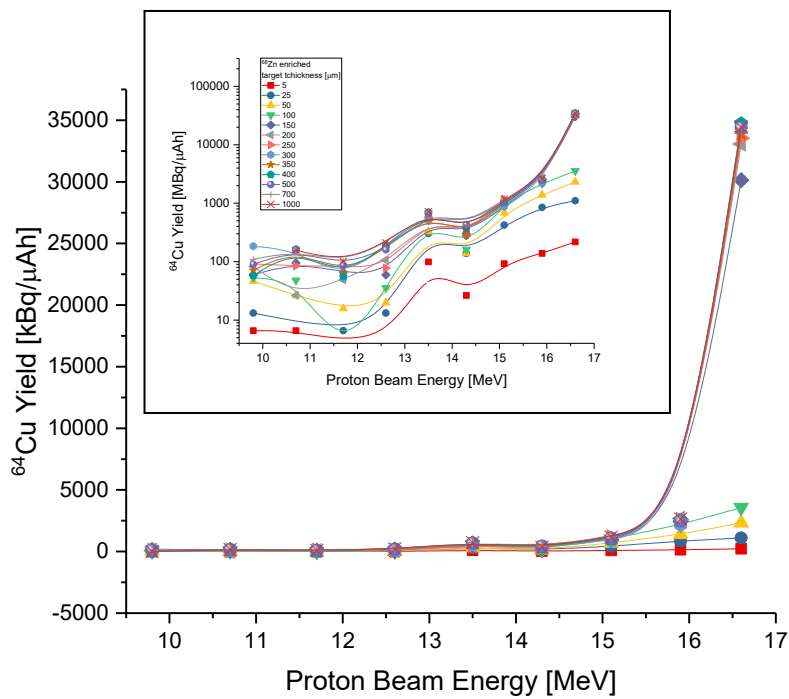


Figure 94 ^{64}Cu (12.700(2) h) yields calculated in FLUKA for ^{68}Zn enriched target (logarithmic scale in insert).

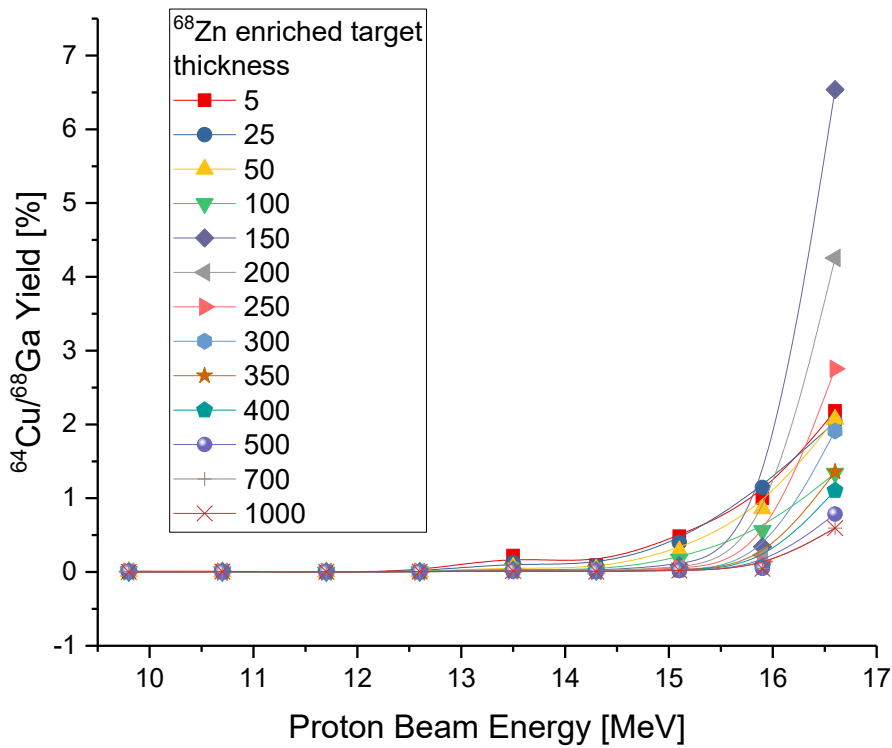


Figure 95 Ratios of the ^{64}Cu to the ^{68}Ga yield vs proton beam energy for ^{68}Zn enriched targets.

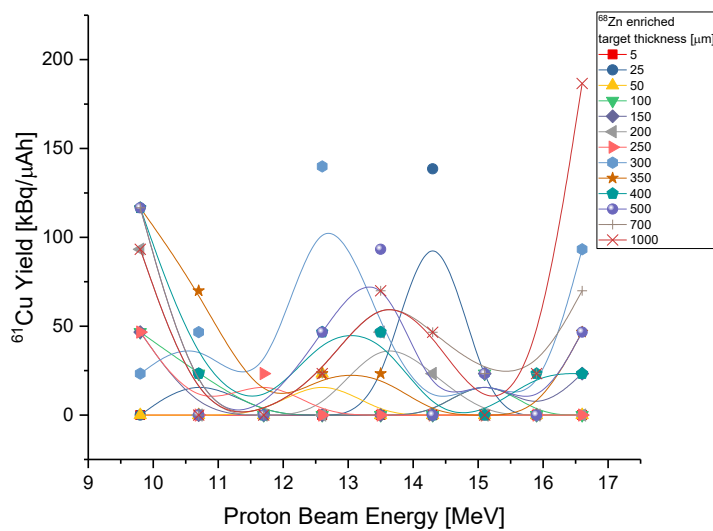


Figure 96 ^{61}Cu (3.333(5) h) yields calculated in FLUKA for ^{68}Zn enriched target.

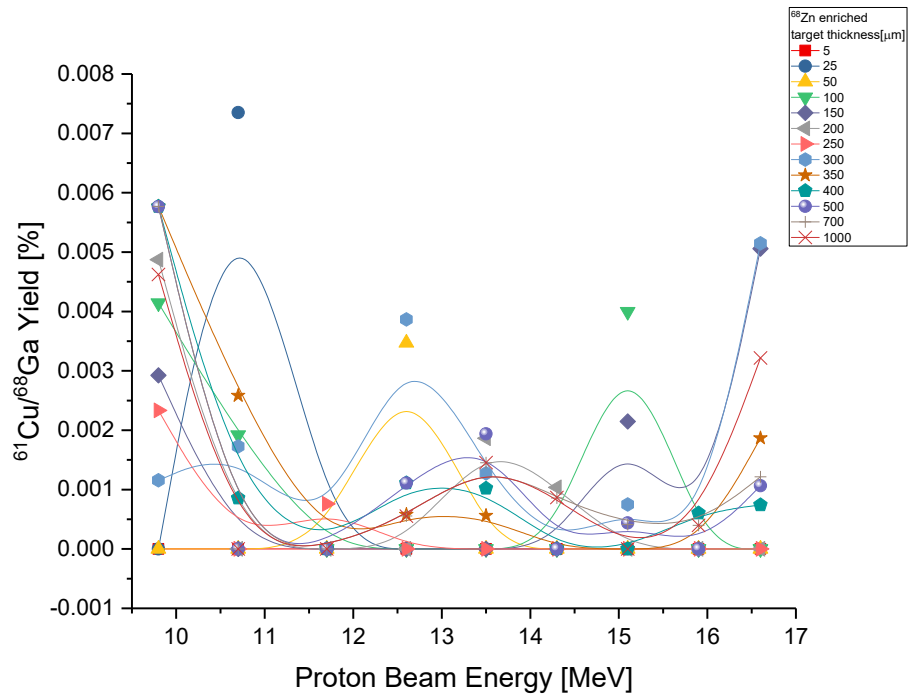


Figure 97 Ratios of the ^{61}Cu to the ^{68}Ga yield vs proton beam energy for ^{68}Zn enriched targets.

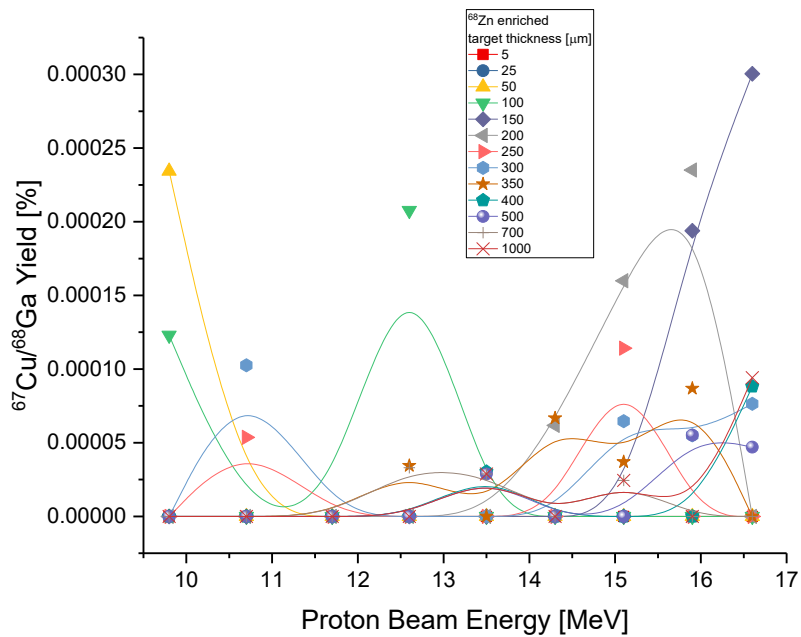


Figure 98 Ratios of the ^{67}Cu (61.83(12) h) to the ^{68}Ga yield vs proton beam energy for ^{68}Zn enriched targets.

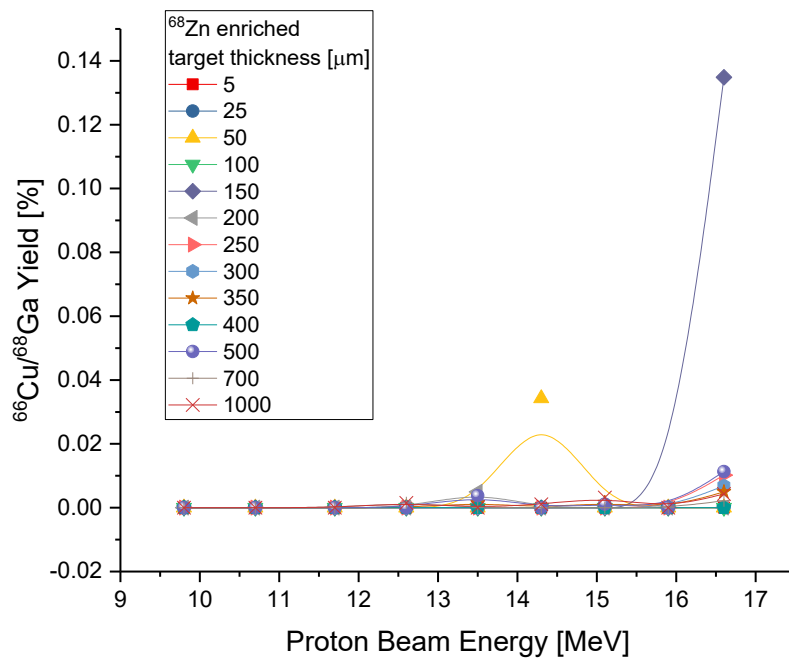


Figure 99 Ratios of the ^{66}Cu (5.120(14) min) to the ^{68}Ga yield vs proton beam energy for ^{68}Zn enriched targets.

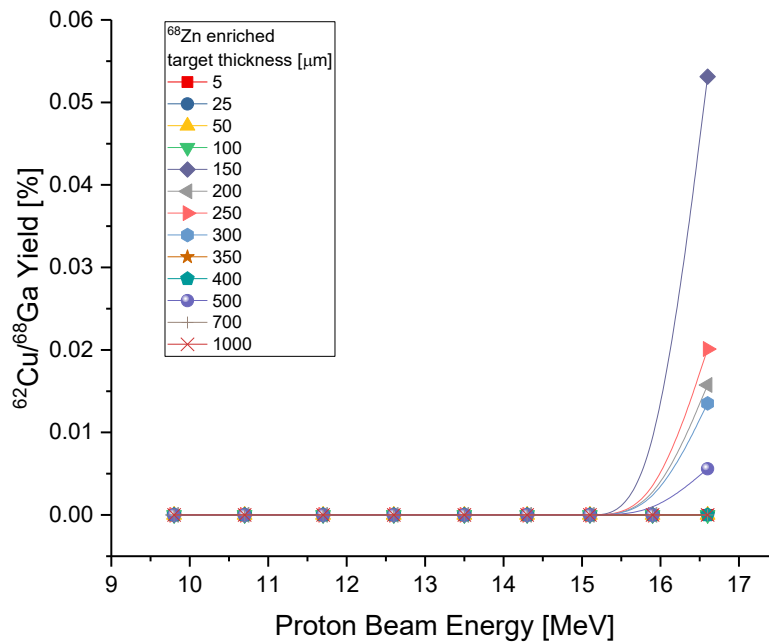


Figure 100 Ratios of the ^{62}Cu (9.673(8) min) to the ^{68}Ga yield vs proton beam energy for ^{68}Zn enriched targets.

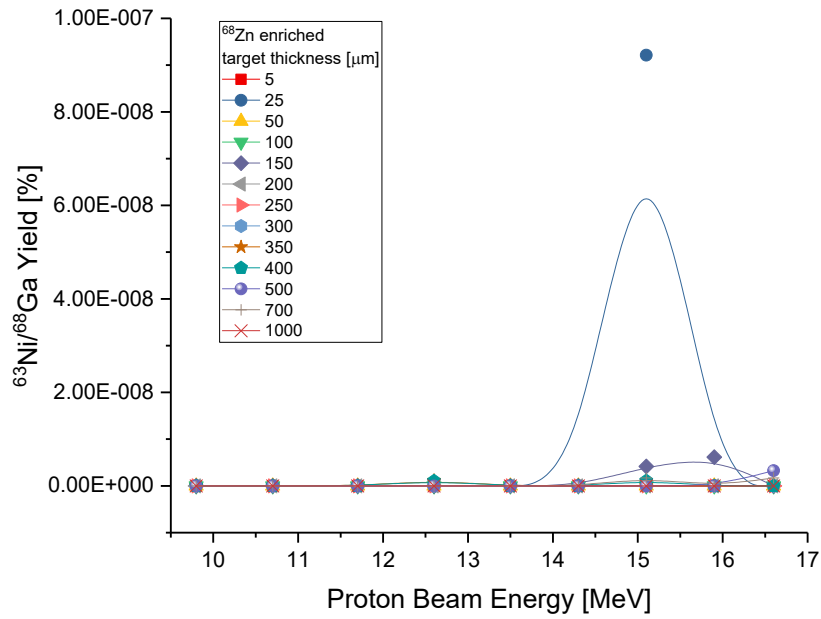


Figure 101 Ratios of the ^{63}Ni (100.1(20) y) to the ^{68}Ga yield vs proton beam energy for ^{68}Zn enriched targets.

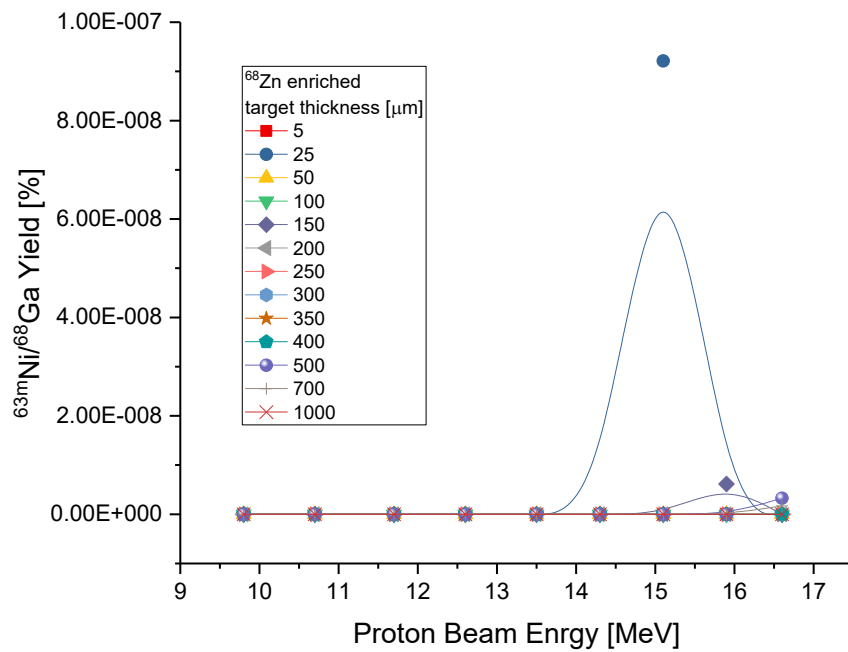


Figure 102 Ratios of the $^{63\text{m}}\text{Ni}$ (1.67(3) μs) to the ^{68}Ga yield vs proton beam energy for ^{68}Zn enriched targets.

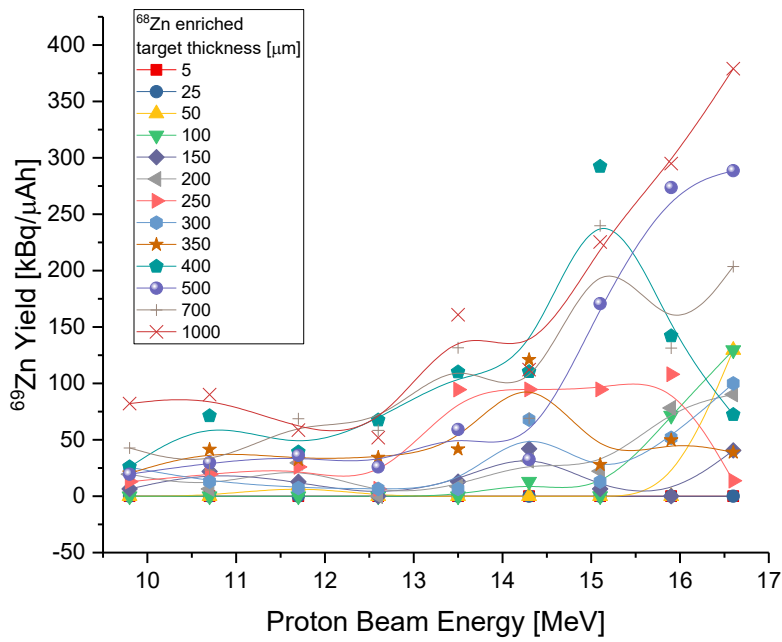


Figure 103 ^{69}Zn (56.4(9) min) yields calculated in FLUKA for ^{68}Zn enriched target.

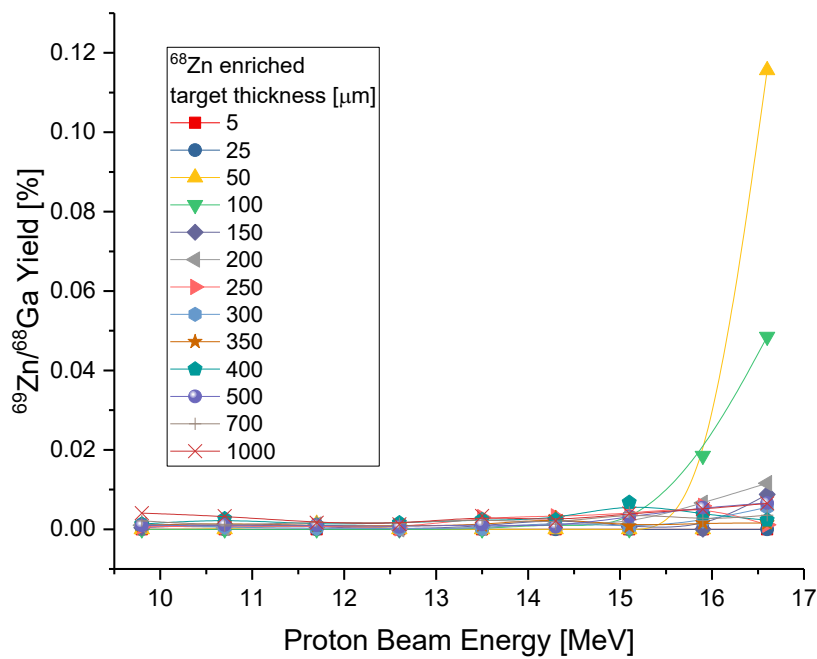


Figure 104 Ratios of the ^{69}Zn to the ^{68}Ga yield vs proton beam energy for ^{68}Zn enriched targets.

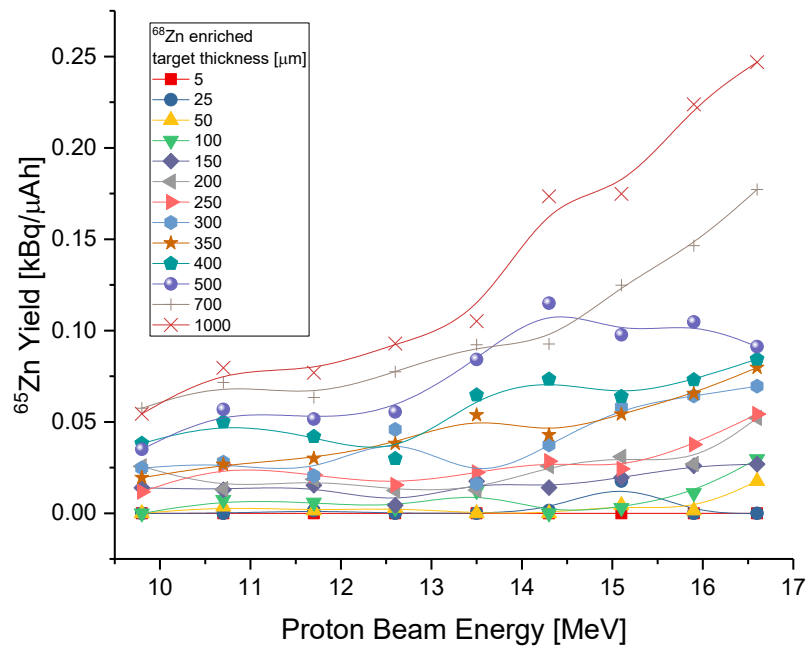


Figure 105 ^{65}Zn (243.66(9) d) yields calculated in FLUKA for ^{68}Zn enriched target.

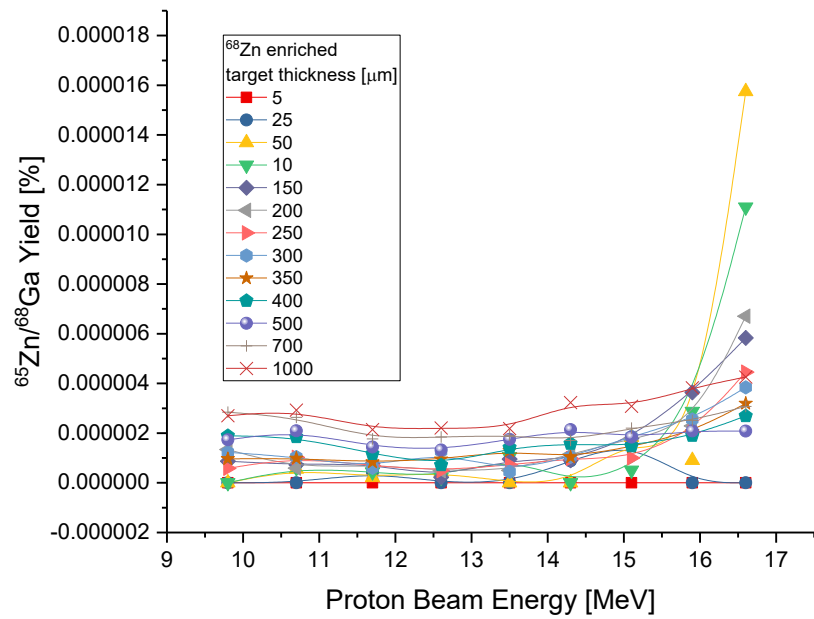


Figure 106 Ratios of the ^{65}Zn to the ^{68}Ga yield vs proton beam energy for ^{68}Zn enriched targets.

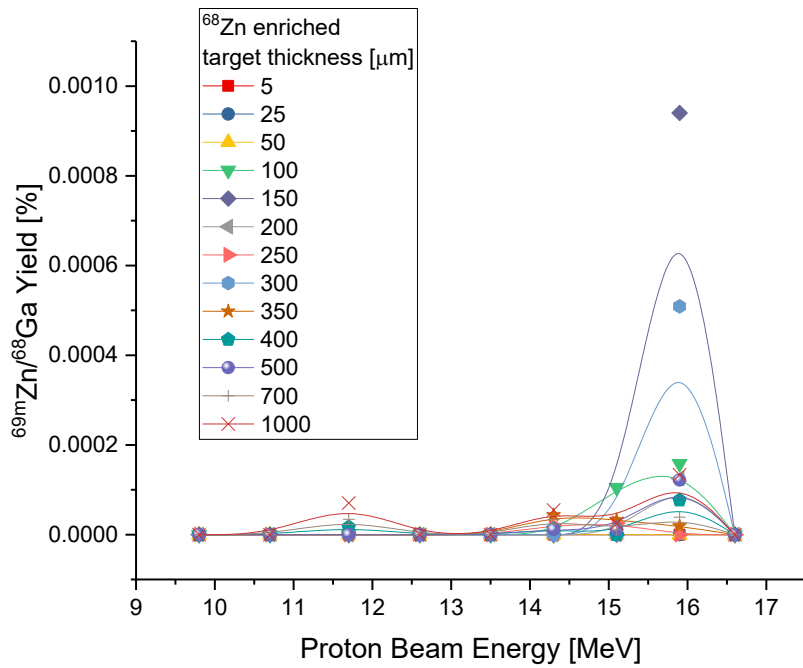


Figure 107 Ratios of the ^{69m}Zn (13.76(2) h) to the ^{68}Ga yield vs proton beam energy for ^{68}Zn enriched targets.

Enriched Zinc-68 solid target proton bombardment – shelf life assessment (Galium-68 content vs time)

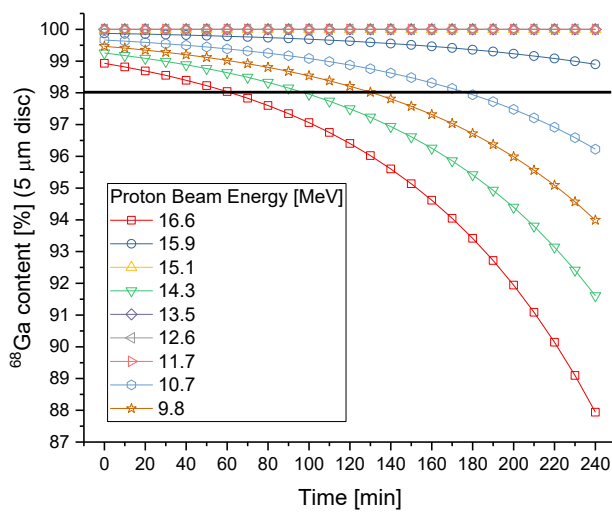


Figure 108 ^{68}Ga content vs time and proton beam energy for ^{68}Zn enriched targets 5 μm of thickness.

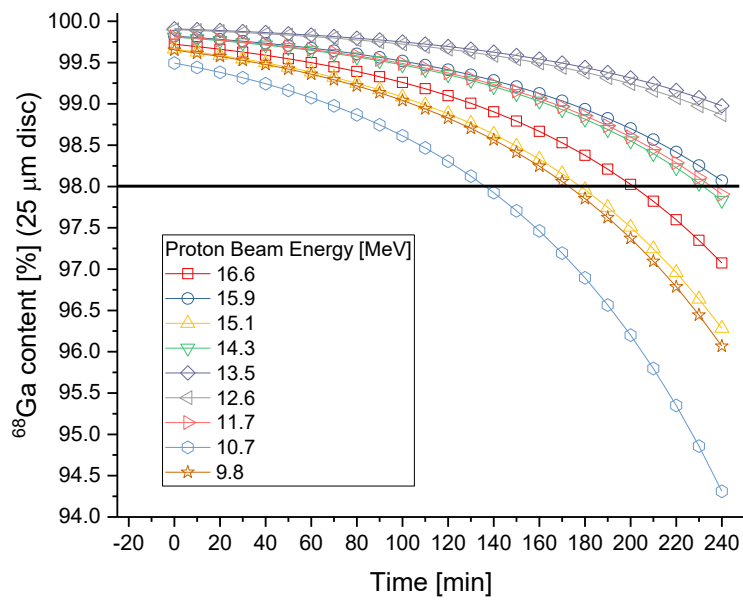


Figure 109 ^{68}Ga content vs time and proton beam energy for ^{68}Zn enriched targets 25 μm of thickness.

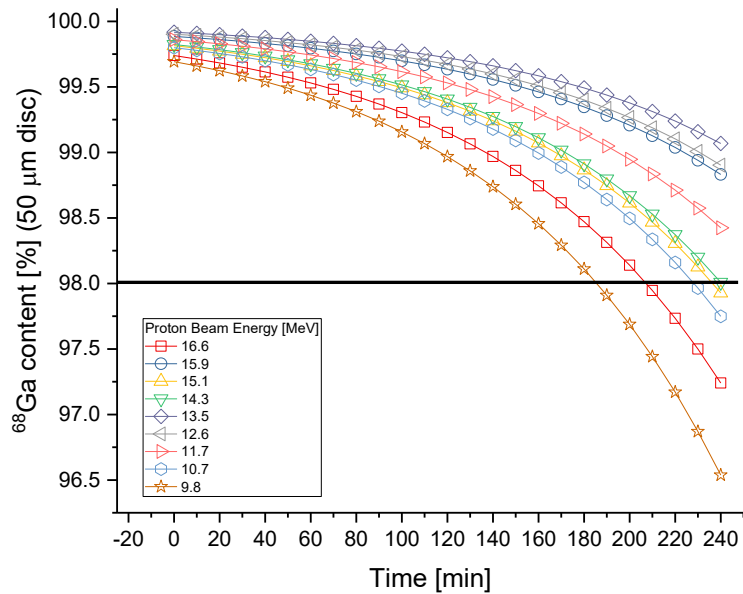


Figure 110 ^{68}Ga content vs time and proton beam energy for ^{68}Zn enriched targets 50 μm of thickness.

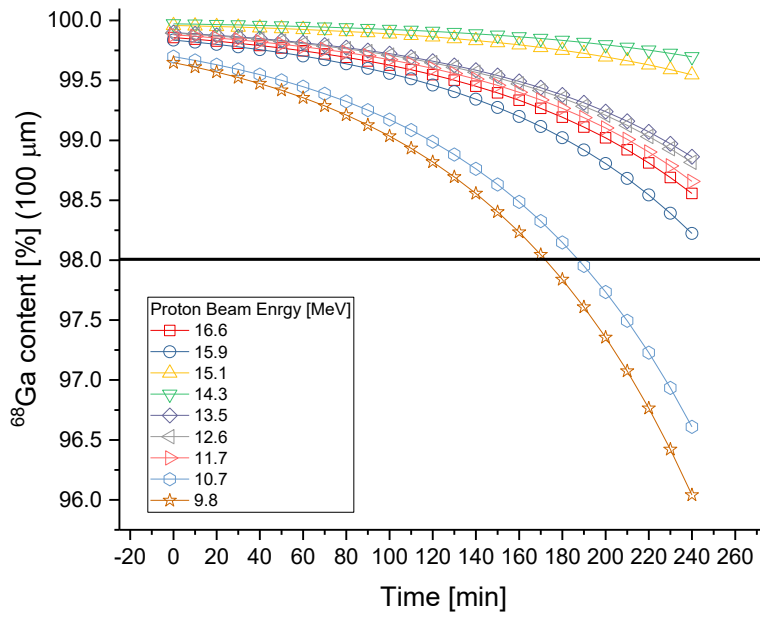


Figure 111 ^{68}Ga content vs time and proton beam energy for ^{68}Zn enriched targets 100 μm of thickness.

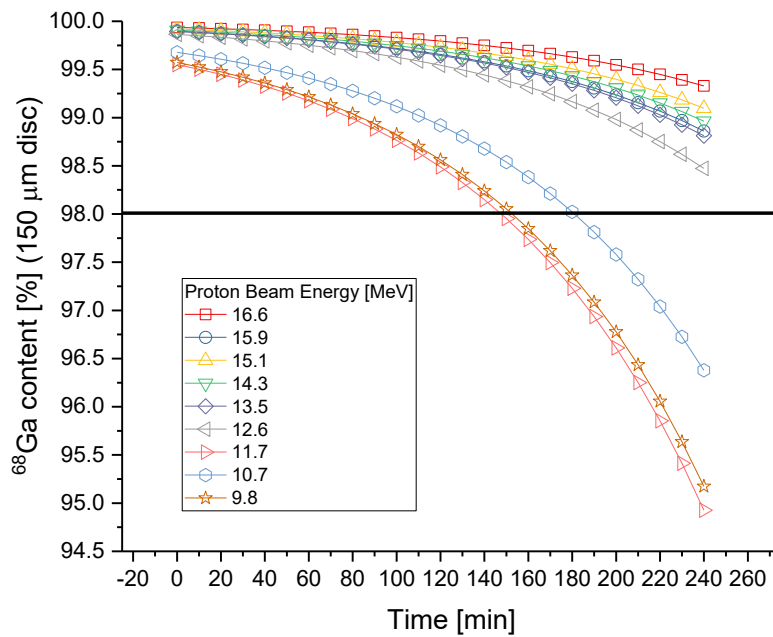


Figure 112 ^{68}Ga content vs time and proton beam energy for ^{68}Zn enriched targets 150 μm of thickness.

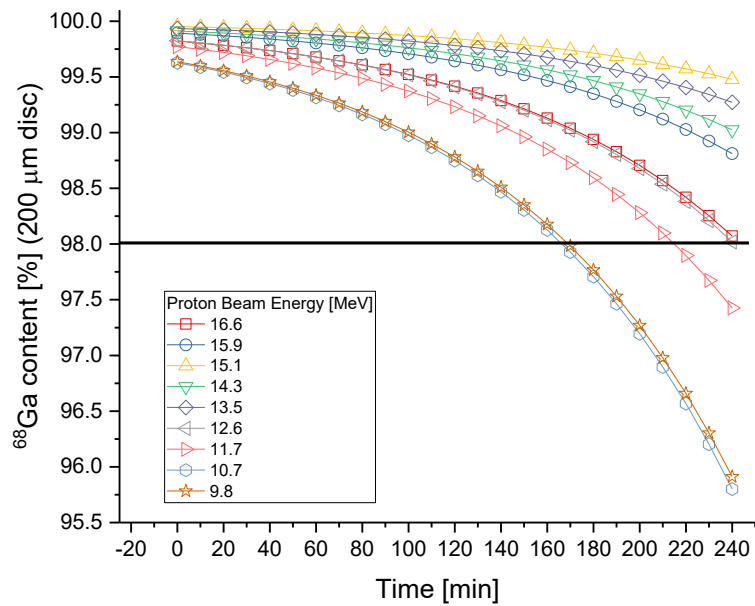


Figure 113 ^{68}Ga content vs time and proton beam energy for ^{68}Zn enriched targets 200 μm of thickness.

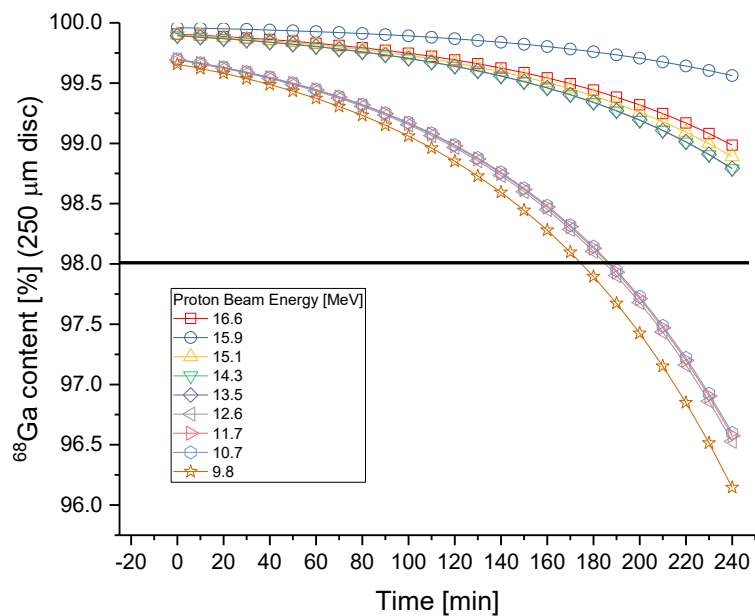


Figure 114 ^{68}Ga content vs time and proton beam energy for ^{68}Zn enriched targets 250 μm of thickness.

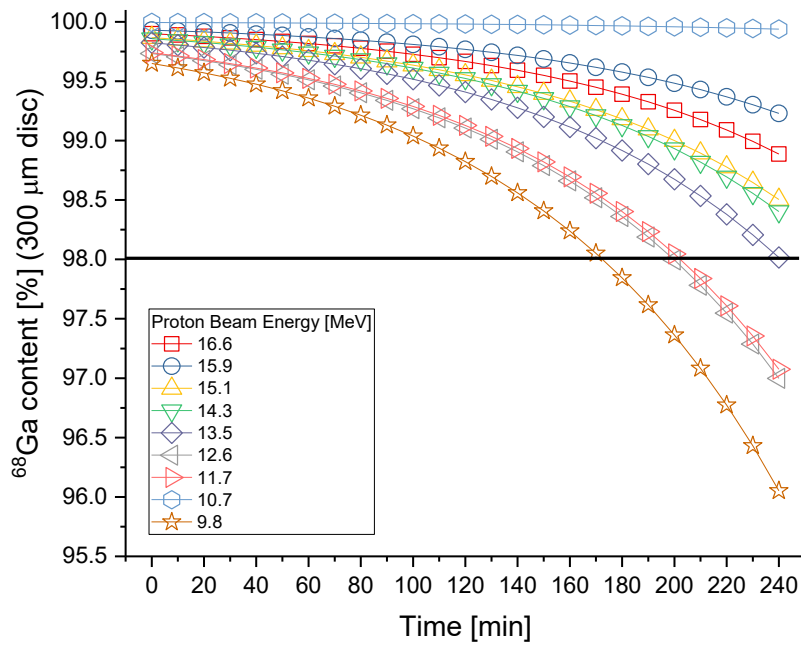


Figure 115 ^{68}Ga content vs time and proton beam energy for ^{68}Zn enriched targets 300 μm of thickness.

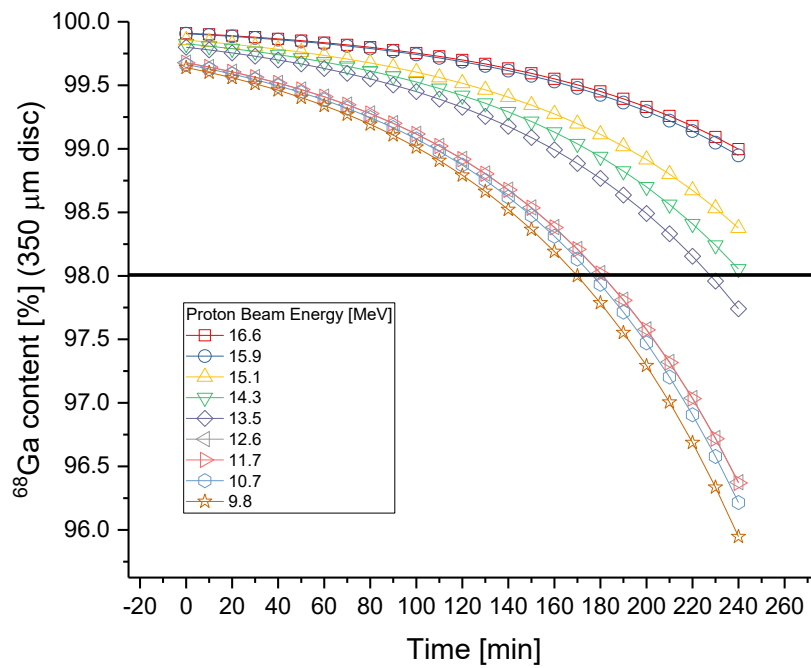


Figure 116 ^{68}Ga content vs time and proton beam energy for ^{68}Zn enriched targets 350 μm of thickness.

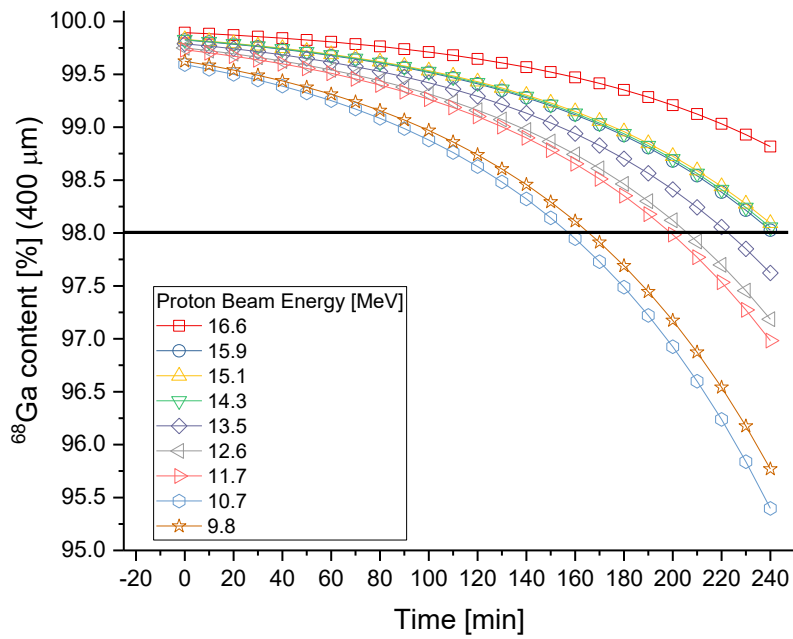


Figure 117 ^{68}Ga content vs time and proton beam energy for ^{68}Zn enriched targets 400 μm of thickness.

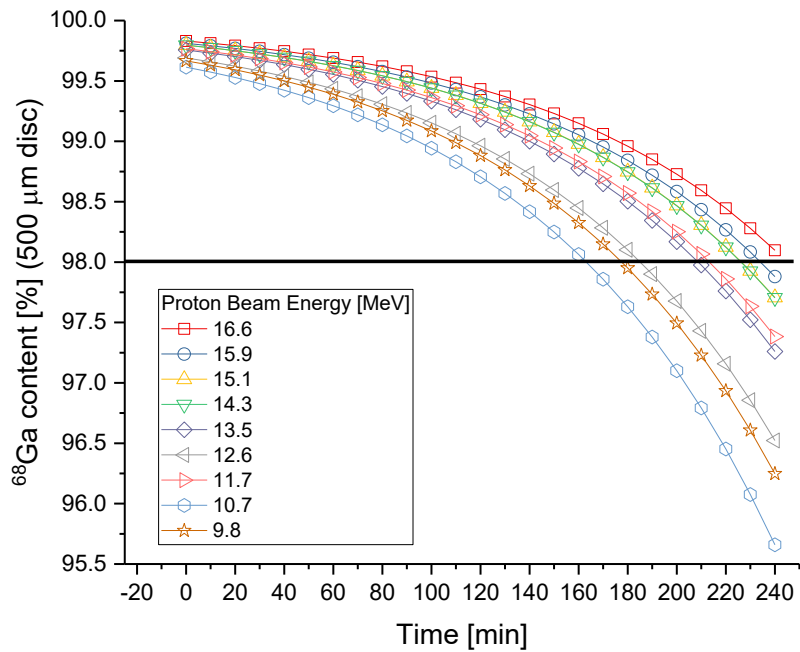


Figure 118 ^{68}Ga content vs time and proton beam energy for ^{68}Zn enriched targets 500 μm of thickness.

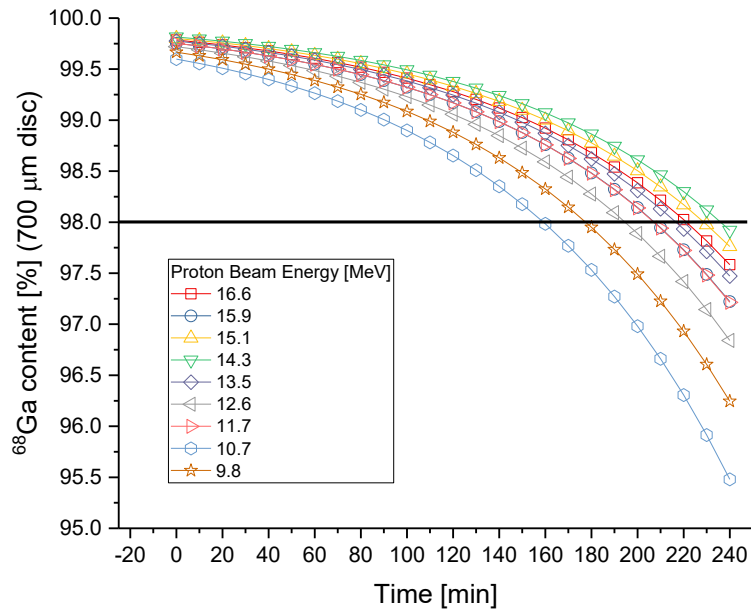


Figure 119 ^{68}Ga content vs time and proton beam energy for ^{68}Zn enriched targets 700 μm of thickness.

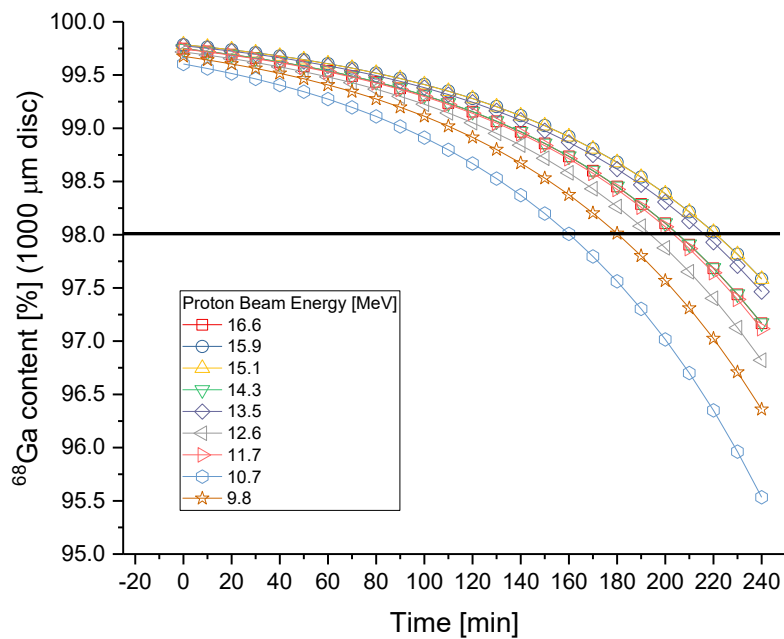


Figure 120 ^{68}Ga content vs time and proton beam energy for ^{68}Zn enriched targets 1000 μm of thickness.

Enriched Zinc-68 solution target proton bombardment – gamma spectroscopy results

For gallium-68 produced in a solution target, gallium-67 (gamma energy 93, 184, 209 and 887 keV) and gallium-66 (1039 keV) were identified as the main impurity radionuclides (Figure 121). For the first production, the activity of gallium-67 was 0.7-0.8% pre-purification and 0.4-0.5% post-purification. Following target improvement (energy degradation), subsequent productions gave corresponding values of 0.17-0.23% and 0.20-0.25%. The activities of gallium-66 were about two orders of magnitude smaller.

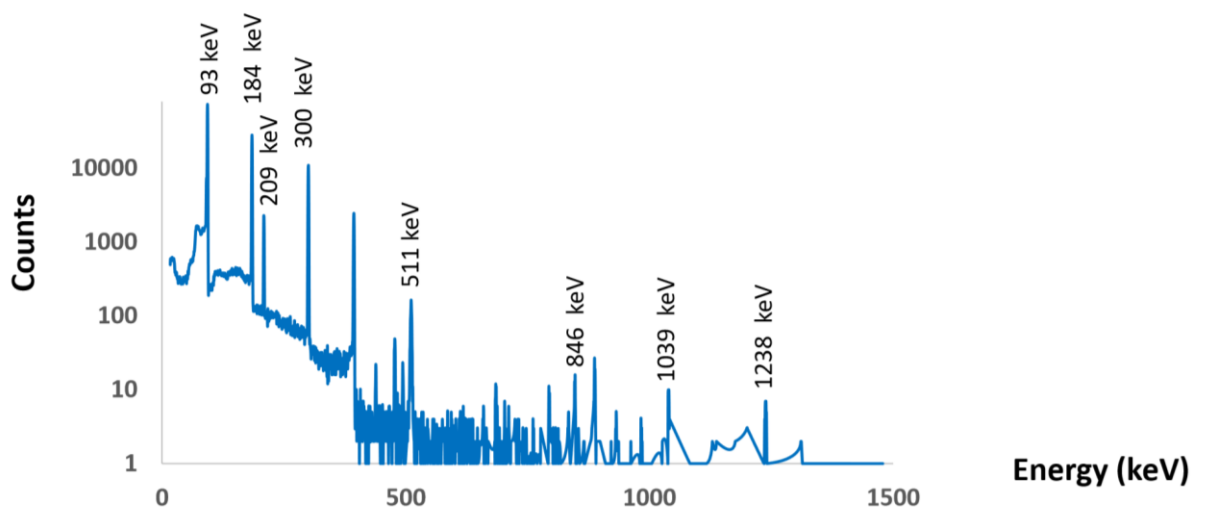


Figure 121 Gallium-68 gamma spectrum for sample produced in solution target.

Discussion

The irradiation of ^{68}Zn by protons was the only available method, in the range of used energies (Figure 75 a), among several possible nuclear reactions [177] as it leads to a large production yield and uses protons, the simplest and most widely available of all cyclotron projectiles. It is generally necessary to bombard isotopically enriched ^{68}Zn as several radioisotopes of gallium with longer half-lives than ^{68}Ga are also co-produced when irradiating natural Zn. However, despite the use of isotopically enriched ^{68}Zn , small amounts of ^{66}Ga and ^{67}Ga will occur as it is not possible to acquire 100% pure ^{68}Zn , and even in the event of pure ^{68}Zn being

available, the proton irradiation of ^{68}Zn leads to the production of ^{67}Ga radioisotopic impurity through the $^{68}\text{Zn}(p,2n)^{67}\text{Ga}$ reaction for proton energies larger than 12.2 MeV (Figure 122). Therefore, the composition of the isotopically enriched ^{68}Zn and the proton energy must be selected wisely to balance yield and achieve a purity suitable for human use [32, 33, 158, 177, 178].

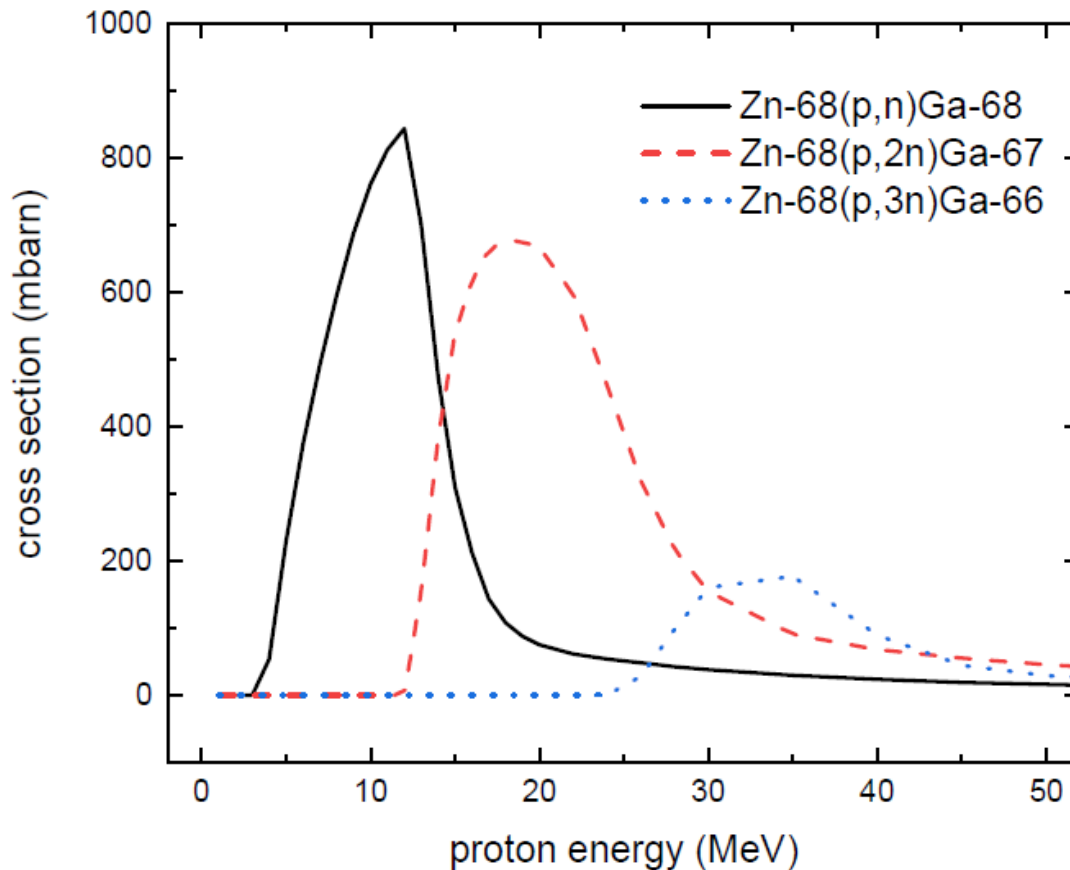


Figure 122 Excitation function for the $^{68}\text{Zn}(p,n)^{68}\text{Ga}$, $^{68}\text{Zn}(p,2n)^{67}\text{Ga}$ and $^{68}\text{Zn}(p,3n)^{66}\text{Ga}$ reactions [179].

FLUKA simulations' results received for ^{68}Zn pure and ^{68}Zn enriched targets confirm the well-known statements from the literature [27] presented above, but also help to find and estimate the yields of the other isotopical impurities that can state a potential risk for human use of the ^{68}Ga labelled product and are not easy to detect by gamma spectroscopy (Figure 121).

Figure 75 b and 84 b, presenting yields of ^{68}Ga productions for range of energies and target thicknesses, shows a fully reasonable picture where the maximums for thin targets lay close or exactly in the same range (10 MeV) like for excitation function shown in Figure 122. For thinner targets effect of energy degradation in the volume of these target is smaller and the energy range for maximum yield corresponds to the energy of excitation function's maximum cross-section. The situation is analogical to ^{89}Zr and ^{48}V production yields, where thicker targets (even a bit more than 5 μm) have their maximum yield shifted towards energies higher than 10 MeV. This effect increases with growing thickness of the target as the target itself provides additional energy degradation for the proton beam reaching the target with initial energy higher than 10 MeV.

To optimize potential solid target production yield of ^{68}Ga it is necessary also to analyse content of the radionuclide impurities and energy range for which they are produced. We can assume that impurities in form of isotopes of other elements than Gallium like Cu, Ni and Zn can be easily removed in the process of chemical purification. This purification procedure should be relatively quick as the ^{68}Ga half-life is only 67.71 min and another phenomenon called shelf life plays significant role. However, reducing the amount of these isotopes and being able to quantify their amounts produced is important to minimise the number of radioactive by-products in this process.

Other two Gallium (^{67}Ga ; $t_{1/2} = 3.26$ days and ^{68}Ga ; $t_{1/2} = 9.49$ hours) isotopes with longer half-lives and yields that cannot be neglected degrade purity of the product with the level raising with elapsed time. Analysis of this relationship, which is the third factor, that should be considered during gallium-68 production optimization, would be based on results shown in the Figures 108 – 120.

Starting from ^{68}Ga yields, to find optimal conditions by getting maximally pure product with possibly longest shelf life and looking at Figures 75b and 84 b one can see that relationship of yield with target thickness and energy is almost the same for pure and enriched ^{68}Zn target. Gallium-67 is only produced in significant quantities above 12.5 MeV and can be avoided using beam energies below this value or thicker targets with slightly higher beam energy. From Figure 84b, increasing the target thickness increases the yield up to 300 μm thickness. Increasing the thickness above this value provides little increase in yield but moves maximum to higher energies where ^{67}Ga is produced. Figures 87 and 88 show that there is no sharp threshold for starting the production of gallium-66 in ^{68}Zn enriched target for considered energy range what agrees with Figure 123 (it is worth to mention that

Figure 122 shows that for pure ^{68}Zn target there is no channel for production of ^{66}Ga below 25 MeV). However, its yields are relatively small between 10 and 14.5 MeV before beginning to increase above this value. Therefore, optimum beam energy to produce ^{68}Ga is around 12.5 MeV as this gives the maximum yield of ^{68}Ga whilst preventing gallium-67 production and minimising gallium-66 production. Increasing the beam energy above 12.5 MeV provides little increase in yield of gallium-68 for target thickness below 300 μm and in fact would lead to lower yields in thinner targets below 150 μm . This agrees completely with ARTMS yields shown in the page 118 and explains why they used beam energies 11 - 12.8 MeV. This value of the used beam energy helps to avoid production of the problematic ^{67}Ga impurity for which 12.5 MeV is the lower production cut-out energy (Figure 122). Figures 66 and 75 confirm that for pure and enriched targets. Figures 77 and 86 show that for both kinds of targets amount of ^{67}Ga related to ^{68}Ga is not higher than 2% up to 14.5 MeV. Situation looks different for ^{66}Ga impurity which production via $^{68}\text{Zn}(p,3n)^{66}\text{Ga}$ can be eliminated using pure ^{68}Zn target and beam energy below 25 MeV (Figure 122). For ^{68}Zn enriched target containing small amounts (0.01 %) of ^{66}Zn reaction $^{66}\text{Zn}(p,n)^{66}\text{Ga}$ becomes available for production of ^{66}Ga impurity (Figure 123), however with much smaller yield and less impact on shelf life of the product than ^{67}Ga .

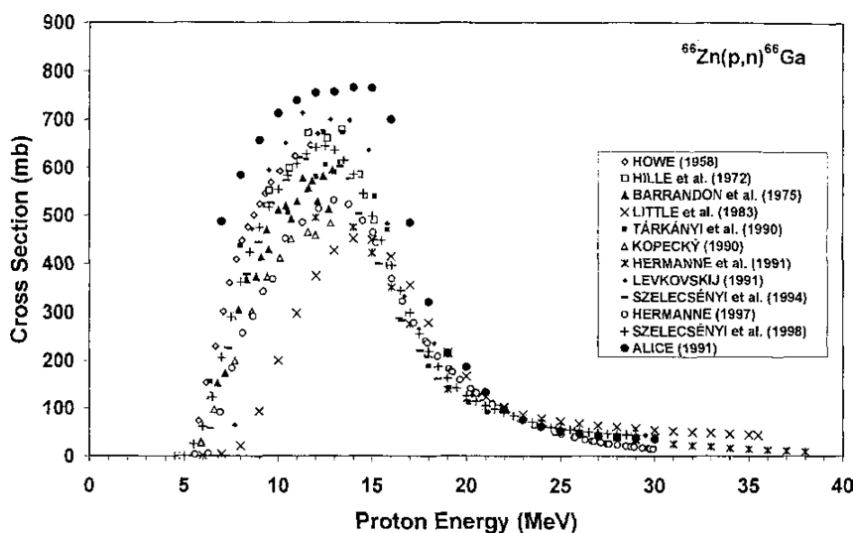


Figure 123 Excitation function for the $^{66}\text{Zn}(p,n)^{66}\text{Ga}$ reactions [179].

Figures 124 and Figure 125 show reactions and cross-sections for other less abundant impurities that might appear as by-products together with ^{68}Ga to compare with FLUKA simulations (Figures 89-107).

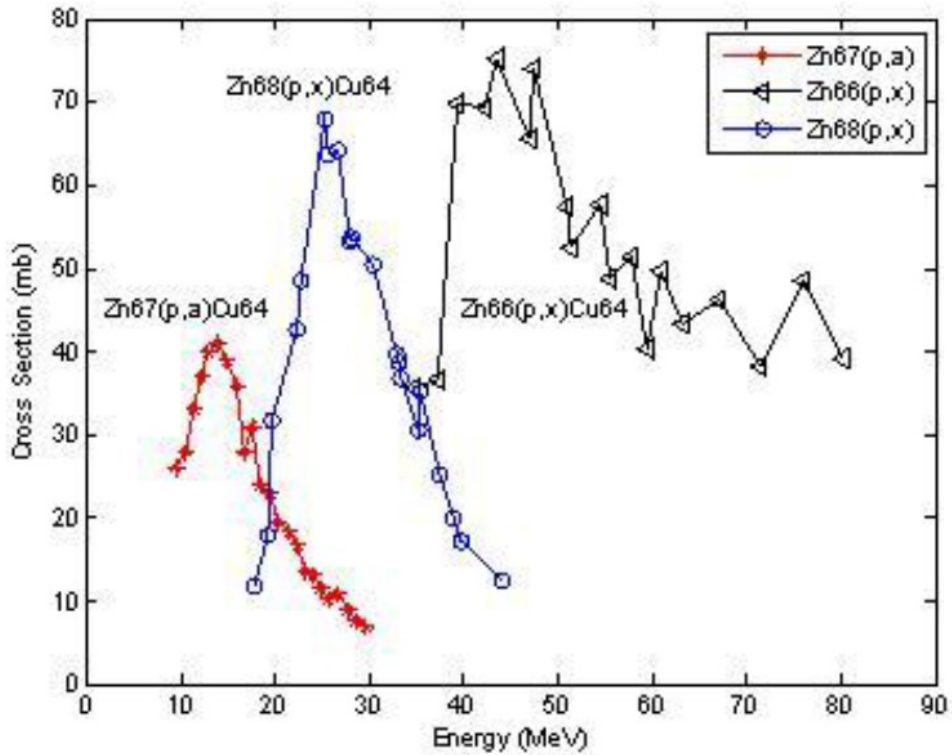


Figure 124 Excitation functions for Cu^{64} of the Three Reactions $\text{Zn}^{68}(\text{p},\text{x})$, $\text{Zn}^{66}(\text{p},\text{x})$ and $\text{Zn}^{67}(\text{p},\text{a})$ [180].

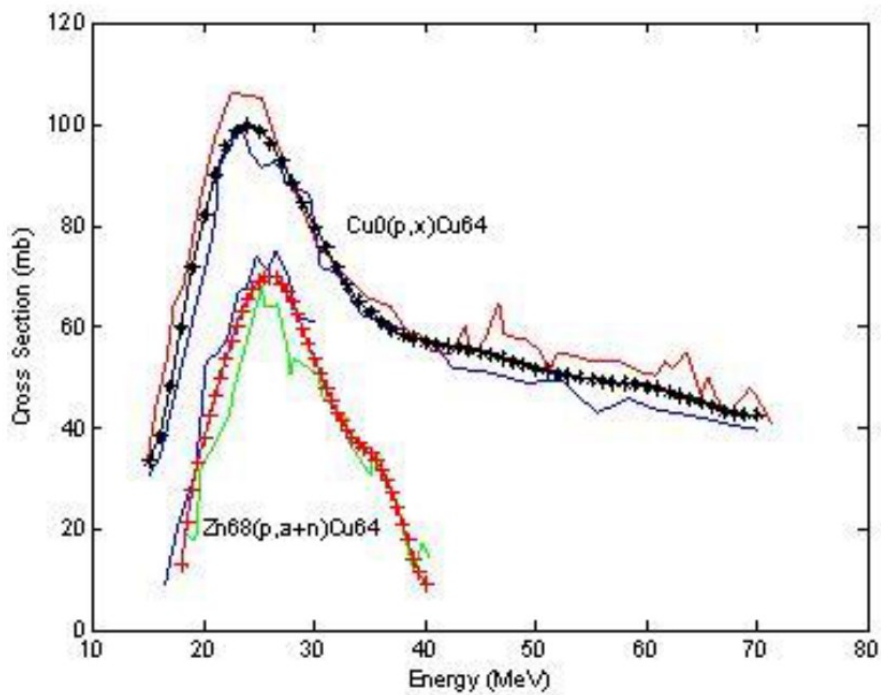


Figure 125 Excitation functions of the Reactions $\text{natCu}(\text{p},\text{x})\text{Cu}^{64}$ and $\text{Zn}^{68}(\text{p},\text{a}+\text{n})\text{Cu}^{64}$ [180].

Conclusion

From discussion of the basic impurities that can appear during ^{68}Ga production and product yields, optimal target thickness lays in the range 100-350 μm . However, looking in the Figures 111-116 one can see decrease of the shelf life from about 4 h to about 2 h with increasing target thickness. Therefore, the cost of increased yield (two times) is shorter shelf life (also two times).

Additionally, for solid target irradiations yields are much higher than for solution targets. One hour run in solution target gives about 5 GBq when solid target irradiation in the same time 180 GBq or more.

Final Conclusions

My Italian colleagues: Dr Mario Marengo and Dr Angelo Infantino, explained to me few facts about Monte Carlo method:

- The perfect Monte Carlo code does not exist.
- Every Monte Carlo code has a more dedicated field of application.
- The experimental measurements validate the simulations and not vice versa.

And most important that the “simulation” gives a result that is “wrong” by nature.

FLUKA is the code that base on Monte Carlo method to simulate transport of the particles in matter. It is still evolving tool that was first designed for high energy phenomena simulations (GeV or more) and is still updated and enriched with new parts of the code that enable research of the new domains in science. FLUKA is a subject of constant verification, validation and testing from scientific groups of whole World.

The aim of this thesis was to show that also cyclotron engineers and physicists can take advantage of using this method for more efficient target design and modification. Even with some problems like not generating separate results for isomeric states of the same isotopes FLUKA seems to be very useful instrument for simulations helping to innovate nuclear medicine and PET. Not only cyclotrons can be modelled with FLUKA, also detectors, PET scanners and whole facilities and vaults in case of the radioprotection studies and dose calculations.

This project shows how FLUKA can be used to optimize production of four subjectively chosen promising radiometals. Also, lot of practical remarks were given that can help others to avoid mistakes and make their cyclotron production safe.

Future perspective that might be continuation of presented here methods and experiments might be use of FLUKA for detecting activation products in the cyclotron parts, Al target holder and Nb degraders or liquid target parts to find possible threats or optimize used materials to avoid them.

Very interesting domain would be simulation of radiometals production in solution targets.

However, the final conclusion is that simulation will never replace a well-designed experiment or measurement but might be very useful in finding the best way of planning and preparation for the best scientific method to receive ground-breaking results.

References

- [1] O. F. Ikotun and S. E. Lapi, "The rise of metal radionuclides in medical imaging: copper-64, zirconium-89 and yttrium-86," (in eng), *Future Med Chem*, vol. 3, no. 5, pp. 599-621, Apr 2011.
- [2] C. S. Cutler, H. M. Hennkens, N. Sisay, S. Huclier-Markai, and S. S. Jurisson, "Radiometals for Combined Imaging and Therapy," *Chemical Reviews*, vol. 113, no. 2, pp. 858-883, 2013/02/13 2013.
- [3] D. Brasse and A. Nonat, "Radiometals: towards a new success story in nuclear imaging?," *Dalton Transactions*, 10.1039/C4DT02911A 2015.
- [4] S. Banerjee, M. R. Pillai, and N. Ramamoorthy, "Evolution of Tc-99m in diagnostic radiopharmaceuticals," (in eng), *Semin Nucl Med*, vol. 31, no. 4, pp. 260-77, Oct 2001.
- [5] R. C. Mease and C. Lambert, "Newer methods of labeling diagnostic agents with Tc-99m," (in eng), *Semin Nucl Med*, vol. 31, no. 4, pp. 278-85, Oct 2001.
- [6] W. Wadsak and M. Mitterhauser, "Basics and principles of radiopharmaceuticals for PET/CT," *European Journal of Radiology*, vol. 73, no. 3, pp. 461-469, 2010/03/01/ 2010.
- [7] D. L. Smith, W. A. Breeman, and J. Sims-Mourtada, "The untapped potential of Gallium 68-PET: the next wave of (6)(8)Ga-agents," (in eng), *Appl Radiat Isot*, vol. 76, pp. 14-23, Jun 2013.
- [8] F. Alves, V. Alves, S. do Carmo, A. C. B. Neves, M. Silva, and A. Abrunhosa, *Production of copper-64 and gallium-68 with a medical cyclotron using liquid targets*. 2017.
- [9] M. K. Pandey, J. F. Byrne, H. Jiang, A. B. Packard, and T. R. DeGrado, "Cyclotron production of (68)Ga via the (68)Zn(p,n)(68)Ga reaction in aqueous solution," *American Journal of Nuclear Medicine and Molecular Imaging*, vol. 4, no. 4, pp. 303-310, 2014.
- [10] M. K. Pandey, H. P. Engelbrecht, J. P. Byrne, A. B. Packard, and T. R. DeGrado, "Production of 89Zr via the 89Y(p,n)89Zr reaction in aqueous solution: effect of solution composition on in-target chemistry," (in eng), *Nucl Med Biol*, vol. 41, no. 4, pp. 309-16, Apr 2014.
- [11] M. A. Deri, B. M. Zeglis, L. C. Francesconi, and J. S. Lewis, "PET imaging with 89Zr: From radiochemistry to the clinic," *Nuclear Medicine and Biology*, vol. 40, no. 1, pp. 3-14, 1// 2013.

- [12] O. T. Dejesus and R. J. Nickles, "Production and purification of ^{89}Zr , a potential PET antibody label," *International Journal of Radiation Applications and Instrumentation. Part A. Applied Radiation and Isotopes*, vol. 41, no. 8, pp. 789-790, // 1990.
- [13] S. Zurrida and U. Veronesi, "Milestones in Breast Cancer Treatment," (in Eng), *Breast J*, Dec 15 2014.
- [14] I. Ihnenfeld Arcienega, P. Imesch, D. Fink, and K. J. Dedes, "Prolonged complete remission of metastatic HER2-positive breast cancer after continuous trastuzumab treatment: a case report and review of the literature," (in Eng), *Target Oncol*, Dec 17 2014.
- [15] Y. Zhang, H. Hong, and W. Cai, "PET tracers based on Zirconium-89," (in eng), *Curr Radiopharm*, vol. 4, no. 2, pp. 131-9, Apr 2011.
- [16] M. Harries and I. Smith, "The development and clinical use of trastuzumab (Herceptin)," (in eng), *Endocr Relat Cancer*, vol. 9, no. 2, pp. 75-85, Jun 2002.
- [17] J. M. Kirkwood, L. H. Butterfield, A. A. Tarhini, H. Zarour, P. Kalinski, and S. Ferrone, "Immunotherapy of Cancer in 2012," *CA: a cancer journal for clinicians*, vol. 62, no. 5, pp. 309-335, 05/10 2012.
- [18] T. K. Nayak and M. W. Brechbiel, "Radioimmunoimaging with longer-lived positron-emitting radionuclides: potentials and challenges," (in eng), *Bioconjug Chem*, vol. 20, no. 5, pp. 825-41, May 20 2009.
- [19] J. Wang, Z.-H. Zou, H.-L. Xia, J.-X. He, N.-S. Zhong, and A.-L. Tao, "Strengths and Weaknesses of Immunotherapy for Advanced Non-Small-Cell Lung Cancer: A Meta-Analysis of 12 Randomized Controlled Trials," *PLoS ONE*, vol. 7, no. 3, p. e32695, 2012.
- [20] G. Zhou and H. Levitsky, "Towards Curative Cancer Immunotherapy: Overcoming Posttherapy Tumor Escape," *Clinical and Developmental Immunology*, vol. 2012, p. 124187, 2012.
- [21] D. J. Vugts and G. A. M. S. van Dongen, " ^{89}Zr -labeled compounds for PET imaging guided personalized therapy," *Drug Discovery Today: Technologies*, vol. 8, no. 2-4, pp. e53-e61, //Summer 2011.
- [22] E. W. Price and C. Orvig, "Matching chelators to radiometals for radiopharmaceuticals," *Chemical Society Reviews*, 10.1039/C3CS60304K vol. 43, no. 1, pp. 260-290, 2014.
- [23] T. J. Wadas, E. H. Wong, G. R. Weisman, and C. J. Anderson, "Coordinating radiometals of copper, gallium, indium, yttrium, and zirconium for PET and

- SPECT imaging of disease," (in eng), *Chem Rev*, vol. 110, no. 5, pp. 2858-902, May 12 2010.
- [24] M. J. Welch, R. Laforest, and J. S. Lewis, "Production of non-standard PET radionuclides and the application of radiopharmaceuticals labeled with these nuclides," (in eng), *Ernst Schering Res Found Workshop*, no. 62, pp. 159-81, 2007.
- [25] E. Rorat, B. Petelenz, B. Marczewska, and E. Ochab, "Thermoluminescence dosimetry of model line sources containing vanadium-48," *Radiation Measurements*, vol. 39, no. 5, pp. 495-501, 10// 2005.
- [26] N. Eigler *et al.*, "Effects of a positron-emitting VANADIUM-48 nitinol stent on experimental restenosis in porcine coronary arteries: An injury–response study," *Cardiovascular Radiation Medicine*, vol. 1, no. 3, pp. 239-251, 7// 1999.
- [27] A. Arbabi, M. Sadeghi, and M. Joharifard, "Irradiation and dosimetry of Nitinol stent for renal artery brachytherapy," (in eng), *Appl Radiat Isot*, vol. 67, no. 1, pp. 129-32, Jan 2009.
- [28] R. D. Hichwa *et al.*, "Vanadium-48: A renewable source for transmission scanning with PET," *Nuclear Instruments and Methods in Physics Research Section B: Beam Interactions with Materials and Atoms*, vol. 99, no. 1–4, pp. 804-806, 5/5/ 1995.
- [29] T. J. Ruth, "The medical isotope crisis: how we got here and where we are going," (in eng), *J Nucl Med Technol*, vol. 42, no. 4, pp. 245-8, Dec 2014.
- [30] J. E. Beaver and H. B. Hupf, "Production of ^{99m}Tc on a Medical Cyclotron: A Feasibility Study," *Journal of Nuclear Medicine*, vol. 12, no. 11, pp. 739-741, November 1, 1971 1971.
- [31] I. Velikyan, "Positron Emitting [^{68}Ga]Ga-Based Imaging Agents: Chemistry and Diversity," *Medicinal Chemistry*, vol. 7, no. 5, pp. 345-379, // 2011.
- [32] I. Velikyan, "Prospective of (^{68}Ga)Ga-Radiopharmaceutical Development," *Theranostics*, vol. 4, no. 1, pp. 47-80, 2014.
- [33] I. Velikyan, " ^{68}Ga -Based Radiopharmaceuticals: Production and Application Relationship," *Molecules*, vol. 20, no. 7, 2015.
- [34] S. V. Smith, "Molecular imaging with copper-64," *Journal of Inorganic Biochemistry*, vol. 98, no. 11, pp. 1874-1901, 11// 2004.
- [35] D. V. F. V. Radchenko, O. K. Bochko, N. A. Lebedev, A. V. Rakhimov, H. Hauser, M. Eisenhut, N. V. Aksenov, G. A. Bozhikov, B. Ponsard, F. Roesch, "Separation of ^{90}Nb from zirconium target for application in immuno-PET.," *Radiochim. Acta*, pp. 433–442, 2014.

- [36] J. P. Holland *et al.*, "Optimizing the production, separation and radiochemistry of ^{90}Nb for PET imaging.," in *World Molecular Imaging Congress 2013*, Georgia, USA, 2013.
- [37] J. Czernin, M. Allen-Auerbach, D. Nathanson, and K. Herrmann, "PET/CT in Oncology: Current Status and Perspectives," *Current Radiology Reports*, vol. 1, no. 3, pp. 177-190, 05/03 2013.
- [38] T. Beyer, "PET: Speed Dating CT or MRI?," *Journal of Nuclear Medicine*, vol. 48, no. 3, p. 331, March 1, 2007 2007.
- [39] W. G. Meyers, "Georg Charles de Hevesy: the father of nuclear medicine. Proceedings of the 26th Annual Meeting," *Journal of Nuclear Medicine*, vol. 20, no. 6, pp. 590-698, June 1, 1979 1979.
- [40] K. Strebhardt and A. Ullrich, "Paul Ehrlich's magic bullet concept: 100 years of progress," *Nat Rev Cancer*, 10.1038/nrc2394 vol. 8, no. 6, pp. 473-480, 06//print 2008.
- [41] R. J. Hicks, "The role of PET in monitoring therapy," *Cancer Imaging*, vol. 5, no. 1, pp. 51-57, 2005.
- [42] S. J. G. Jasna Mihailovic, Ronan P. Killeen *FDG PET/CT in Clinical Oncology Case Based Approach with Teaching Points*. Springer Berlin Heidelberg, 2012.
- [43] R. J. Hicks, "Beyond FDG: novel PET tracers for cancer imaging," *Cancer Imaging*, vol. 4, no. 1, pp. 22-24, 2004.
- [44] P. G. Abrams and A. R. Fritzberg, *Radioimmunotherapy of Cancer*. CRC Press, 2000.
- [45] H. Herzog, F. Rösch, G. Stöcklin, C. Lueders, S. M. Qaim, and L. E. Feinendegen, "Measurement of Pharmacokinetics of Yttrium-86 Radiopharmaceuticals with PET and Radiation Dose Calculation of Analogous Yttrium-90 Radiotherapeutics," *Journal of Nuclear Medicine*, vol. 34, no. 12, pp. 2222-2226, December 1, 1993 1993.
- [46] M. A. Avila-Rodriguez, J. A. Nye, and R. J. Nickles, "Production and separation of non-carrier-added ^{86}Y from enriched ^{86}Sr targets," (in eng), *Appl Radiat Isot*, vol. 66, no. 1, pp. 9-13, Jan 2008.
- [47] I. Verel, G. W. Visser, R. Boellaard, M. Stigter-van Walsum, G. B. Snow, and G. A. van Dongen, " ^{89}Zr immuno-PET: comprehensive procedures for the production of ^{89}Zr -labeled monoclonal antibodies," (in eng), *J Nucl Med*, vol. 44, no. 8, pp. 1271-81, Aug 2003.

- [48] P. K. E. Börjesson *et al.*, "Radiation Dosimetry of ⁸⁹Zr-Labeled Chimeric Monoclonal Antibody U36 as Used for Immuno-PET in Head and Neck Cancer Patients," *Journal of Nuclear Medicine*, vol. 50, no. 11, pp. 1828-1836, November 1, 2009 2009.
- [49] G. A. van Dongen and M. J. Vosjan, "Immuno-positron emission tomography: shedding light on clinical antibody therapy," (in eng), *Cancer Biother Radiopharm*, vol. 25, no. 4, pp. 375-85, Aug 2010.
- [50] M. Shokeen and C. J. Anderson, "Molecular imaging of cancer with copper-64 radiopharmaceuticals and positron emission tomography (PET)," (in eng), *Acc Chem Res*, vol. 42, no. 7, pp. 832-41, Jul 21 2009.
- [51] M. Shokeen and T. J. Wadas, "The development of copper radiopharmaceuticals for imaging and therapy," (in eng), *Med Chem*, vol. 7, no. 5, pp. 413-29, Sep 2011.
- [52] R. Banerjee, R. Banerjee, Ed. *Nanotechnology, Diagnosis and Treatment of Cancers*. Narosa Publishing House 2011, p. 286.
- [53] B. G. Nair, S. Hanna Varghese, R. Nair, Y. Yoshida, T. Maekawa, and D. Sakthi Kumar, "Nanotechnology Platforms; An Innovative Approach to Brain Tumor Therapy," *Medicinal Chemistry*, vol. 7, no. 5, pp. 488-503, // 2011.
- [54] S. A. Mousa and D. J. Bharali, "Nanotechnology-Based Detection and Targeted Therapy in Cancer: Nano-Bio Paradigms and Applications," *Cancers*, vol. 3, no. 3, pp. 2888-2903, 2011.
- [55] M. Brandt, J. Cardinale, M. L. Aulsebrook, G. Gasser, and T. L. Mindt, "An Overview of PET Radiochemistry, Part 2: Radiometals," *Journal of Nuclear Medicine*, vol. 59, no. 10, pp. 1500-1506, October 1, 2018 2018.
- [56] J. Humm, A. Rosenfeld, and A. Del Guerra, "From PET detectors to PET scanners," (in English), *European Journal of Nuclear Medicine and Molecular Imaging*, vol. 30, no. 11, pp. 1574-1597, 2003/11/01 2003.
- [57] S. Reardon, "Whole-body PET scanner produces 3D images in seconds," *Nature*, vol. 570, pp. 285-286, 2019.
- [58] T. K. Lewellen, "Recent developments in PET detector technology," *Physics in Medicine and Biology*, vol. 53, no. 17, p. R287, 2008.
- [59] S. Joao, C. Ben, and P. Mike, "Review on the characteristics of radiation detectors for dosimetry and imaging," *Physics in Medicine and Biology*, vol. 59, no. 20, p. R303, 2014.
- [60] J. P. Holland, M. J. Williamson, and J. S. Lewis, "Unconventional nuclides for radiopharmaceuticals," (in eng), *Mol Imaging*, vol. 9, no. 1, pp. 1-20, Feb 2010.

- [61] I. A. E. AGENCY, *Therapeutic Radionuclide Generators: $^{90}\text{Sr}/^{90}\text{Y}$ and $^{188}\text{W}/^{188}\text{Re}$ Generators* (Technical Reports Series, no. 470). Vienna: INTERNATIONAL ATOMIC ENERGY AGENCY, 2009.
- [62] I. A. E. AGENCY, *Alternative Technologies for ^{99}Tc Generators* (IAEA TECDOC Series, no. 852). Vienna: INTERNATIONAL ATOMIC ENERGY AGENCY, 1996.
- [63] I. A. E. AGENCY, *Manual for Reactor Produced Radioisotopes* (IAEA TECDOC Series, no. 1340). Vienna: INTERNATIONAL ATOMIC ENERGY AGENCY, 2003.
- [64] F. Benard *et al.*, "Implementation of Multi-Curie Production of ($^{99\text{m}}$)Tc by Conventional Medical Cyclotrons," (in eng), *J Nucl Med*, vol. 55, no. 6, pp. 1017-22, Jun 2014.
- [65] E. National Academies of Sciences and Medicine, *Opportunities and Approaches for Supplying Molybdenum-99 and Associated Medical Isotopes to Global Markets: Proceedings of a Symposium*. Washington, DC: The National Academies Press, 2018, p. 86.
- [66] P. Schaffer *et al.*, "Direct Production of $^{99\text{m}}\text{Tc}$ via $^{100}\text{Mo}(p,2n)$ on Small Medical Cyclotrons," *Physics Procedia*, vol. 66, pp. 383-395, 2015/01/01/ 2015.
- [67] I. A. E. AGENCY, *Cyclotron Produced Radionuclides: Principles and Practice* (Technical Reports Series, no. 465). Vienna: INTERNATIONAL ATOMIC ENERGY AGENCY, 2008.
- [68] I. A. E. AGENCY, *Cyclotron Produced Radionuclides: Physical Characteristics and Production Methods* (Technical Reports Series, no. 468). Vienna: INTERNATIONAL ATOMIC ENERGY AGENCY, 2009.
- [69] H. Paganetti and T. Bortfeld, *Proton Beam Radiotherapy - The State of the Art1*. 2005.
- [70] W. Levin, H. Kooy, J. S. Loeffler, and T. Delaney, *Proton beam therapy*. 2005, pp. 849-54.
- [71] E. T. Committee, "Radiopharmacy: An Update," *Technologist's Guide*, pp. 52-71, 2019.
- [72] J. P. d. Lima, "Nuclear Medicine Physics (*Alves F.* Cyclotron and radionuclide production)," *CRC Press*, 2011.
- [73] M. A. Synowiecki, L. R. Perk, and J. F. W. Nijsen, "Production of novel diagnostic radionuclides in small medical cyclotrons," (in eng), *EJNMMI radiopharmacy and chemistry*, vol. 3, no. 1, pp. 3-3, 2018.

- [74] S. M. Qaim, "Decay data and production yields of some non-standard positron emitters used in PET," (in eng), *Q J Nucl Med Mol Imaging*, vol. 52, no. 2, pp. 111-20, Jun 2008.
- [75] A. Dabkowski, Paisey, S., Talboys, M., and Marshall, C., "Optimization of Cyclotron Production for Radiometal of Zirconium 89," *Acta Physica Polonica A*, vol. 127, no. 5, pp. 1479-1482, 2015.
- [76] J. J. Livingood, *Principles of Cyclic particle accelerators*. London: D. van Nostrand Co, 1961.
- [77] W. Scharf and J. V. Siebers, *Biomedical particle accelerators*. American Institute of Physics, 1994.
- [78] Unknown, *Radcraft Publications*, vol. 18, no. 9, p. 23, 1947.
- [79] M. Sadeghi, M. Enferadi, and M. Bakhtiari, "Accelerator production of the positron emitter zirconium-89," *Annals of Nuclear Energy*, vol. 41, pp. 97-103, 3// 2012.
- [80] A. Wooten *et al.*, "Routine Production of ⁸⁹Zr Using an Automated Module," *Applied Sciences*, vol. 3, no. 3, p. 593, 2013.
- [81] M. Walther *et al.*, "Implementation of ⁸⁹Zr production and in vivo imaging of B-cells in mice with ⁸⁹Zr-labeled anti-B-cell antibodies by small animal PET/CT," (in eng), *Appl Radiat Isot*, vol. 69, no. 6, pp. 852-7, Jun 2011.
- [82] A. Ciarmatori *et al.*, "Some experimental studies on ⁸⁹Zr production," in *Radiochimica Acta International journal for chemical aspects of nuclear science and technology* vol. 99, ed, 2011, p. 631.
- [83] A. al-obaidi, A. Dabkowski, C. Marshall, and W. Evans, *Abstract: Radionuclide impurities in cyclotron-produced gallium-68 and zirconium-89 for positron emission tomography*. 2018.
- [84] O. Lebeda, E. J. van Lier, J. Stursa, J. Ralis, and A. Zyuzin, "Assessment of radionuclidic impurities in cyclotron produced (^{99m}Tc)," (in eng), *Nucl Med Biol*, vol. 39, no. 8, pp. 1286-91, Nov 2012.
- [85] M. K. Pandey, A. Bansal, H. P. Engelbrecht, J. F. Byrne, A. B. Packard, and T. R. DeGrado, "Improved production and processing of ⁸⁹Zr using a solution target," *Nuclear Medicine and Biology*, vol. 43, no. 1, pp. 97-100, 1// 2016.
- [86] C. Hoehr *et al.*, "Radiometals from liquid targets: ^{94m}Tc production using a standard water target on a 13MeV cyclotron," *Applied Radiation and Isotopes*, vol. 70, no. 10, pp. 2308-2312, 2012/10/01/ 2012.
- [87] S. J. C. do Carmo, P. J. H. Scott, and F. Alves, "Production of radiometals in liquid targets," *EJNMMI Radiopharmacy and Chemistry*, vol. 5, no. 1, p. 2, 2020/01/10 2020.

- [88] E. Oehlke *et al.*, "Production of Y-86 and other radiometals for research purposes using a solution target system," *Nuclear Medicine and Biology*, vol. 42, no. 11, pp. 842-849, 11// 2015.
- [89] R. Dölling, "BEAM DIAGNOSTICS FOR CYCLOTRONS," in *The 19th International Conference on Cyclotrons and their Applications*, Lanzhou, China, 2010, pp. 344 - 350: Institute of Modern Physics, Chinese Academy of Sciences.
- [90] ElexCommerce, COSTIS - Operating Manual TS04-80.00.00.01: Elex Commerce, 2007. [Online]. Available.
- [91] V. Hanemaayer *et al.*, "Solid targets for ^{99m}Tc production on medical cyclotrons," *AIP Conference Proceedings*, vol. 1509, no. 1, pp. 120-124, 2012.
- [92] J. Klug *et al.*, "Design of target systems for the high-yield production of Tc-99m with a cyclotron," *J NUCL MED MEETING ABSTRACTS*, vol. 54, no. 2_MeetingAbstracts, pp. 608-, May 1, 2013 2013.
- [93] P. Schaffer *et al.*, "Assessing the potential of using the Mo-100(p,2n)Tc-99m transformation as a means of producing Curie-quantities of Tc-99m on existing cyclotron infrastructure," *Journal of Labelled Compounds & Radiopharmaceuticals*, vol. 54, pp. S247-S247, 01/01 2011.
- [94] *Nuclear Medicine Resources Manual 2020 Edition*. Vienna: INTERNATIONAL ATOMIC ENERGY AGENCY, 2020.
- [95] C. O'Farrell, M. Zimmer, N. McDonald, and S. Spies, "Accuracy of the F-18 calibration setting with a Capintec dose calibrator," *Journal of Nuclear Medicine*, vol. 49, no. supplement 1, pp. 435P-435P, 2008.
- [96] T. T. Böhlen *et al.*, "The FLUKA Code: Developments and Challenges for High Energy and Medical Applications," *Nuclear Data Sheets*, vol. 120, pp. 211-214, 6// 2014.
- [97] A. Ferrari, P. R. Sala, A. Fassò, and R. J., " FLUKA: a multi-particle transport code," *CERN-2005-10*, vol. INFN/TC_05/11, no. SLAC-R-773, 2005.
- [98] M. P. W. Chin, T. T. Böhlen, A. Fassò, A. Ferrari, P. G. Ortega, and P. R. Sala, "FLUKA and PENELOPE simulations of 10 keV to 10 MeV photons in LYSO and soft tissue," *Radiation Physics and Chemistry*, vol. 95, pp. 170-173, 2// 2014.
- [99] A. Fasso, A. Ferrari, and P. Sala, "Radiation transport calculations and simulations," *Radiation protection dosimetry*, vol. 137, pp. 118-33, 09/01 2009.

- [100] "D - Some Popular Monte Carlo Codes for Particle Transport," in *Exploring Monte Carlo Methods*, W. L. Dunn and J. K. Shultis, Eds. Amsterdam: Elsevier, 2012, pp. 347-371.
- [101] A. Ferrari, P. R. Sala, A. Fassò, and R. J., "FLUKA: a multi-particle transport code," *CERN-2005-10*, vol. INFN/TC_05/11, no. SLAC-R-773, 2005.
- [102] G. Battistoni *et al.*, "The FLUKA code: description and benchmarking," (in English), *Hadronic Shower Simulation Workshop*, vol. 896, no. 1, pp. 31-49, 2007.
- [103] A. Fasso *et al.*, "The FLUKA code: present applications and future developments," 07/23 2003.
- [104] A. F. A. Fass`o, J. Ranft, P.R. Sala "FLUKA: Performances and Applications in the Intermediate Energy Range," *OECD Documents*, pp. 287–304, 1995.
- [105] A. Ferrari, Sala, P., Fassò, A., Ranft, J., "Fluka: a multi-particle transport code.," *Tech. Rep. CERN-2005-10*, vol. INFNTC-0511, SLAC-R-773, 2005.
- [106] G. Battistoni *et al.*, "Overview of the FLUKA code," *Annals of Nuclear Energy*, vol. 82, pp. 10-18, 2015/08/01/ 2015.
- [107] T. T. Böhlen *et al.*, "Benchmarking nuclear models of FLUKA and GEANT4 for carbon ion therapy," *Physics in Medicine and Biology*, vol. 55, no. 19, pp. 5833-5847, 2010/09/16 2010.
- [108] G. Battistoni, F. Cappucci, N. Bertolino, M. G. Brambilla, H. S. Mainardi, and A. Torresin, "FLUKA Monte Carlo simulation for the Leksell Gamma Knife Perfexion radiosurgery system: homogeneous media," (in eng), *Phys Med*, vol. 29, no. 6, pp. 656-61, Nov 2013.
- [109] A. Infantino *et al.*, "Prediction of 89Zr production using the Monte Carlo code FLUKA," *Applied Radiation and Isotopes*, vol. 69, no. 8, pp. 1134-1137, 8// 2011.
- [110] S. Vichi *et al.*, "Activation studies for the decommissioning of PET cyclotron bunkers by means of Monte Carlo simulations," *Radiation Physics and Chemistry*, vol. 174, p. 108966, 2020/09/01/ 2020.
- [111] K. Parodi, A. Ferrari, F. Sommerer, and H. Paganetti, "Clinical CT-based calculations of dose and positron emitter distributions in proton therapy using the FLUKA Monte Carlo code," *Physics in Medicine and Biology*, vol. 52, no. 12, pp. 3369-3387, 2007/05/17 2007.
- [112] A. Infantino *et al.*, "Radiation Protection Studies for Medical Particle Accelerators using Fluka Monte Carlo Code," *Radiation Protection Dosimetry*, vol. 173, no. 1-3, pp. 185-191, 2016.

- [113] W. S. Kozłowska *et al.*, "FLUKA particle therapy tool for Monte Carlo independent calculation of scanned proton and carbon ion beam therapy," *Physics in Medicine & Biology*, vol. 64, no. 7, p. 075012, 2019/03/29 2019.
- [114] S. M. Brugger *et al.*, "A phylogenetically conserved cis-regulatory module in the *Msx2* promoter is sufficient for BMP-dependent transcription in murine and *Drosophila* embryos," *Development*, vol. 131, no. 20, pp. 5153-5165, 2004.
- [115] M. Brugger, A. Ferrari, S. Roesler, and L. Ulrici, "Validation of the FLUKA Monte Carlo code for predicting induced radioactivity at high-energy accelerators," *Nuclear Instruments and Methods in Physics Research Section A: Accelerators, Spectrometers, Detectors and Associated Equipment*, vol. 562, pp. 814-818, 06/01 2006.
- [116] F. Ballarini *et al.*, "The physics of the FLUKA code: Recent developments," *Advances in Space Research*, vol. 40, pp. 1339-1349, 12/31 2007.
- [117] B. J. Beattie, K. S. Pentlow, J. O'Donoghue, and J. L. Humm, "A Recommendation for Revised Dose Calibrator Measurement Procedures for ⁸⁹Zr and ¹²⁴I," *PLOS ONE*, vol. 9, no. 9, p. e106868, 2014.
- [118] J. P. Holland, Y. Sheh, and J. S. Lewis, "Standardized methods for the production of high specific-activity zirconium-89," (in eng), *Nucl Med Biol*, vol. 36, no. 7, pp. 729-39, Oct 2009.
- [119] J. C. Knight *et al.*, "Scaling-down antibody radiolabeling reactions with zirconium-89," *Dalton Transactions*, 10.1039/C5DT04774A vol. 45, no. 15, pp. 6343-6347, 2016.
- [120] M. U. Khandaker, K. Kim, M.-W. Lee, K.-S. Kim, G. Kim, and N. Otuka, "Investigations of ⁸⁹Y(p,x)^{86,88,89}Zr, ^{86m+g,87g,87m,88g}Y, ^{85g}Sr, and ^{84g}Rb nuclear processes up to 42 MeV," *Nuclear Instruments and Methods in Physics Research Section B: Beam Interactions with Materials and Atoms*, vol. 271, pp. 72-81, 1/15/ 2012.
- [121] H. M. Uddin M. S., M. Baba, F. Tarkanyi, F. Ditroi, "Experimental studies on excitation functions of the proton-induced activation reactions on yttrium.," *Appl. Radiat. Isot.*, vol. 63, no. 3, pp. 367-374, 2005.
- [122] H. T.-D. S. Poniger, H. Panopoulos, A. Scott, "Fully automated production of Zr-89 using IBA Nirta and Pinctada Systems - Poster Session 2-11," in *WTTC15*, 2015.
- [123] J. M. Link, K. A. Krohn, and M. J. O'Hara, "A simple thick target for production of ⁸⁹Zr using an 11 MeV cyclotron," *Applied Radiation and Isotopes*, vol. 122, pp. 211-214, 4// 2017.

- [124] M. L. Bonardi, E. Rizzio, M. Gallorini, F. Groppi, and H. S. Mainardi, "Improved radiochemical separation of no-carrier-added vanadium-48 from proton irradiated titanium target," *Journal of Radioanalytical and Nuclear Chemistry*, journal article vol. 263, no. 1, pp. 23-28, January 01 2005.
- [125] M. Sadeghi, M. Mahmodi, T. Kakavand, and C. Tenreiro, "Simulation of vanadium-48 production using MCNPX code," *Nuclear Technology and Radiation Protection*, vol. 27, no. 3, pp. 269-273, // 2012.
- [126] *Charged Particle Cross-Section Database for Medical Radioisotope Production: Diagnostic Radioisotopes and Monitor Reactions*. Vienna: INTERNATIONAL ATOMIC ENERGY AGENCY, 2001.
- [127] E. Sabbioni *et al.*, "Metallobiochemistry of current environmental levels of trace metals: A new method of cyclotron production of ^{48}V for toxicological studies," *Journal of Radioanalytical and Nuclear Chemistry*, journal article vol. 134, no. 1, pp. 199-208, November 01 1989.
- [128] F. H. Nielsen and E. O. Uthus, "The Essentiality and Metabolism of Vanadium," in *Vanadium in Biological Systems: Physiology and Biochemistry*, N. D. Chasteen, Ed. Dordrecht: Springer Netherlands, 1990, pp. 51-62.
- [129] I. Shtangeeva, "Scandium," vol. 20, 2004.
- [130] L. Deilami-nezhad, L. Moghaddam-Banaem, M. Sadeghi, and M. Asgari, "Production and purification of Scandium-47: A potential radioisotope for cancer theranostics," *Applied Radiation and Isotopes*, vol. 118, pp. 124-130, 2016/12/01/ 2016.
- [131] O.-. NEA, "2017 Medical Isotope Supply Review: $^{99}\text{Mo}/^{99\text{m}}\text{Tc}$ Market Demand and Production Capacity Projection 2017-2022," *The Supply of Medical Radioisotopes*, April 2017 2017.
- [132] C. H. Green, "Technetium-99m production issues in the United Kingdom," (in eng), *Journal of medical physics*, vol. 37, no. 2, pp. 66-71, 2012.
- [133] G. Krzysztozek, "The Characteristics and Irradiation Capabilities of MARIA Research Reactor in NCBJ Świerk," *EPJ Web of Conferences*, vol. 115, p. 01004, 2016.
- [134] *Technetium-99m Radiopharmaceuticals: Status and Trends*. Vienna: INTERNATIONAL ATOMIC ENERGY AGENCY, 2010.
- [135] *Cyclotron Based Production of Technetium-99m*. Vienna: INTERNATIONAL ATOMIC ENERGY AGENCY, 2017.
- [136] *Non-HEU Production Technologies for Molybdenum-99 and Technetium-99m*. Vienna: INTERNATIONAL ATOMIC ENERGY AGENCY, 2013.

- [137] B. A. Neilly, Sarah ; Ballinger, Jim ; Buscombe, John ; Clarke, Rob ; Ellis, Beverley ; Flux, Glenn ; Fraser, Louise ; Hall, Adrian ; Owen, Hywel ; Paterson, Audrey ; Perkins, Alan ; Scarsbrook, Andrew., "Future Supply of Medical Radioisotopes for the UK Report 2014.," *ArXiv.org.*, 2015.
- [138] "<https://shinemed.com>."
- [139] *Nuclear Security Culture*. Vienna: INTERNATIONAL ATOMIC ENERGY AGENCY, 2008.
- [140] *Preventive and Protective Measures against Insider Threats*. Vienna: INTERNATIONAL ATOMIC ENERGY AGENCY, 2008.
- [141] K. Mang'era *et al.*, "Processing and evaluation of linear accelerator-produced $^{99}\text{Mo}/^{99\text{m}}\text{Tc}$ in Canada," *Journal of Radioanalytical and Nuclear Chemistry*, vol. 305, no. 1, pp. 79-85, 2015/07/01 2015.
- [142] G. Pupillo, J. Esposito, F. Haddad, N. Michel, and M. Gambaccini, "Accelerator-based production of ^{99}Mo : a comparison between the $^{100}\text{Mo}(p,x)$ and $^{96}\text{Zr}(\alpha,n)$ reactions," *Journal of Radioanalytical and Nuclear Chemistry*, vol. 305, no. 1, pp. 73-78, 2015/07/01 2015.
- [143] K. Nakai *et al.*, "Feasibility studies towards future self-sufficient supply of the ^{99}Mo - $^{99\text{m}}\text{Tc}$ isotopes with Japanese accelerators," *Proceedings of the Japan Academy, Series B*, vol. 90, no. 10, pp. 413-421, 2014.
- [144] M. Fujiwara *et al.*, "Production of medical $^{99\text{m}}\text{Tc}$ isotope via photonuclear reaction," *Physics of Particles and Nuclei*, vol. 48, no. 1, pp. 124-133, 2017/01/01 2017.
- [145] V. Bychenkov, A. Brantov, and G. Mourou, "Tc-99m production with ultrashort intense laser pulses," *Laser and Particle Beams*, vol. 32, pp. 605-611, 12/01 2014.
- [146] IAEA, "Final report of the coordinated research project On Accelerator-based Alternatives to Non-HEU Production of Mo-99 /Tc-99m," no. Supporting Material, 2016.
- [147] J. E. Beaver and H. B. Hupf, "Production of $^{99\text{m}}\text{Tc}$ on a medical cyclotron: a feasibility study," (in eng), *J Nucl Med*, vol. 12, no. 11, pp. 739-41, Nov 1971.
- [148] S. M. Qaim, S. Sudár, B. Scholten, A. J. Koning, and H. H. Coenen, "Evaluation of excitation functions of $^{100}\text{Mo}(p,d+pn)^{99}\text{Mo}$ and $^{100}\text{Mo}(p,2n)^{99\text{m}}\text{Tc}$ reactions: Estimation of long-lived Tc-impurity and its implication on the specific activity of cyclotron-produced $^{99\text{m}}\text{Tc}$," *Applied Radiation and Isotopes*, vol. 85, pp. 101-113, 2014/02/01/ 2014.
- [149] M. Das *et al.*, "Production and separation of $^{99\text{m}}\text{Tc}$ from cyclotron irradiated ^{100}Mo /naturalMo targets: a new automated module for separation of $^{99\text{m}}\text{Tc}$

- from molybdenum targets," *Journal of Radioanalytical and Nuclear Chemistry*, vol. 310, pp. 423-432, 03/19 2016.
- [150] P. Martini *et al.*, "In-house Cyclotron Production of High-purity Tc-99m and Tc-99m Radiopharmaceuticals," *Applied Radiation and Isotopes*, vol. 139, 05/01 2018.
- [151] M. R. A. Rovais, K. Aardaneh, G. Aslani, A. Rahiminejad, K. Yousefi, and F. Boulouri, "Assessment of the direct cyclotron production of 99mTc: An approach to crisis management of 99mTc shortage," *Applied Radiation and Isotopes*, vol. 112, pp. 55-61, 2016/06/01/ 2016.
- [152] C. Brown, "Will new isotope sources be ready in time?," (in eng), *CMAJ : Canadian Medical Association journal = journal de l'Association medicale canadienne*, vol. 188, no. 4, pp. 252-252, 2016.
- [153] A. Celler, X. Hou, F. Bénard, and T. Ruth, "Theoretical modeling of yields for proton-induced reactions on natural and enriched molybdenum targets," *Physics in Medicine and Biology*, vol. 56, no. 17, p. 5469, 2011.
- [154] K. Gagnon *et al.*, "Cyclotron production of 99mTc: Experimental measurement of the $^{100}\text{Mo}(p,x)^{99}\text{Mo}$, ^{99}mTc and ^{99}gTc excitation functions from 8 to 18 MeV," *Nuclear Medicine and Biology*, vol. 38, no. 6, pp. 907-916, 2011/08/01/ 2011.
- [155] S. V. Selivanova *et al.*, "Radiation dose from cyclotron-produced 99mTc-radiopharmaceuticals based on their experimentally determined isotopic composition," *Nuclear Medicine and Biology*, vol. 41, no. 7, p. 649, 2014/08/01/ 2014.
- [156] S. Lapi, "Direct production of $^{99\text{m}}\text{Tc}$ using a small medical cyclotron," United States 2017-10-03 2017.
- [157] R. P. Baum and H. R. Kulkarni, "THERANOSTICS: From Molecular Imaging Using Ga-68 Labeled Tracers and PET/CT to Personalized Radionuclide Therapy - The Bad Berka Experience," (in eng), *Theranostics*, vol. 2, no. 5, pp. 437-447, 2012.
- [158] M. N. Aslam, N. Amjed, and S. M. Qaim, "Evaluation of excitation functions of the $^{68,67,66}\text{Zn}(p,xn)^{68,67,66}\text{Ga}$ and $^{67}\text{Zn}(p,\alpha)^{64}\text{Cu}$ reactions: Validation of evaluated data through comparison with experimental excitation functions of the $^{\text{nat}}\text{Zn}(p,x)^{66,67}\text{Ga}$ and $^{\text{nat}}\text{Zn}(p,x)^{64}\text{Cu}$ processes," *Applied Radiation and Isotopes*, vol. 96, pp. 102-113, 2015/02/01/ 2015.
- [159] A. Jalilian, A. Novinrooz, F. Sedeh, S. Moradkhani, A. Rajamand, and J. Solati, "Evaluation of [^{67}Ga]Citrate in The Detection of Various

- Microorganism Infections in Animal Models," *Iranian Journal of Nuclear Medicine*, vol. 17, 01/01 2009.
- [160] A. Jalilian, "An overview on Ga-68 radiopharmaceuticals for positron emission tomography applications," *Iran J Nucl Med*, vol. 24, pp. 1-10, 01/01 2016.
- [161] N. Kalsy and S. Vinjamuri, "Should we stop offering indium-111 octreotide scans in favour of gallium-68 PET-CT scans in the UK?," *Nuclear Medicine Communications*, vol. 37, no. 12, pp. 1221-1222, 2016.
- [162] S. Singh, R. Poon, R. Wong, and U. Metser, "68Ga PET Imaging in Patients With Neuroendocrine Tumors: A Systematic Review and Meta-analysis," (in eng), *Clin Nucl Med*, vol. 43, no. 11, pp. 802-810, Nov 2018.
- [163] G. Treglia, P. Castaldi, G. Rindi, A. Giordano, and V. Rufini, "Diagnostic performance of Gallium-68 somatostatin receptor PET and PET/CT in patients with thoracic and gastroenteropancreatic neuroendocrine tumours: a meta-analysis," (in eng), *Endocrine*, vol. 42, no. 1, pp. 80-7, Aug 2012.
- [164] D. Wild *et al.*, "Comparison of 68Ga-DOTANOC and 68Ga-DOTATATE PET/CT within patients with gastroenteropancreatic neuroendocrine tumors," (in eng), *J Nucl Med*, vol. 54, no. 3, pp. 364-72, Mar 2013.
- [165] I. Rauscher, T. Maurer, W. P. Fendler, W. H. Sommer, M. Schwaiger, and M. Eiber, "(68)Ga-PSMA ligand PET/CT in patients with prostate cancer: How we review and report," (in eng), *Cancer imaging : the official publication of the International Cancer Imaging Society*, vol. 16, no. 1, pp. 14-14, 2016.
- [166] C. Y. Lin, M. T. Lee, C. L. Lin, and C. H. Kao, "Comparing the Staging/Restaging Performance of 68Ga-Labeled Prostate-Specific Membrane Antigen and 18F-Choline PET/CT in Prostate Cancer: A Systematic Review and Meta-analysis," (in eng), *Clin Nucl Med*, vol. 44, no. 5, pp. 365-376, May 2019.
- [167] I. Rauscher *et al.*, "Matched-pair comparison of 68Ga-PSMA-11 and 18F-PSMA-1007 PET/CT: frequency of pitfalls and detection efficacy in biochemical recurrence after radical prostatectomy," *Journal of Nuclear Medicine*, June 28, 2019 2019.
- [168] *Production of Long Lived Parent Radionuclides for Generators: 68Ge, 82Sr, 90Sr and 188W*. Vienna: INTERNATIONAL ATOMIC ENERGY AGENCY, 2010.
- [169] H. T. Bach *et al.*, "Improving the survivability of Nb-encapsulated Ga targets for the production of 68Ge," *Nuclear Instruments and Methods in Physics Research Section B: Beam Interactions with Materials and Atoms*, vol. 299, pp. 32-41, 2013/03/15/ 2013.

- [170] J. M. Fitzsimmons and L. Mausner, "Production scale purification of Ge-68 and Zn-65 from irradiated gallium metal," *Applied Radiation and Isotopes*, vol. 101, pp. 60-64, 2015/07/01/ 2015.
- [171] G. Meinken, S. Kurczak, L. Mausner, K. Kolsky, and S. Srivastava, "Production of high specific activity ^{68}Ge at Brookhaven National Laboratory," *Journal of Radioanalytical and Nuclear Chemistry*, vol. 263, pp. 553-557, 01/01 2005.
- [172] S. K. Egamediev, S. Khujaev, and A. I. Muminov, "Production of carrier-free germanium-68 by alpha-particle bombardment zinc cyclotron target," in *Cyclotrons and Their Applications 2001*, 2001, vol. 600, p. 55.
- [173] F. Roesch, "Maturation of a key resource - the germanium-68/gallium-68 generator: development and new insights," (in eng), *Curr Radiopharm*, vol. 5, no. 3, pp. 202-11, Jul 2012.
- [174] J. W. Engle *et al.*, "Very high specific activity $^{66/68}\text{Ga}$ from zinc targets for PET," (in eng), *Applied radiation and isotopes : including data, instrumentation and methods for use in agriculture, industry and medicine*, vol. 70, no. 8, pp. 1792-1796, 2012.
- [175] M. Pandey, H. Jiang, J. Byrne, A. Packard, and T. DeGrado, "Cyclotron production of ^{68}Ga using a solution target," *Journal of Nuclear Medicine*, vol. 55, no. supplement 1, p. 434, May 1, 2014 2014.
- [176] M. Pandey, J. Byrne, H. Jiang, A. Packard, and T. Degrado, "Cyclotron production of (^{68}Ga) via the $(^{68}\text{Zn}(p,n)(^{68}\text{Ga})$ reaction in aqueous solution," *American journal of nuclear medicine and molecular imaging*, vol. 4, pp. 303-10, 07/01 2014.
- [177] F. Szelecsényi, Z. Kovács, K. Nagatsu, K. Fukumura, K. Suzuki, and K. Mukai, "Investigation of direct production of ^{68}Ga with low energy multiparticle accelerator," (in English), *Radiochimica Acta*, vol. 100, no. 1, p. 5, 2012.
- [178] F. Szelecsényi, T. E. Boothe, E. Tavano, M. E. Plitnikas, and F. Tárkányi, "Compilation of cross sections/thick target yields for ^{66}Ga , ^{67}Ga and ^{68}Ga production using Zn targets up to 30 MeV proton energy," *Applied Radiation and Isotopes*, vol. 45, no. 4, pp. 473-500, 1994/04/01 1994.
- [179] *Gallium-68 Cyclotron Production*. Vienna: INTERNATIONAL ATOMIC ENERGY AGENCY, 2019.
- [180] K. H. A. MAHER NASER NAOOM, NAWAL FATAH NAJI, "CROSS SECTIONS AND YIELDS CALCULATIONS FOR COPPER-64 PRODUCTION INDUCED BY DEUTERONS AND PROTONS," *International Journal of Physics and Research (IJPR)*, vol. 3, no. 3, pp. 13-20, Aug 2013.

Appendix

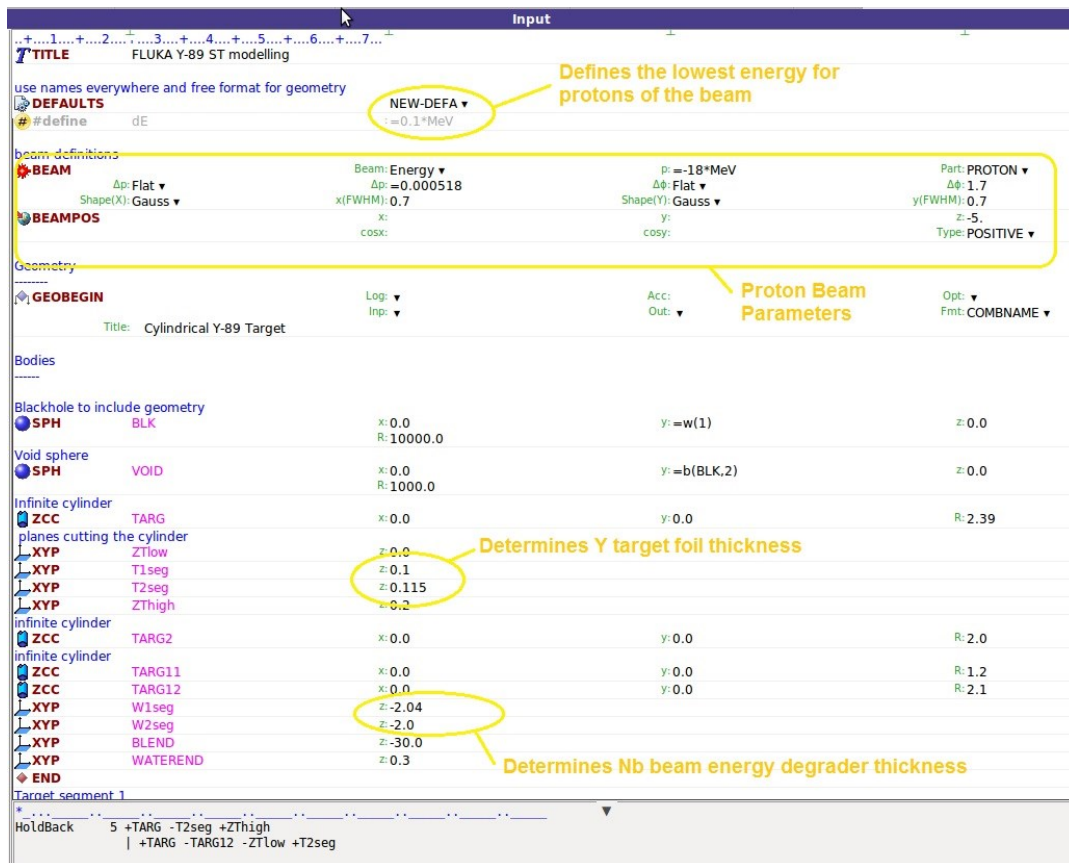


Figure 126 File editor FLAIR view with first page of the input file open, showing crucial parameters setting for FLUKA simulation of ^{89}Zr production.

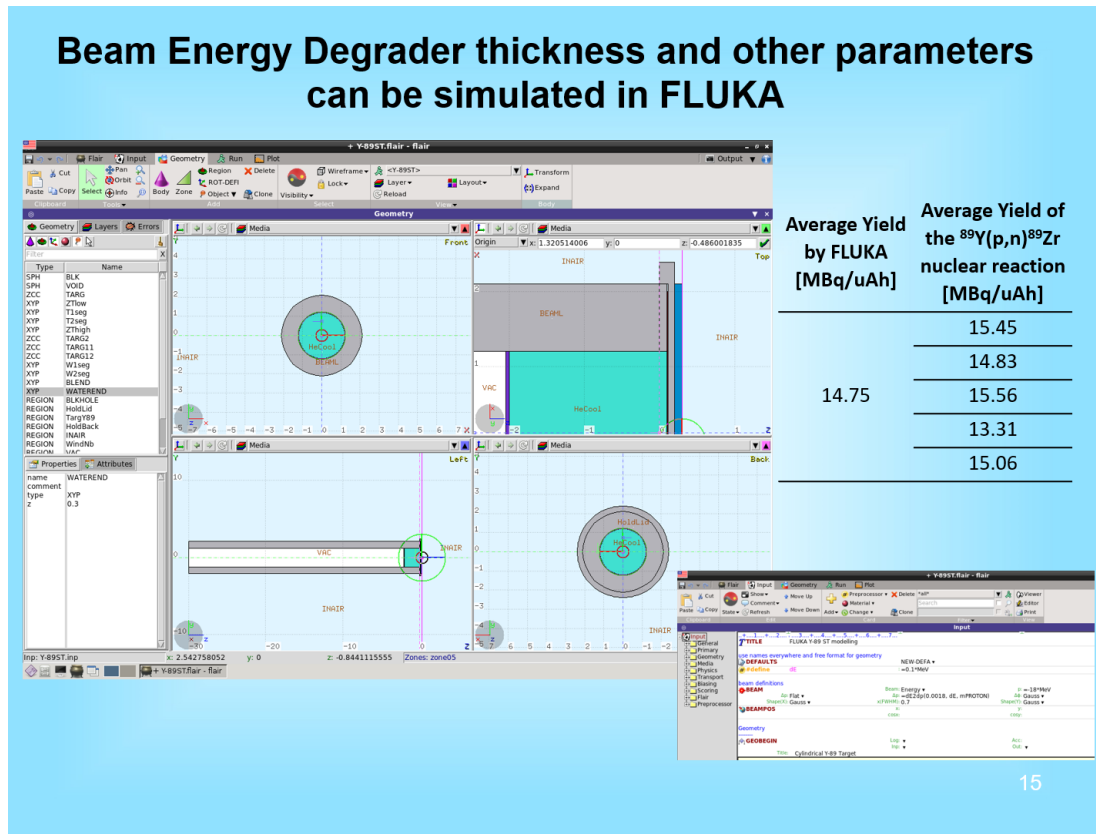
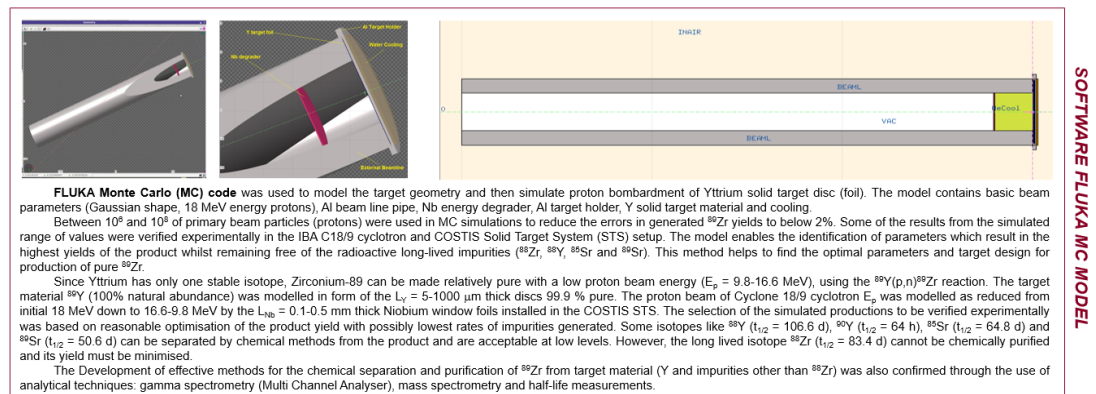
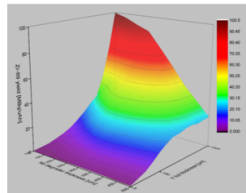


Figure 127 Regions and materials definition in geometry editor.

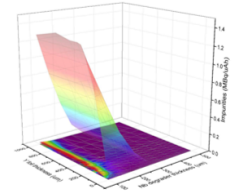


RESULTS of those simulations that have been verified experimentally are shown in the table below demonstrating the accuracy of the model.

L_{nb} [μ m] E_p [MeV]	L_y [μ m]	Experimental ⁸⁹ Zr Yield [MBq/uAh]	Simulated ⁸⁹ Zr Yield [MBq/uAh]	Simulated ⁸⁹ Zr Yield Error [%]
400 (11.7)	150	15.56	16.62	0.22
	200	23.30	21.88	0.48
	300	30.74	30.79	0.68
350 (12.6)	200	24.41	23.55	1.75
	300	33.68	34.58	0.99



3D map on the left presents levels of the ⁸⁹Zr yields received from the FLUKA MC simulations (errors < 2%)



Set of 3D maps on the right is showing levels of the impurities generated by the FLUKA model to compare the yield of the most abundant ⁸⁹Zr relative to the other unwanted products with very low yields (almost flat). It is clearly seen that yield of ⁸⁹Zr drops from 1.4 (5 to 10 % of typical product yield) at maximum to almost 0 MBq/uAh for 350 μ m and thicker Nb foils.

The ⁸⁹Zr and ⁸⁶Zr yields from all simulations are shown in 3D plots above. The aim was to find the highest simulated product yield with no ⁸⁶Zr impurities generated (at accuracy of $10^6 - 10^8$ primary protons) using target disc thickness less than 500 μ m and then validate them by cyclotron productions and postproduction analysis. The 150 μ m thick Y target, previously used for routine productions of ⁸⁹Zr in PETIC, has been replaced by one 300 μ m thick and beam energy degradation was reduced to 350 μ m Nb foil, resulting in an increased yield of more than double (**from 15.6 to 33.7 MBq/uAh**) for isotopically pure product, as predicted by the simulations. It is important to consider also the yields of the impurities in the process of possible optimization. Some short-lived isotopes like ^{89m}Zr disappear after few hours (4 to 6 h), others like Zr⁸⁸ should be eliminated by good production planning (parameters optimization).

Figure 128 Examples of the 3D presentations of the FLUKA results.

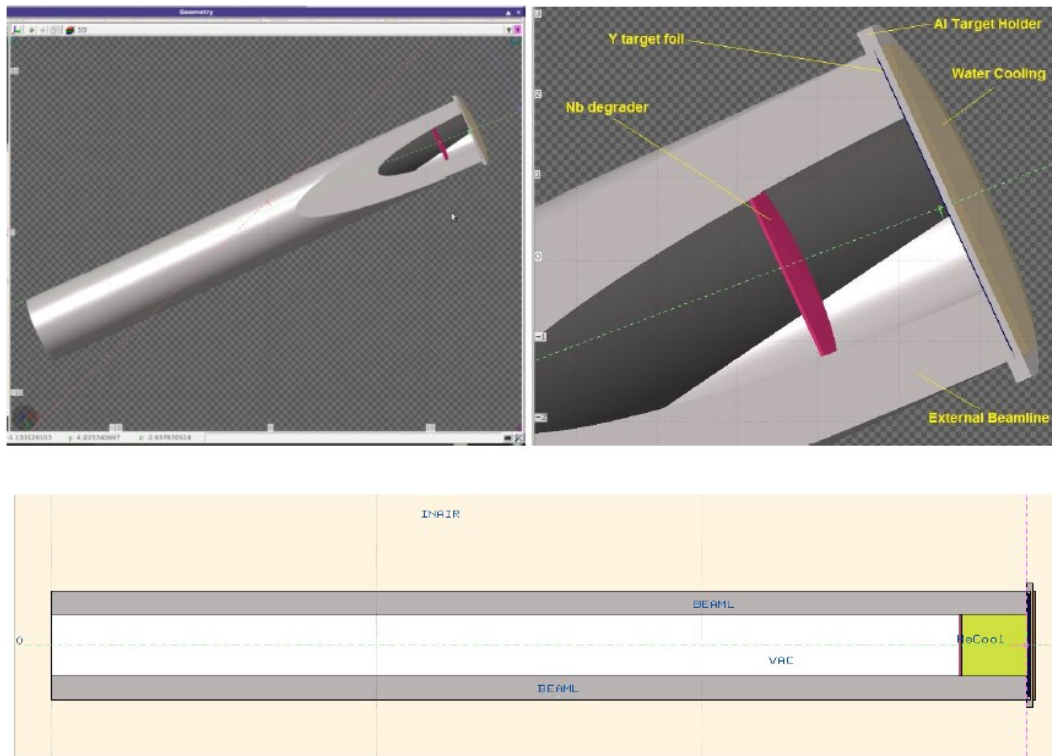


Figure 129 Screenshots from the FLAIR geometry editor.


```

C:\Users\adam\Documents\PHD\MET\Results\Zr-89_Prod_var_prim-corrected\Nb300\Nb300Y-89Zr_80_hab.h4
File Edit Options Encoding Help
Detector #: 1
actin
# R/Z Isotopes:
98 33 0.000 0.000
98 34 0.000 0.000
98 35 0.000 0.000
98 36 0.000 0.000
98 37 0.000 0.000
98 38 0.000 0.000
98 39 881.5 66.67
98 40 0.000 0.000
98 41 0.000 0.000
98 42 0.000 0.000
98 43 0.000 0.000
99 33 0.000 0.000
99 34 0.000 0.000
99 35 0.000 0.000
99 36 0.000 0.000
99 37 0.000 0.000
99 38 0.000 0.000
99 39 3.664E+07 0.5255
99 40 3.499E+07 0.5255
99 41 0.000 0.000
99 42 0.000 0.000
99 43 0.000 0.000
99 44 0.000 0.000
99 45 0.000 0.000
99 46 0.000 0.000
99 47 0.000 0.000
99 48 0.000 0.000
99 49 0.000 0.000
99 50 0.000 0.000
99 51 0.000 0.000
99 52 0.000 0.000
99 53 0.000 0.000
99 54 0.000 0.000
99 55 0.000 0.000
99 56 0.000 0.000
99 57 0.000 0.000
99 58 0.000 0.000
99 59 1.544 9.746
99 60 1.865E+04 9.746
99 61 0.000 0.000
99 62 0.000 0.000
99 63 0.000 0.000

```

Figure 131 Example of the file with results for FLUKA simulation of ^{89}Zr production.

Figure 132 displays two screenshots of a FLUKA simulation results file, showing the output for the production of ^{48}V . The top screenshot shows the results for detector n: 1, and the bottom screenshot shows the results for detector n: 2. Both screenshots display a list of isotopes and their corresponding production rates.

The top screenshot (Detector n: 1) shows the following data:

Isotope	Production Rate
49 16	0.000
49 17	0.000
49 18	0.000
49 19	0.000
49 20	0.000
49 21	0.000
49 22	0.000
49 23	1.7075E+04
49 24	0.000
49 25	0.000
49 26	0.000
48 16	0.000
48 17	0.000
48 18	0.000
48 19	0.000
48 20	0.000
48 21	0.000
48 22	0.000
48 23	5.5875E+06
48 24	0.000
48 25	0.000
48 26	0.000
47 16	0.000
47 17	0.000
47 18	0.000
47 19	0.000
47 20	0.000
47 21	1.1745E+04
47 22	0.000
47 23	9.6525E+07
47 24	0.000
47 25	0.000
47 26	0.000
46 16	0.000
46 17	0.000
46 18	0.000
46 19	0.000
46 20	0.000
46 21	4.922
46 22	0.000
46 23	3.8755E+07
46 24	0.000
46 25	0.000
46 26	0.000
45 16	0.000
45 17	0.000
45 18	0.000
45 19	0.000
45 20	0.000
45 21	0.000
45 22	0.000
45 23	0.000
45 24	0.000
45 25	0.000
45 26	0.000
44 16	0.000
44 17	0.000
44 18	0.000
44 19	0.000
44 20	0.000
44 21	3.1552E+06
44 22	0.000
44 23	0.000
44 24	0.000
44 25	0.000
44 26	0.000

The bottom screenshot (Detector n: 2) shows the following data:

Isotope	Production Rate
48 17	0.000
48 18	0.000
48 19	0.000
48 20	0.000
48 21	0.000
48 22	0.000
48 23	5.5875E+06
48 24	0.000
48 25	0.000
48 26	0.000
47 16	0.000
47 17	0.000
47 18	0.000
47 19	0.000
47 20	0.000
47 21	1.1745E+04
47 22	0.000
47 23	9.6525E+07
47 24	0.000
47 25	0.000
47 26	0.000
46 16	0.000
46 17	0.000
46 18	0.000
46 19	0.000
46 20	0.000
46 21	4.922
46 22	0.000
46 23	3.8755E+07
46 24	0.000
46 25	0.000
46 26	0.000
45 16	0.000
45 17	0.000
45 18	0.000
45 19	0.000
45 20	0.000
45 21	0.000
45 22	0.000
45 23	0.000
45 24	0.000
45 25	0.000
45 26	0.000
44 16	0.000
44 17	0.000
44 18	0.000
44 19	0.000
44 20	0.000
44 21	3.1552E+06
44 22	0.000
44 23	0.000
44 24	0.000
44 25	0.000
44 26	0.000
43 16	0.000
43 17	0.000
43 18	0.000
43 19	0.000
43 20	0.000
43 21	1.6213E+06
43 22	0.000
43 23	0.000
43 24	0.000
43 25	0.000
43 26	0.000

Figure 132 Example of the file with results for FLUKA simulation of ^{48}V production.

